Nuclear Fuel Recycling:

Are There NO Issues?

Michael Alexander Chimes, M.Chem (Hons.)

This Thesis is Submitted for the degree

of Doctor of Philosophy

Engineering Department

Lancaster University

August 2022

Declaration

The work described in this thesis was conducted in the Department of Engineering, Lancaster University between October 2015 and August 2022. I declare that the work in this thesis has been done by myself and has not been submitted elsewhere for the award of any other degree.

Michael Chimes

Abstract

In reprocessing flowsheets for spent nuclear fuel, one challenge which needs to be addressed is the controlled routing of neptunium. This is of importance as neptunium, along with the other minor actinides, contributes significantly to the long-term radiotoxicity of radioactive waste and can be highly mobile in the environment. Its presence across various reprocessing streams also contributes to the radiolysis of the nitric acid medium as well as other species present. Radiolysis of nitric acid, largely due to Pu/minor actinide alpha emission and fission product gamma emission, gives rise to significant in-process concentrations of redox-active nitrous acid; the following chemical reactions of this radiolytically generated HNO_2 then giving rise to a range of similarly active nitrogen-oxygen redox species such as NO_2, N_2O_4 and NO.

The effect of the concentrations of nitrous and nitric acid on the extent of oxidation of neptunium is dependent on the HNO_3:HNO_2 ratio - control of the Np(V)/nitrous ratio has been found to be key in achieving near-complete Np extraction as Np(VI).

However, previous work attempting to fit Np(V) oxidation data to the current accepted kinetic expressions has shown inconsistencies, most especially with respect to

i. The key oxidant in the forward going conversion of Np(V) to Np(VI); and
ii. The nature of the so-generated reductant for the reverse reduction of Np(VI) to Np(V).

Thermodynamic analysis based on the redox potentials of possible nitrogen-oxygen species present within a spent fuel reprocessing scheme suggests that the key oxidant in the reaction outlined in point i. above, is N_2O_4. This oxidation of NpO_2^+ by N_2O_4 would thereby generate NO, a hitherto unconsidered species with the capacity to act as the reductant in the reverse reduction of Np(VI) back to Np(V) – thus addressing point ii. above. Therefore, examination of the kinetics with respect to the net production of the known reducing agent NO is needed to determine its role in the oxidation/reduction reactions of the actinides.

In order to support method development prior to experiments on real neptunium samples, work has been performed to look at the electrochemical behaviour of both nitrous acid and nitric oxide, and reduction reactions have been performed using vanadium as a non-radioactive analogue for neptunium. Whilst vanadium shows similar electrochemical potentials for the VO_2^+ reduction to VO^{2+} to the reduction of Np(VI) to Np(V), making it a good thermodynamic analogue, the removal of the bonded oxygen in the vanadium system has been seen to make it kinetically slower. Experiments have been performed to investigate the reduction of both the VO_2^+ and NpO_2^{2+} species by NO. These experiments have allowed for the deduction of a mechanism of reaction to be proposed which addresses the inconsistences in the accepted kinetic expression previously found and detailed above.

Acknowledgements

Firstly, I would like to thank my supervisor Prof Colin Boxall for all his help, support, and encouragement throughout my PhD tenure.

I would also like to thank my industrial supervisor Robin Taylor at the National Nuclear Laboratory, and both the Next Generation Nuclear Centre for Doctoral Training and the Lloyd's Register Foundation for the funding to allow me to undertake this project.

It would be amiss of me to not also extend my thanks to Richard Wilbraham, Michael Bromley, Dominic Laventine, and all the other students and staff, both past and present, within the group and department for their support throughout my PhD, be it technical or otherwise.

Finally, thanks to Mum, Dad, Richard, and Josh for their continued support through the entirety of my seemingly everlasting education, and for always believing I would remain the perpetual student.

Contents

List of Figures

List of Tables

List of Abbreviations

AGR	Advanced Gas-cooled Reactor
AHA	Aceto-hydroxamic acid
CCE	Chemical-Chemical-Electrochemical
CEC	Chemical-Electrochemical-Chemical
COEX	Coextraction
CV	Cyclic Voltammetry
EC'	Electrochemical-Catalytic chemical
ECC	Electrochemical-Chemical-Chemical
ECE	Electrochemical-Chemical-Electrochemical
FHA	Formo-hydroxamic acid
GC	Glassy Carbon
GDF	Geological Disposal Facility
HA	Highly Active
LET	Linear Energy Transfer
LSC	Liquid Scintillation Counting
LWR	Light Water Reactor
MOX	Mixed Oxide Fuel
NHE	Normal Hydrogen Electrode
NNL	National Nuclear Laboratory
NOx	Nitrogen Oxide
NUEX	Neptunium Uranium Extraction
OK	Odourless Kerosene
PP	Plutonium Purification

PUREX	Plutonium Uranium Reduction Extraction
PWR	Pressurised Water Reactor
S/A	Ratio of Organic Solvent to Aqueous Phase
SNF	Spent Nuclear Fuel
TBP	Tributyl phosphate
Thorp	Thermal Oxide Reprocessing Plant
UKAEA	United Kingdom Atomic Energy Authority
UP	Uranium Purification
UREX	Uranium Extraction
UV-VIS-NIR	Ultraviolet-Visible-near-IR

1 Introduction

1.1 Nuclear Power and the Low Carbon Economy

1.1.1 Current Nuclear Power

On the forefront of the minds of many of the world's population and touted as the world's biggest problem by scientists worldwide, climate change looks to cause irreparable damage to ecosystems. Yet with electricity demands continuing to rise, Figure 1-1,[1, 2] due to factors such as increased population and urbanisation, the need to develop the production of electricity from sustainable sources becomes more and more important.

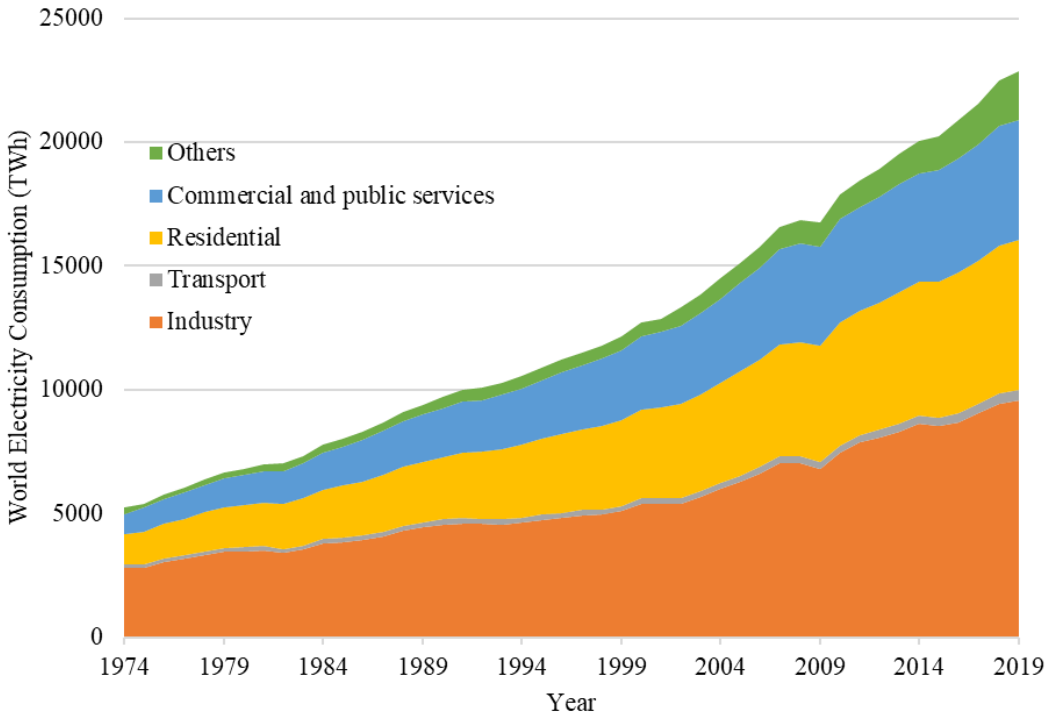

Figure 1-1 Growth of world electricity consumption from 1974-2019.[1, 2]

Following World War II, both western nations and the Soviet Union began to turn to focus on the development of technologies which could utilise the power recently discovered and demonstrated in nuclear reactions through the use of nuclear weapons, for generation of electricity.[3] In the United Kingdom, development of this new nuclear reactor technology, as

well as providing nuclear material for the country's defence purposes, was to be the remit of the United Kingdom Atomic Energy Authority (UKAEA). This resulted in the world's first commercial nuclear power station to be built at Calder Hall and opened in 1956; a Magnox type reactor which used uranium metal fuel, a graphite moderator, and were carbon dioxide cooled.[4] Between 1956 and 1971, a total of 26 Magnox reactors were built in the UK, which was then followed by 14 advanced gas-cooled reactors (AGR) being built between 1976 and 1989, and one pressurised water reactor (PWR) being built in 1995.[5]

Now the second largest generator of low carbon energy, nuclear power provides approximately 10% of the world's electricity from over 450 operational nuclear reactors in more than 30 countries.[6-8] Currently in the UK, nuclear power accounts for approximately 15% of the electricity supply annually and has a total capacity of 6.5 GWe, with this being generated from 15 operational reactors across 8 nuclear power station sites.[9-12] With half of these expected to close within the next 5 years, the resulting energy shortfall will need to be made up to keep up with growing energy demands. Current UK policy to account for this closure of currently operational nuclear reactors is to support a number of new nuclear builds,[13] resulting in an increase on previous nuclear capacity of 16 GWe new nuclear capacity.[11, 14] For this purpose, a number of proposals have been made, the most advanced of which being the construction of Hinkley Point C, but also include new reactors at Sizewell and Bradwell (expected commercial operation around 2030), among others.

However, with any future increase in nuclear capacity in the UK resulting in increased amounts of spent nuclear fuel (SNF), the need to be able to store and dispose of any newly generated radiological wastes, as well as of legacy wastes, becomes of increasing importance. As part of the management of radioactive waste, the reprocessing of SNF offers potential benefits to both the geological disposal of waste and the manufacture of new fuel materials. The removal of fissile actinides from SNF will facilitate a decreased radiological heat burden on any proposed geological disposal facility (GDF) wherein highly active fission products will be disposed,

while the use of reprocessed uranium for the manufacture of new UO_2 or mixed metal oxide fuels (MOX) will decrease demand for uranium from primary sources.[15, 16]

The UK's historic Thermal Oxide Reprocessing Plant (Thorp) ceased operation in 2018 and its Magnox reprocessing site closed in July 2022. As well as these closures, current UK policy is that of an open fuel cycle, in which SNF is disposed of without prior reprocessing after being allowed to cool both thermally and radioactively within an interim storage facility. Both the closure of UK reprocessing sites and the UK's open fuel cycle policy, mean that the design of any GDF for the disposal of SNF would need to be able to account for the heat burden of wastes and have the design life to cope with the long timescales involved to allow decay of radionuclides due to the long half-life transuranics.[17] However, no GDF is currently available in the UK, and one is not expected to receive the first waste until at least the 2040s as a suitable site has yet to have been identified.[18] Due to these potential issues, the option of operating a closed fuel cycle must remain available in order to potentially address the need to store and dispose of any newly generated wastes and the absence of any current solution for producing a GDF.

Therefore, for this purpose, as well as for the purpose of retaining knowledge and expertise in the UK across the whole fuel cycle, research and development is still being undertaken in order to develop advanced reprocessing techniques which look to be proliferation resistant, more cost effective, and generate less wastes than current reprocessing options.[19, 20]

1.1.2 Reprocessing of Spent Nuclear Fuel

Due to factors such as differing reactor types, operating conditions, fuel types, and cooling times, the composition of SNF can vary greatly, with most of the known elements being present to varying degrees. One such example of SNF composition, calculated by Hiezl[21] using the FISPIN fuel depletion code, is given in Table 1-1. This complex mixture therefore poses significant challenges in its management through either direct disposal or reprocessing.

Elements	Amount / mol	mol %
U + Pu + Np + Am + Cm	4093.94	94.91271
Zr	33.93	0.786623
Nd + Sm + Eu + Gd + Pr + Tb	32.53	0.754166
Gaseous (Kr, Xe, He)	32.2	0.746515
Mo	26.26	0.608804
Ru + Tc	21.89	0.507491
Ba	14.01	0.324804
Rb + Cs	13.3	0.308343
Ce	12.72	0.294897
Pd	8.33	0.19312
La	6.67	0.154635
Y	4.08	0.09459
Sr	3.46	0.080216
Rh	3.44	0.079752
Te + Se	3.12	0.072333
I + Br	1.46	0.033848
Rest of the elements	1.155	0.026777
Cd + Ag	0.727	0.016855
Sn + Sb	0.152	0.003524

Table 1-1 Elements present in spent nuclear fuel after 100 years cooling time for 25 GWd/t U burn-up. Reproduced from Hiezl.[21]

Reprocessing of spent nuclear fuel is important in the nuclear fuel cycle for the management of wastes, and for the recovery and recycle of Pu generated by the U-238 activation process and unused U. Currently, commercial reprocessing is largely done using this extraction in the PUREX (Plutonium Uranium Reduction EXtraction) process, with spent uranium metal and uranium oxide-based fuels currently being reprocessed in France (La Hague), Japan (Rokkasho-mura), and Russia (Mayak) and Thorp in the UK having also utilised the PUREX process up until its recent closure.[22, 23] The PUREX process involves extraction of tetravalent and

hexavalent actinides using tributyl phosphate (TBP) in order to separate the U and Pu from the rest of the waste.[24, 25]

Whilst PUREX currently does not involve any recovery and recycling of the minor actinides (Np, Am, Cm), it will be an important part of any future reprocessing scheme, with new processes such as i-SANEX and GANEX seeking to recover the minor actinides.[26, 27] By including the recovery and recycling of the minor actinides in a future reprocessing scheme, the long term radiotoxicity of radioactive wastes as well as the heat burden on a geological disposal facility can be reduced.[28]

The three key stages involved in any reprocessing of spent nuclear fuel are the head-end stage, the central solvent extraction process, and the product finishing. Each of these stages will now be covered in turn.

Spent nuclear fuel undergoes a head-end process first to prepare it for the solvent extractions in the chemical plant. At Thorp, when under operation, this was integrated into one building and consisted of shearing of the intact spent fuel pins followed by dissolution in nitric acid, which was then centrifuged to remove solid, insoluble wastes. This dissolution was done through an oxidative process wherein the uranium dioxide was oxidised to uranyl by nitric acid, as given in equation 1.1, where x depends on the concentration of nitric acid.[29] The efficiency of this oxidative dissolution is usually improved by performing it at elevated temperature to reduce the time taken.[30] Further improvements to this dissolution process, in particular in when looking at dissolution of MOX fuel, have also been studied, such as the use of an electrochemically generated redox mediator, such as Ce(IV) or Ag(II), as a method of oxidising the uranium/plutonium oxides present.[31-33]

$$3UO_2 + 4(2+x)HNO_3 \rightarrow 3UO_2(NO_3)_2 + 2(1-x)NO + 6xNO_2 + 2(2+x)H_2O \qquad 1.1$$

Following dissolution of the spent fuel, the PUREX extraction scheme, for which a simplified flowsheet is shown in Figure 1-2 using the information given in Burrows *et al.*[34], then utilises the organic phase extractant ligand TBP in an organic solvent such as odourless kerosene (OK), to separate the uranium and plutonium present from the fission products and minor actinides.

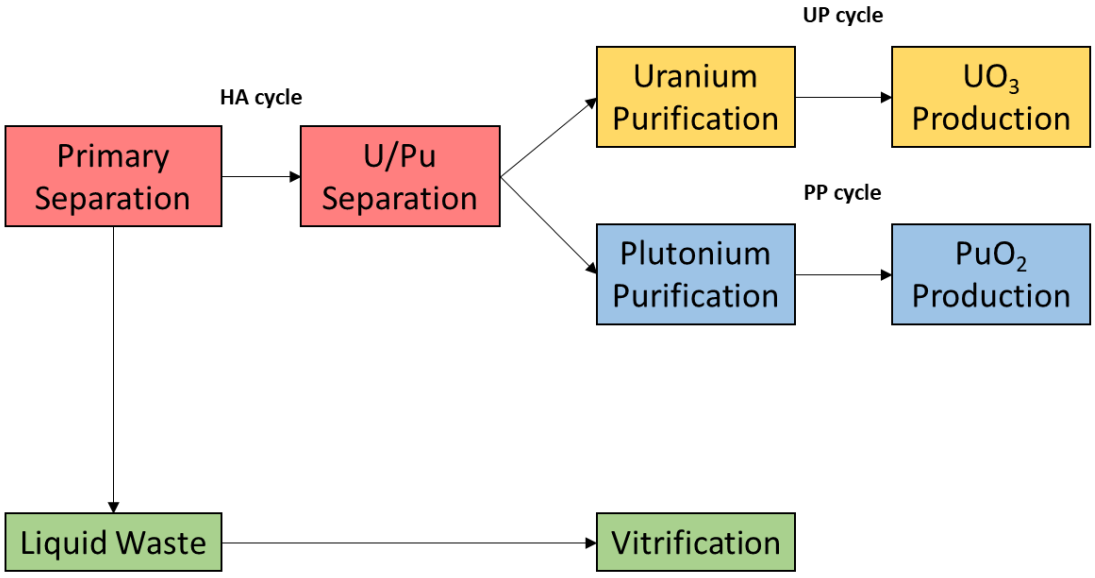

Figure 1-2 Flowsheet of chemical separation at Thorp.

The PUREX process separates the uranium and plutonium present from the fission products and minor actinides by making use of the different accessible oxidation states of both uranium and plutonium, illustrated by the Latimer diagrams shown in Figure 1-3, to transfer the uranium and plutonium between the aqueous and organic solvent phases.

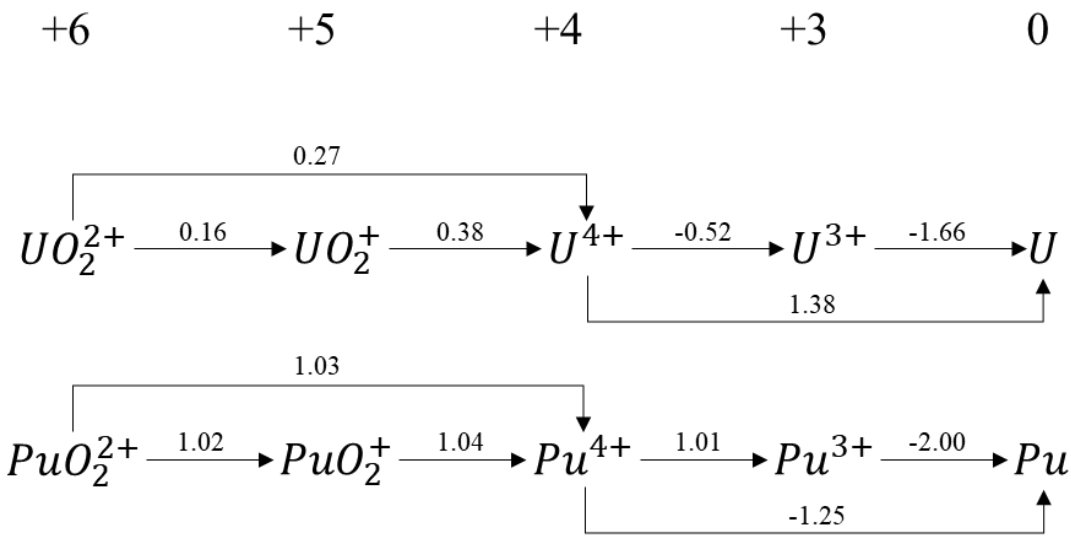

Figure 1-3 Latimer diagrams for a) Uranium and b) Plutonium in acid solution.

The amount of a species that will be in each of a given organic and aqueous phase can be quantified using its distribution coefficient, as defined in equation 1.2 for cases in which the ratio of the organic to aqueous volumes is 1:1, where D is the distribution coefficient, $[M]_{org}$ is the concentration of species M in the organic phase, and $[M]_{aq}$ is the concentration of species M in the aqueous phase. From this equation, we can see that larger distribution coefficient values will mean more of the species will be within the organic phase when at equilibrium.

$$D = \frac{[M]_{org}}{[M]_{aq}} \qquad 1.2$$

Distribution coefficient values vary according to both acidity of the aqueous phase and oxidation state of the metal ion, Figure 1-4. This makes it possible to implement selective extractions of different metals ions by either changing the acidity of the contacted aqueous phase, or by the addition of redox active reagents to change the oxidation state of the metal ion.

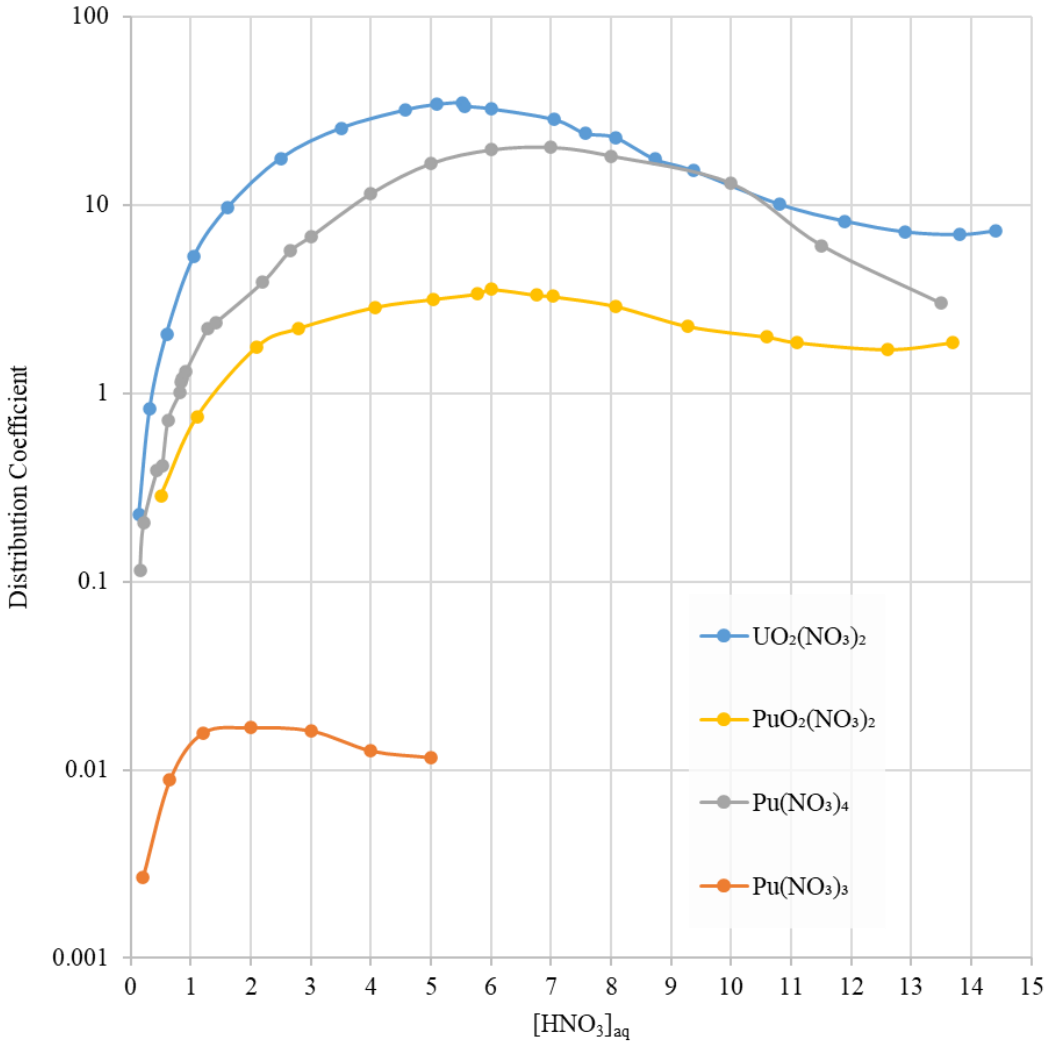

Figure 1-4 Distribution coefficients of some uranium and plutonium species at varying nitric acid concentrations when contacted with 19% TBP in kerosene. Graph produced using data taken from Alcock et al.[35] and Best et al.[36]

For the PUREX process, this change in distribution coefficient is utilised when TBP/OK is shaken with an aqueous layer containing U or Pu in a high concentration of HNO_3 (i.e. approximately 2-6 mol dm^{-3}).[37] This causes the equilibria in equations 1.3 and 1.4 to move to the right, forming a U/Pu-NO_3-TBP complex, which subsequently goes into the organic

phase. When TBP/OK containing the U/Pu-NO_3^--TBP complex is shaken with dilute acid (approximately 0.1 mol dm^{-3}) the equilibrium will move to the left because the NO_3^- concentration in the aqueous phase is very low and the U/Pu thus goes into the aqueous phase.

$$Pu^{4+}{}_{(aq)} + 4NO_3{}^-{}_{(aq)} + 2TBP_{(org)} \rightleftharpoons [Pu(NO_3)_2(TBP)_2]_{(org)} \quad 1.3$$

$$UO_2{}^{2+}{}_{(aq)} + 2NO_3{}^-{}_{(aq)} + 2TBP_{(org)} \rightleftharpoons [UO_2(NO_3)_2(TBP)_2]_{(org)} \quad 1.4$$

The transfer of the uranium and plutonium nuclides between the aqueous and organic phases is therefore based on the ability of the Pu(IV) and U(VI) to form complexes with TBP and nitrate that are soluble in the organic phase. Fission products will largely not form these complexes due to their tendency to not form stable higher oxidation states and thus be softer in comparison to the hexavalent and tetravalent uranium/plutonium ions. The TBP will therefore preferentially coordinate to the hexavalent and tetravalent uranium/plutonium ions through its hard-base coordinating oxygen based on the hard/soft acid/base theory which states that hard acids react faster and form stronger bonds with hard bases.

In order to then separate the uranium and plutonium from each other, a reductant is then added in order to reduce the Pu(IV) present to Pu(III). Usually this reductant is in the form of U(IV) which has a lower reduction potential of 0.38 V *vs.* NHE as the U(V)/U(IV) when compared to that of 0.918 V *vs.* NHE for the Pu(IV)/Pu(III) electrochemical couple.[38] The U(IV) can therefore thermodynamically reduce the Pu(IV) present to Pu(III). Since the Pu(III) formed does not readily form a complex with TBP, the plutonium then transfers back over into a fresh nitric acid solution due to the Pu(III) being more readily soluble in the aqueous phase as seen from the distribution coefficients for the $Pu(NO_3)_3$ complex seen in Figure 1-4, leaving the $UO_2(NO_3)_2(TBP)_2$ in the organic phase. Finally, by contacting the uranium containing organic phase with another aqueous nitric acid phase of much lower acidity the uranium is transferred into the lower acidity aqueous phase. This extraction occurs due to the much lower value for

the distribution coefficient at lower nitric acid concentrations, Figure 1-4. By now having the uranium separated into its own aqueous phase, it can then undergo a finishing stage consisting of heating up to 400-500°C[39] to reform it as UO_2 for either disposal or fabrication as a fuel. Similarly, by having Pu in its own aqueous phase also, the Pu can either be sent for disposal or mixed back into the U in the desired ratio for fabrication of MOX fuel, with the average plutonium content of commercial MOX fuel being approximately 9.5%.[40] By stripping all species from the organic phase, it allows the extractant TBP to be reused for further solvent extractions. The full PUREX flowsheet is shown in Figure 1-5.[37]

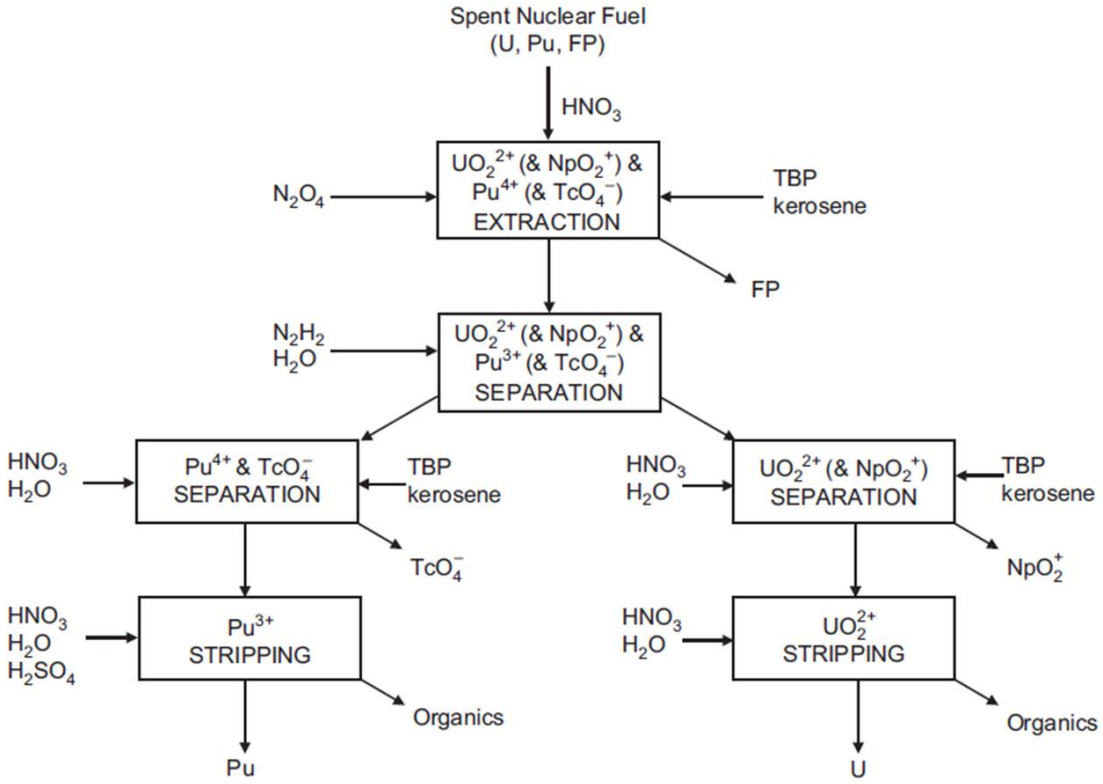

Figure 1-5 PUREX Flowsheet reproduced from Natrajan and Langford Paden.[37]

Up until its recent closure, the chemical separations plant at Thorp implemented PUREX through the use of three-cycles, Figure 1-2, an initial separation cycle (HA cycle), a uranium purification cycle (UP cycle), and a plutonium purification cycle (PP cycle). In the HA cycle, pulsed columns were used to extract U/Pu into 30% TBP in OK, leaving the fission products in

an aqueous nitric acid phase which was then sent for vitrification. The U and Pu were then separated from each other with pulsed columns.[34, 41] The UP cycle was done to remove contaminants such as Np, Pu, and Ru from the uranium steam using mixer settlers and the PP cycle was done for purification of the plutonium stream from mainly technetium, and residual uranium using pulsed columns.

Finally, the finishing stage is then done in order to convert the uranyl nitrate and plutonium nitrate solutions to UO_3 and PuO_2 respectively.[41] For the uranyl nitrate this conversion is done by a thermal denitration process, equation 1.5, whereas the plutonium nitrate conversion is done using an oxalate precipitation, equations 1.6 and 1.7.[42-44]

$$UO_2(NO_3)_2 \rightarrow UO_3 + 2NO_2 + \frac{1}{2}O_2 \qquad 1.5$$

$$Pu(NO_3)_4 + 2H_2C_2O_4 + 6H_2O \rightarrow Pu(C_2O_4)_2 \cdot 6H_2O + 4HNO_3 \qquad 1.6$$

$$Pu(C_2O_4)_2 \cdot 6H_2O \xrightarrow{calcine} PuO_2 + 2CO + 2CO_2 + 6H_2O \qquad 1.7$$

In the reprocessing flowsheet for spent nuclear fuel, one of the major challenges is that of the routing of neptunium. This problem of the routing of neptunium is due to its ready interconversion between the (IV), (V), and (VI) oxidation states and their differing extractability. The ability of these oxidation states to all coexist in aqueous solution under conditions typical of conventional PUREX makes the controlled selective extraction of neptunium difficult to realise. The kinetics and mechanisms of different neptunium redox reactions, and hence the control of the neptunium oxidation states present within a reprocessing scheme, are therefore important to be fully understood. Since these redox reactions are largely brought about by the presence of nitrogen oxide (NOx) species, reactions of these species with the various oxidation states of neptunium need to be understood.

1.2 Control of Neptunium in PUREX

1.2.1 The Neptunium Routing Issue

Neptunium presents particular difficulties in the context of nuclear fuel reprocessing due to its long half-life (the most stable isotope being Np-237 with a half-life of 2.14 million years[45]), environmental mobility as the pentavalent actinyl ion (NpO_2^+),[46-49] and its tendency to be readily convertible between, and hence present as, the (IV), (V), and (VI) oxidation states. This convertibility between oxidation states are due to a number of redox reactions which occur in nitric acid, including the disproportionation of Np(V), Equation 1.8.[50] Several investigations into this reaction have shown how the forward and reverse of this disproportionation are affected by variables such as type of acid present, ionic strength and temperature.[51-55]

$$2NpO_2^+ + 4H^+ \rightleftharpoons NpO_2^{2+} + Np^{4+} + 2H_2O \qquad 1.8$$

The existence of these three oxidation states in nitric acid causes the neptunium to be split between the organic and aqueous phases during reprocessing, Figure 1-6.[56, 57]

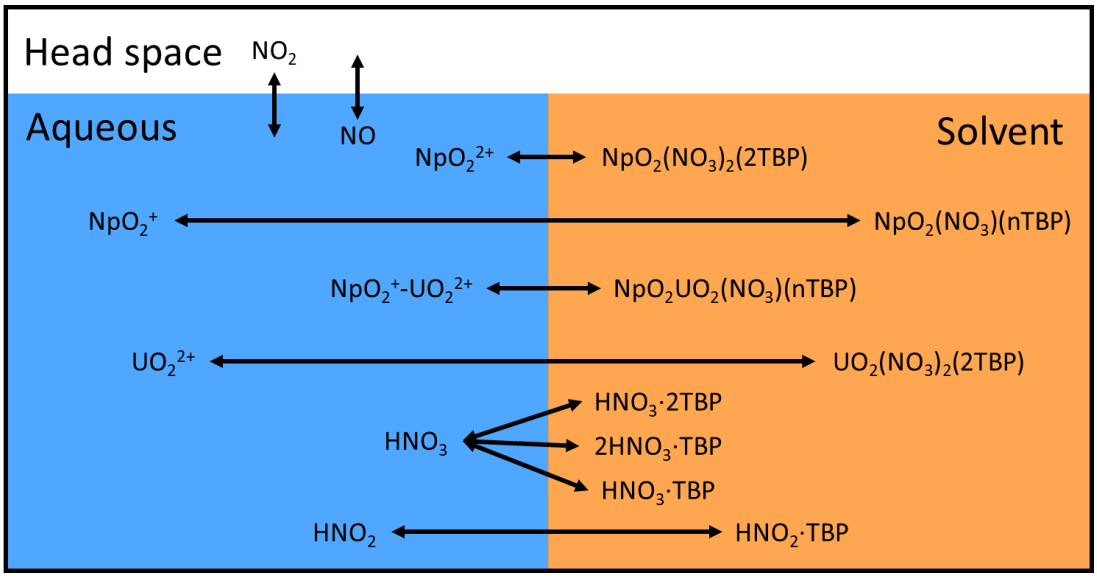

Figure 1-6 Simplified diagram for the transfer of species between organic and aqueous phases.[56, 57]

The neptunium routing issue is one that needs to be resolved in the development of 'next generation' reprocessing techniques such as advanced PUREX, NUEX (Neptunium Uranium Extraction), UREX (URanium EXtraction), NPEX (Neptunium Plutonium Extraction), and COEX (COEXtraction).[23, 58] In these processes, the objective is that the neptunium would be routed with the Pu to give a Np/Pu product which could be used for fabrication of MOX fuel.[59] Alternatively other options would be to completely reject the neptunium to the high activity raffinate and vitrify with the fission products and actinides, or to separate between the first cycle and the U/Pu split forming a dedicated neptunium stream, Figure 1-7.[60] Improvement of neptunium routing in reprocessing would likely reduce the complexity and therefore cost of reprocessing plants, due to reducing the number of process steps.[61]

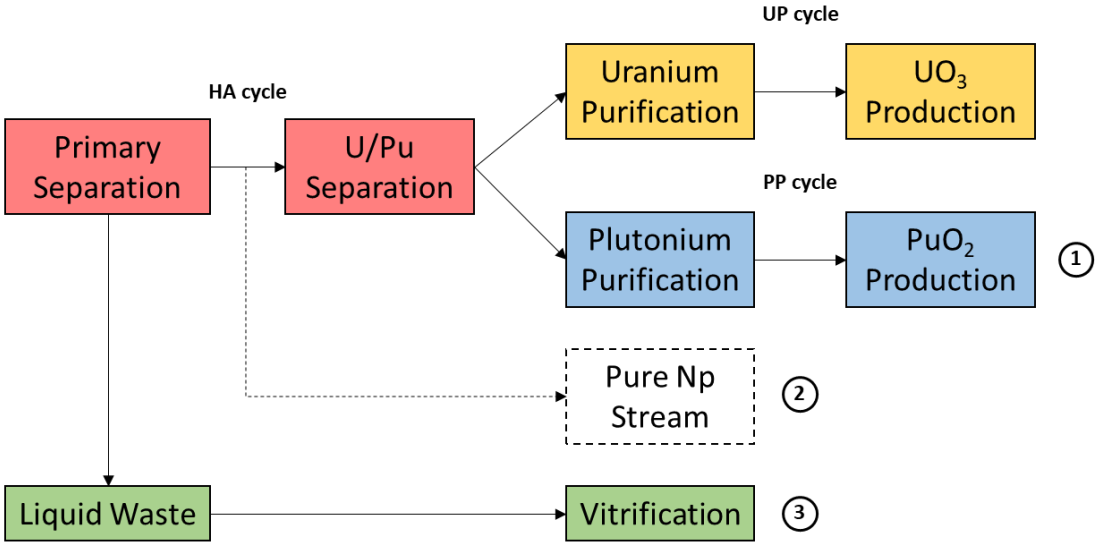

Figure 1-7 Diagram outlining three potential neptunium routing options. 1. Routing of the Np with the Pu to give a Np/Pu product, 2. Separation of the Np to its own dedicated stream, 3. Routing of the Np to the high activity raffinate for disposal along with the fission products and actinides.

In order to produce a dedicated Np stream after the U/Pu split, or to route the neptunium with the plutonium to give a Pu/Np product, addition of hydroxamic acids has been proposed. Both formo- and aceto-hydroxamic acid (FHA and AHA) have both been shown to be suitable for neptunium stripping from the organic phase to the aqueous phase as these small ligands have the ability to preferentially complex tetravalent actinides. As well, FHA and AHA have the

ability to reduce Np(VI) to Np(V) rapidly[62-65] a reaction that is advantageous from a Np routing perspective as the Np(V) will then be stripped back into the aqueous phase along with the hydroxamate-complexed Np(IV). In addition, if the hydroxamate-driven reduction of Np(VI) to Np(V) can be coupled with the disproportionation of Np(V) to form Np(VI) and Np(IV), then a potential route to convert all Np(VI) and Np(V) to hydroxamate-strippable Np(IV) becomes available.

On dissolution of the spent nuclear fuel within the context of conventional PUREX-based reprocessing, the neptunium exists mainly as Np(V) which is effectively inextractable into the TBP organic phase.[66] Extraction of the neptunium happens due to it being oxidised to the more highly extractable Np(VI),[24] mainly driven by the nitric acid, equation 1.9.

$$2NpO_2^+ + NO_3^- + 3H^+ \rightleftharpoons 2NpO_2^{2+} + HNO_2 + H_2O \qquad 1.9$$

This oxidation is complicated by the presence of HNO_2, which, at low concentrations catalyse the forward reaction, while at higher concentrations both catalyses the forward reaction and, through Le Chatelier's principle, causes a shift in the position of equilibrium back to the reduced Np(V) species. Since nitrous acid may also be extracted to the organic phase, the Np-HNO_2 redox reactions need to be understood in both phases.[67] Disproportionation of Np(V) can also occur, giving Np(VI) and Np(IV). Whilst Np(IV) is also extractable, its interchangeability between itself and the pentavalent state is slow due to the required rearrangement of its primary coordination sphere and therefore high activation barrier.[68] It has been shown that in Thorp approximately 34% of Np entering the initial extraction cycle is routed to the high activity raffinate,[27, 69] while it has been shown that only approximately 25% is rejected in the first separation at La Hague.[22] In both instances, the balance of Np is forwarded to the subsequent UP and PP stages.

The routing of neptunium could be dictated by more careful control of its oxidation state in solution. It is believed this can be done using relatively simple modifications to the current PUREX flowsheet in order to adjust concentrations of HNO_2 and HNO_3 in solution. The speciation of neptunium is also dependant on factors such as uranium loading, temperature, radiation, and contactor residence times. However, taking all these factors into account requires the kinetics of the neptunium redox reactions to be well understood in the context of kinetic rate equations that are still largely disputed in the literature. Control of these nitrogen oxide species is critical to neptunium routing and therefore the focus of this literature review is to look at nitrate chemistry in the context of nuclear fuel reprocessing and neptunium speciation.

1.2.2 Mechanism of the Oxidation of Neptunium(V)

As stated above, upon dissolution of the spent nuclear fuel within conventional PUREX-based reprocessing, the neptunium exists mainly as Np(V). While neptunium speciation in the context of the PUREX process has been widely studied by many authors,[56, 70-77] in regards to both the equilibrium of equation 1.9 and the kinetics of oxidation, the actual form of the rate equation is still largely disputed with recent work done by Edwards showing that either of the oxidants proposed by Koltunov were strong enough oxidants to drive the thermodynamic oxidation of Np(V). Based on this observation, the kinetics of the system were first to be looked at, with the thermodynamics and redox potentials of possible oxidants present being examined using the redox ladder presented later in this section, Figure 1-8. In order to achieve full control of neptunium in an advanced PUREX process, the kinetics of both the oxidation and reduction reactions need to be accurately modelled in both the aqueous nitric and organic TBP/OK phase.

Siddall and Dukes[70] reported a dependence of the rate of oxidation on the fourth power of nitric acid concentration which was quantified by Koltunov[78] as given in equation 1.10, while also showing an independence on the concentration on nitrous acid above 5×10^{-5} mol dm^{-3}. The proposed mechanism was outlined using these results and is given in equations 1.11 to

1.13. In this mechanism, the rate determining step is predominantly the activation/protonation of the NpO_2^+ ion shown in equation 1.11, other than at low concentrations of HNO_2 where the oxidation step of equation 1.12 becomes rate determining. Subsequent studies by other authors raised concerns about the validity of results given by Siddall and Dukes due to the use of extraction into 30% TBP-dodecane as the experimental method for determining the amount of Np(VI) present. These concerns are due to the assumption for the extraction method that solvent reactions can be neglected. However, works by Moulin[74] and by Tochiyama[79] using other spectrophotometric experimental methods have shown the underlying analytical methods used by Siddall and Dukes to be valid. These both showed that the results from Siddall and Dukes were not skewed by the rate of solvent reactions and extraction, which would cause determined orders of reaction to be inaccurate.

$$-\frac{d[Np(V)]}{dt} = k[Np(V)][HNO_3]^4 \qquad 1.10$$

$$NpO_2{}^+ + nH^+ \rightleftharpoons Np(V)^* \ (activated\ state) \qquad 1.11$$

$$Np(V)^* + HNO_2 \rightleftharpoons NpO_2{}^{2+} + NO + (n-1)H^+ + H_2O \qquad 1.12$$

$$H_2O + 2NO + NO_3{}^- + H^+ \rightleftharpoons 3HNO_2 \qquad 1.13$$

By contrast, Koltunov[72, 78] suggested the activation of the NpO_2^+ ion, equation 1.11 was unlikely to be the rate determining step in this mechanism as similar protonation reactions of UO_2^+ and PuO_2^+ have been shown to be fast. Therefore, Koltunov used the data from the study and applied activity coefficients for nitric acid in order to account for differing degrees of deprotonation of HNO_3 at differing nitric acid concentrations. This showed that the order of reaction with respect to HNO_3 should be 3 in equation 1.10. The following mechanism could then be suggested for the reaction as shown in equations 1.14 and 1.15. This mechanism

proposed by Koltunov, however, does not explain the apparent dependence of the reaction on HNO_2 concentration below 5×10^{-5} mol dm^{-3} which was seen in the Siddall and Dukes paper.

$$2H^+ + NO_3{}^- \rightleftharpoons NO_2{}^+ + H_2O \quad 1.14$$

$$NpO_2{}^+ + NO_2{}^+ \rightarrow NpO_2{}^{2+} + NO_2 \quad 1.15$$

Further kinetic studies into the oxidation of Np(V) by Koltunov, considering the oxidation by HNO_2, led to the following rate equation seen in equation 1.16. This therefore suggested a mechanism in which the oxidants formed were NO_2 and NO^+ in a fast decomposition of HNO_2. The mechanism, outlined in equations 1.17 to 1.20, was then suggested incorporating this information.

$$-\frac{d[Np(V)]}{dt} = [Np(V)](k_1[H^+]^{0.5}[NO_3{}^-]^{0.5}[HNO_2]^{0.5} + k_2[H^+][HNO_2]) \quad 1.16$$

$$HNO_2 + H^+ + NO_3{}^- \rightleftharpoons 2NO_2 + H_2O \quad 1.17$$

$$HNO_2 + H^+ \rightleftharpoons NO^+ + H_2O \quad 1.18$$

$$NpO_2{}^+ + NO_2 \rightleftharpoons NpO_2{}^{2+} + NO_2{}^- \quad 1.19$$

$$NpO_2{}^+ + NO^+ \rightleftharpoons NpO_2{}^{2+} + NO \quad 1.20$$

Investigations by Moulin[74] and Tochiyama[75] obtained similar kinetic expressions, equations 1.21 and 1.22 respectively, when comparing *via* spectrophotometric (i.e. UV-visible spectrometry) and distribution (i.e. extraction into 30% TBP-dodecane) methods, and when using different solvents for extraction.

$$-\frac{d[Np(V)]}{dt} = \frac{[HNO_2][NO_3^-][Np(V)]\left(k_\gamma[H^+] + k_\delta[H^+]^2 + k_\varepsilon[HNO_2]\right)}{[HNO_2] + [Np(V)]} \quad 1.21$$

$$-\frac{d[Np(V)]}{dt} = k_1[Np(V)][HNO_2]^{0.5}[H^+]^{0.5}[NO_3{}^-]^{0.5} = k_1[Np(V)][HNO_2]^{0.5}[HNO_3] \quad 1.22$$

Moulin's re-investigations[74] of the kinetics found the rate of oxidation to be dependent on the $[HNO_2]/[Np(V)]$ ratio, where $[HNO_2] << [Np(V)]$ showed a rate proportional to HNO_2 but independent of [Np(V)], and *vice versa*. The mechanism suggested by Moulin, equations 1.23 to 1.27, involved a protonated form of Np(V) and a polar form of nitrogen peroxide, N_2O_4.

$$HNO_2 + H^+ \rightleftharpoons NO^+ + H_2O \quad 1.23$$

$$NO_3{}^- + NO^+ \rightleftharpoons N_2O_4 \quad 1.24$$

$$NpO_2{}^+ + H^+ \rightleftharpoons NpO_2H^{2+} \quad 1.25$$

$$N_2O_4 + NO^+ \rightleftharpoons N_2O_3 + NO_2{}^+ \quad 1.26$$

$$NpO_2H^{2+} + N_2O_4 \rightleftharpoons NpO_2{}^{2+} + H^+ + NO_3{}^- + NO \quad 1.27$$

Tochiyama[75] used a form of the Koltunov equation given in equation 1.16 where the k_2 term, associated with the NO^+ oxidant, describes a minor reaction to give equation 1.22. A mechanism consistent with this rate equation was proposed which was the same as one of the pathways given by Koltunov, where the decomposition of HNO_2 gives the oxidant NO_2 for oxidation of Np(V), equations 1.17 and 1.19. The resulting NO_2^- ion is then protonated, regenerating HNO_2.

Previous work by Edwards within this laboratory focused on fitting experimental data for the oxidation of Np(V) obtained by the National Nuclear Laboratory (NNL) to rate equations using the gPROMS commercial chemical process modelling software. The rate expressions used by Edwards for this study were that of Koltunov given in equation 1.16, Moulin given in equation 1.21, and Tochiyama given in equation 1.22 for the forward reaction and that of Precek and Paulenova for the reverse reaction (discussed further in Section 1.2.3). Due to the nature of these modelling studies being done over the full time period of the reaction of up to 80 minutes, as opposed to the initial rate studies done by Koltunov/Moulin/Tochiyama, it was seen that the rate dependence on temperature and nitric acid could be accurately modelled, whilst rates as a function of $[HNO_2]$ showed poor fits. This was proposed to be due to differences in the nature of the reductant between the experiments conducted at NNL and by Precek and Paulenova, which will be discussed further in Section 1.2.3.

In examining the electrochemical potentials of species involved it was found that the oxidation mechanism proposed by Koltunov was not thermodynamically possible as neither of the proposed oxidants, NO_2 or NO^+ in equations 1.19 and 1.20 respectively, are strong enough oxidants to oxidise the Np(V) to Np(VI). This can be seen from the redox ladder shown in Figure 1-8 NO_2 or NO^+ couples are seen to be lower than that for the Np(VI)/Np(V) couple seen at 1.24V.

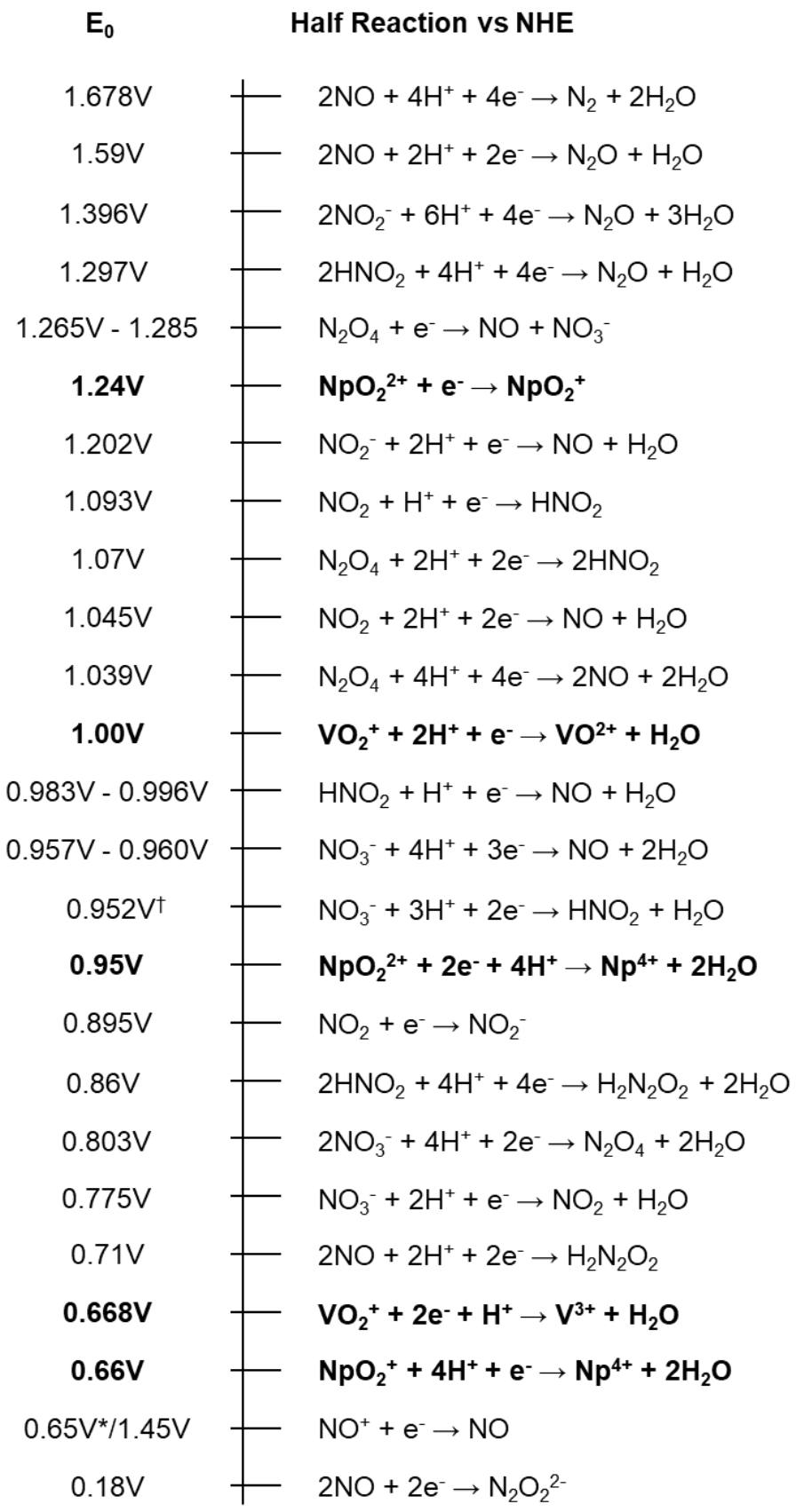

Figure 1-8 Redox ladder showing standard reduction potentials measured at standard room temperature and pressure against a normal hydrogen electrode (NHE) for relevant neptunium, vanadium, and nitrogen oxide reductions. Starred value taken from Topol and Osteryoung[80], daggered value taken from Tochiyama et al.[76], and all other values either taken directly or calculated from Bard et al.[81] Reduction potentials of metal ions are shown in bold for clarity.

As alluded to in the redox ladder shown in Figure 1-8, some uncertainty exists as to the redox potential for the oxidation of NO, with the two most common values cited in the literature between 1.45 V *vs* NHE reported by Bard *et al.* to 0.65 V *vs* NHE reported by Topol and Osteryoung[80, 82-85]. Bennett and Kelmers have found that, in 3 mol dm^{-3} HNO_3, NO gas was seen to be a better reductant than NO_2 gas for the reduction of Pu(VI) to Pu(IV).[86] As the standard redox potential for the PuO_2^{2+}/Pu^{4+} couple is found to be 1.03 V *vs* NHE[81], this therefore suggests that the value of Topol and Osteryoung is the best available for the NO/NO^+ couple and thus that NO would not be a strong enough oxidant to oxidise Np(V) to Np(VI). However, this value shows that NO may be capable of acting as a reductant in reducing Np(VI) to Np(V), which will be discussed further below. In order to verify the value of 0.65 V *vs* NHE reported by Topol and Osteryoung a detailed study of the redox potential of the NO/NO^+ couple, which agrees with this conclusion, is the subject of Section 3.1 in Chapter 3.

The four reactions at the top of the redox ladder shown in Figure 1-8 are all multielectron processes involving two nitrogen containing species, HNO_2 or NO, reacting to yield dinitrogen species such as N_2 and N_2O. They are therefore multistep processes with the quoted redox potentials being associated with the overall reaction rather than any individual step. However, given the behaviour of HNO_2 under acid conditions described by equation 1.18 and what is known from the work of Topol and Osteryoung[80] about the potential for the reduction of the so-formed NO^+ (E = 0.65 V vs NHE, see Section 1.2.3 below), it is highly likely that it is the reduction of NO that is driving these processes. As there is little to no NO initially present in the solutions studied by either Siddall and Dukes, Koltunov, Moulin *et al.*, Tochiyama *et al.* or, subsequently, ourselves (see below), it is not unreasonable to discount its involvement in the oxidation of Np(V) under discussion here. Thus, it is unlikely that the four reactions at the top of Figure 1-8's redox ladder are driving the oxidation of Np(V) in any of the studies discussed above.

There will, however, be some N_2O_4 present in solution as a result of the dimerization of NO_2 produced by the well-studied equilibrium reaction given by equation 1.17. The potential for the

one electron reduction of N_2O_4 given in Equation 1.28 was found to be in the range 1.265-1.285 V *vs.* NHE. This calculation was done using the known potentials for the half equations given in Equations 1.29, 1.30, and 1.32 which are 1.039, 0.957, and 0.803 V respectively. The potential for Equation 1.28 could then be calculated as in Equations 1.31 and 1.33.

$$N_2O_4 + e^- \rightleftharpoons NO_3^- + NO \quad 1.28$$

$$N_2O_4 + 4H^+ + 4e^- \rightleftharpoons 2NO + H_2O \quad 1.29$$

$$NO_3^- + 4H^+ + 3e^- \rightleftharpoons NO + 2H_2O \quad 1.30$$

$$E = (4 \times 1.039) - (3 \times 0.957) = 4.156 - 2.871 = 1.285V \quad 1.31$$

$$2NO_3^- + 4H^+ + 2e^- \rightleftharpoons N_2O_4 + H_2O \quad 1.32$$

$$E = (3 \times 0.957) - (2 \times 0.803) = 2.871 - 1.606 = 1.265V \quad 1.33$$

It has therefore been proposed that N_2O_4 was a possible oxidant for Np(V). This is consistent with observations by Moulin, equations 1.21 where the kinetics depend on the $[HNO_2]/[Np(V)]$ ratio. Moulin's mechanism, wherein N_2O_4 is the oxidant, equations 1.23 to 1.27, could then be shown to give the overall reaction for the oxidation of NpO_2^+ by HNO_2, equation 1.34. The resulting production of NO, which is a known reductant, could therefore also play a role in the speciation of neptunium and the effect of this is yet to be studied. This reduction of Np(VI) by NO can be seen to be thermodynamically viable from the reduction potentials found for both the Np(VI)/Np(V) and NO/NO^+ couples which are at 1.24 V *vs.* NHE and 0.65 V *vs.* NHE respectively. The possibility of this reduction occurring is also supported by previous work done by Bennett and Kelmers, in which NO gas was seen to be a better reductant than NO_2 gas for the reduction of Pu(VI) to Pu(IV).[86]

$$NpO_2^{2+} + H^+ + HNO_2 \rightleftharpoons NpO_2^{2+} + H_2O + NO \quad 1.34$$

1.2.3 Mechanism of the Reduction of Neptunium(VI)

Investigations into the reverse reaction have not been as extensive and is likely due to the reaction being limited by extraction of the Np(VI) into the organic phase in a PUREX process. One suggestion for the mechanism of this reaction comes from Koltunov who suggested a scheme involving a pathway with nitric oxide as the reductant, equations 1.35 to 1.38, and derived a rate equation, equation 1.39.

$$3HNO_2 \rightleftharpoons 2NO + HNO_3 + H_2O \quad 1.35$$

$$NpO_2^{2+} + NO \rightleftharpoons NpO_2NO^{2+} \quad 1.36$$

$$NpO_2NO^{2+} + H_2O \rightleftharpoons NpO_2^{+} + HNO_2 + H^+ \quad 1.37$$

$$NpO_2^{2+} + NO_2^{-} \rightleftharpoons NpO_2^{+} + NO_2 \quad 1.38$$

$$\frac{d[Np(V)]}{dt} = [Np(VI)]\left(k_1\frac{[HNO_2]}{[H^+]} + k_2\frac{[HNO_2]^{1.5}}{[H^+]^{0.5}[NO_3^{-}]^{0.5}}\right) \quad 1.39$$

Woods investigated the reduction of Np(VI) by HNO_2 and found it to be first order with respect to both reactants. Further exploration of the dependence of the rate on $[H^+]$ allowed for determination of the rate equation, equation 1.40, and a mechanism for the reaction given by equations 1.41 to 1.43.[87]

$$-\frac{d[Np(VI)]}{dt} = [Np(VI)][HNO_2]\left(k_1 + \frac{k_2}{[H^+]}\right) \quad 1.40$$

$$NpO_2^{2+} + HNO_2 \rightarrow NpO_2^{+} + H^+ + NO_2 \quad 1.41$$

$$NpO_2^{2+} + NO_2^- \rightarrow NpO_2^+ + NO_2 \quad 1.42$$

$$NpO_2^{2+} + \cdot NO_2 + H_2O \rightarrow NpO_2^+ + 2H^+ + NO_3^- \quad 1.43$$

Most recently, a study by Precek and Paulenova investigating the reduction of Np(VI) also showed that the rate was first order with respect to [Np(VI)] but showed that the order with respect to HNO_2 was 1.2.[88] This report gave a rate equation for the reduction, equation 1.44, which was in agreement with previous results of Shilin and Nazarov as cited by Precek and Paulenova[88]. The reaction mechanism given by Koltunov above is consistent with this kinetic expression and the equation given by Precek and Paulenova can be considered as a condensed form of that of Koltunov.

$$-\frac{d[Np(VI)]}{dt} = k\frac{[Np(VI)][HNO_2]^{1.2}}{[H^+]} \quad 1.44$$

The mechanism for the reduction of Np(VI) by HNO_2 in nitric acid can therefore be shown to proceed *via* two pathways, as shown in equations 1.45 and 1.46, wherein the nitric oxide is formed *via* the decomposition of nitrous acid as per equation 1.35.

Pathway 1:

$$NpO_2^{2+} + NO_2^- \rightleftharpoons NpO_2^+ + NO_2 \quad 1.45$$

Pathway 2:

$$NpO_2^{2+} + NO + H_2O \rightleftharpoons NpO_2^+ + HNO_2 + H^+ \quad 1.46$$

The kinetic expressions for both pathways can be obtained as outlined in equations 1.47 to 1.54, wherein k_1 is the rate constant for pathway 1, k_2 is the rate constant for pathway 2, equation 1.48 is the equilibrium expression for the dissociation of nitrous acid, and equation 1.52 is the equilibrium expression for the decomposition of nitrous acid to nitric oxide given by equation 1.35. Simplification of equation 1.53 is done using the assumption that [NO3-] = [H+] to give equation 1.54, which is valid under the condition that there are no other acids or additional nitrate present.

$$Rate = k_1[Np(VI)][NO_2{}^-] \quad 1.47$$

$$\textit{Since;} \qquad K_{HNO2} = \frac{[H^+][NO_2{}^-]}{[HNO_2]} \quad 1.48$$

$$Rate = k_1 K_{HNO2}[Np(VI)]\frac{[HNO_2]}{[H^+]} \quad 1.49$$

$$Rate = \frac{k_1'[Np(VI)][HNO_2]}{[H^+]} \quad 1.50$$

$$Rate = k_2[Np(VI)][NO] \quad 1.51$$

$$\textit{Since;} \qquad K_{NO} = \frac{[NO]^2[NO_3^-][H^+]}{[HNO_2]^3} \quad 1.52$$

$$Rate = k_2[Np(VI)]\frac{K_{NO}^{0.5}[HNO_2]^{1.5}}{[NO_3^-]^{0.5}[H^+]^{0.5}} \quad 1.53$$

Since in nitric acid $[NO_3^-] = [H^+]$,

$$Rate = k_2'[Np(VI)]\frac{[HNO_2]^{1.5}}{[H^+]} \quad 1.54$$

Therefore, from these mechanistic pathways, orders of reaction can be obtained with respect to nitrous acid of 1 and 1.5 for pathway 1 and pathway 2 respectively. By combining the two

kinetic expressions given for the two pathways in equations 1.50 and 1.54, it is clear that this is consistent with equation 1.39, and is therefore consistent with the observed order of reaction of 1.2, seen in equation 1.44, when the observed rate equation is a combination of these two pathways.

Within the work done by Edwards mentioned above in modelling NNL data to the rate equations for both the oxidation and reduction directions, rates as a function of [HNO_2] were seen to produce poor fits. In order to improve the accuracy of these models, a modified version of the equation given by Precek and Paulenova, equation 1.44, was needed in order to produce better fits of the model to experimental data. These improved fits were obtained when the order with respect to [HNO_2] was 0.5 rather than 1.2.[89] It was therefore suggested that this modification to the rate expression given by Precek and Paulenova was due to the difference in nature of the reductants between those experiments and those conducted at NNL. Within the work done by Precek and Paulenova, cuvettes in which the experiments were performed were uncapped, which will have allowed any volatile nitrogen oxide species to escape and thus the reductant to be controlled as nitrous acid. Reductions performed by NNL, however, were done within capped cuvettes, allowing or the build-up of volatile nitrogen oxide species, such as NO as a product of equation 1.34, and hence additional pathways to reduction of Np(V).

Again as discussed above, Bennett and Kelmers have found that, in 3 mol dm^{-3} HNO_3, NO gas was seen to be a better reductant than NO_2 gas for the reduction of Pu(VI) to Pu(IV)[86] indicating that NO may be capable of reducing Np(VI) to Np(V). Reduction of Np(VI) to Np(V) by NO, which may be present as a product of the Np(V) oxidation to Np(VI) by N_2O_4, has therefore been studied within this work (Section 4.2).

Through modelling the kinetics of the Np(VI) reduction – Np(V) oxidation reactions we ultimately need to know how speciation changes in various conditions. In the PUREX process, conditions that may change are concentrations of HNO_3 and HNO_2 (and thus redox stress by the oxidation and reduction reactions promoted by nitrous as described above), temperature,

absorbed radiation dose, and ratio of organic solvent to aqueous phase (S/A). The next Section will focus on the first of these conditions i.e. the concentrations of nitric and nitrous acid.

1.2.4 Effect of Nitric and Nitrous Acid Concentration

The effect of the concentrations of HNO_3 and HNO_2 on the extent of oxidation of Np(V) to Np(VI) has previously been seen to be dependent on the HNO_3:HNO_2 ratio.[79] From a review of the current literature, it can be seen that an increase in the concentration of HNO_3 gives an increase in the extent of oxidation and hence the amount of Np(VI) at steady state. However, it is also understood that an increasing concentration of HNO_2 leads to an increase in Np(V). These affects are consistent with the equilibrium equation 1.9, where, through application of Le Chatelier's principle, the addition of HNO_3 or HNO_2 will thermodynamically drive the equilibrium to the right or left respectively. The kinetic effect on the addition of nitrous acid however is more complex, as the oxidation in absence of nitrous acid is slow. There is then a significant increase in rate of oxidation on the addition of between 1×10^{-5} mol dm^{-3} and 1×10^{-4} mol dm^{-3} $NaNO_2$, and further addition leads to a less substantial change, or no change, in the rate due to the reduction reaction also being accelerated by addition of nitrous acid.[90]

1.2.5 Effect of Absorbed Dose

The effect of absorbed dose, which is a measure of the energy deposited in matter by ionising radiation per unit mass, is important due to the being a source of HNO_2 as described in Section 1.3.2. In γ-irradiated solutions with an absorbed dose of approximately 1.3 kGy of initially predominant Np(V), oxidation was enhanced compared to non-irradiated solutions and is likely attributable to strongly oxidising radicals such as ·OH and $\cdot NO_3$ as well as the radiolytically generated nitrous acid.[91] Irradiation of solutions initially containing predominantly Np(VI) tend to show an induction period in the reduction of the Np(VI) present up to approximately 1 kGy in which the small amount of Np(V) present is oxidised, Figure 1-9.[91, 92] This initial oxidation has been shown to be not due to the presence of dissolved oxygen and is likely due

to oxidising radicals produced by irradiation.[93] A study by Mincher *et al.* also showed that the rate of reduction of Np(VI) was increased after irradiation had finished. This was attributed to the strong oxidising radicals being depleted due to their short lifetimes and the longer lived radiogenic nitrous acid still being present.[93]

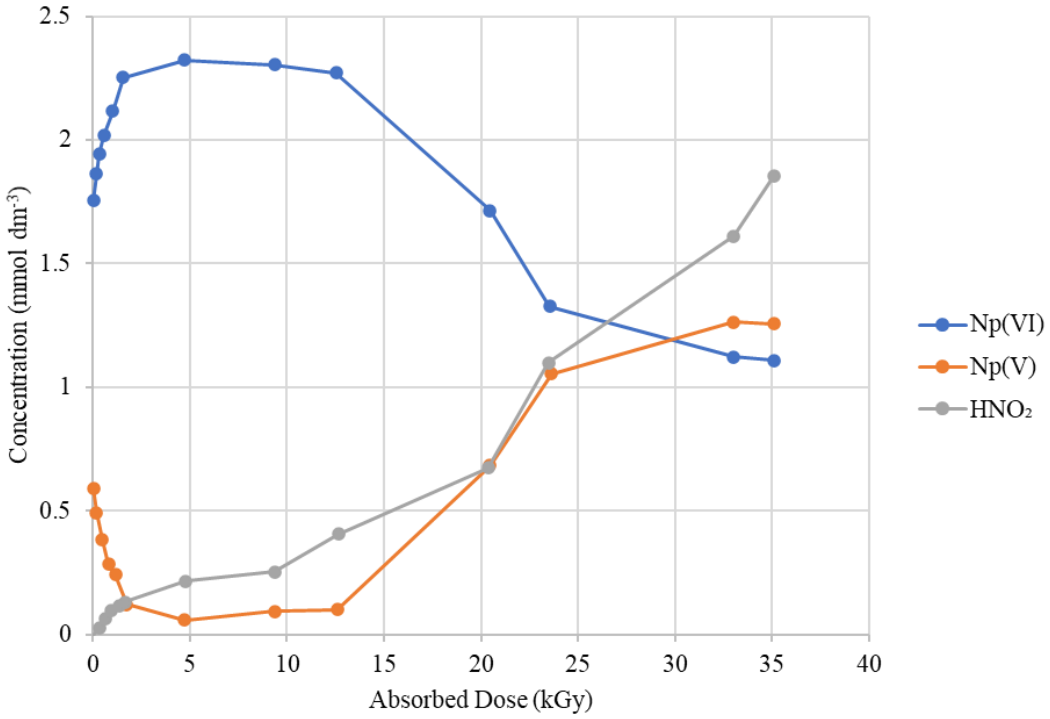

Figure 1-9 Concentrations of Np(V), Np (VI), and HNO_2 against absorbed dose in 4 mol dm^{-3} HNO_3 solution initially containing predominantly Np(VI)[92]

1.2.6 Effect of Scavengers and Temperature

The use of nitrous scavengers to prevent the formation of Np(V) by back-reduction of Np(VI), and thus ensure full extraction of neptunium as Np(VI) in the context of an advanced reprocessing flowsheet (Section 1.2.1), has been investigated by Precek *et al*.[94] In this study, the use of vanadium(V) was to reoxidise any Np(V) back to Np(VI) and the use of methyl urea and acetamide was to scavenge any HNO_2 formed and prevent Np(VI) reduction. Methyl urea was found to be fully decomposed after irradiation in concentrations between 1 and 10 mmol dm^{-3} and hence was seen to have no effect the amount of HNO_2 formed during irradiation. A decrease in radiolytically generated HNO_2 was observed for increasing methyl

urea concentrations of between 10 mmol dm^{-3} and 20 mmol dm^{-3}, with no free HNO_2 detected in samples containing methyl urea concentrations of > 100 mmol dm^{-3}. However, higher concentrations of methyl urea were actually found to promote reduction of Np(VI), with the tetravalent Np(IV) oxidation state becoming predominant at higher absorbed doses. One suggestion for the predominance of the tetravalent oxidation state as opposed to the pentavalent oxidation state produced from the reduction of Np(VI) by HNO_2, was suggested to be due to the further reduction of Np(V) by the presence of accumulated H_2O_2. Whilst the presence of hydrogen peroxide in irradiated solutions of nitric acid is usually negligible due to its scavenging by nitrous acid, as per equation 1.55, the presence of higher concentrations of methyl urea scavenging the nitrous acid would prevent its subsequent scavenging of, and hence accumulation of, hydrogen peroxide.

$$HNO_2 + H_2O_2 \rightarrow HNO_3 + H_2O \qquad 1.55$$

Another explanation for the predominance of the tetravalent oxidation state would be due to the disproportionation of Np(V) to Np(IV) and Np(VI), with the Np(VI) being reduced again by either HNO_2 or H_2O_2.

Therefore, whilst the presence of methyl urea was not able to prevent the reduction of Np(VI) through the scavenging of the HNO_2 reductant, use of methyl urea could still have application in reprocessing due to the extractability of Np(IV) into TBP. The additions of vanadium(V) or acetamide were found to have no effect on the final speciation of neptunium in irradiated solutions.

Higher temperature shows preference for the Np(VI) oxidation state which is consistent with the reported endothermicity of the oxidation reaction.[90, 95] An increase in temperature also shows an increase in rate up to 50°C, however further temperature increase shows visible loss of NOx due to increased decomposition of the nitrous acid present. While data obtained was

admitted to be of poor quality above 50°C, it suggested an apparent slower rate of oxidation at temperatures higher than 50°C, likely due to the above mentioned loss of NOx.[61]

1.2.7 Two Phase Studies on Neptunium Distribution

The effects of the variables discussed in Sections 1.2.4 to 0 on neptunium speciation in nitric acid have been studied in solely in the context of the aqueous phase. However, the effects of the presence of the organic TBP phase have also been studied throughout the literature. These studies allow for the validation of these effects within a PUREX process, and hence the efficient extraction of neptunium as either the (IV) or (VI) oxidation state along with the uranium and plutonium present (if also in appropriate extractable oxidation states, see Section 1.1.2).

In a mixed phase system, any Np(V) produced due to radiogenic nitrous acid accumulation will be present in the aqueous phase; thus irradiation will lower the distribution ratio.[66] Studies within the literature also show lower yields of Np(V) to have been reported for the reduction of Np(VI) in irradiated solutions of nitric acid in the presence of an organic phase, which is likely due to stabilisation of the hexavalent oxidation state by TBP complexation.[92] For mixed-phase and pure aqueous phase systems, yields of nitrous acid were also shown to be approximately equal in irradiated solutions of both 2 mol dm^{-3} and 6 mol dm^{-3} nitric acid. However, irradiation of 0.5 mol dm^{-3} nitric acid was shown to have a significant increase in HNO_2 for the mixed-phase system. The effect of this was reduction of the Np(VI) present to Np(V) and stripping of the Np(V) to the aqueous phase.

Studies have also show that the effect of U-loading is to increase the rate of oxidation of Np(V) to Np(VI) with increasing U concentration. This was explained by presence of U causing a lower extractability of HNO_2 into the organic phase. However, in modelling the system it was shown that the order with respect to $[H^+]$ in the kinetic equation for the oxidation of Np(V), equation 1.16, needed to be altered to give a satisfactory fit to experimental data. In the presence of U, the power had to be changed to 2 from the original value of 0.5 and to 1.3 with no U

present. This difference in power on addition of U shows that the increased oxidation rate cannot solely be due to lower extractability of HNO_2.[96]

At an elevated temperature of 50°C, increasing the S/A ratio from 1 to 2 showed no effect on the rate of oxidation or the position of the final equilibrium. This is likely due to the maximum rate of oxidation having been reached due to the increased temperature. However, at lower temperature the rate of oxidation was faster for S/A ratio of 1. This can be explained by the extraction of HNO_2 being less at lower S/A ratios when looking at an increase in the S/A ratio from 1 to 2, and by the aqueous concentration of HNO_3 being higher.[61] This increase in the rate of Np(V) oxidation when looking at a S/A ratio of 1 for the lower temperature studied will like result in higher extraction of neptunium to the organic phase due to Np(VI) having a higher distribution coefficient than Np(VI).

The presence of nitrogen oxide species will therefore have significant effect on the speciation of neptunium, and all possible sources of these species need to be well understood in the development of a reprocessing plant. This is especially important due to nitric acid being present in high concentrations as the main aqueous constituent of the PUREX reprocessing flowsheet and the high radioactivity of the solution of spent fuel.

1.3 Sources of Nitrogen Oxide Species

1.3.1 Dissolution of Spent Nuclear Fuel

One of the more important nitrogen oxide species involved in the context of a spent nuclear fuel reprocessing scheme is nitrous acid. This is present in varying concentrations across the chemical separation process for spent nuclear fuel due to several different production pathways and its instability.

The primary source of nitrous acid is from the dissolution of the oxide fuel. Upon dissolution of the uranium oxide (Section 1.1.2), nitric acid is reduced to give a range of NOx species, equations 1.56 to 1.58, which can then form nitrous acid by disproportionation.[29, 97-101] This production of nitrous acid makes the dissolution of fuel autocatalytic as the increase in [HNO_2] increases the rate of dissolution and subsequently generates more nitrous acid.[102-104] Whilst this autocatalytic behaviour might be favourable in the dissolution of SNF, the increase in HNO_2 and other NOx species will affect the oxidation states of metal ions present and hence their extractability in later separation stages of reprocessing.

$$3UO_2 + 4(2+x)HNO_3 \rightarrow 3UO_2(NO_3)_2 + 2(1-x)NO + 6xNO_2 + 2(2+x)H_2O \quad 1.56$$

$$UO_2 + 4HNO_3 \rightarrow UO_2(NO_3)_2 + 2NO_2 + 2H_2O \quad 1.57$$

$$UO_2 + 2HNO_3 + 2HNO_2 \rightarrow UO_2(NO_3)_2 + 2NO + 2H_2O \quad 1.58$$

The rate of spent fuel dissolution will therefore depend on the kinetics of both the separate nitric and nitrous acid reaction pathways' rates.[30] Due to the autocatalytic nature of the dissolution reaction, after a slow induction period, the rate of dissolution will steadily increase as HNO_2 is generated and therefore transition to the more rapid nitrous acid oxidation pathway.

From this production of nitrous acid by dissolution of SNF, it can be seen that across the whole of a reprocessing flowsheet, the concentration of nitrous acid will be highest at the first stages of the chemical separation process and will decrease through the process due to nitrous acid decomposition and less NOx gases being produced through dissolution as it nears completion.

1.3.2 Radiolysis of Nitric Acid

Nitrous acid is also produced by radiolysis of nitric acid. Many studies have been done into both the photolysis and radiolysis as these are both important for atmospheric and nuclear chemistry processes.[105-108] Studies have shown that radiolysis of nitrate and nitrite solutions affect the concentrations of various oxidising and reducing species. This is due to the nitrate and nitrite ions competing for the reactions with radical species such as ·OH, $\cdot e_{aq}^-$, and $\cdot O_2^-$. It was also shown that the ratio of nitrate to nitrite ion was strongly dependant on pH, while being nearly independent of initially dissolved nitrogen species concentration. The dependency on pH seen is due to a decrease in the number of oxidising ·OH radicals in irradiated nitrate and nitrite solutions when moving from a pH of 6.0 to a higher pH of 10.6, whilst the concentration of reducing $\cdot e_{aq}^-$, and $\cdot O_2^-$ radicals remains approximately constant across pH. With the fewer oxidising ·OH radicals for NO_2^- to react with to reform NO_3^- at higher pH, nitrite ions therefore become dominant at pH values > 9.7.[105]

Final products for the γ-radiolysis of nitric acid solutions are HNO_2, O_2 and H_2. The yields of HNO_2 and O_2 can be rationalised by the mechanism below, equation 1.59.[109] The oxygen atom produced in this reaction is likely to be in the triplet state in order to react with a nitrate ion to produce molecular oxygen and a nitrite ion, equation 1.60.[110]

$$NO_3^- \xrightarrow{\gamma} O + NO_2^- \qquad 1.59$$

$$O(^3P) + NO_3^- \rightarrow O_2 + NO_2^- \qquad 1.60$$

As well as this direct radiolysis of nitric acid, nitrite ions may also be formed by reaction of a nitrate ion with a solvated electron from the radiolysis of water, equations 1.61 to 1.64.[111]

$$NO_3^- + e_{aq}^- \rightarrow NO_3^{2-} \quad 1.61$$

$$NO_3^{2-} + H^+ \rightarrow HNO_3^- \quad 1.62$$

$$HNO_3^- \rightarrow OH^- + NO_2 \quad 1.63$$

$$2NO_2 + H_2O \rightarrow NO_3^- + 2H^+ + NO_2^- \quad 1.64$$

A number of researchers have reported on the irradiation of nitric acid of various concentrations, showing nitrite yields to increase with both increasing dose and nitrate ion concentration with no limit being apparent.[91, 109-112] The latter dependence is shown in Figure 1-10. However, work done by Precek *et al.* have shown that while the concentration of nitrite is found to increase with increasing dose, the rate of production in the presence of neptunium was found to slow significantly after ~1 kGy absorbed dose in 4 mol dm^{-3} HNO_3, due to consumption by Np(VI).[112] It has also been shown in studies by Mincher *et al.* and by Daniels and Wigg that there is negligible change in the yield of nitrous acid with variation in temperature between 25°C and 60°C or intensity of irradiation.[91, 111]

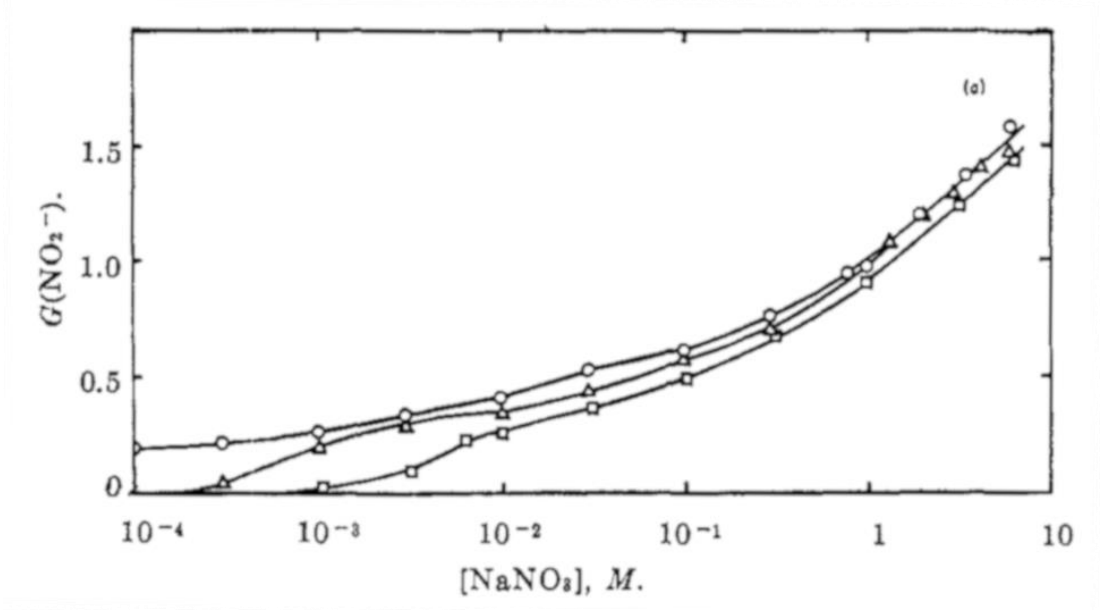

Figure 1-10 Dependence of yield of nitrite on nitrate concentration in neutral solution that have been purged with helium (circles), aerated (triangles) and oxygen saturated (squares).[111]

Studies done by Kazanjian *et al.* into the effect of the type of irradiation has shown that the yield of nitrous acid varied due to linear energy transfer (LET) effects.[113] This study by Kazanjian *et al.* showed that yields of nitrous acid were appreciably lower for α irradiation than that for β/γ but was shown to continually increase for α irradiation with acidity while yields began to decrease above 1 mol dm^{-3} acid concentration for β/γ. This contrasted with the studies done by Daniels and Wigg of nitrite yield in neutral solutions which were shown to continually increase.[111] Results from Kazanjian *et al.* showed that up to a HNO_3 concentration of 1 mol dm^{-3} a maximum concentration of nitrite was eventually reached with increased dose. Although above 1 mol dm^{-3} HNO_3, nitrite yields continued to increase linearly with dose, Figure 1-11, this could be due to the maximum yield not yet having been reached on the timescales for which the experiments were conducted. Kazanjian *et al.* suggested from these results that when comparing the direct radiolysis of nitrate to that of water, where there is a significant change in the yields of molecular and radical products, then there will be an increase in nitrite yield for γ irradiation. Also, direct radiolytic decomposition of undissociated nitric acid, which would become more significant at higher concentrations, would produce NO_2 and

an oxidising ·OH radical rather than the reducing ·O radical. The NO_2 may then react with water to produce nitric acid and nitrite, the latter reacting with the ·OH radical to produce NO_2 and hydroxide, so reducing the net yield of nitrite.

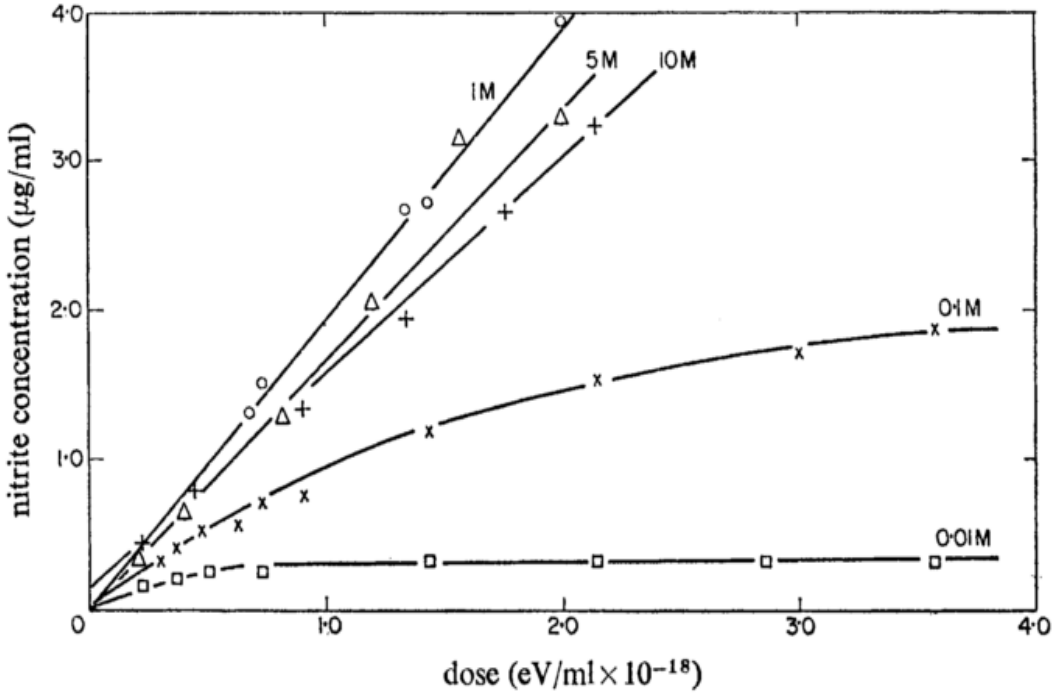

Figure 1-11 Nitrite yield for γ–irradiation of various concentrations of nitric acid.[113]

1.3.3 Decomposition of Nitrous Acid

Concentration of nitrous acid would be seen to decrease throughout the chemical separation process used for the reprocessing of SNF, due to decomposition. The decomposition of nitrous acid, which produces NOx gases, can be described by rate equations such as that proposed by Abel and Schmidt, equation 1.65[114] who showed a dependence on concentration of HNO_2 to the fourth power. It was also shown by this study that the overall stoichiometry of the reaction is given by equation 1.66.[115, 116]

$$-\frac{d[HNO_2]}{dt} = \frac{k_{fwd}[HNO_2]^4}{[NO]^2} \quad 1.65$$

$$3HNO_2 \rightarrow 2NO + NO_3{}^- + H^+ + H_2O \quad 1.66$$

Solutions of nitrous acid quickly establish an equilibrium which produces dissolved NOx. These reactions proceed *via* N_2O_3 and N_2O_4 intermediates which exist in equilibrium with NO and NO_2. The presence of O_2 influences the rate of decomposition due to oxidising the NO produced in the reaction to NO_2 and driving the decomposition of HNO_2.[117] Nitric oxide is also important as the rate of decomposition of nitrous acid is initially rapid but then slows due to accumulation of NO as per the equilibrium described by equation 1.66. The mechanism for the decomposition of HNO_2 to give nitric acid and NO can be given as in equations 1.67 to 1.70, where the dependence on concentration of HNO_2 to the fourth power and we get a net loss of $3HNO_2$ as seen in equation 1.66:

$$2HNO_2 \rightleftharpoons N_2O_3 + H_2O \quad 1.67$$

$$N_2O_3 \rightleftharpoons NO + NO_2 \quad 1.68$$

$$2NO_2 \rightleftharpoons N_2O_4 \quad 1.69$$

$$N_2O_4 + H_2O \rightleftharpoons HNO_2 + NO_3^- + H^+ \quad 1.70$$

The presence of the nitrate ion or nitric acid, which would be present in reprocessing has been shown to increase the rate of decomposition of nitrous acid due to formation of N_2O_4 *via* the reverse of equation 1.70. An increase in temperature also shows an increase in the rate of decomposition.[115, 118]

Due to the decomposition of nitrous acid being dependant on the release of NOx gases, it has been shown that the decomposition can be greatly reduced by reducing the headspace above the solution.[119]

1.3.4 Nitrous Acid Detection Methods

The importance of nitrous acid in the speciation of various elements within SNF reprocessing, such as the Np(V)/Np(VI) equilibrium, equation 1.9, and its ability to undergo decomposition to a range of other NOx species makes its accurate and convenient detection necessary.

Currently, one common method to determine the concentration of nitrous acid in solution at sub-millimolar concentration ranges is *via* a colorimetric method. This involves the addition of a colour reagent, such as p-nitroaniline and azulene or commonly Griess reagent, which consists of naphthylethylenediamine dihydrochloride suspended in water and sulphanilamide in phosphoric acid to react with the nitrite ion to form an azo dye which is then analysed spectrophotometrically.[120-122] While this has the advantages of being independent of pH, temperature, and, to some extent, volume of reagents, the method has the disadvantage of being reasonably complex through its use of multiple reagents. Use of an *in situ* technique would allow easier, non-destructive measurement of HNO_2 concentration.

Direct detection of nitrous acid by UV-vis spectrophotometry is possible through the use of a number of characteristic peaks due to $n_0\pi^*$ absorption between approximately 346 nm and 386 nm.[123] Whilst the use of UV-vis spectrophotometry would allow for *in situ* quantification of nitrous acid by either doing the reaction within a cuvette or through the use a flow cell, the presence of other chemical species with overlapping absorbances would add a level of complexity to its quantification.

Electrochemical detection has also been shown within the literature to be suitable for the detection of nitrous acid in a range of systems using a variety of strategies such as voltammetric, potentiometric and impedimetric methods.[122] These detection methods allow for the possibility of *in situ* analysis, and have good limits of detection in the nanomolar range through the use of either electrode surface modifications or nitrite specific ionophore membranes.

Studies into the feasibility of the use of an electrochemical sensor suitable for the detection of nitrous acid in the concentration ranges needed for proposed reduction experiments will be described in Chapter 3.

1.4 Vanadium Reduction by Nitrous Acid

To minimize radiological exposure risks associated with using neptunium in investigation of the redox reaction of Np(VI) with nitrogen oxide species, a non-active Np(VI) analogue is required. In this work, the use of vanadium(V) as the Np(VI) analogue was investigated, beginning with the V(V)/HNO_2 system as an analogue for the Np(VI)/HNO_2 system that was well characterised by Precek and Paulenova[88]. Subsequent work was then undertaken in order to extend understanding of the reduction of V(V) to the V(V)/NO system.

Vanadium(V) has previously been used as an analogue for neptunium[124, 125] and was chosen as an analogue due to the electrochemical potential for the VO_2^+/VO^{2+} couple being similar to that of the NpO_2^{2+}/NpO_2^+ couple.[81] In comparing the electrochemical potentials of the VO_2^+/VO^{2+} couple and NpO_2^{2+}/NpO_2^+ couple, with values of 1.00 V and 1.24 V respectively, with those of the various nitrogen oxide standard potentials, Figure 1-8 we can predict that certain redox reactions of nitrous acid, such as the NO_2/NO_2^- couple with an electrochemical potential of 0.895 V, should be able to reduce V(V) in a similar manner to Np(VI).

A second reason for using vanadium was the structural similarities, with V(V) showing formation of the pervanadyl ion containing two oxygens, much like the formation of the neptunyl ion – although, unlike the neptunyl oxygens, the O-V-O bond has been shown to be bent, with bond angles ranging from 104° to 107°.[126] Some differences can also be expected in the respective rates of reduction of V(V) to V(IV) and Np(VI) to Np(V) due to breaking of a metal oxygen bond in the former reaction but not the latter, with the VO_2^+/VO^{2+} couple therefore being expected to exhibit slower reduction kinetics than the NpO_2^{2+}/NpO_2^+ couple. This may be advantageous in making the time dependence of the V(V) reduction process easier to measure.

To assess the use of vanadium as an analogue for neptunium when looking specifically at the reduction by nitrous acid and nitric oxide, the literature was reviewed for work done on this reduction reaction.

Studies on the reduction of vanadium(V) by nitrous acid have been previously conducted by Dikshitulu *et al*.[127] in perchloric acid. This study proposed that the reduction of V(V) occurs *via* the mechanism outlined in equations 1.71 to 1.73, with the associated rate equation being as shown in equation 1.74. However, upon critical review of this paper, it became apparent that the proposed mechanism was not fully supported by the reported experimental findings as the orders of reactions in the kinetic expressions did not match those which could be taken from the increase in rates with changes in the concentrations of different species. Therefore, due to this, and due to study done by Dikshitulu *et al*. showing that the reaction is slowed by the presence of the low concentrations of generated nitrate ions, further work is needed in order to address these points and fully elucidate the vanadium nitrous mechanism in nitric acid solution.

$$VO_2^+ + H_3O^+ \overset{K}{\rightleftharpoons} V(OH)_3^{2+} \quad 1.71$$

$$V(OH)_3^{2+} + HONO \underset{k_2}{\overset{k_1}{\rightleftharpoons}} NO_3^- + V(III) + 2H_2O \quad 1.72$$

$$VO_2^+ + V(III) \overset{k_3}{\rightarrow} 2VO^{2+} \quad 1.73$$

$$Rate = \frac{-d[V(V)]}{dt} = \frac{2k_1k_3K[VO_2^+]^2[HNO_2][H^+]}{k_2[NO_3^-] + k_3[VO_2^+]} \quad 1.74$$

With the literature having been reviewed with regards to the aspects of nitrous acid chemistry specifically relevant to the speciation of neptunium, the factors affecting neptunium speciation within a reprocessing scheme, and the relevant chemistry of vanadium as an analogue, it was apparent that a range of nitrogen oxide species affect speciation and that there was a need to look further at both the mechanism of Np(VI) and V(V) reduction by HNO_2 (the latter again as a non-active surrogate system) and the potential role of NO in this mechanism. Therefore, in

order to further the understanding of the neptunium/nitrogen oxide system, the following objectives were laid out to be studied in this work;

- Investigate the electrochemistry of NO and elucidated the oxidation potential of the NO/NO^+ couple
- Determine suitability/feasibility of the use of electrochemical quantification of HNO_2 during V(V)/Np(VI) reduction experiments
- Establish the suitability of V(V) as an analogue in wider studies of the reduction of Np(VI) by nitrogen-oxygen containing species
- Determine the role of NO in the reduction of V(V) to V(IV)
- Verify the observed results on the V(V) reduction by NO are applicable to the Np(VI) system

To address these, experiments were done to look at the redox behaviour of nitrous acid and nitric oxide (Chapter 3), the reduction of vanadium by nitrous acid and nitric oxide (Chapter 4), and the reduction of neptunium by nitric oxide (Chapter 5).

2 Experimental and Methods

2.1 Chemicals and Materials

2.1.1 Chemicals

All chemicals used were purchased from Sigma-Aldrich Ltd. (Gillingham, Dorset, UK) at AnalaR grade or higher and used without further purification, nitric acid was ACS reagent grade and similarly used without further purification. Vanadium (V) was prepared by dissolution of sodium metavanadate, $NaVO_3$ in nitric acid. Solutions of nitrous acid were prepared by dissolution of sodium nitrite in nitric acid, where the nitrite anions were immediately protonated due to it being a relatively weak acid, pKa = 3.35.[128] Nitrous acid was prepared immediately before use in order to minimize decomposition. 68% nitric acid was used for preparation of all HNO_3 solutions. Vanadium (IV) solutions for use in the determination of the attenuation coefficient were prepared using vanadyl sulphate, $VOSO_4 \cdot xH_2O$. In order to correctly determine the concentration of V(IV) in vanadyl sulphate solutions created, and hence determine the attenuation coefficient from created calibration curves (Section 2.3), the number of waters of crystallization present was determined using both thermogravimetric-mass spectrometry analysis and elemental analysis (Appendix A) to be x = 3.

All solutions were prepared using distilled, deionized water prepared to 18 MΩ cm resistivity using a Direct-Q® 3 UV Water Purification System (Millipore, Watford, UK).

Nitric oxide gas was purchased through BOC (Guildford, UK), of 99.5% minimum purity and was bubbled through a 2 mol dm^{-3} NaOH solution before use to remove any traces of nitrogen dioxide gas present.[129] Full details of the experimental set up for experiments involving nitric oxide are outlined in Section 2.5.

2.1.2 Neptunium Solution, Preparation and Recovery

Neptunium was obtained as the Np-237 isotope ($t_{1/2}$ = 2.144 × 10^6 years) from NNL. The solution obtained came as a neptunyl nitrate solution, in a mix of the +V and +VI oxidation states, at an activity of 101.2 kBq in 10 mL of 0.5 mol dm^{-3} HNO_3. This corresponds to a concentration of Np of 1.65 mmol dm^{-3}, calculated by using the specific activity of Np-237 taken as 2.59 × 10^7 Bq g^{-1}.[130] Solution impurities were assessed before delivery by gamma spectroscopy at NNL. Ingrowth of the protactinium-233 daughter was assessed each day until a steady state of Pa-233 was reached using the calculations as seen in Appendix B, Table B-1 based on this initial purity – where *m* is the mass of the given nuclide, on the given day (with *f* indicating the mass formed and *r* indicating the mass remaining), $t_{1/2}$ is the half-life of the given nuclide in days ($t_{1/2,Np}$ = 781,635,000 days, $t_{1/2,Pa}$ = 27 days), a_{Pa} is the specific activity of Pa-233 (7.77 × 10^{14} Bq g^{-1})[131], and *A* is the activity present of the given nuclide, with A_{Np0} being the initial activity of Np-237 (101.2 kBq). The percentage given is the percentage of the Pa-233 activity compared to the initial Np-237 activity.

From these calculations, it was seen that the ingrowth of Pa-233 reached a steady state at an activity of approximately 102% that of the initial Np-237 activity after approximately 200 days, Figure 2-1. This steady state was also seen to correspond to a mass of Pa-233 present on the order of 10^{-10} g. Therefore, due to the amounts of Pa-233 being low, as well as having no electrochemical potentials in the region of those being studied,[81] it was decided that further purification was not required before running Np reduction experiments.

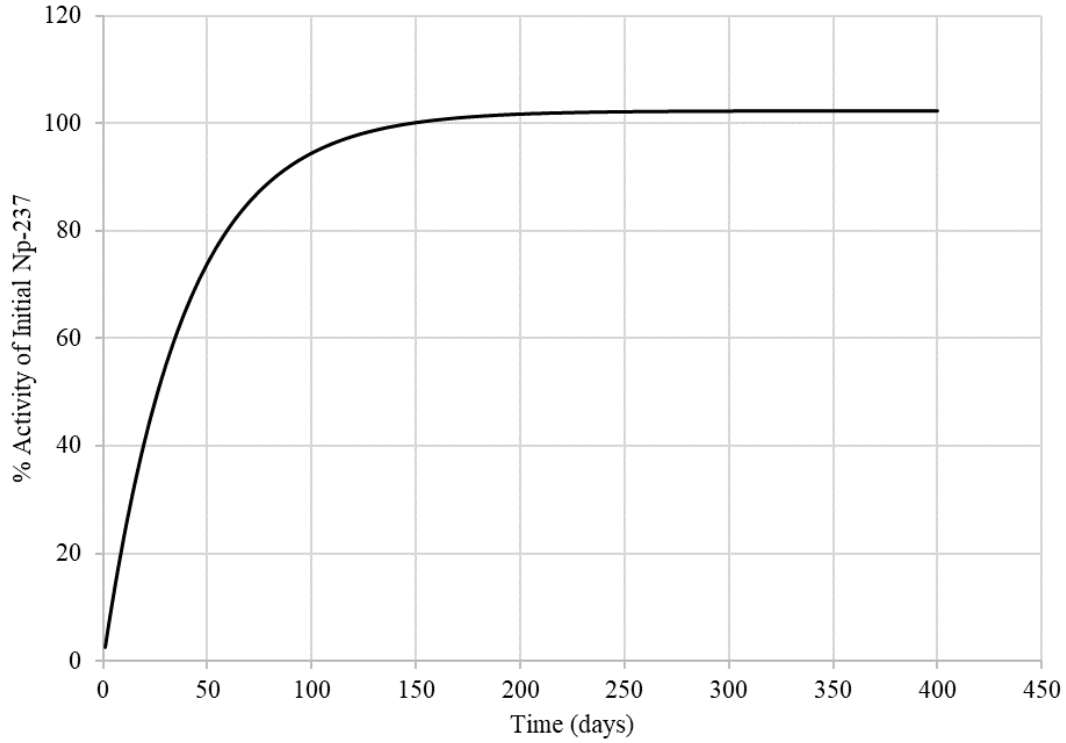

Figure 2-1 Ingrowth of Pa-233 activity as a percentage of the initial Np-237 activity.

Solutions of Np(VI) were prepared by quantifying total neptunium concentration using liquid scintillation counting and by utilising bulk electrolysis in order to condition the neptunium stock to the correct oxidation state. This electrooxidation of Np(V) to Np(VI) was done by applying a potential of 1.4 V *vs.* Ag/AgCl between Pt mesh working and counter electrode, separated by a vycor frit. The extent of the conversion from the 5+ to the 6+ oxidation state was monitored using UV-vis spectroscopy. Following the electrolysis, more than 95% of Np existed in the 6+ oxidation state, with the remainder being in the 5+ state.

Neptunium waste solutions were recovered for use as new stock solutions through a multi-step recycling process. First, the aggregated waste solution, typical volume 300 cm^3, is gently heated on a stirred hotplate to evaporate excess H_2O and reduce the overall volume to approximately 2 mL. The resulting solution was then re-diluted with desired concentration acid for the next set of experiments and this evaporation/dilution repeated several times to ensure any of the previous acid concentration had been removed and the concentration of acid was correct. The volumetrically reduced solution was then made up to a final volume in a volumetric flask using

the desired acidity. The activity of the new stock solution was quantified using liquid scintillation counting (LSC) to ensure no significant loses of Np have occurred.

2.2 Electrochemical Methods and Instrumentation

Cyclic voltammetry of both nitrite and nitric oxide solutions was performed using a PGSTAT100 potentiostat from Autolab (Windsor Scientific Ltd.), and neptunium cyclic voltammograms were measured using an EmStat3+ from PalmSens (Houten, Netherlands) from within a negative pressure glovebox. The use of a negative pressure glovebox was required for all neptunium experiments in order to minimise radiation exposure in both routine operations and in the event of an accident.

Platinum and gold working electrodes used were prepared using metal wire, setting them into glass, and polishing them to reveal just the wire cross section. Both platinum and gold wires of 250 μm diameter, used for the fabrication of micro-electrodes, were obtained from Advent Research Materials (Oxford, England), at 99.95% and 99.99+% purity. Glassy carbon (GC) working electrodes used were prepared from glassy carbon rods by setting them into resin and polishing them to reveal the cross section. Glassy carbon rods of 1 mm diameter, used for the fabrication of micro-electrodes, were obtained from VWR. Before use, electrodes were polished with diamond paste of decreasing size (6 μm, 3 μm, and 1 μm) and then sonicated in an ultrasound bath to remove any embedded diamond particles from the electrode surface.

For all electrochemical experiments a Pt mesh purchased from Advent Research Materials (Oxford, England) was used as the counter electrode, along with Ag/AgCl reference electrodes, purchased from Bioanalytical Systems, Inc. (West Lafayette, Indiana, USA). Unless stated otherwise all potentials have been quoted *vs* Ag/AgCl.

2.3 Spectroscopic Methods and Instrumentation

For ultraviolet–visible spectroscopy, a wide UV–VIS-NIR range of 300–1,000 nm was monitored by either a Shimadzu UV-2600 UV-Vis spectrophotometer (Shimadzu UK Ltd., Milton Keynes, UK) spectrophotometer or an OceanOptics™ (Oxford, UK) HR2000 spectrophotometer (fibre optic system) with combined deuterium/halogen light source, DH-2000 BAL. Use of the OceanOptics™ fibre optics system allowed for the recording of absorbance on all selected wavelengths within the 300–1,000 nm range simultaneously, from within a negative pressure glovebox. Before each experimental run, a baseline reading was recorded for the working acid media in the absence of any metal ions, this reading was then subtracted from sample measurements to give a clear and consistent baseline. To minimize noise, each spectrum was taken by averaging 5 successive scans and boxcar smoothing was employed for each absorbance measurement.

In order to account for any changes in the baseline over the course of the reaction, each spectrum was baseline corrected during post-acquisition data processing. In the case of the reductions of vanadium by nitrous acid this was done by baseline correcting with respect to a single point with an absorbance of zero, whereas in the case of the reductions of vanadium by nitric oxide it was done with respect to an isosbestic point for a given total vanadium concentration which was calculated from calibration spectra of V(IV) and V(V). In order to ensure the correct vanadium speciation was present, full spectral scans were recorded before each experimental run and compared with Choi *et al*.[132]

2.3.1 Determination of Molar Attenuation Coefficients

Concentrations of V(V), V(IV), HNO_2 and Np(V) were calculated using the absorbance values at either 386 nm, 770 nm, or 981 nm depending on the position of the absorbance peaks, and the attenuation coefficients for the individual species which were determined as follows. Firstly, other species that were determined to be potentially present using the redox ladder in Figure 1-8 (such as NO_2, N_2O, N_2O_3, N_2O_4, etc.) were considered for possible spectral interferences; however, none were found to have significant absorbance at the relevant wavelengths. Attenuation coefficients were found for V(IV), V(V) and HNO_2 using individual solutions of $VOSO_4 \cdot xH_2O$, $NaVO_3$, and $NaNO_2$ respectively. These solutions were made of known concentrations by dissolving the relevant species in 0.5 mol dm^{-3} HNO_3. The attenuation coefficient for Np(V) was found using the stock solution of neptunium supplied by NNL (Section 2.1.2). The solution being measured was then diluted sequentially with 0.5 mol dm^{-3} HNO_3 in order to give a range of concentrations to be measured by UV-vis spectrophotometry. The range of concentrations chosen for a given species was based upon the intended experimental working range, solubilities and, in the case of $NaNO_2$, minimization of decomposition. Specimen spectra recorded at concentrations in the vicinity of the mid-point of the calibration plot for each species are shown in Figure 2-2 to Figure 2-5. It should be noted here that whilst Figure 2-4 shows the full spectral range taken, data for the absorbance recorded below 355 nm was not used for analysis due to possible deviation from linearity seen above absorbances of approximately 1.5. Therefore, as stated above, determination of [V(V)] was done using the absorbance at 386 nm.

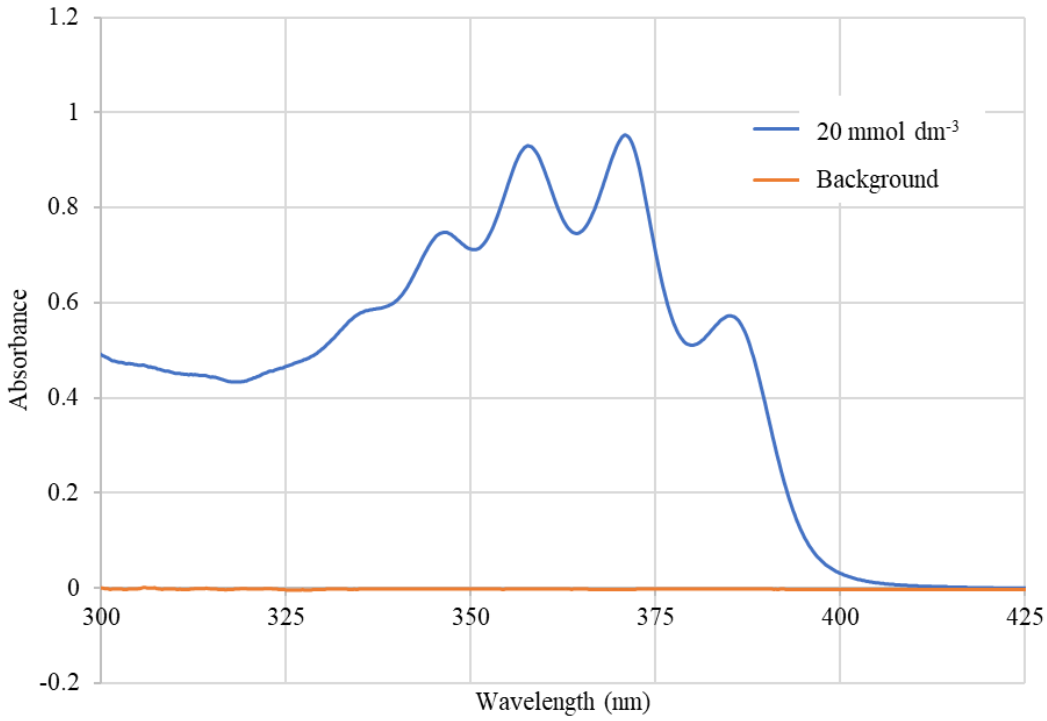

Figure 2-2 UV-vis spectra of 20 mmol dm^{-3} nitrous acid in 0.5 mol dm^{-3} HNO_3.

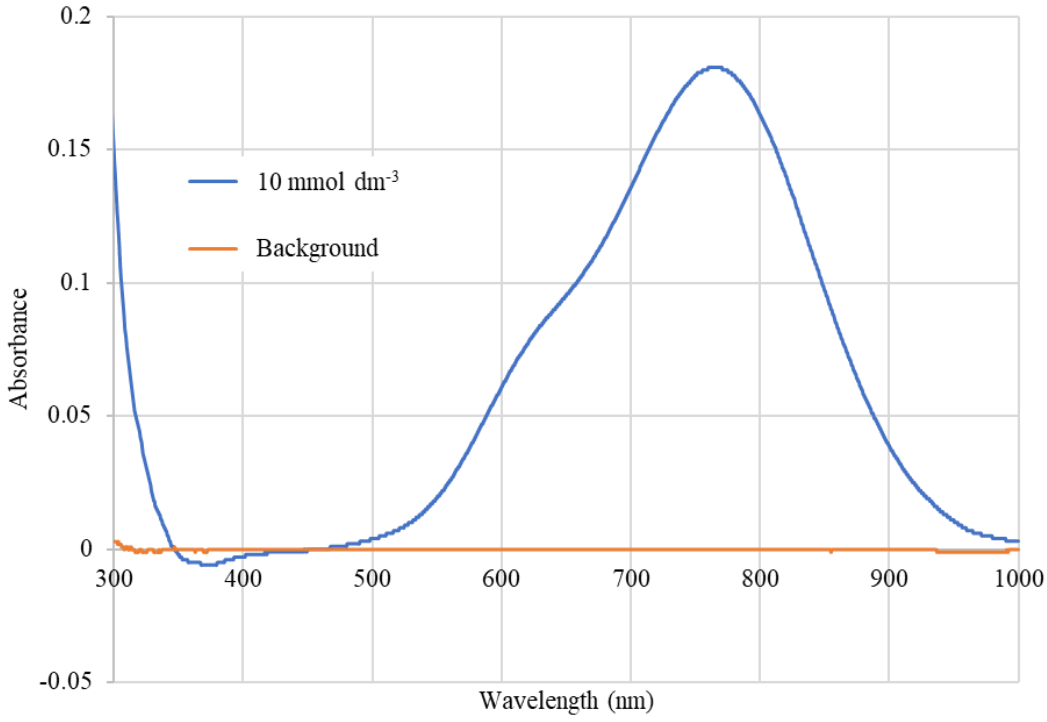

Figure 2-3 UV-vis spectra of 10 mmol dm^{-3} V(IV) in 0.5 mol dm^{-3} HNO_3.

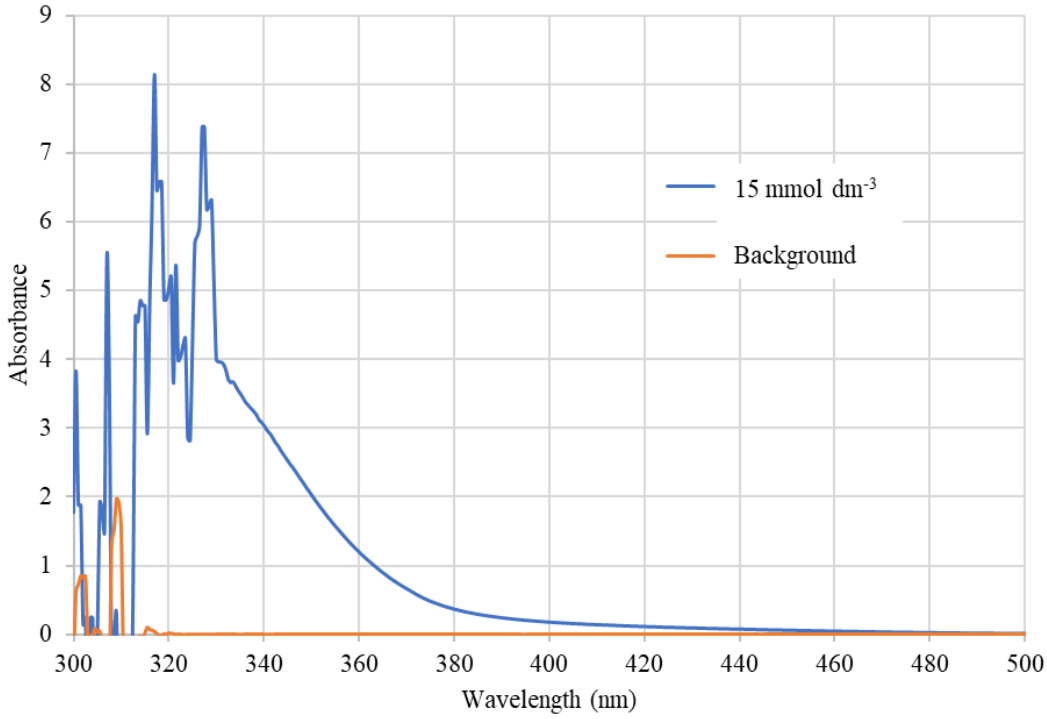

Figure 2-4 UV-vis spectra of 15 mmol dm^{-3} V(V) in 0.5 mol dm^{-3} HNO_3.

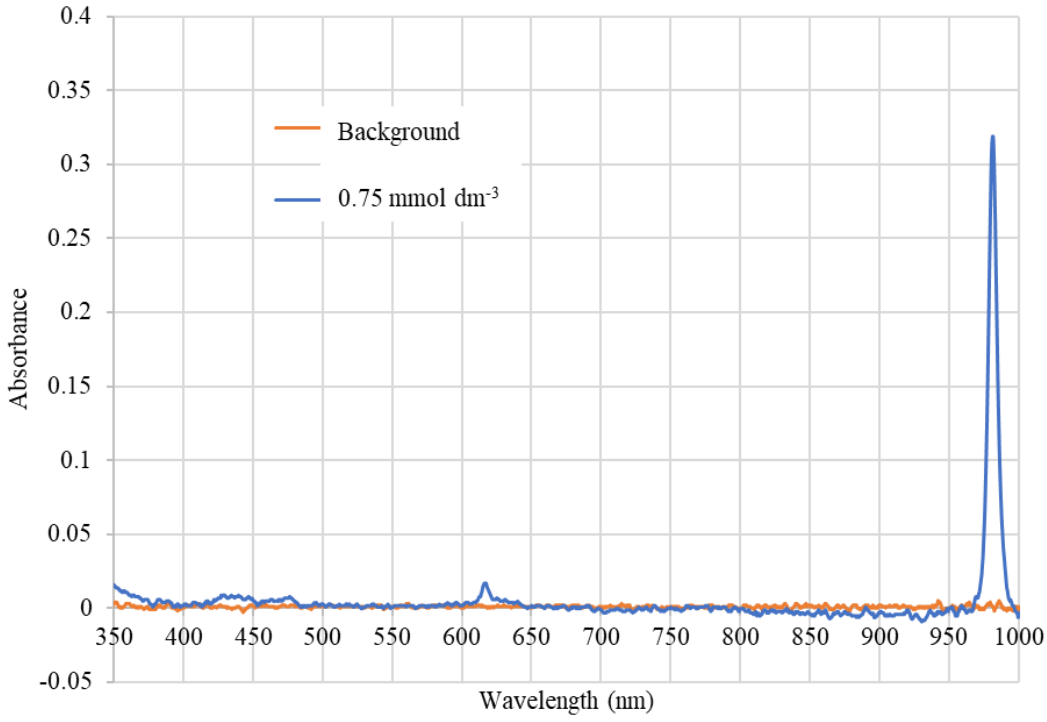

Figure 2-5 UV-vis spectra of 0.75 mmol dm^{-3} Np(V) in 0.5 mol dm^{-3} HNO_3.

Calibration curves could then be produced by plotting the absorbance at a given wavelength *vs* concentration. The calibration curves for V(IV) at 770 nm and V(V)at 386 nm, HNO_2 at 386 nm, and Np(V) at 981 nm are shown in Figure 2-6, Figure 2-7, and Figure 2-8 respectively. The attenuation coefficient could then be calculated from the gradient of these plots using the Beer-Lambert law. It should be noted that the attenuation coefficients for both V(IV) and V(V) are similar due to not taking the absorbance at the peak height for V(V) so as to not be evaluating the value in a region of high absorption where non-linearity might be observed.

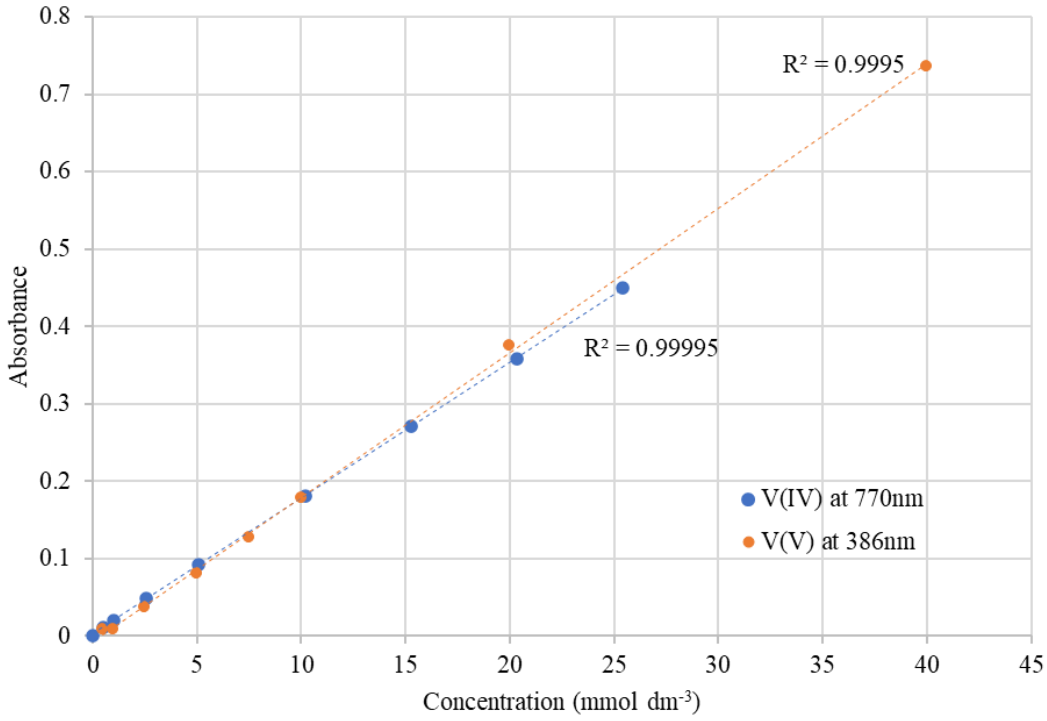

Figure 2-6 Plot of Absorbance at 770 nm vs V(IV) Concentration and Absorbance at 386 nm vs V(V) Concentration in 0.5 mol dm^{-3} HNO_3.

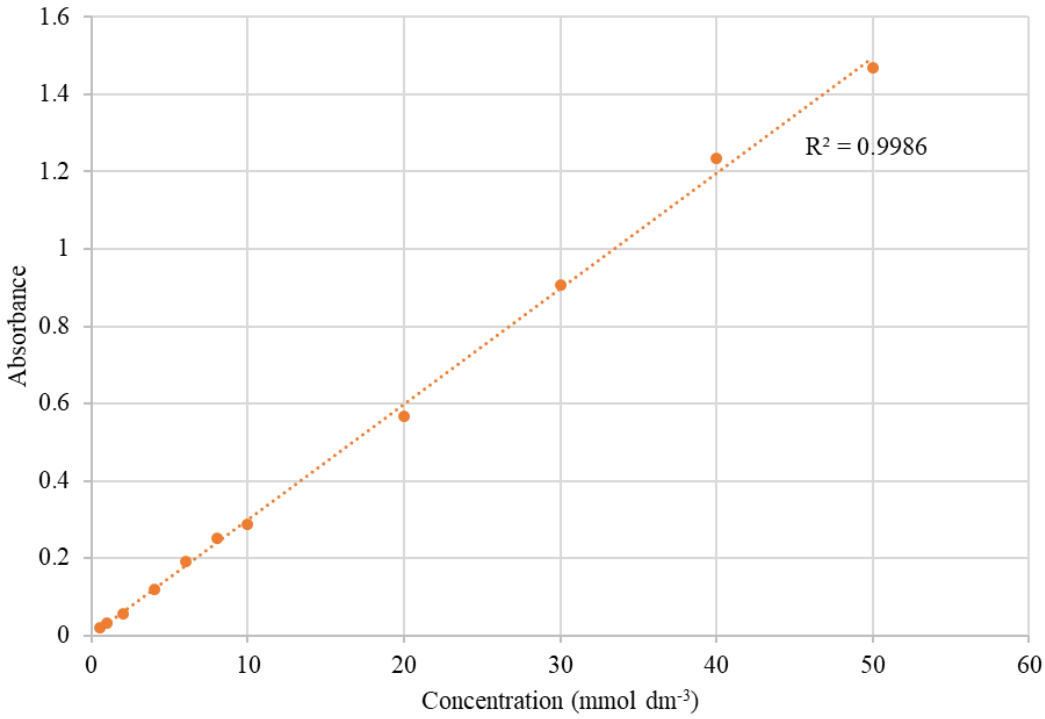

Figure 2-7 Plot of Absorbance at 386 nm vs HNO_2 Concentration in 0.5 mol dm^{-3} HNO_3.

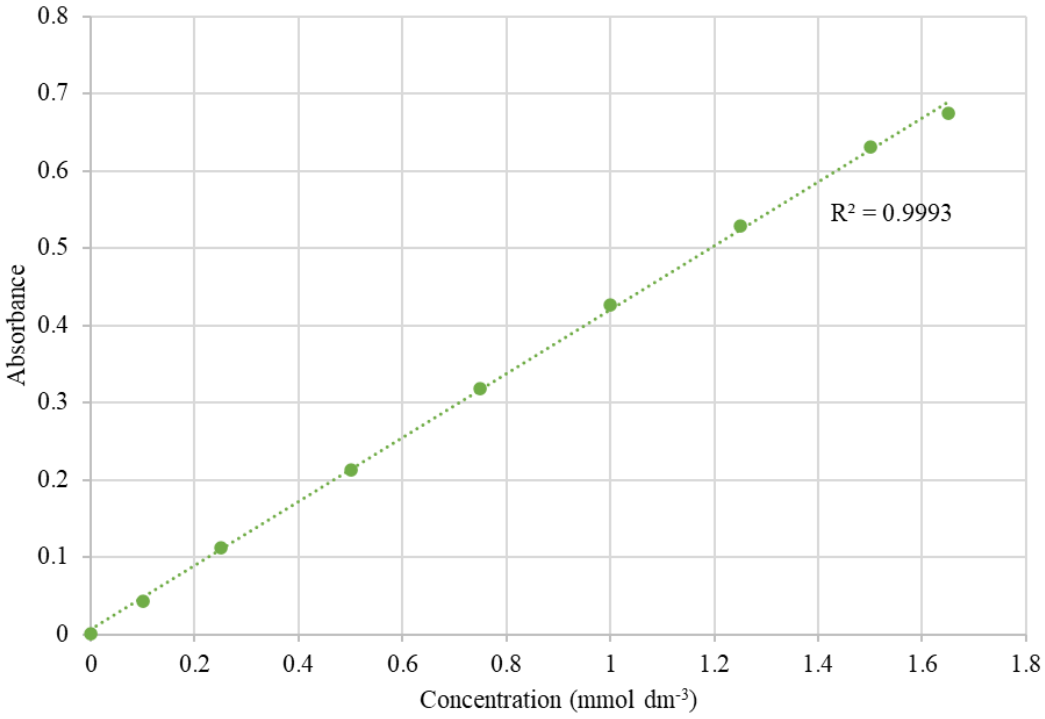

Figure 2-8 Plot of Absorbance at 981 nm vs NpO_2^+ Concentration in 0.5 mol dm^{-3} HNO_3.

Values for the attenuation coefficients are outlined in Table 2-1 along with values given in the literature for comparison.

Species	**Calibration wavelength / nm**	**R^2 value for calibration plot**	**Experimentally Determined Attenuation Coefficient / $dm^3\ mol^{-1}\ cm^{-1}$**	**Literature Attenuation Coefficient / $dm^3\ mol^{-1}\ cm^{-1}$**	**Ref.**
VO^{2+}	770	0.99995	17.6	17.17	[133]
VO_2^+	386	0.9995	18.7	11.55	[132]
HNO_2	386	0.9986	29.9	32.97	[115]
NpO_2^+	981	0.9993	414.1	395	[134]

Table 2-1 Table of Experimentally Determined Attenuation Coefficients on 0.5 mol dm^{-3} HNO_3 and Attenuation coefficients from the Literature.

2.3.2 Determination of Different Vanadium Oxidation State Concentrations

For spectra where both V(V) and HNO_2 were present, the absorbance at 770 nm was used in order to first calculate the concentration of V(IV) in solution, the concentration of V(V) could also be calculated by subtracting the V(IV) concentration from the total known vanadium concentration. Since this relies on the assumption that all V(V) is converted to V(IV), the presence of any lower oxidation states of vanadium, specifically V(III), was checked for, and were deemed not to be present due to the absence of any significant absorption peaks between 550 nm and 600 nm, this being the region in which V(III) is seen to absorb.[132] Other vanadium species arising from potential cation-cation interactions[135-137] of the metal ion at higher concentrations may account for any deviation from a linear dependence of vanadium absorbance on its concentration in experiments involving varying HNO_2 concentrations. However, whilst cation-cation interactions are well known for both V(IV) and V(V) species in solution at higher acidities,[135] the acidities used in this study would not be expected to form cation-cation complexes.[136] This is supported by the shape of the V(IV) peak present in our UV-vis spectra being comparable to that of the mononuclear cation.[137]

Based on the above considerations, nitrous acid concentration could then be calculated, taking the total absorbance at 386 nm to be the sum of the absorbances due to V(V) and HNO_2. The absorbance due to HNO_2 could then be calculated to be the difference in the total absorbance and the absorbance due to V(V), calculated using the V(V) attenuation coefficient and V(V) concentration. This absorbance could then be used to calculate HNO_2 concentration using the HNO_2 attenuation coefficient.

2.3.3 Determination of Reaction Kinetics for Reduction of both V(V) and Np(VI)

Reduction reactions were monitored by UV-vis spectroscopy for up to 3 hours, recording the full spectral range at regular intervals. The extent of reaction could therefore be seen by looking at the increase in the V(IV) peak at 770 nm, Figure 2-9.

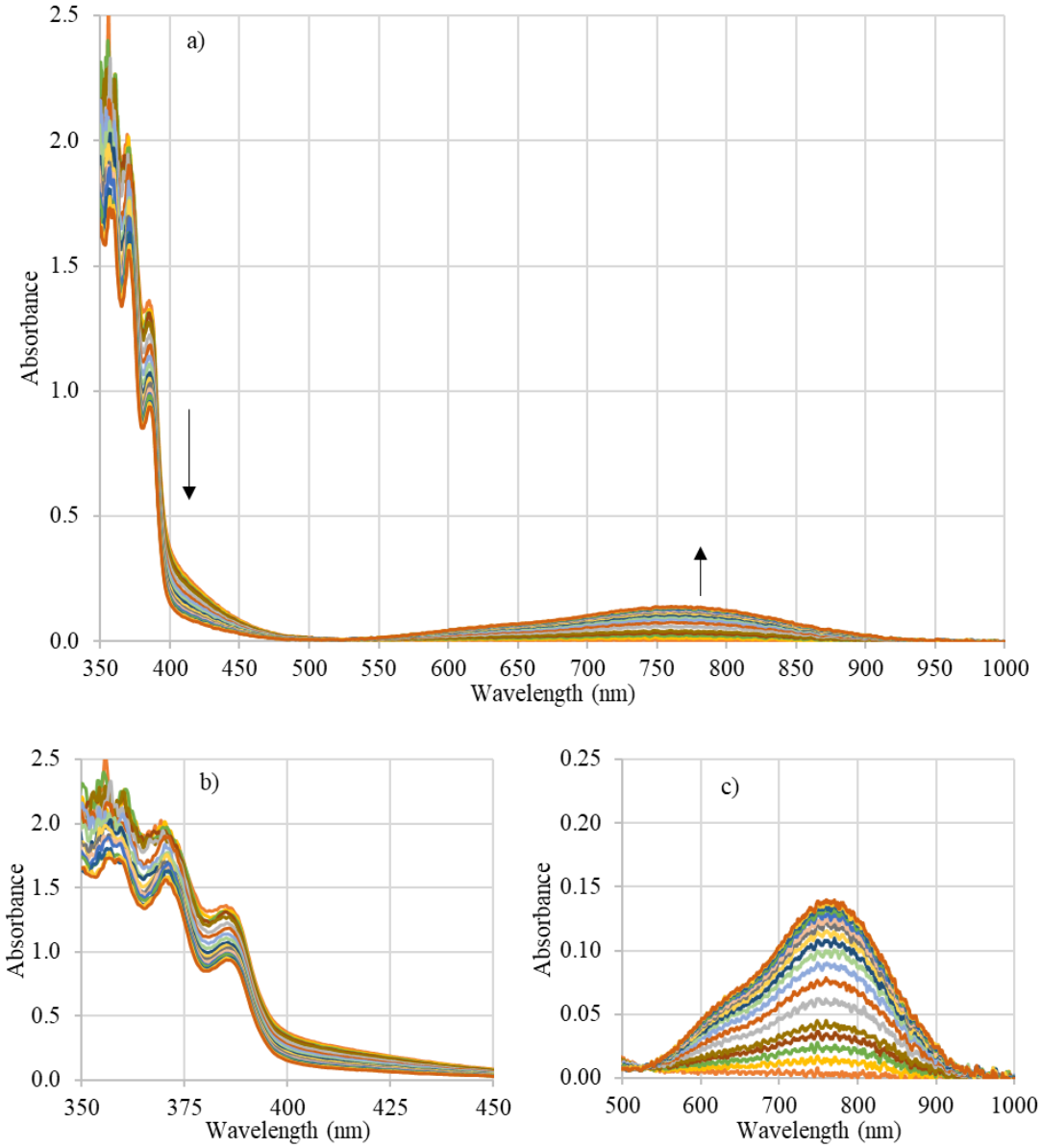

Figure 2-9 Spectral change for the V(V) reduction by HNO_2 every 2.5 mins over the course of 3 hours showing a) the full spectral range, b) the V(V) and HNO_2 absorbance range, and c) the V(IV) absorbance range. Over this time, we see a decrease in the absorbance at approx. 386 nm due to loss of V(V) and nitrite and increase in the V(IV) peak at 770 nm.

Plots were then made of concentration of V(IV) *vs* time, Figure 2-10, and the initial rate was calculated using the first 15 minutes of data points for reductions by HNO_2 performed in Section 4.1, using the data points from 10 to 30 minutes for reductions by NO performed in Section 4.2, and data points from 2 to 10 minutes for reductions by NO performed in Chapter 5, over which near-linearity is observed and fitting a slope of least squares linear regression. An initial induction period was left out for NO-bubbled reductions due to no reduction of the metal species over this time. This is likely due to a short time being needed to work its way through the bubbling setup outlined in Section 2.5 and saturate the reaction solution with NO. The gradients of these slopes were then used to plot log-log plots to give the order of reaction with respect to a given reactant. Rate constants were then also calculated using these reaction orders. Errors in these plots were determined by looking at the errors in baseline measurements along with pipetting and weight errors in order to give an error for each point.

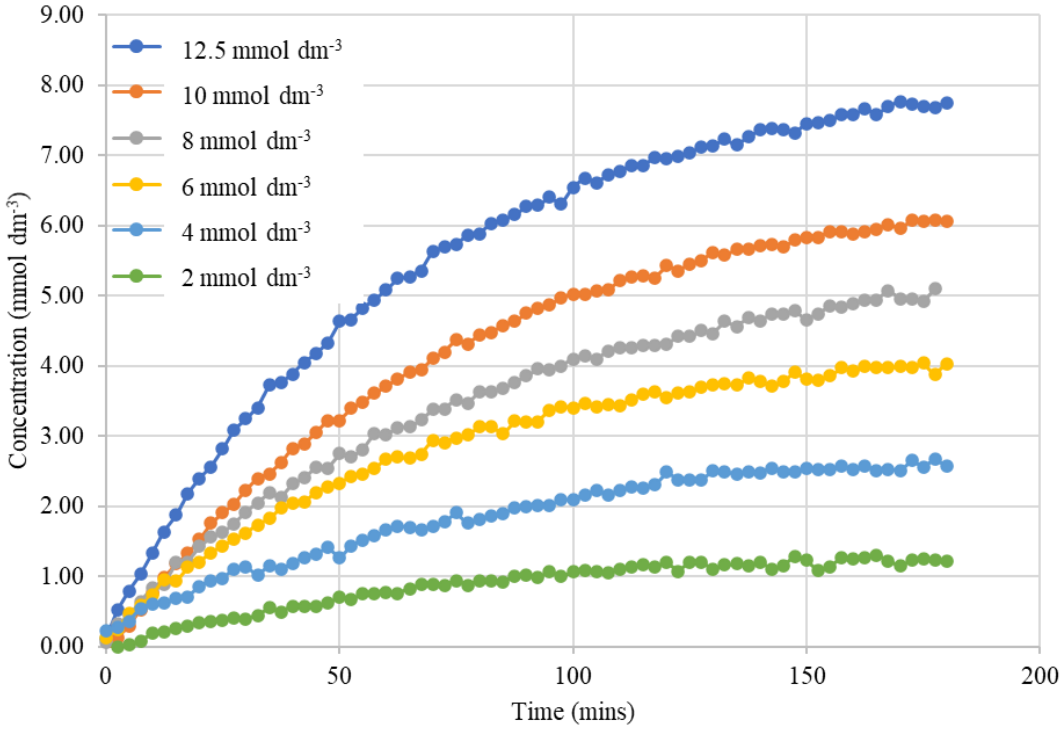

Figure 2-10 Plot of concentration of V(IV) vs time for the reduction of varying initial V(V) concentrations by 30 mmol dm^{-3} HNO_2 in 0.1 mol dm^{-3} HNO_3.

2.3.4 Liquid Scintillation Counting

LSC was used to quantify the amount of neptunium present in the newly formed stock solution after the waste had been recycled to ensure minimal loses had occurred. To prepare the samples for this, a 0.1 mL aliquot was taken and added to a shatterproof glass vial and diluted to 1 mL with water. A 0.1 mL aliquot was then taken of this diluted solution and added to a new shatterproof glass vial along with scintillant cocktail. At each dilution stage the vial was sealed and weighed for accuracy. Finally, this was sealed and counted on a PerkinElmer Tri-Carb 3170TR/SL Liquid Scintillation Analyzer. The activity of the neptunium present was then calculated from the total activity using an equilibrium value for the activity of the protactinium-233 daughter due to ingrowth which had previous been seen to be 102% the activity of the neptunium.

2.4 Modelling Methodology

Modelling work to determine rate constants for the individual pathways of the postulated mechanism for the vanadium/nitrous acid system was done using MATLAB software by Alexander Jackson at Lancaster University. This was done using a set of defined rate and discretised time differential equations (further outlined in Section 4.1.6) to track the concentrations of different species over the course of the reduction. Rate parameters were then adjusted manually until the model was seen to be within ±10% error of the majority of experimental data points and a chi-squared statistical test indicated a good fit. Use of a chi-squared statistical test compares a calculated chi-squared value to a critical value for a given number of degrees of freedom. If the calculated chi-squared value is below that of the critical value, then there is a high correlation between the two sets of data.

2.5 Bubbling Setup

Difficulties in both the preparation and handling of NO solutions of known concentrations meant that experiments involving NO were done using gaseous NO, with the gas being bubbled through any reaction vessel at a known flow rate. Due to NO readily forming NO_2 in the presence of oxygen, any reactor setup would also need to be purged with inert gas before experiments. Therefore, in order to perform studies of reduction reactions by NO, a bubbling setup was established, Figure 2-11.

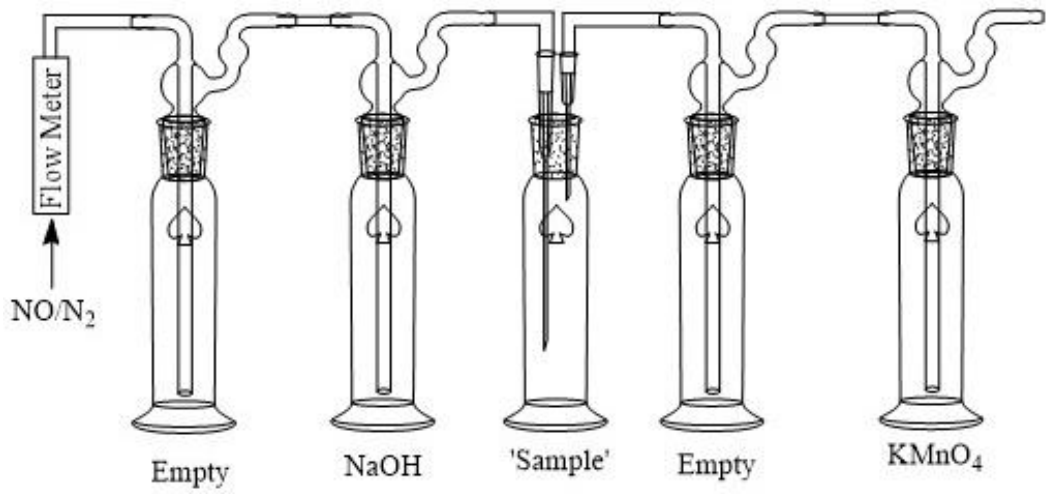

Figure 2-11 Schematic diagram of bubbling setup used for experiments involving nitric oxide.

This consisted of a switchable feed of either pure nitrogen gas (for the purposes of deoxygenation of the system) or nitric oxide into a variable area flow meter purchased from Cole-Parmer, followed by a series of Drechsel bottles with connections made using Tygon tubing. These Drechsel bottles contained either 2 mol dm^{-3} NaOH solution for the purpose of purifying the incoming nitric oxide gas,[129] $KMnO_4$ solution for scrubbing outgoing excess nitric oxide gas before release to the atmosphere, or were empty to prevent any backflow of the solutions when switching gases. The 'sample' Drechsel bottle containing the desired experimental solution and was sealed using a rubber septum which was pierced using needles to allow for the flow of gas both in and out. Additionally, the use of a sealed rubber septum

allowed for the electrodes required for the experiments outlined in Section 3.1 to be submerged in solution whilst maintaining an anoxic environment.

For reduction experiments of V by NO (Section 4.2), NO gas was flowed into the reaction vessel at a rate of 150 mL min^{-1}, with this flow rate being sufficient to generate a saturated solution of NO, with a concentration of approximately 3.02 mmol dm^{-3}.[138] Sampling of the vanadium solution for UV-vis measurements was done using a 1 mm pathlength flow cell cuvette (Hellma 170-QS), with the reaction solution being pumped at a rate of 1.5 mL min^{-1} using a peristaltic pump (Masterflex C/L® Analog Variable-Speed Pump). Again, in order to maintain an anoxic environment, the reaction vessel was sealed using a rubber septum with both NO gas flow and flow cell sampling for UV-vis measurements being done using needles. The sample vessel could also be changed to a more appropriately sized vessel for the neptunium experiments outlined in Chapter 5. In order to achieve the smaller NO gas flow rates of 20 mL min^{-1} required for the neptunium reduction experiments, the flow meter was also changed to an Alicat MCS-500SCCM-D/5M mass flow controller, which would allow for flow rates down to 5 cm^3 STP min^{-1}.

3 Electrochemistry of Nitrogen-Oxygen Species

In order to assess the thermodynamic and kinetic feasibility of nitric oxide playing a role in the Np(V)/Np(VI) equilibrium reaction, there was a need to first establish the thermodynamics of Np(VI) reduction by NO through elucidation of the reduction potential for the $NO^+ + e^- \rightarrow NO$ reduction. This need is especially important given the uncertainty that surrounds the value of the reduction potential for this process with existing literature values being reported in the range of 0.65 to 1.45 V *vs.* NHE.[80, 82-85] Thus, it was determined that the reduction potential to be used for the purpose of this study should be measured experimentally.

In addition to this, a method was required to quantitatively measure nitrous acid *in situ* during its reduction reaction with either neptunium or vanadium. Therefore, the electrochemical behaviour of nitrous acid was examined on a number of different electrode materials for the purpose of developing an electrochemical sensor for HNO_2.

3.1 Electrochemistry of Nitric Oxide

Cyclic voltammetry was used as the main means by which to investigate the electrochemistry of NO and for the elucidation of its oxidation potential. This was performed by first sparging, with nitrogen, a solution containing either 1 mol dm^{-3} $NaNO_3$ or 1 mol dm^{-3} H_2SO_4 as electrolyte. This was in order to remove dissolved molecular oxygen from solution, so minimising the formation of other redox active NOx species by reaction between NO and O_2. A cyclic voltammogram (CV) was taken of the sparged solution in order to provide a reference baseline. Using the NO bubbling set-up outlined in Section 2.5, the solution was then bubbled with NO gas. In the first instance, these CV measurements were performed using platinum as the working electrode material.

3.1.1 Behaviour in 1 mol dm^{-3} H_2SO_4 Solutions

As a result of bubbling NO gas through 1 mol dm^{-3} H_2SO_4, it was possible to record CVs that showed the presence of an electrochemical process not seen in the reference CVs measured of the system prior to NO bubbling, that we attribute to being due to the NO/NO^+ couple. These CVs, shown in Figure 3-1, showed slight peaks in the background scans which can be attributed to the well-studied surface oxidation behaviour of platinum in sulphuric acid.[139]

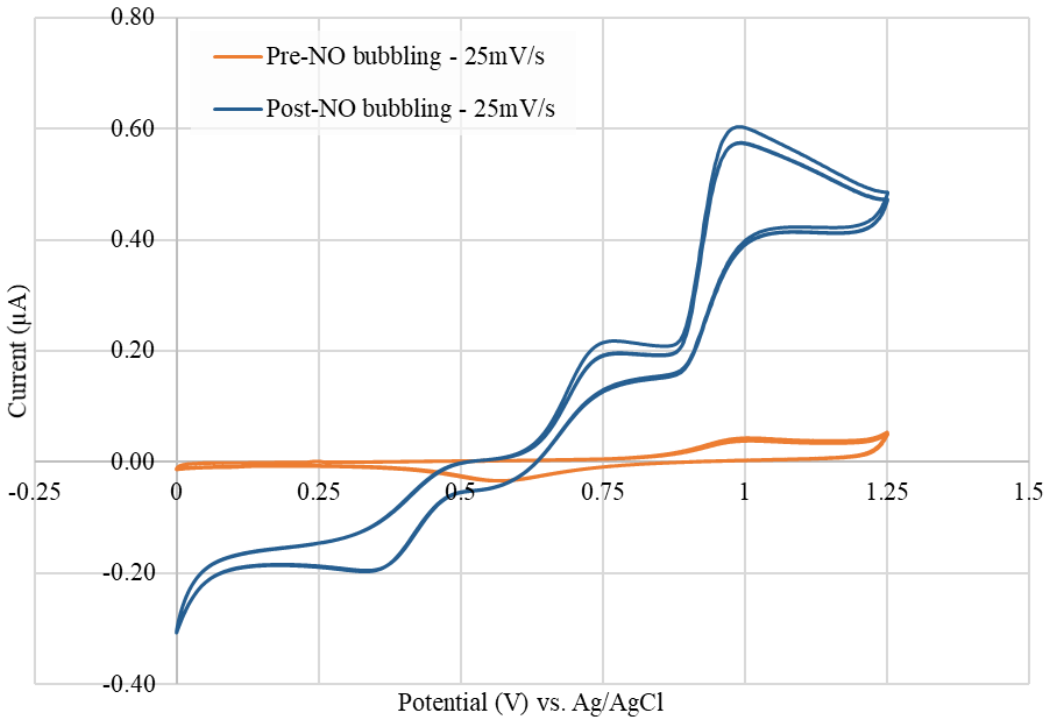

Figure 3-1 Cyclic voltammograms of 1 mol dm^{-3} H_2SO_4 both before and after bubbling with NO gas. Scan rate = 100 mV s^{-1}.

Within the CV of the NO sparged solution, the peak present at approximately 0.7 V *vs.* Ag/AgCl, can be assigned to the oxidation of NO. This peak potential is consistent with the standard electrode potential for the NO/NO^+ electrochemical couple of 6.5 V *vs.* Ag/AgCl reported by Topol, Osteryoung and Christie[80]. Importantly, the peak potential of 0.7 V *vs.* Ag/AgCl and the E^0 of Topol, Osteryound and Christie both have values that are more negative than that for the Np(V)/Np(VI) couple of 1.24 V *vs.* NHE[81] – meaning

that it would be thermodynamically possible for any NO formed during the oxidation of Np(V) by nitric acid to reduce the Np(VI) back to Np(V).

A second, more positive oxidation peak seen at approximately 1 V *vs.* Ag/AgCl in the scans conducted in NO-purged solutions is also seen in the scans recorded from the pre-NO bubbled solution, the currents associated with the former being substantially larger than the latter. In the case of the latter, non-NO sparged solutions, this peak can be attributed to the well-studied surface oxidation behaviour of platinum in sulphuric acid. However, in the case of the former, NO-sparged solutions, the observed larger currents are due to both the surface oxidation behaviour of platinum *and* the electrochemistry of nitrite/nitrous acid in the NO-sparged system. By taking the onset of this peak as approximately 0.85 V *vs.* Ag/AgCl (1.047 *vs.* NHE), we can see that this is in line with the potential for the oxidation couple given by Equation 3.1, which has been found to have a literature value of 1.093 V *vs.* NHE.[81] This peak has also been seen in previous studies into the electrochemical oxidation of nitrite done by Wang *et al.*, and Casella and Salvi with differences in the potential being likely due to differences in pH used.[140, 141]

$$NO_2 + H^+ + e^- \rightarrow HNO_2 \qquad 3.1$$

As no nitrous acid is expected to be present within the solution due to the initial sparging and removal of oxygen from the experimental system, the apparent presence of nitrous acid and hence its oxidation peak must therefore be explained. The presence of both of the two anodic peaks, however, can be rationalised through the application of a so called electrochemical-chemical-electrochemical (ECE) mechanism. In an ECE mechanism the initial electrochemical step is followed by a chemical step, which forms an electroactive product which then goes on to give a second electrochemical step.[142, 143] Within the NO sparged electrolyte, we therefore propose that the expanded ECE mechanism outlined in equations 3.2 to 3.6 is taking place.

$$NO \rightarrow NO^+ + e^- \quad 3.2$$

$$NO^+ + H_2O \rightarrow HNO_2 + H^+ \quad 3.3$$

$$HNO_2 \rightarrow NO_2 + e^- + H^+ \quad 3.4$$

$$2NO_2 \overset{slow}{\rightleftharpoons} N_2O_4 \quad 3.5$$

$$N_2O_4 + H_2O \rightarrow HNO_2 + HNO_3 \quad 3.6$$

Subsequently as a result of this mechanism, the reduction of dissolved NO^+ and NO_2 species produced by equations 3.2 and 3.4 respectively will give rise to the peaks seen within the reverse cathodic scan.

3.1.2 Behaviour in 1 mol dm^{-3} $NaNO_3$ Solutions

In a similar approach to that employed with sulphuric acid solutions immediately above, CVs were recorded from pre- and post-NO sparged solutions of 1 mol dm^{-3} $NaNO_3$. That, in the case of the NO-sparged solutions, showed the presence of an electrochemical process that we attribute to being due to the NO/NO^+ couple. As in the case of the sulphuric acid electrolytes employed immediately above, the CVs measured on platinum in the presence of bubbling with NO showed the presence of two anodic peaks at approximately 0.7 V *vs.* Ag/AgCl and at 0.85 V *vs.* Ag/AgCl – neither of which were seen in the background trace recorded in the absence of NO bubbling, see Figure 3-2.

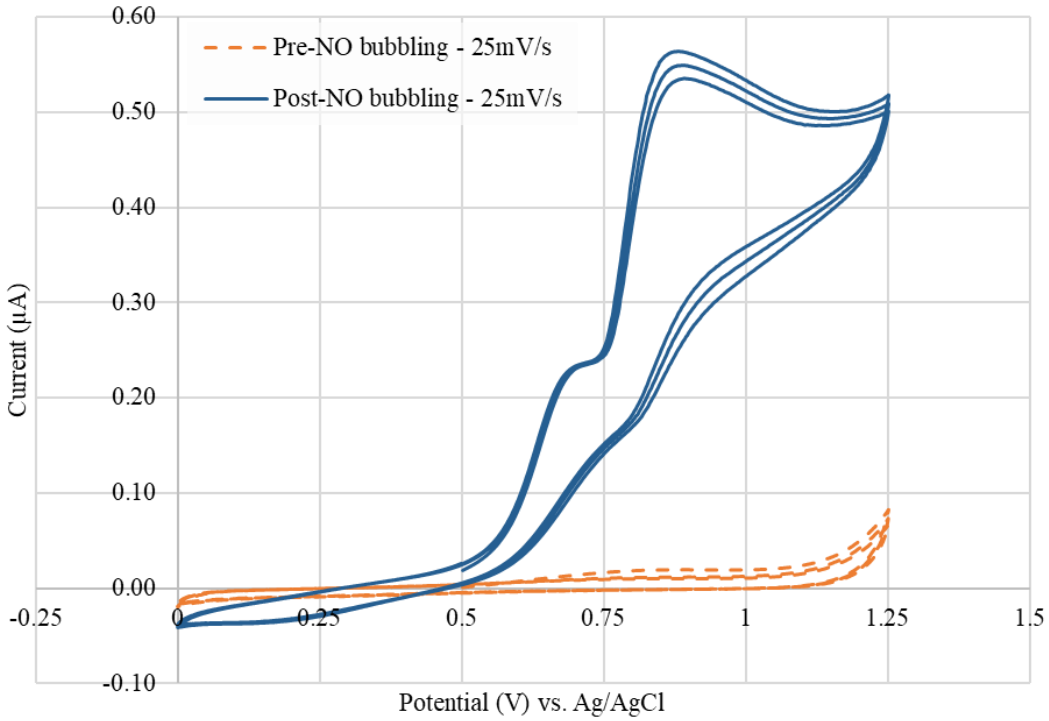

Figure 3-2 Cyclic voltammograms of 1 mol dm^{-3} $NaNO_3$ both before and after bubbling with NO gas. Scan rate = 100 mV s^{-1}.

As was detailed previously in sulphuric acid solutions, the presence of a nitrous/nitrite oxidation peak at 0.85 V vs Ag/AgCl can be explained through the use of an ECE mechanism, wherein the NO^+ formed by the initial electro-oxidation of NO, resulting in the peak at 0.7 V *vs.* Ag/AgCl, reacts with H_2O to form HNO_2, which then undergoes a second electrochemical step. However, unlike within the sulphuric acid, no peaks were seen within the reverse cathodic scan corresponding to the reductions of the NO^+ and NO_2 species. The absence of these reduction peaks suggests a change in the ECE mechanism occurring due to the presence of the nitrate ion. A consequently slightly modified ECE mechanism is outlined in equations 3.7 to 3.11, with presence of the NO_3^- ion allowing for an additional chemical step, outlined in equation 3.8, to occur after the initial electro-oxidation. This change in the chemical step may result in a quicker formation, and hence larger concentrations of the N_2O_4 species, which in turn may result in the reaction of equation 3.9 occurring more quickly. This reaction then results in the formation of HNO_3 and HNO_2, the latter of which can then undergo another

electrochemical step, equation 3.10, resulting in the formation of NO_2 which may dimerise to reform N_2O_4, equation 3.11.

$$NO \rightarrow NO^+ + e^- \quad 3.7$$

$$NO^+ + NO_3^- \rightarrow N_2O_4 \quad 3.8$$

$$N_2O_4 + H_2O \rightarrow HNO_2 + HNO_3 \quad 3.9$$

$$HNO_2 \rightarrow NO_2 + e^- + H^+ \quad 3.10$$

$$2NO_2 \overset{slow}{\rightleftharpoons} N_2O_4 \quad 3.11$$

The net result of this putative reaction scheme is then the formation electrochemically inactive HNO_3, formed faster than previously seen in H_2SO_4. This proposed rapid conversion of electrochemically active nitrogen-oxygen species to nitric then offers a potential explanation as to why no reduction wave is seen in the reverse cathodic scan of the NO-sparged solutions seen in Figure 3-2.

It can also be seen that the peak attributed to the nitrite couple is seen to shift to slightly lower potentials in $NaNO_3$ solution when compared to that recorded in H_2SO_4. This shift in the potential can be attributed to the difference in pH of the solutions, where in the higher pH of the 1 mol dm^{-3} $NaNO_3$ solution, the nitrite exists predominantly as unprotonated HNO_2, and the redox equation therefore shifts from that shown in equation 3.1 to that shown in equation 3.12. As previously, by taking the onset of this peak as approximately 0.65 V *vs.* Ag/AgCl (0.847 V *vs.* NHE), we can see that this is in line with the potential for the oxidation couple which has been found to have a literature value of 0.895 V *vs.* NHE.[81]

$$NO_2 + e^- \rightarrow NO_2^-$$ 3.12

Whilst the potential for the nitrite couple has shifted to be slightly lower in $NaNO_3$ than in H_2SO_4, as would be expected in the higher acidity media, the value of the NO/NO^+ couple is still at similar potentials in both media, and seen well below that of the Np(V)/Np(VI) couple. Therefore, it can be seen that the presence of NO within a nuclear fuel reprocessing scheme should be thermodynamically capable of reducing Np(VI) down to Np(V).

With the NO oxidation potential shown to occur at potentials where the reduction of either Np(VI) or V(V) would be thermodynamically viable, a method was required to quantitatively measure nitrous acid *in situ* during its reduction reaction with either neptunium or vanadium. Therefore, the electrochemical behaviour of nitrous acid was examined on a number of different electrode materials for the purpose of developing an electrochemical sensor for HNO_2.

3.2 Feasibility Study of Electrochemical Detection of Nitrous Acid

In order to monitor the consumption of nitrous acid during the reduction of either neptunium or vanadium, the use of electrochemical quantification of HNO_2/nitrite was examined to determine its suitability.

Whilst electrochemical methods are well known for the detection of nitrite, many studies focus on the quantification of nitrite in the micromolar concentration range and use a number of electrode surface modification techniques for the purpose of enhancing selectivity and sensitivity.[122] Within this work however, the feasibility of the use of electrochemical techniques for detection in the millimolar concentration range using simple, non-modified surface electrode materials was to be investigated and compared to use of spectroscopic techniques. This study was to be done in the millimolar concentration range in order to be applicable to the concentrations to be used in experiments performed on the reduction of either Np(VI) or V(V) by nitrous acid (Section 4.1). The use of millimolar concentrations for these experiments were in turn chosen to allow for a good signal-to-noise ratio in the identification and quantification of the metal species present by UV-vis spectroscopy, whilst facilitating the safe handling of neptunium.

In order to determine the suitability of electrochemical techniques for the detection of nitrite and its consumption within the metal ion reduction reactions to be studied, the behaviour of nitrous acid, vanadium, and neptunium were looked at on a range of electrode materials by using cyclic voltammetry. Unless stated otherwise, these where all done at a scan rate of 100 mV s^{-1}. Platinum, gold, and glassy carbon were used as different electrode materials to check the different current responses on each of these materials to improve the accuracy of the electrochemical sensor. From these cyclic voltammograms, the current response could then be used to determine nitrous acid concentration using the Randles-Sevcik equation of equation 3.13a which, at 25°C, may be rewritten in simplified form as equation 3.13b.[142, 144] Use of equation 3.13b requires that the following unitary convention is adopted: i_p, the

peak current, is given in amperes; *n* is the stoichiometric number of electrons involved in the electrode reaction; *A* is the electrode area in cm^2; D_O is the diffusion coefficient of species O in $cm^2\ s^{-1}$; C_O is the concentration of species O in mol cm^{-3}; and *v* is the scan speed in V s^{-1}.

$$i_p = 0.4463nFAC_O\left(\frac{nF}{RT}\right)^{0.5} v^{0.5} D_O^{0.5} \quad 3.13a$$

$$i_p = (2.69 \times 10^5) n^{1.5} A {D_O}^{0.5} C_O v^{0.5} \quad 3.13b$$

3.2.1 Electrochemical Measurements on Platinum

3.2.1.1 Nitrous Acid Response

Cyclic voltammograms were performed using a 250 µm Pt micro-disc working electrode for varying nitrous acid concentrations, Figure 3-3, between 1 mmol dm^{-3} and 100 mmol dm^{-3} in a solution of 0.5 mol dm^{-3} nitric acid. Responses seen in CVs showed an anodic peak potential at approximately 1.1 V *vs.* Ag/AgCl which can be attributed, similarly to the peak seen previously at approximately 1 V *vs.* Ag/AgCl in Figure 3-1, to the oxidation of nitrite/nitrous acid

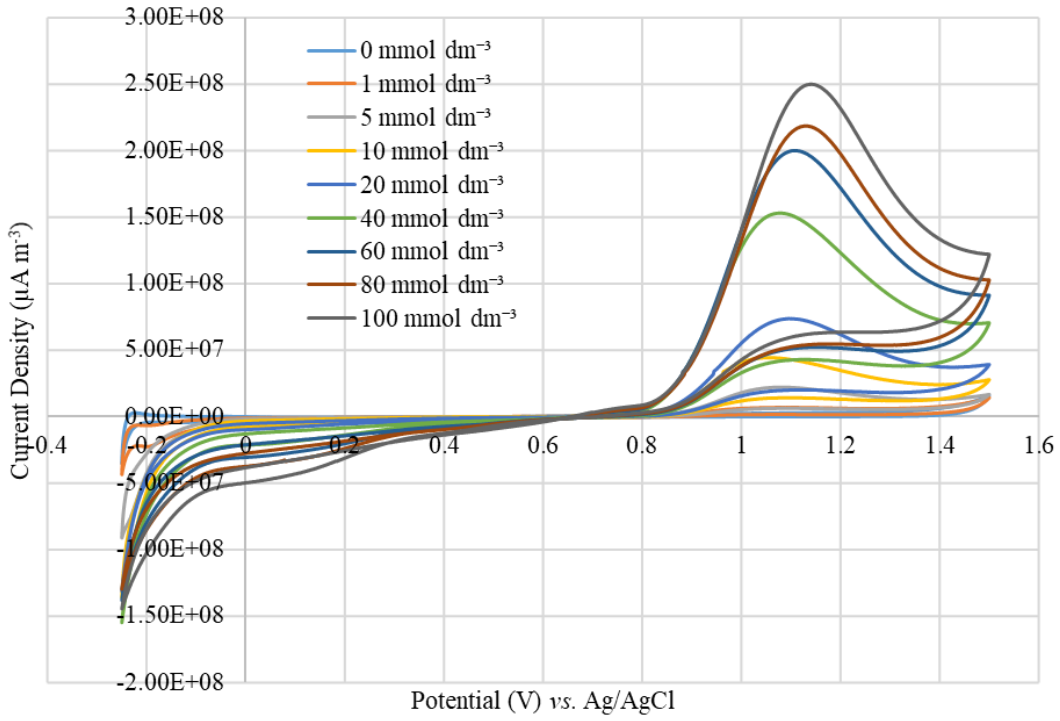

Figure 3-3 Cyclic voltammograms of varying concentrations of HNO_2 in 0.5 mol dm^{-3} HNO_3 on Pt (250 µm diameter) showing the final scan only for clarity. Scan rate = 100 mV s^{-1}.

Plots of the current measured at 1.1 V *vs.* Ag/AgCl for the anodic waves *vs.* the concentration of nitrous acid were created, Figure 3-4, and linear trendlines shown were calculated using data for concentrations ≤ 60 mmol dm^{-3} with R^2 values obtained of > 0.989. Extension of these trendlines to higher nitrous concentrations indicated that the current observed at 80 mmol dm^{-3} and 100 mmol dm^{-3} are lower than might be expected on the basis of the linear i *vs* $[HNO_2]$ behaviour seen at $[HNO_2] \leq 60$ mmol dm^{-3}.

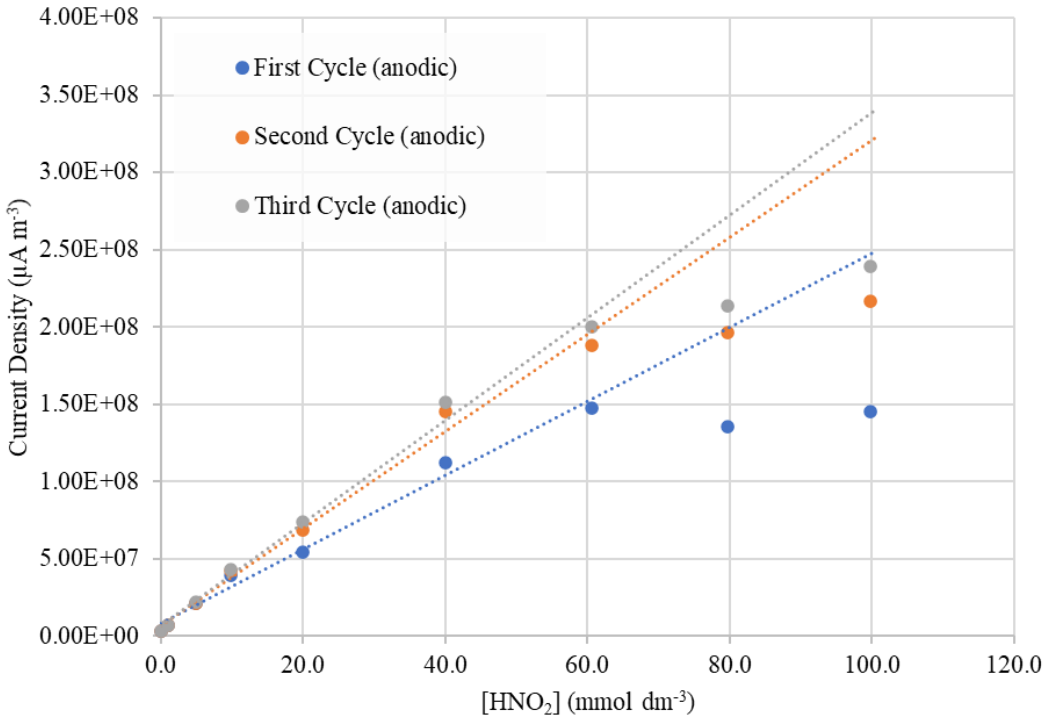

Figure 3-4 Plots of current measured at 1.1 V vs [HNO_2] in 0.5 mol dm^{-3} HNO_3 on Pt (250 µm diameter). Currents taken from both the first, second and third anodic scans.

From this plot it could be seen that nitrous acid concentrations on the order of millimolar could be detected using electrochemical methods with a Pt working electrode. As can be seen from equation 3.13, this limit of detection obtainable by using an electrochemical method could also be improved by increasing the electrode area, however, this was impractical for the neptunium reduction experiments which were to be done within small volume reaction vessels for radiological safety reasons.

The deviation from linear behaviour seen here for the current response at the 80 mmol dm^{-3} and 100 mmol dm^{-3} nitrous acid concentrations is most likely indicative of surface adsorption of an intermediate species in the overall electrode process. This adsorption we postulate to be of the NO/NO^+ in accordance with the work of Vetter, Abel and Schmid, and Balbaud.[145-149] These authors gave the elementary steps involved in the reduction of nitrate to nitrous in accordance with equations 3.14 to 3.17.

$$HNO_2 + H^+ \rightleftharpoons NO^+ + H_2O \quad 3.14$$

$$NO^+ + e^- \rightleftharpoons NO \quad 3.15$$

$$HNO_3 + NO \rightleftharpoons HNO_2 + NO_2 \quad 3.16$$

$$2NO_2 + H_2O \rightleftharpoons HNO_3 + HNO_2 \quad 3.17$$

This mechanism will obtain in homogenous solution but will, according to Balbaud *et al*.[149], be promoted in a heterogeneous manner on Pt (the most electrocatalytically active of the electrode materials used within the studies done in Section 3.2) *via* the adsorption of NO/NO^+ at the electrode surface. It is not unreasonable to assume that the same mechanism will operate during the reverse reaction, i.e. the oxidation of nitrous acid to nitric acid.

In such a system/mechanism, at low nitrous acid concentrations, the number of adsorption sites occupied by NO will be linearly proportional to the $[HNO_2]$ in accordance with standard isotherm behaviour such as seen within the Langmuir adsorption model. At high nitrous acid concentrations, the sites will become saturated – especially if the desorption process associated with the electro-oxidised NO^+ is slow – thus causing the observed effect, wherein the overall observed oxidation current value at high nitrous acid concentrations was lower than would be expected from a simple linear dependence of current on $[HNO_2]$.

3.2.1.2 Vanadium Response

In order to check for any current response at the same potentials as the nitrite oxidation peak seen at 1.1 V *vs.* Ag/AgCl from other species relevant to the Np(VI)/V(V) reduction studies, a cyclic voltammogram was then taken of 25 mmol dm^{-3} V(IV) in 0.5 mol dm^{-3} HNO_3, Figure 3-5. In these CVs, a peak could be seen with an onset at approximately 1.1 V *vs.* Ag/AgCl which could be attributed to the oxidation of V(IV) to V(V), given within the literature as 0.8 V *vs.* Ag/AgCl (1.0 V *vs.* NHE)[81]. The oxidation peak for this couple has therefore been

seen to be displaced by approximately 300 mV in the anodic direction from the E^0 value given in the literature. Likewise, the reduction of V(V) back to V(IV) can be assigned to the peak within the cathodic scan with an onset potential of approximately 0.55 V *vs.* Ag/AgCl, which is again displaced by an overpotential of approximately 250-300 mV from the literature value given above, with the displacement this time being in the cathodic direction. These overpotentials are not unexpected given that the redox process involves the breaking/formation of a V-O bond in going from either the V(V) to V(IV) or *vice versa*, so favouring irreversible-type electrode kinetics.

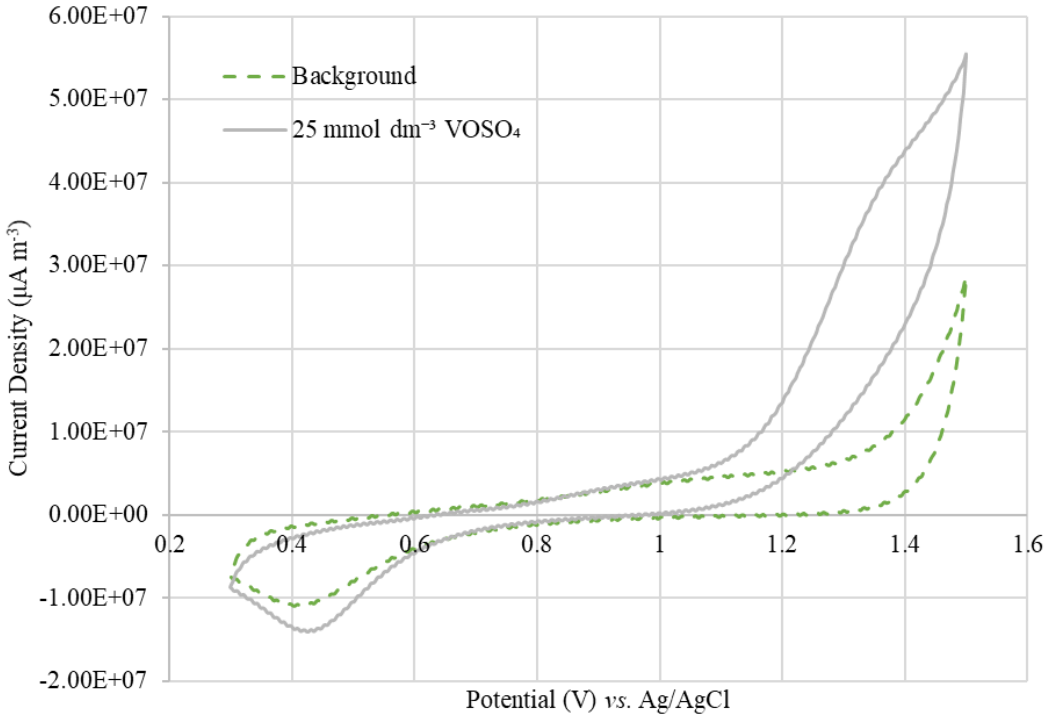

Figure 3-5 CVs of 25 mmol dm^{-3} V(IV) in 0.5 mol dm^{-3} HNO_3 on Pt (250 µm diameter) showing the final scan only for clarity. Scan rate = 100 mV s^{-1}.

From these CVs, it could therefore be seen that amperometric measurement, and hence quantification, of nitrous acid in the presence of V(IV) would be possible through calibration of the measured current within the electrode kinetics-derived potential window afforded by the irreversibility of the VO_2^+/VO^{2+} couple on Pt, as at these applied potentials, the resulting current

would be solely due to the oxidation of nitrous acid and not due to the oxidation of any vanadium present.

3.2.1.3 Neptunium Response

A cyclic voltammogram was also taken of the NNL provided neptunium stock solution, detailed in Section 2.1.2, 1.65 mmol dm^{-3} Np in 0.5 mol dm^{-3} HNO_3, Figure 3-6, as another species relevant to the Np(VI)/V(V) reduction studies to be undertaken, in order to check for possible overlapping of oxidation peaks and hence interference in the quantification of nitrous acid.

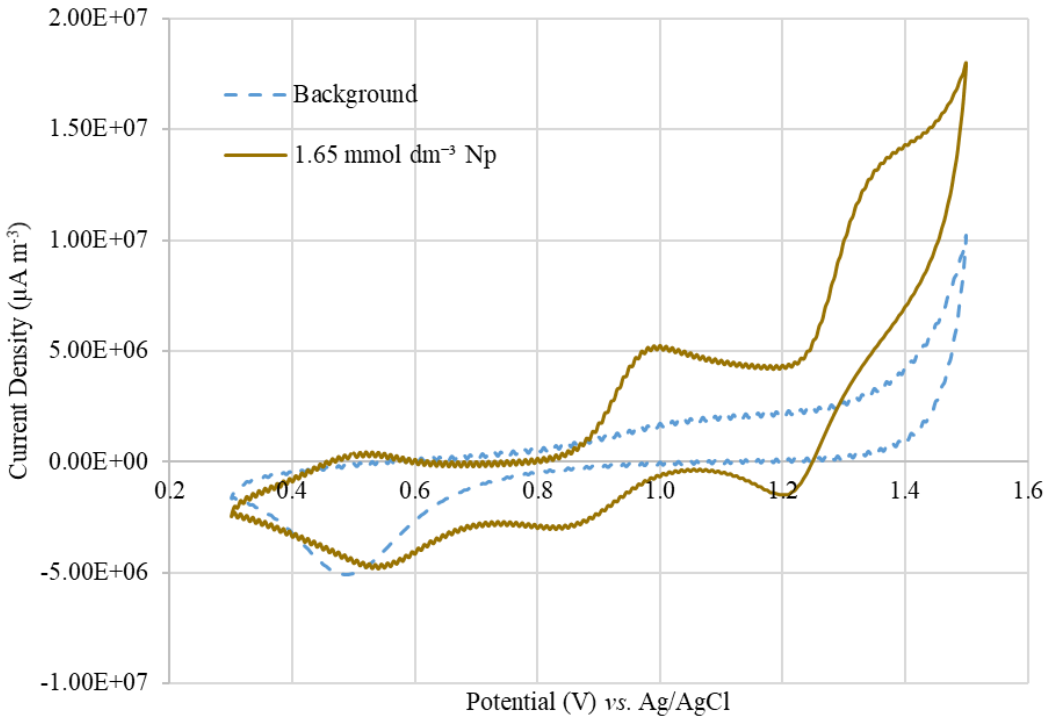

Figure 3-6 CVs of 1.65 mmol dm^{-3} Np(V) in 0.5 mol dm^{-3} HNO_3 on Pt (250 µm diameter) showing the final scan only for clarity. Scan rate = 100 mV s^{-1}.

The oxidation peak observed at approximately 1 V *vs.* Ag/AgCl is consistent with the formal potential for the oxidation of NpO_2^+ to NpO_2^{2+} in 1 mol dm^{-3} HNO_3 of 0.943 V *vs.* NHE when taking the onset of the peak as approximately 0.80 V *vs.* Ag/AgCl (0.997 *vs.* NHE),.[81] The oxidation peak present at approximately 1.35 V *vs.* Ag/AgCl has been previously seen by Chatterjee *et al.* and has been attributed to the NpO_2^{2+}-assisted solvent oxidation.[150] Whilst

this NpO_2^{2+}-assisted solvent oxidation is not described within the literature, we propose here that this is due to an electrochemical-catalytic chemical (EC') mechanism, from the perspective of the neptunium couple, in which the electrochemical step of oxidation of Np(V) to Np(VI) is followed by a chemical step which regenerates the reactant species for the electrochemical step, said chemical step being caused by the reductive effect of electrogenerated H_2O_2 and $HO_2\cdot$ species. For the NpO_2^{2+}-assisted solvent oxidation, the initial electrochemical step is the electrochemical generation of either the H_2O_2 or $HO_2\cdot$ species from water which have electrochemical potentials of 1.56 V *vs.* Ag/AgCl and 1.45 V *vs.* Ag/AgCl respectively.[151] Both of these species can then act as reductants for the Np(VI) giving Np(V), themselves being oxidised to oxygen, due to their electrochemical potentials of 0.50 V *vs.* Ag/AgCl and -0.25 V *vs.* Ag/AgCl respectively.[151] This Np(V) is then reoxidised at the electrode back to Np(VI), which can be reduced by more $H_2O_2/HO_2\cdot$, creating an EC' cycle for neptunium oxidation and enhancing the measured current. Whilst the above proposed mechanism hasn't been verified here due to being outside the scope of this work, further work could potentially be done to verify this by fitting experimental data to the mathematical models developed by Nicholson and Shain for an EC' system.[143]

Both the Np(V)/Np(VI) and the Np-assisted solvent oxidation peaks described above are seen to be close to that of the NO_2/HNO_2 couple previously seen at 1.1 V *vs.* Ag/AgCl, making the quantification of nitrous acid using the oxidation of HNO_2 more difficult due to currents within the 0.9 V to 1.1 V range resulting from the NpO_2^+ oxidation.

Due to the current response from both the NpO_2^{2+}/NpO_2^+ redox couple, and the Np-assisted solvent oxidation recorded in the neptunium CVs being measured at comparable potentials to that of the nitrite oxidation peak, the use of Pt as the working electrode material for the quantification of nitrous acid by electrochemical methods during reduction reactions was not feasible. Consequently, further experiments were conducted on alternative electrode materials to determine whether reversibility differences in the electrode kinetics for the redox couples of interest on those materials may afford a voltage window for the selective amperometric

measurement of one couple or other (as was seen to be the case for the measurement of nitrous in the presence of V(V)/V(IV) in Figure 3-3 and Figure 3-5 above).

3.2.2 Electrochemical Measurements on Gold

3.2.2.1 Nitrous Acid Response

Cyclic voltammograms were performed for comparable solution systems to those done using a 250 µm Pt micro-disc working electrode, Section 3.2.1.1, using a 250 µm Au micro-disc working electrode, with nitrous acid concentrations varying between 1 mmol dm^{-3} and 100 mmol dm^{-3} in solutions of 0.5 mol dm^{-3} nitric acid, Figure 3-7. These showed similar response to those on Pt, with the main oxidation peak being attributable to the HNO_2/NO_2 redox couple. However, at all nitrous concentrations studied, this peak was seen to have shifted to slightly to less-positive potentials than that for the same peak in the analogous studies on Pt; specifically, for the Au electrode used in collecting the data of Figure 3-7, the anodic current peak occurs at approximately 0.9 V *vs.* Ag/AgCl compared to 1.1 V *vs.* Ag/AgCl recorded when using a Pt working electrode as per Figure 3-3.

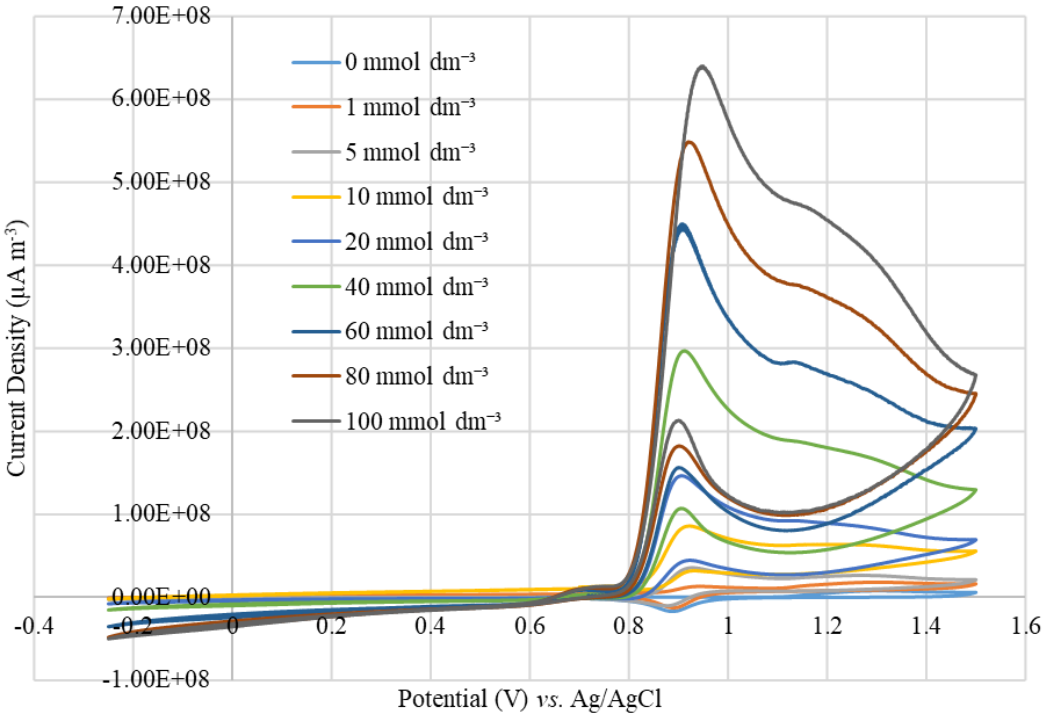

Figure 3-7 Cyclic voltammograms of varying concentrations of HNO_2 in 0.5 mol dm^{-3} HNO_3 on Au (250 µm diameter) showing the final scan only for clarity. Scan rate = 100 mV s^{-1}.

Plots of the maximum current measured between 0.8 and 1.0 V *vs.* Ag/AgCl for the anodic wave *vs.* the concentration of nitrous acid were created, Figure 3-8. Due to Au being less electrocatalytically active than the Pt used in Section 3.2.1.1, the oxidation will occur predominantly in the homogeneous manner in the solution phase, as opposed to heterogeneously with the aforementioned adsorption of NO onto the surface of the electrode – leading to the expectation that the plateauing of the peak current with increasing nitrous acid concentration seen in Pt electrode-measured data of Figure 3-4 will not be seen on the Au electrode employed in this section. This expectation was confirmed by good linearity being seen across the whole nitrous acid concentration range for the plots of oxidation wave peak current *vs.* [HNO_2] of Figure 3-8, with R^2 values > 0.99 being obtained.

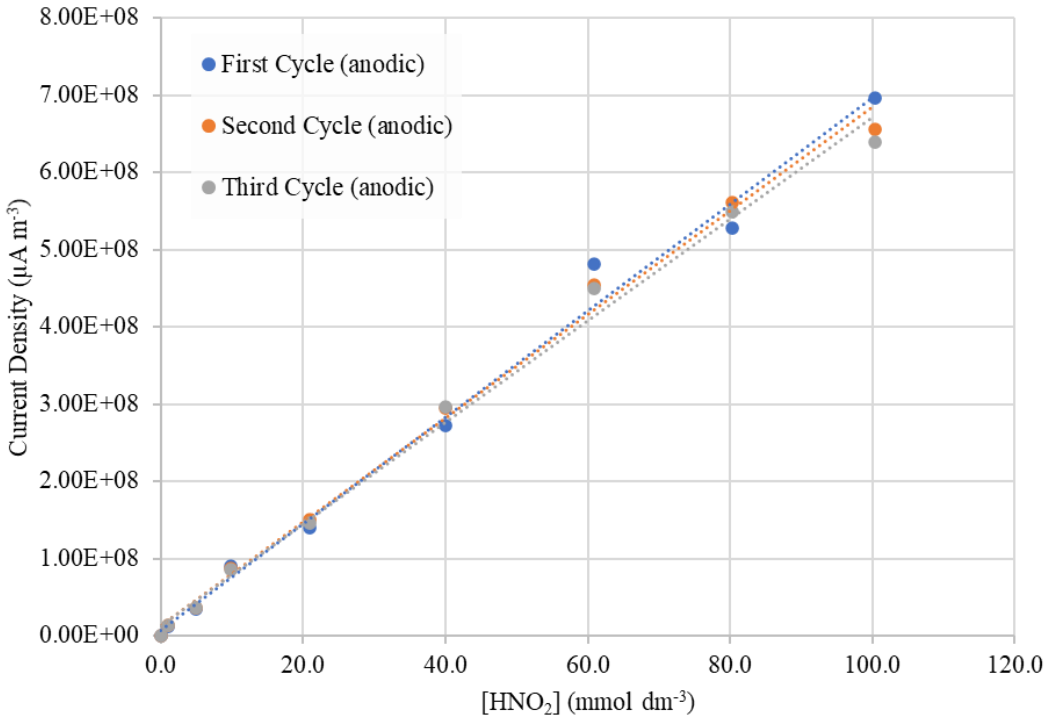

Figure 3-8 Plots of max current measured between 0.8 V and 1 V vs [HNO_2] in 0.5 mol dm^{-3} HNO_3 on Au (250 µm diameter).

From this plot it could be seen that, as was seen on Pt in Section 3.2.1.1, limits of detection on the order of millimolar were found when using a Au working electrode. Whilst the limits of detection could again be improved by increasing the electrode area, this was impractical for the neptunium reduction experiments to be performed, for radiological safety reasons.

A secondary peak at approximately 1.2 V *vs.* Ag/AgCl can also be seen in the CVs, which is likely due to inherent electrochemical behaviour of Au in HNO_3 as this can also be seen in the absence of HNO_2 within the 0 mmol dm^{-3} voltammogram. This behaviour is similar to that seen by Shackleford *et al.* where, at sufficiently high scan rates, deposition of a layer of Au oxide as a passive layer causes current to stop flowing.[152] This Au electrode behaviour is also seen to affect the observed CVs of both V and Np in Sections 3.2.2.2 and 3.2.2.3 respectively.

In order to test that the anodic peak current occurring at approximately 0.9 V *vs.* Ag/AgCl was primarily due to the presence of HNO_2 and not convoluted with the electrochemical behaviour

of the Au surface, scan rate studies were performed using a solution of 60 mmol dm^{-3} HNO_2 in 0.5 mol dm^{-3} HNO_3. Figure 3-9 shows the resultant plot of the peak current *vs.* the square root of the scan rate for these cyclic voltammograms, recorded over a range of scan rates between 5 mV s^{-1} and 750 mV s^{-1}. From this figure it can be seen that a linear dependence was seen when plotting the peak current *vs.* the square root of the scan rate for the peak at 0.9 V *vs.* Ag/AgCl, with R^2 values of > 0.994, showing that the process associated with this oxidation peak is dependent on diffusion of the solution. Since the oxidation of the Au electrode surface would not be expected to display this from-solution diffusion control, the oxidation peak at approximately 0.9 V *vs.* Ag/AgCl can be attributed to the nitrous acid redox couple.

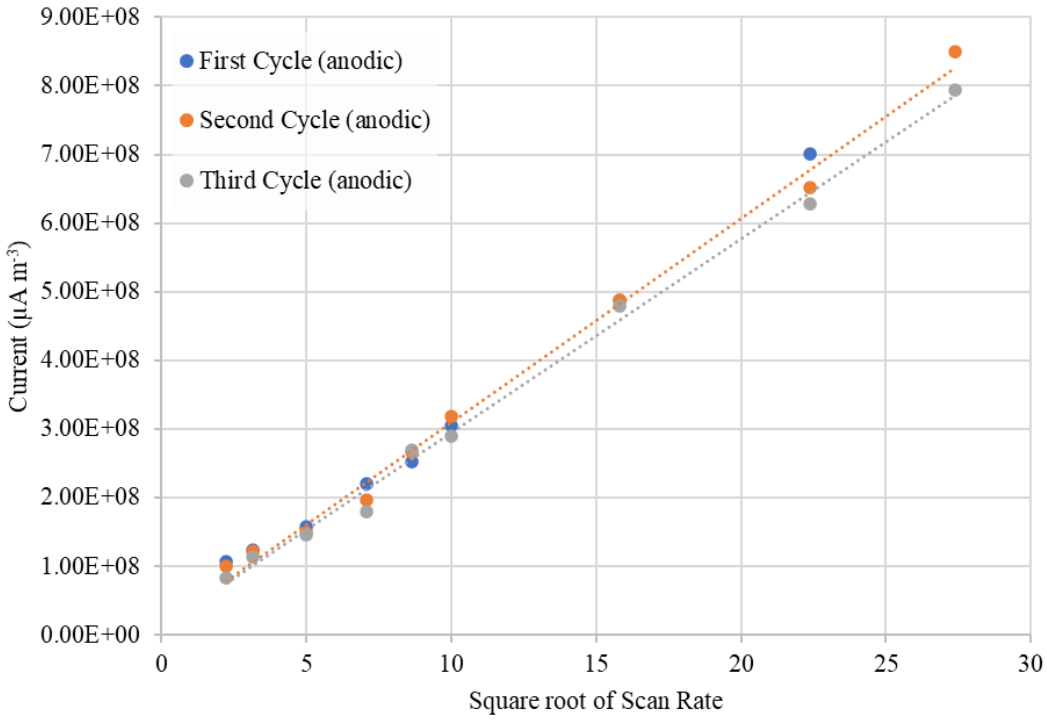

Figure 3-9 Plot of Current at 0.94V vs the square root of the Scan Rate for a solution of 60 mmol dm^{-3} HNO_2 in 0.5 mol dm^{-3} HNO_3.

3.2.2.2 Vanadium Response

As was done previously on Pt, any current response at the same potentials as the nitrite oxidation peak seen at 0.9 V *vs.* Ag/AgCl from other species relevant to the reduction studies was to be checked for. In the first instance this was to be done for vanadium by measuring a cyclic voltammogram of 25 mmol dm^3 V(IV) in 0.5 mol dm^3 HNO_3, with the results of these being shown in Figure 3-10.

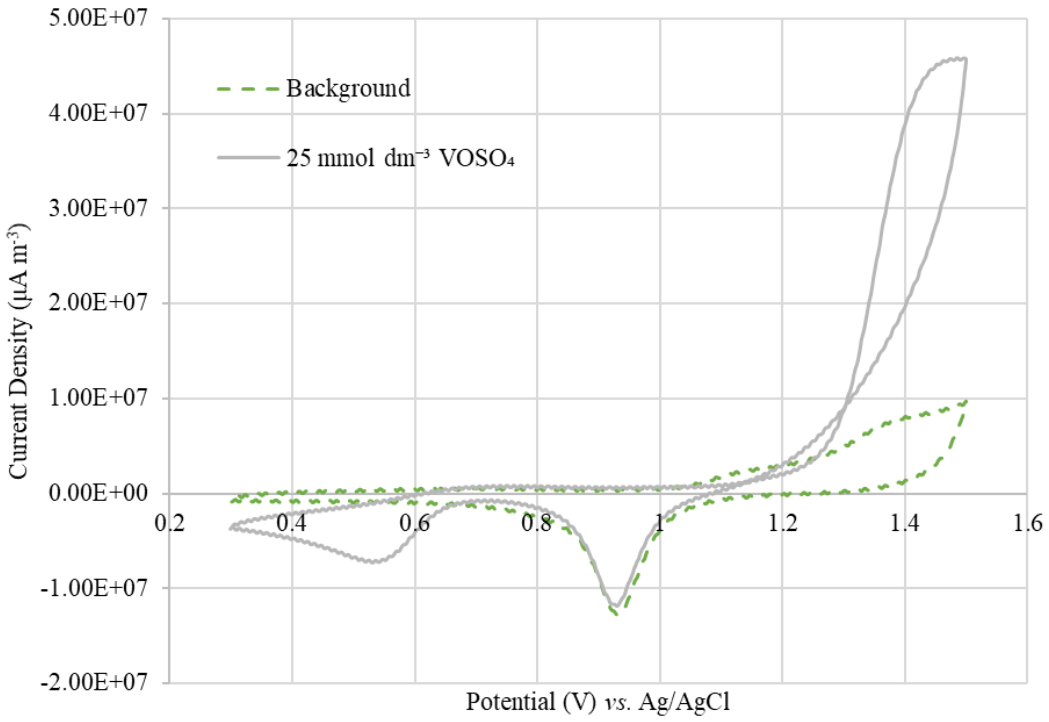

Figure 3-10 CVs of 25 mmol dm^{-3} V(IV) in 0.5 mol dm^{-3} HNO_3 on Au (250 µm diameter) showing the final scan only for clarity. Scan rate = 100 mV s^{-1}.

These CVs are comparable to those reported by Chen and Liu[136], with peaks being seen at approximately 1.45 V *vs.* Ag/AgCl in the anodic scan and 0.55 V *vs.* Ag/AgCl in the cathodic scan which can be assigned to the V(V)/V(IV) redox couple.[81] Similarly to as was seen for CVs of V(IV) on Pt in Figure 3-5, both the reduction and oxidation peaks for this couple are displaced by 250-300 mV in the cathodic and anodic directions respectively. This again is likely due to the irreversibility of the V(V)/V(IV) couple which involves the breaking/formation of a

V-O bond. This irreversibility is also seen to cause a hysteresis loop within the vanadium CV between 1.1 V *vs.* Ag/AgCl and 1.3 V *vs.* Ag/AgCl.

Amperometric measurement, and hence quantification, of nitrous acid in the presence of V(IV) would therefore again be possible – as was seen on Pt in section 3.2.1.2 – due to the electrode kinetics-derived potential window afforded by the irreversibility of the VO_2^+/VO^{2+} couple providing a region in which the resulting current would be solely due to the oxidation of nitrous acid and not due to the oxidation of any vanadium present.

3.2.2.3 Neptunium Response

Current responses of neptunium on Au were then measured by running CVs of 1.65 mmol dm^{-3} neptunium in 0.5 mol dm^{-3} HNO_3, Figure 3-11. The electrochemical behaviour of the neptunium on Au was seen to create a type of hysteresis loop where the peak current of the cathodic scan was seen to reach current higher than that of the anodic scan. This can be attributed to the electrochemical behaviour of Au in HNO_3 as explained in Shackleford *et al.*[152] and similarly to what was seen previously for the CVs of HNO_2 in Section 3.2.2.1. The effect of this Au behaviour is to cause a drop in current above approximately 1.3 V *vs.* Ag/AgCl as a passivating layer of Au oxide is formed. Within the reverse cathodic scan, currents are then seen to increase again at approximately 1.3 V *vs.* Ag/AgCl as the Au oxide layer is dissolved. This passivating of the Au electrode surface and turning off of current can be seen more readily in the CVs of Np than those for HNO_2 due to the smaller concentrations of the former than the latter.

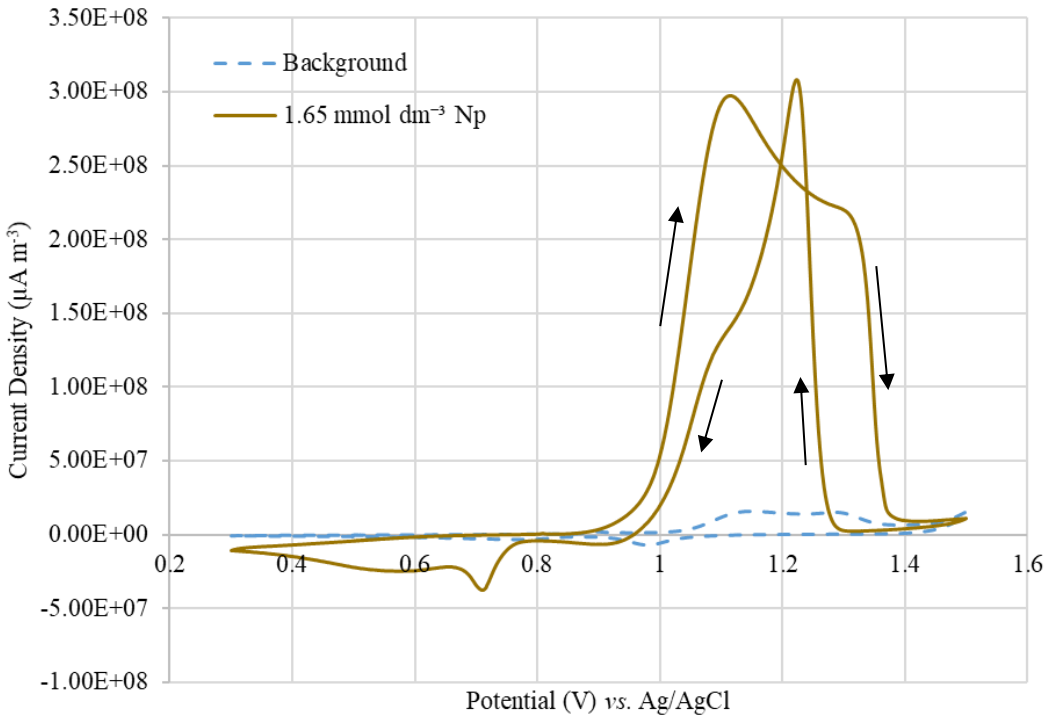

Figure 3-11 CVs of 1.65 mmol dm^{-3} Np(V) in 0.5 mol dm^{-3} HNO_3 on Au (250 µm diameter) showing the final scan only for clarity. Scan rate = 100 mV s^{-1}. Presence of a hysteresis loop seen within these scans was attributed to the inherent electrochemical behaviour of Au in HNO_3, wherein formation of a gold oxide layer causes passivation of the electrode surface during the anodic scan, with the dissolution of this layer during cathodic scan causing re-activation of the electrode surface.

The shift in the oxidation peak potential of the nitrous acid on Au to approximately 0.9 V *vs.* Ag/AgCl and the absence of a significant current response of the neptunium on Au at 0.9 V *vs.* Ag/AgCl meant that quantification of the nitrous acid independent of any neptunium present would be possible by measuring current at a held potential. However, due to the low current response at lower concentrations of nitrous acid meant that limits of detection would be on the order of 1 mmol dm^3. This limit of detection was seen to be comparable to that when using UV-vis to detect nitrite (Section 3.2.4) and would therefore need to be improved in order to detect lower amounts of nitrous acid. Whilst this improvement could be made by increase the area of the working electrode, this would mean that the electrode would need to be larger and would not fit within the small volume reaction vessel in which the reduction experiments were to be performed. Also, the use of gold as an electrochemical sensor material for the detection of HNO_2 is complicated by the inherent behaviour of the Au surface in HNO_3 as seen for both solutions of nitrous acid and neptunium.

3.2.3 Electrochemical Measurements on Glassy Carbon

3.2.3.1 Nitrous Acid Response

The final material for the response of nitrous acid to be tested on was glassy carbon. Therefore, as previously, cyclic voltammograms were done for varying nitrous acid concentrations, Figure 3-12, between 1 mmol dm^{-3} and 100 mmol dm^{-3} in solutions of 0.5 mol dm^{-3} nitric acid. In comparison to the CVs on both Pt and Au which showed anodic peak potentials of 1.1 V *vs.* Ag/AgCl and 0.9 V *vs.* Ag/AgCl respectively for the peak attributed to the HNO_2/NO_2 redox couple, this peak was seen to shift to slightly more positive potentials on glassy carbon, reaching a maximum current at approximately 1.39 V *vs.* Ag/AgCl. This oxidation was also seen to just produce a singular peak as was seen on Pt and unlike on Au, strongly suggesting that no inherent background behaviour associated with the of the electrode material itself was being observed.

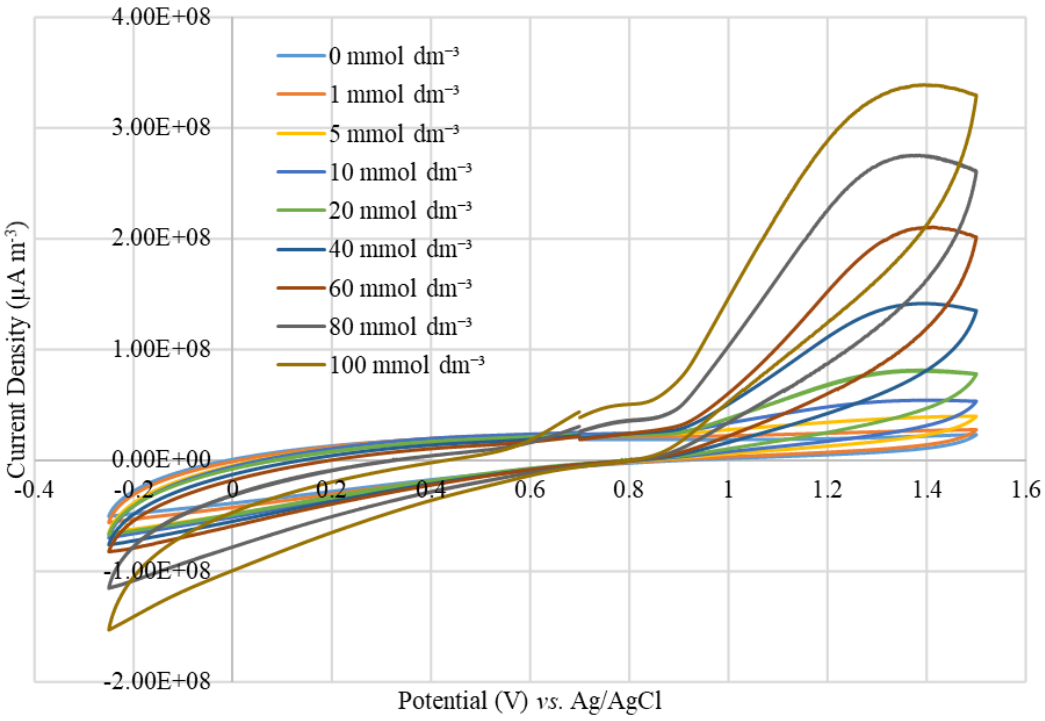

Figure 3-12 Cyclic voltammograms of varying concentrations of HNO_2 in 0.5 mol dm^{-3} HNO_3 on Glassy Carbon (1 mm diameter) showing the final scan only for clarity. Scan rate = 100 mV s^{-1}.

Plots of the peak current measured at 1.4 V *vs.* Ag/AgCl for the anodic wave *vs.* the concentration of nitrous acid were created, Figure 3-13. Good linearity was seen for these across the whole nitrous acid concentration range with R^2 values > 0.998 for anodic scan currents. This indicates that, as seen in Section 3.2.2.1 on Au, over the concentration range studied, the oxidation of HNO_2 was occurring predominantly *via* a homogeneous route as opposed to a heterogeneous route.

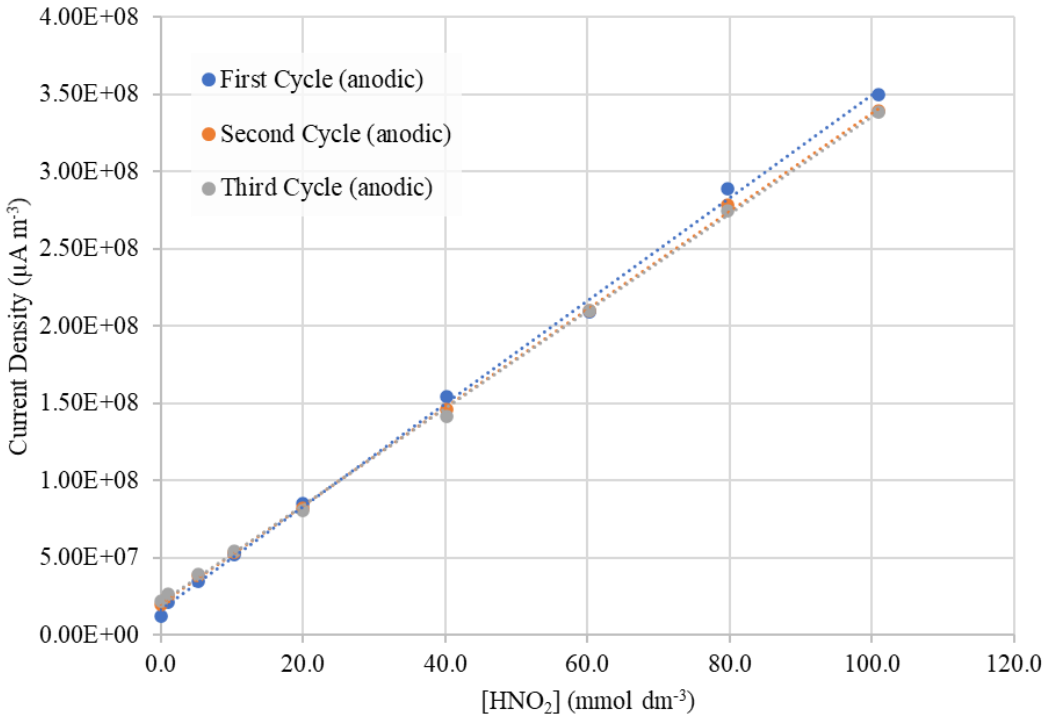

Figure 3-13 Plots of current measured at 1.4 V vs [HNO_2] in 0.5 mol dm^{-3} HNO_3 on Glassy Carbon (1 mm diameter).

From this plot it could be seen that, whilst the electrode area of the glassy carbon (GC) working electrode was larger than that of the Pt and Au electrodes used in Section 3.2.1 and 3.2.2, limits of detection for nitrous acid concentrations were still seen to be on the order of millimolar. Improvement of this limit of detection by increasing the electrode area, whilst possible, would again be impractical for the neptunium reduction experiments for radiological safety reasons.

3.2.3.2 Vanadium Response

As was done previously on both Pt and Au, any current response at the same potentials as the nitrite oxidation peak seen at 1.39 V *vs.* Ag/AgCl from other species relevant to the planned vanadium(V)/neptunium(VI) metal ion reduction studies was to be checked for. Cyclic Voltammograms of 25 mmol dm^3 V(IV) as VO^{2+} on glassy carbon, shown in Figure 3-14, appeared to show no oxidation peaks in the vicinity of ~+1 V where the onset of V(IV) oxidation might be expected to occur, as was seen previously in the analogous data recorded on Pt and Au electrodes shown in Figure 3-5 and Figure 3-10. Furthermore, the voltammograms showed only marginally increased currents over that of the background 0.5 mol dm^3 HNO_3, again suggesting the absence of any V(IV) oxidation. This is likely due to the metal-oxygen bond formation derived irreversibility of the VO_2^+/VO^{2+} couple making both the oxidation and reduction reactions difficult to occur on a GC electrode.

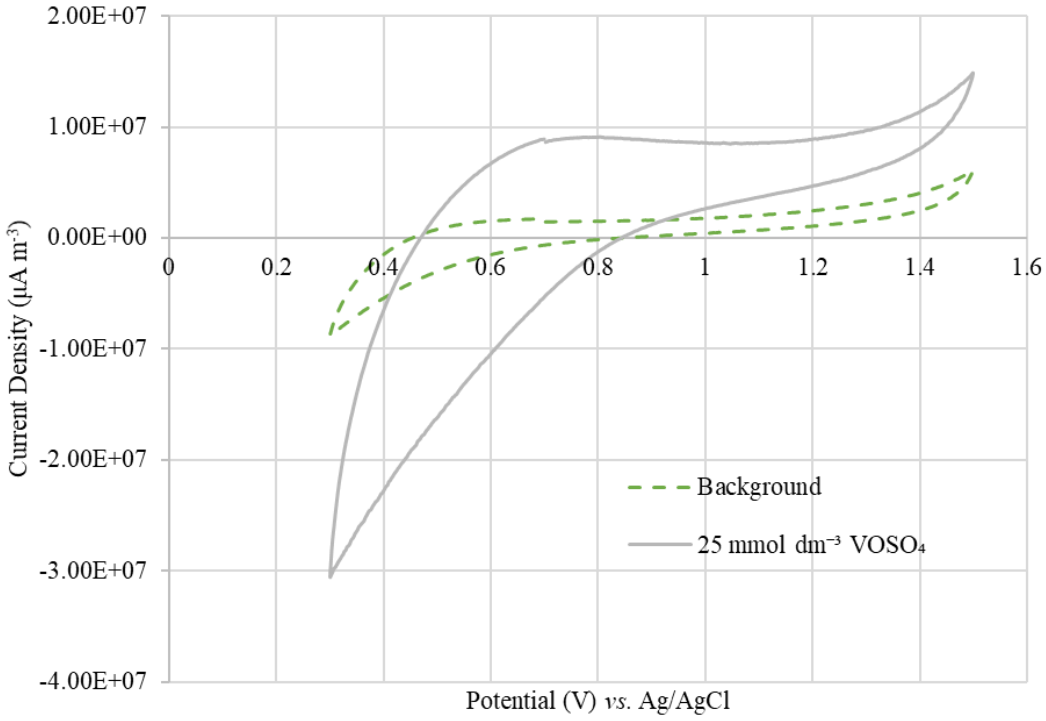

Figure 3-14 CVs of 25 mmol dm^{-3} V(IV) in 0.5 mol dm^{-3} HNO_3 on GC (250 µm diameter) showing the final scan only for clarity. Scan rate = 100 mV s^{-1}.

Amperometric measurement, and hence quantification, of nitrous acid in the presence of V(IV) would therefore again be possible due to the absence of an observed V(IV) oxidation peak allowing measured currents to be solely due to the oxidation of nitrous acid and not due to the oxidation of any vanadium present.

3.2.3.3 Neptunium Response

In behaviour similar to that seen for the oxidation of V(IV) immediately above, cyclic voltammograms of 1.65 mmol dm^{-3} NpO_2^+ on glassy carbon showed only slightly increased currents over that of the background 0.5 mol dm^{-3} HNO_3, Figure 3-15, with no obvious peak associated with Np(V) oxidation. This is consistent with previously seen absence of neptunium redox processes on glassy carbon as mentioned in Chatterjee *et al*.[150] The increases in currents for the neptunium CV when compared to background can be attributed to the increase in ionic strength of the solution.[142]

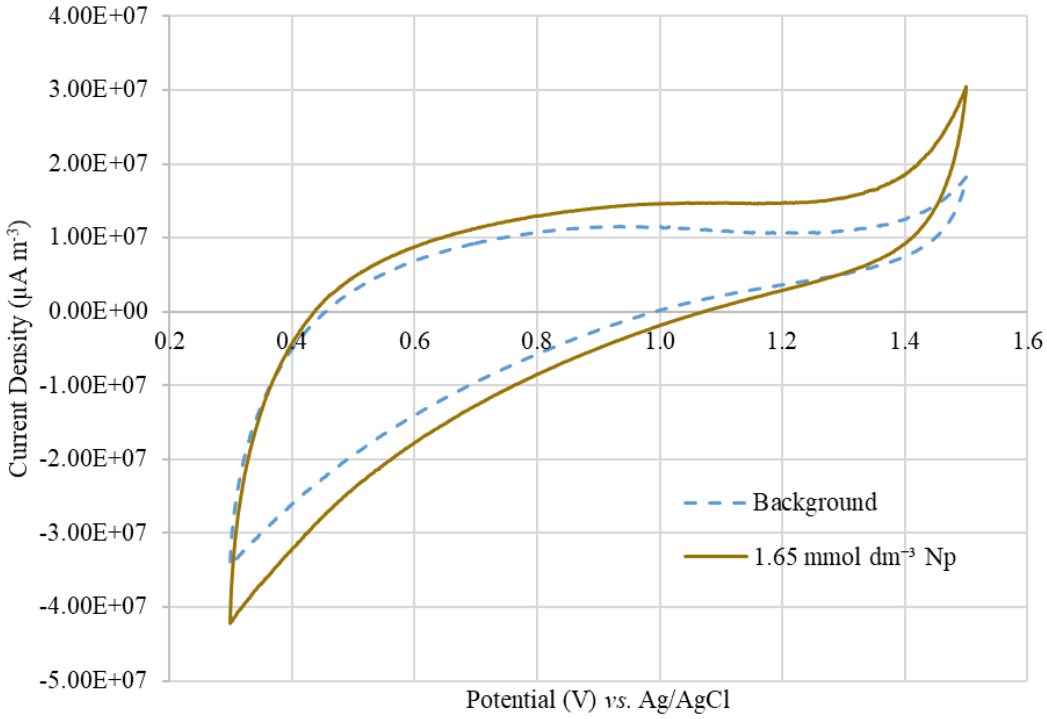

Figure 3-15 CVs of 1.65 mmol dm^{-3} Np(V) in 0.5 mol dm^{-3} HNO_3 on Glassy Carbon (1 mm diameter) showing the final scan only for clarity. Scan rate = 100 mV s^{-1}.

The use of glassy carbon as an electrode material for the quantification of nitrous acid in the presence of vanadium or neptunium has therefore been seen to be feasible due to the absence of a current from either vanadium or neptunium, whilst showing good linear dependence of measured current on the concentration of nitrous acid. However, whilst increased current responses on glassy carbon compared to Au result in improved limits of detection, the physical size of glassy carbon electrodes used here made them unsuitable for use within the small-scale neptunium reduction studies to be performed within this work. Resolving this issue through use of smaller glassy carbon microelectrodes was not possible due to these not being commercially available at the time, with glassy carbon microelectrode arrays only recently being seen in the literature.[153-155] Likewise, scaling up of the neptunium reduction experiments to resolve this issue was also not possible for reasons of radiological safety and to limit operator exposure. Therefore, the use of UV-vis spectroscopy was also examined in order to determine if this could provide a more suitable method for the detection and quantification of the various species present in the experiments to be performed.

3.2.4 Spectroscopic Measurements

Given the radiological safety-derived difficulties associated with implementing electrochemical detection in Np-bearing samples, the use of UV-vis spectrometry was examined as an alternate method for the quantification of nitrous acid, as well as other key species present, i.e. V and Np, for the purposes of monitoring subsequent reduction reactions of V(V) and Np(VI). For this, UV-vis spectra were taken of HNO_2, V(IV), V(V), and Np(V) in 0.5 mol dm^{-3} nitric acid, Figure 3-16 to Figure 3-19 respectively. Spectra of the different species were done over a range of concentrations applicable to those for which the reduction experiments would be conducted, in order to obtain attenuation coefficients for each of the species by creating Beer-Lambert plots, Figure 2-6 to Figure 2-8, whilst it should be noted that in the cases of Figure 3-16 and Figure 3-18 absorbances above approximately 1.5 were not used for analysis due to possible deviation from linearity seen. These plots, along with the calculated attenuation coefficient values and their compared literature values are given in Table 2-1 in Section 2.3.

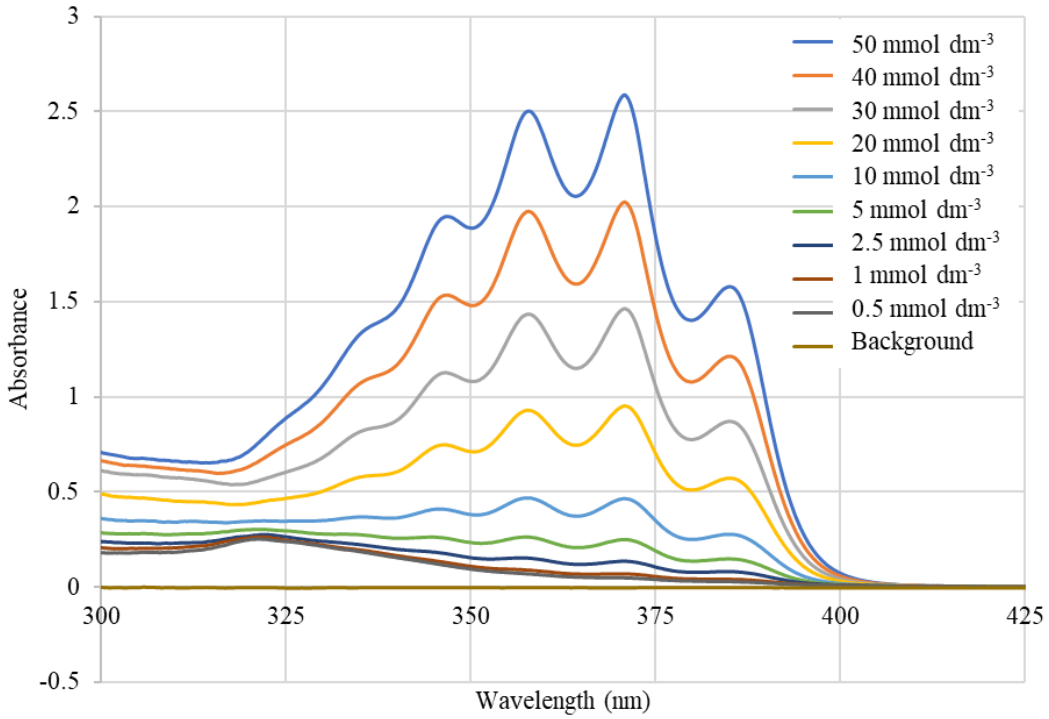

Figure 3-16 UV-vis spectra of varying concentrations of nitrous acid in 0.5 mol dm^{-3} HNO_3.

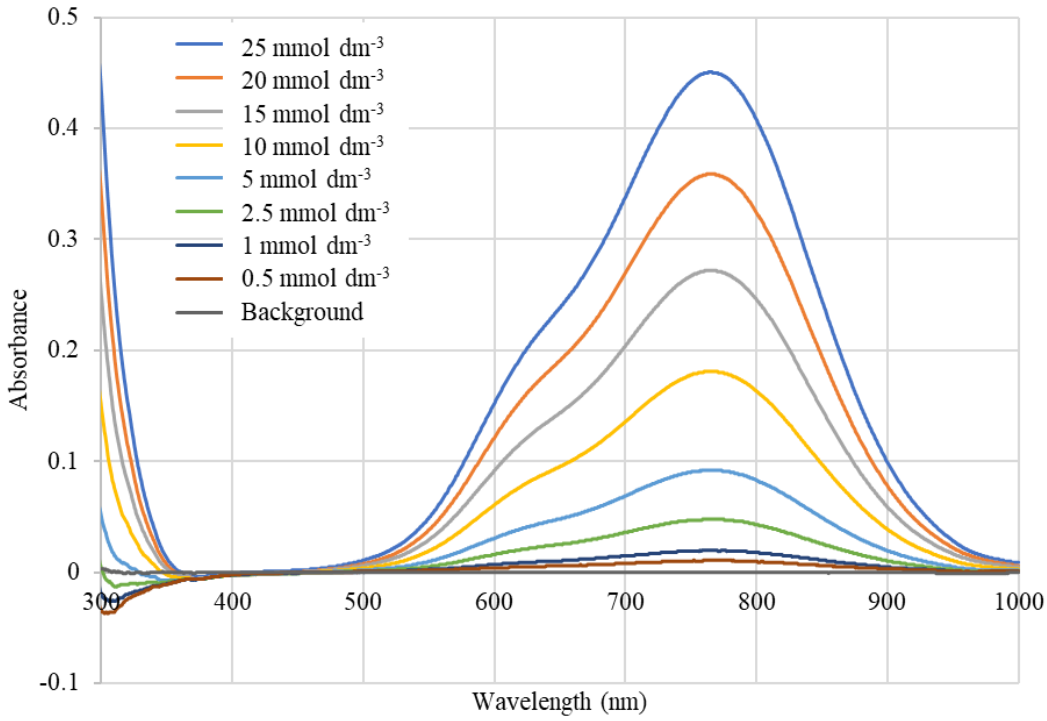

Figure 3-17 UV-vis spectra of varying concentrations of V(IV) in 0.5 mol dm^{-3} HNO_3.

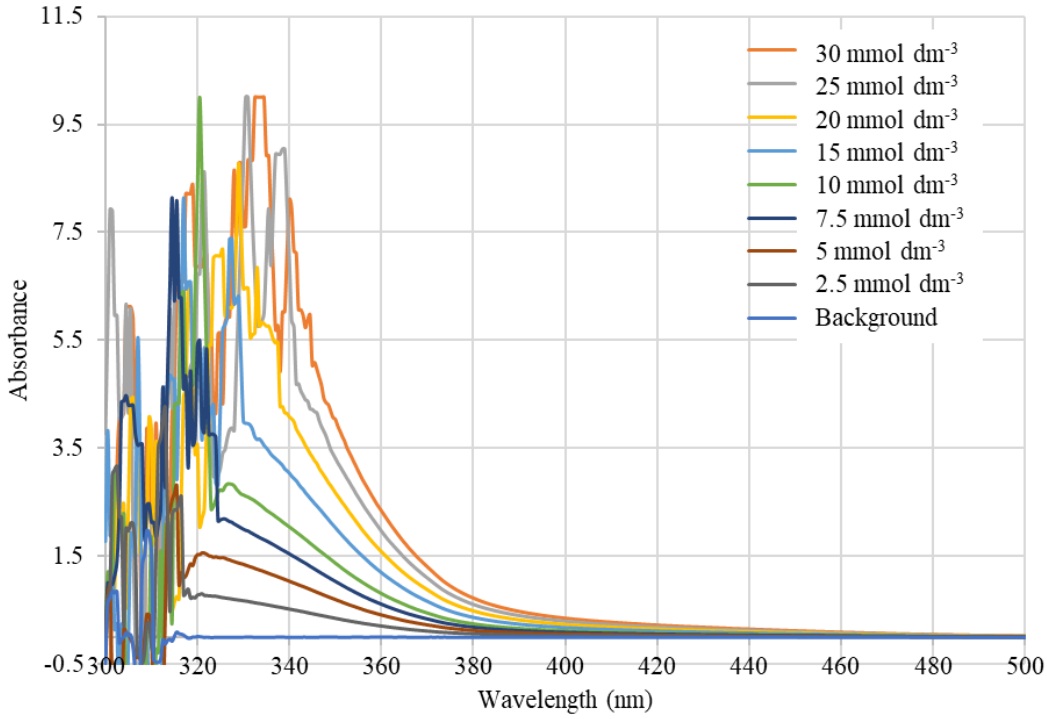

Figure 3-18 UV-vis spectra of varying concentrations of V(V) in 0.5 mol dm^{-3} HNO_3.

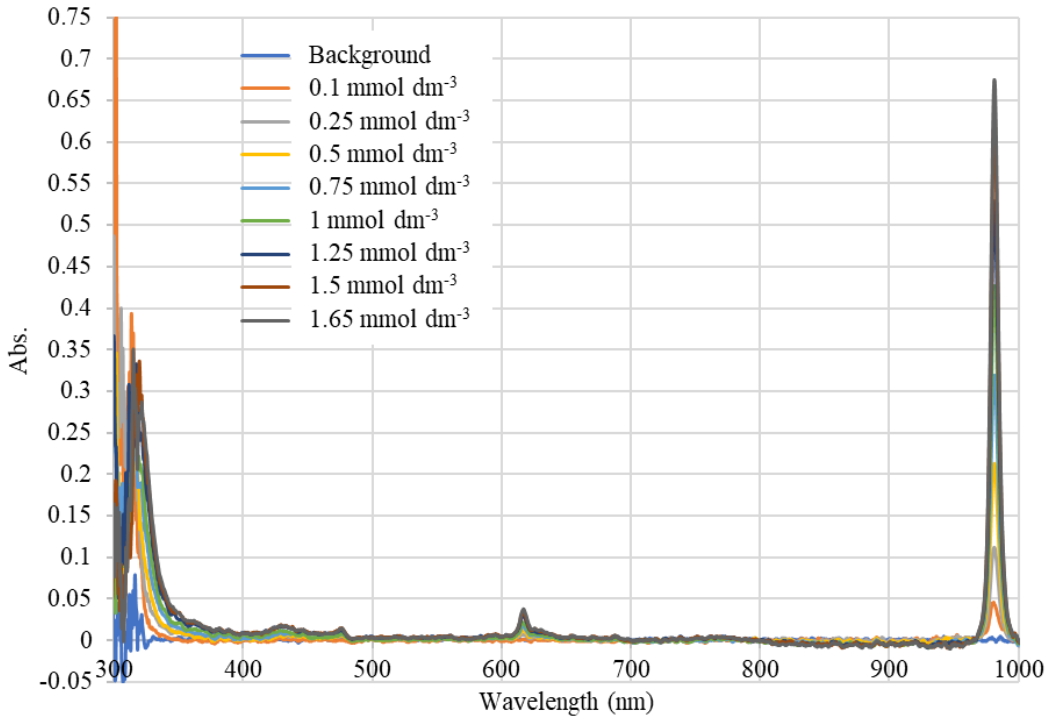

Figure 3-19 UV-vis spectra of varying concentrations of Np(V) in 0.5 mol dm^{-3} HNO_3.

Due to the strong absorbance band seen for Np(V) at 981 nm allowing for quantification of Np(V) in the sub-millimolar range, and hence providing better limits of detection than those seen above for electrochemical methods, it was decided that UV-vis spectroscopy of Np(V) would be used to monitor the progress of the performed Np(VI) reduction reactions. Whilst in principle the absorbance band for Np(VI) seen at wavelengths below 450 nm could also be used for the monitoring of the reduction reactions to be performed,[156] the strong Np(V) absorbance peak and the overlap of the Np(VI) peak with that of nitrous acid meant that quantification of the different Np species would be done using the absorbance seen at 981 nm.

Due to the Np(VI) reduction reactions being monitored by UV-vis spectroscopy, spectroscopic quantification of V by the same method would also need to be utilised in developing the method using a non-active surrogate. However, one potential issue with the use of UV-vis as a detection method of nitrous acid in the presence of vanadium could be seen due to the absorbance

wavelengths of the nitrous acid and the V(V) overlapping. However, due to the position of the V(IV) absorbance peaks being separate, the concentration of V(IV) could be determined, and this could be used, along with the known total V concentration, to determine the concentration of V(V) and hence HNO_2. More details of these calculations are given in Section 2.3.

By performing the above-described deconvolution of the nitrous/vanadium spectral signals to determine concentrations of HNO_2, V(IV), and V(V), UV-vis spectroscopy could therefore be used for the quantification of nitrous acid in the presence of either vanadium or neptunium ions. Limits of detection on the order of millimolar concentrations were seen, similar to those obtained for the electrochemical methods explored above, were obtained. Since UV-vis spectroscopy could also be deployed for the quantification of the metal oxidation states present (i.e. V(V) and V(IV) in the non-active method development studies and Np(V) in the active work), it was decided that this method would be used over electrochemical methods for the quantification of nitrous acid with the vanadium/neptunium reduction reactions to be performed.

3.3 Chapter Summary

The development of an electrochemical sensor has been seen to be feasible using either gold or glassy carbon as an electrode material due to the different position of the Np and HNO_2 current peaks on gold and due to the absence of a current response for Np on glassy carbon. The limit of detection obtainable by using an electrochemical method could also be improved by increasing the electrode area, however, this was impractical for the neptunium reduction experiments which were to be done within small volume reaction vessels for radiological safety reasons. Therefore, the achievable limits of detection of the two quantification methods explored above means that the use of UV-vis is much more practical and reliable method to sense nitrous acid at the concentrations within this study. For this reason, and since UV-vis spectroscopy is to be utilised for quantification of the different metal oxidation states present anyway, for future reduction experiments concentrations of nitrous acid were determined by UV-vis, with any overlapping species being considered by the subtraction of their calculated absorbance – as detailed in Section 2.3.

As discussed at the end of Section 3.1.2, the onset of NO oxidation occurs at a potential at which the reduction of either Np(VI) or V(V) would be thermodynamically viable, highlighting the feasibility of direct reduction of Np(VI) and V(V) by NO and suggesting work could be started to look at both the reduction of vanadium and neptunium by nitric oxide. For the purposes of method development and in order to assess the validity of using vanadium as a neptunium analogue, initial experiments were to be done looking at the reduction of V(V) by both HNO_2 and by NO.

4 Vanadium as a Neptunium Analogue

4.1 Nitrous Acid-Driven Reduction of Vanadium(V)

As a means through which to minimise the radiological exposure associated with radioactive neptunium, vanadium(V) was used as a suitable non-active Np(VI) analogue for the investigation of its reduction by nitrogen oxide species. In the first instance, we focused on determining how well the V(V)/HNO_2 system serves as an analogue for the well characterised Np(VI)/HNO_2 system[88], as a means to establish the suitability of V(V) as an analogue in wider studies of the reduction of Np(VI) by nitrogen-oxygen containing species. Studies were then extended to the V(V)/NO system in order in investigate, through this surrogate system, the role of NO in the reduction of Np(VI) to Np(V), and hence the speciation of neptunium, within the context of nuclear fuel reprocessing.

4.1.1 Reaction Order with Respect to V(V)

Reaction orders were determined by the method of initial rates wherein the reaction is repeated multiple times under controlled conditions, varying the concentration of one reactant at a time. Accordingly, to determine the order with respect to V(V), reduction reactions were carried out at a range of V(V) concentrations in both 0.1 mol dm^{-3} HNO_3 and 0.1 mol dm^{-3} H_2SO_4, with the initial [HNO_2] kept constant at 30 mmol dm^{-3}. Measured plots of [V(IV)] *vs.* time as a function of the initial [V(V)], given in Appendix C-1, showed that increases in the initial V(V) concentrations were seen to lead to an increase in the initial reaction rate, taken as the first 15 minutes of data points, over which near-linearity is observed. At times longer than 15 minutes the concentration of V(IV) was seen to slowly plateau over the full time for which the reaction was run of up to 15 hours. This observed plateau was either due to full conversion of the vanadium to the +IV oxidation state in the case of reactions performed in sulfuric acid, or due to equilibrium being reached with the competing reoxidation of V(IV) to V(V) in the case of reactions performed in nitric acid. This equilibrium observed in nitric acid is further discussed

in section 4.1.3.3. By plotting the log of the initial rate of V(IV) generation *vs.* the log of the initial V(V) concentration, Figure 4-1, the reaction order could be found with respect to [V(V)] from the gradient.

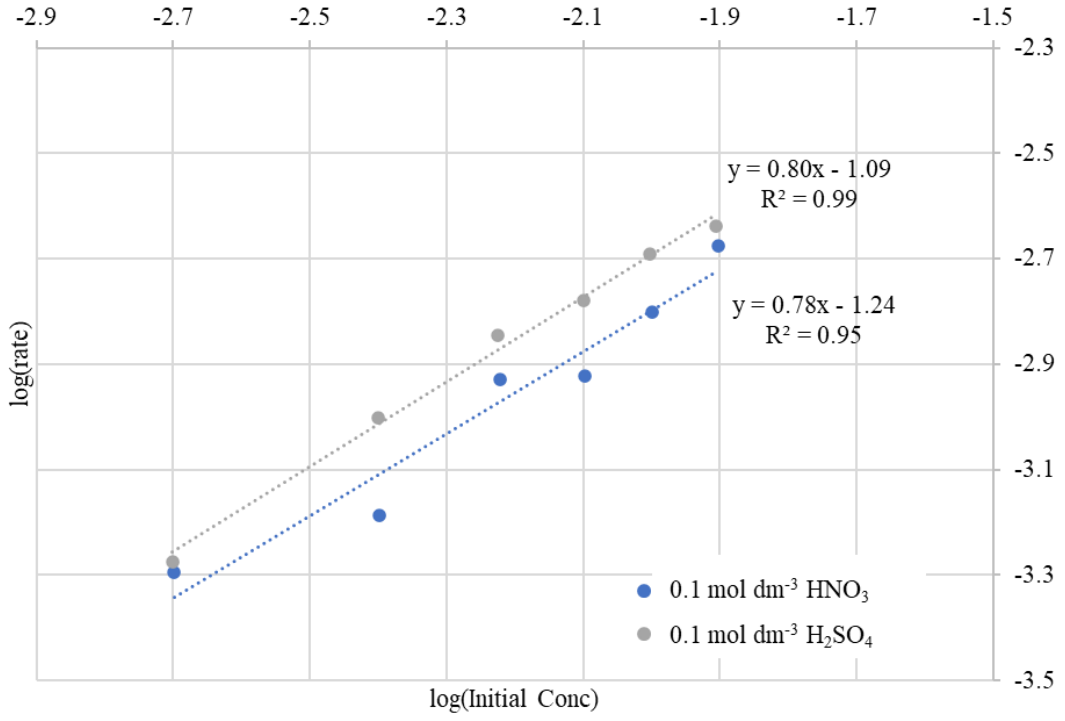

Figure 4-1 Determination of reaction orders with respect to V(V) in HNO_3 and H_2SO_4. (initial conditions: $[HNO_2]$ = 30 mmol dm^{-3}, $[VO_2^+]$ = 2-12.5 mmol dm^{-3})

From this analysis, reaction orders with respect to V(V) were found to be 0.78 and 0.80 in HNO_3 and H_2SO_4 respectively. A possible explanation for the order with respect to V(V) being slightly less than 1 is that, under certain circumstances, vanadium ions in aqueous solution are known to undergo cation-cation interactions.[135-137] However cation-cation interactions, known to occur between V(V) and V(IV) in aqueous solution, are most likely to occur at higher total V concentrations greater than 0.24 mol dm^{-3} and higher acidities with acid concentrations greater than 3 mol dm^{-3}.[135, 157] Neither the total vanadium concentrations nor the acidities employed in the studies reported here exceed these thresholds, suggesting that cation-cation

interactions will not play a role in determining the form of the data shown in Figure 4-1. This conclusion is supported by the shape of the V(IV) peak present in the measured UV-vis spectra (see Figure 2-3), wherein the intensity of slight shoulder peak seen at approximately 625 nm is low compared to the main V(IV) absorbance peak at 770 nm, this being consistent with the literature for that of the mononuclear cation.[136, 137]

Given the closeness of the observed orders with respect to V(V) to unity, these were therefore deemed to be 1, in agreement with that of the order with respect to Np(VI) of 1 derived for both pathways 1 and 2 of the mechanism for Np(VI) reduction by nitrous reported by Precek and Paulenova, see equations 1.45 to 1.54 in Chapter 1, Section 1.2.3.[88] This suggests a similar mechanism may be occurring in the reduction of V(V) by nitrous acid which is further discussed in Section 4.1.5.

4.1.2 Reaction Order with Respect to HNO_2

Reduction reactions were also performed at varying HNO_2 concentration in 0.1 mol dm^{-3} HNO_3 and 0.1 mol dm^{-3} H_2SO_4, with initial V(V) concentration kept constant at 15 mmol dm^{-3}, in order to determine the order of reaction with respect to nitrous acid. Measured plots of [V(IV)] *vs.* time as a function of the initial [HNO_2], given in Appendix C-2, showed that these again showed an increase in the initial reaction rate along with an increase in the initial HNO_2 concentration. As per Figure 4-1, plots of log(initial rate) *vs.* log([HNO_2]) were constructed as shown in Figure 4-2 and orders determined from the slopes of the resultant regression lines.

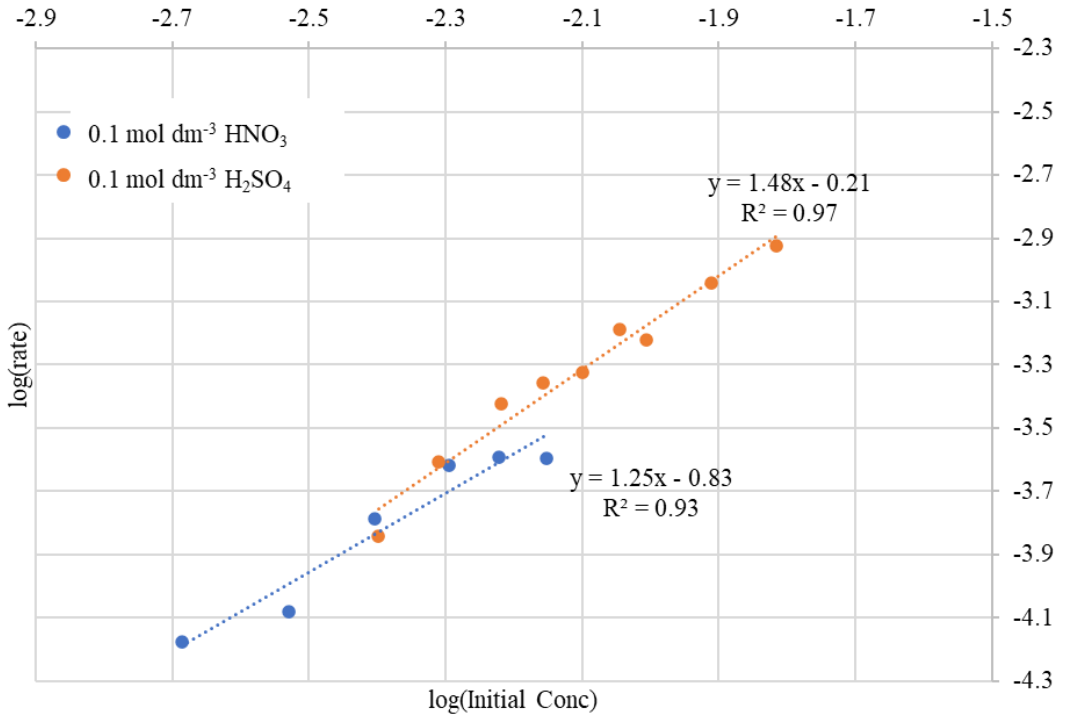

Figure 4-2 Determination of reaction orders with respect to HNO_2 in HNO_3 and H_2SO_4. (initial conditions: $[VO_2^+]$ = 15 mmol dm^{-3}; $[HNO_2]$ = 2-15 mmol dm^{-3})

The reaction order for the reduction of V(V) with respect to HNO_2 concentration across the range of 2 to 7 mmol dm^{-3} in 0.1 mol dm^{-3} HNO_3 was determined to be 1.25. This observation is in good agreement with the value of 1.2 reported with respect to HNO_2 concentration in the reduction of Np by HNO_2 in HNO_3 by Precek and Paulenova[88] – a result that they attribute to the existence of two parallel pathways for the reduction of Np(VI), one involving reduction by HNO_2 directly and a second involving NO as a product of the disproportionation of HNO_2, see equations 1.45 to 1.54 in Chapter 1, Section 1.2.3. This will be discussed in detail in Section 4.1.5. However it bears mentioning here that, once again, the agreement between the reaction orders with respect to HNO_2 for the reduction of V(V) by nitrous acid reported here with that reported by Precek and Paulenova for Np(VI) reduction by nitrous acid suggests similar mechanisms operates in both the V and Np systems. However, the order of 1.48 obtained in Figure 4-2 from the data recorded in H_2SO_4 indicates a different balance between the two

parallel pathways from that which is obtained in HNO_3 and this will also be discussed further in Section 4.1.5.2.

4.1.3 Effect of Varying H^+ and NO_3^- Concentrations

4.1.3.1 Reaction Order with Respect to H^+ and NO_3^-

The reaction order with respect to the dissociation products of HNO_3, H^+ and NO_3^-, were also determined using the method of initial rates, Figure 4-3. This was done by varying H^+ or NO_3^- concentration independently, using KNO_3 as a source of nitrate ions and $HClO_4$ as a source of H^+ ions. Measured plots of [V(IV)] *vs.* time as a function of the either the initial $[H^+]$ or initial $[NO_3^-]$ are given in Appendix C-3.

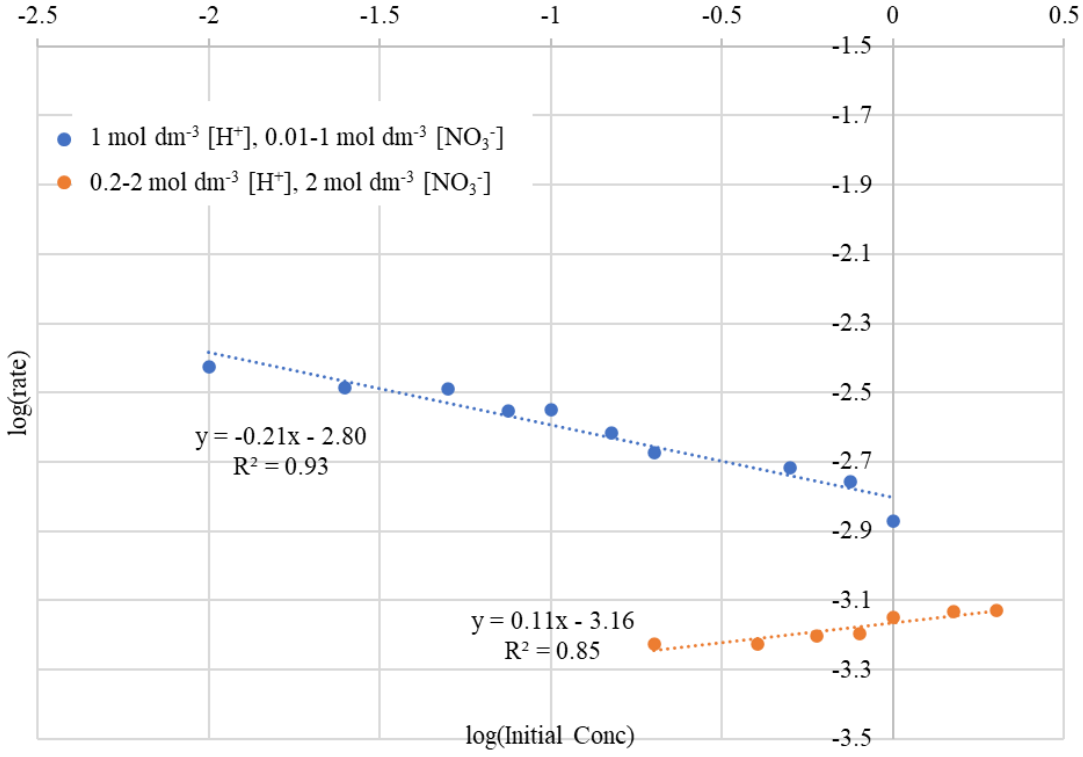

Figure 4-3 Determination of reaction orders with respect to H^+ in a solution of KNO_3 and NO_3^- in a perchloric acid solution. (initial conditions: $[VO_2^+] = 12.5$ mmol dm^{-3}, $[HNO_2] = 30$ mmol dm^{-3}).

For reactions performed at $[H^+] < 75$ mmol dm^{-3}, reduction of V(V) was not seen to occur and are hence not shown in the plot of Figure 4-3. The reasoning for the reaction not occurring at lower $[H^+]$/higher pH will be discussed in the next section, Section 4.1.3.2.

From this analysis, the dependencies of the rate of reaction on these species were seen to be small and close to an observed zero order. This is in contrast to the rate of reaction for the reduction of Np(VI) reported by Precek and Paulenova which shows an inverse dependence on $[H^+]$, see equation 1.44 in Chapter 1, Section 1.2.3.[88] However, through the use of subsequent modelling work, described in detail in Section 4.1.6, and through examination of the half equation for the reduction of V(V) to V(IV), the difference in the observed reaction order for $[H^+]$ in the reduction of V(V) by nitrous acid can be reconciled with that for the reduction of Np(VI) by nitrous acid reported by Precek and Paulenova.[88] This change in dependence on $[H^+]$ is proposed to be due initial protonation of the vanadyl ion, and a change in the validity of assumptions made in calculating the rate equation in different acidic media and is explained further in Section 4.1.5.

4.1.3.2 Observed Absence of Reaction at Low Acidity

During the experiments performed as part of the last section, Section 4.1.3.1, it was noted that V(V) reduction did not occur at $[H^+] < 75$ mmol dm^{-3}. This is likely due to the decrease in the formal potential of the VO_2^+/VO^{2+} couple with decreasing pH, a known phenomenon within the literature.[158] This causes the value of the formal potential for the reduction of VO_2^+/VO^{2+} couple to fall below that of the HNO_2 half equation at sufficiently low $[H^+]$ making the reaction no longer thermodynamically viable. Using the Nernst equation, equation 4.1,[142] along with the potential values at pH = 0 in Figure 1-8, the formal potential of the VO_2^+/VO^{2+} couple can be recalculated at a pH of 1.13 which corresponds with $[H^+] = 75$ mmol dm^{-3}. These calculations, which can be seen in equations 4.2 to 4.12, result in the new formal potential at a pH of 1.13 to be 0.87 V, having shifted from the literature given value of 1 V.

$$E = E^0 + \frac{RT}{nF} ln\left(\frac{C_{Ox}}{C_{Red}}\right) \quad 4.1$$

$$E = E^0 + \frac{RT}{nF} ln\left(\frac{[VO_2^+][H^+]^2}{[VO^{2+}]}\right) \quad 4.2$$

$$E = E^0 + \frac{RT}{nF}\left(ln\left(\frac{[VO_2^+]}{[VO^{2+}]}\right) + ln[H^+]^2\right) \quad 4.3$$

$$E = E^0 + \frac{RT}{nF}\left(ln\left(\frac{[VO_2^+]}{[VO^{2+}]}\right) + 2.303 \times log[H^+]^2\right) \quad 4.4$$

$$E = E^0 + \frac{RT}{nF}\left(ln\left(\frac{[VO_2^+]}{[VO^{2+}]}\right) + 2.303 \times 2 \times pH\right) \quad 4.5$$

Since we are looking at how E changes with a change in pH;

$$E = E^0 + \frac{RT}{nF}\left(ln\left(\frac{[VO_2^+]}{[VO^{2+}]}\right) + 2.303 \times 2 \times \Delta pH\right) \quad 4.6$$

$$E = E^0 + \frac{RT}{nF}\left(ln\left(\frac{[VO_2^+]}{[VO^{2+}]}\right) + 2.303 \times 2 \times (pH_{old} - pH_{new})\right) \quad 4.7$$

$$E = E^0 + \frac{RT}{nF}\left(ln\left(\frac{[VO_2^+]}{[VO^{2+}]}\right) + ln[H^+]_{old}^2 - 2.303 \times 2 \times pH_{new}\right) \quad 4.8$$

$$E = E^0 + \frac{RT}{nF} ln\left(\frac{[VO_2^+][H^+]_{old}^2}{[VO^{2+}]}\right) - 0.059 \times 2 \times pH_{new} \quad 4.9$$

Since given reduction potential is 1 V;

$$E^0 + \frac{RT}{nF} ln\left(\frac{[VO_2^+][H^+]_{old}^2}{[VO^{2+}]}\right) = 1 \quad 4.10$$

Therefore;

$$E = 1 - 0.118 \times 1.13 \quad 4.11$$

$$E = 0.87 \quad 4.12$$

This newly calculated formal potential of 0.87 V is approximately 130 mV lower than that of the value shown in Figure 1-8 and below that of the HNO_2 reduction potential of 0.895 V, as also seen in Figure 1-8. Thus, the apparent stopping of the reduction reaction at proton concentrations < 75 mmol dm^{-3} can be explained by a shift in the formal potential of the VO_2^+/VO^{2+} couple to a value that results in the reduction by HNO_2 being thermodynamically non-viable.

4.1.3.3 Effect of Nitrate Concentration on Percentage Conversion

As Np(V) has also been seen to undergo nitrous acid catalysed oxidation to Np(VI) in nitric acid media, Section 1.2.2, the effect of the possible nitrous acid catalysed re-oxidation of V(IV) to V(V) in nitric acid on the percentage conversion of V(V) to V(IV) during the reduction of V(V) by nitrous acid was also to be investigated. For this purpose, data from initial rate experiments which were performed as part of Section 4.1.3.1 wherein reduction of V(V) were performed in varying $[NO_3^-]$, were analysed further to look at the effect of $[NO_3^-]$ on the percentage conversion of V(V) to V(IV) observed at long reaction times – not just the first 15 minutes. Percentage conversions were analysed at reaction times of 7 hours, after which time the concentration of V(IV) was seen to be invariant with time indicating that equilibrium had been obtained. The results of this analysis are shown in Figure 4-4 as a plot of the percentage conversion of V(V) to V(IV) *vs.* the nitrate ion concentration.

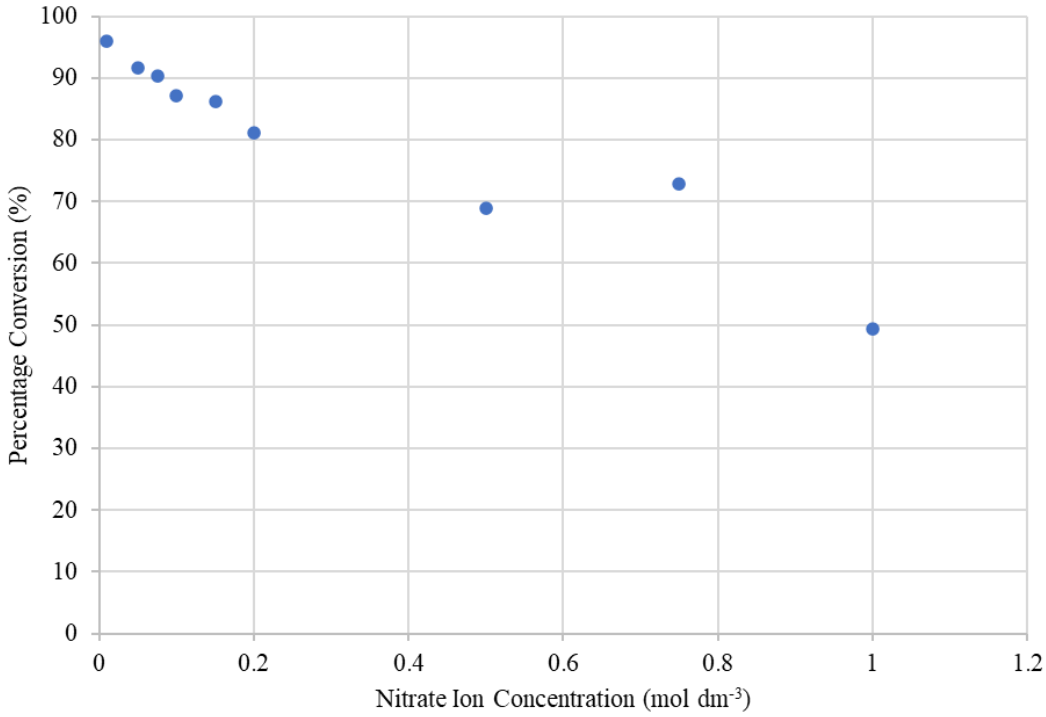

Figure 4-4 Change in percentage conversion of V(V) to V(IV) in the presence of varying concentrations of nitrate ion. (initial conditions: [VO_2^+] = 12.5 mmol dm^{-3}, [HNO_2] = 30 mmol dm^{-3}, [H^+] = 1 mol dm^{-3}).

From this we can see that the percentage conversion at equilibrium decreases with increasing [NO_3^-], with the vanadium seen to reach chemical equilibrium at approximately 50% conversion to the VO^{2+} in 1 mol dm^{-3} NO_3^-. In contrast to this, the experiments conducted in sulphuric acid as part of Sections 4.1.1 and 4.1.2, i.e. in the absence of any deliberately added nitrate, were seen to undergo complete stoichiometric conversion of V(IV) to V(V).

4.1.4 Reaction orders with respect to SO_4^{2-} and ClO_4^-

Reaction orders with respect to, and hence the effect of, SO_4^{2-}, and ClO_4^- concentrations on the reduction of V(V) by HNO_2 were again found from the slopes of plots of the log of the initial rate of V(IV) generation *vs.* the log of the initial V(V) concentration, Figure 4-5. Measured plots of [V(IV)] *vs.* time as a function of the either the initial [SO_4^{2-}] or initial [ClO_4^-] are given in Appendix C-4. Varying the initial concentration each of anions was seen to have minimal

effect on the initial reaction rate. From these plots we can see that the orders with respect to $[SO_4^{2-}]$, or $[ClO_4^-]$ are approximately 0.10, and 0.06 respectively. These are sufficiently small when compared to the other orders of reaction seen for the species studied that they can both be assumed to be zero order. Therefore, these species will have negligible direct involvement in the mechanism of reaction.

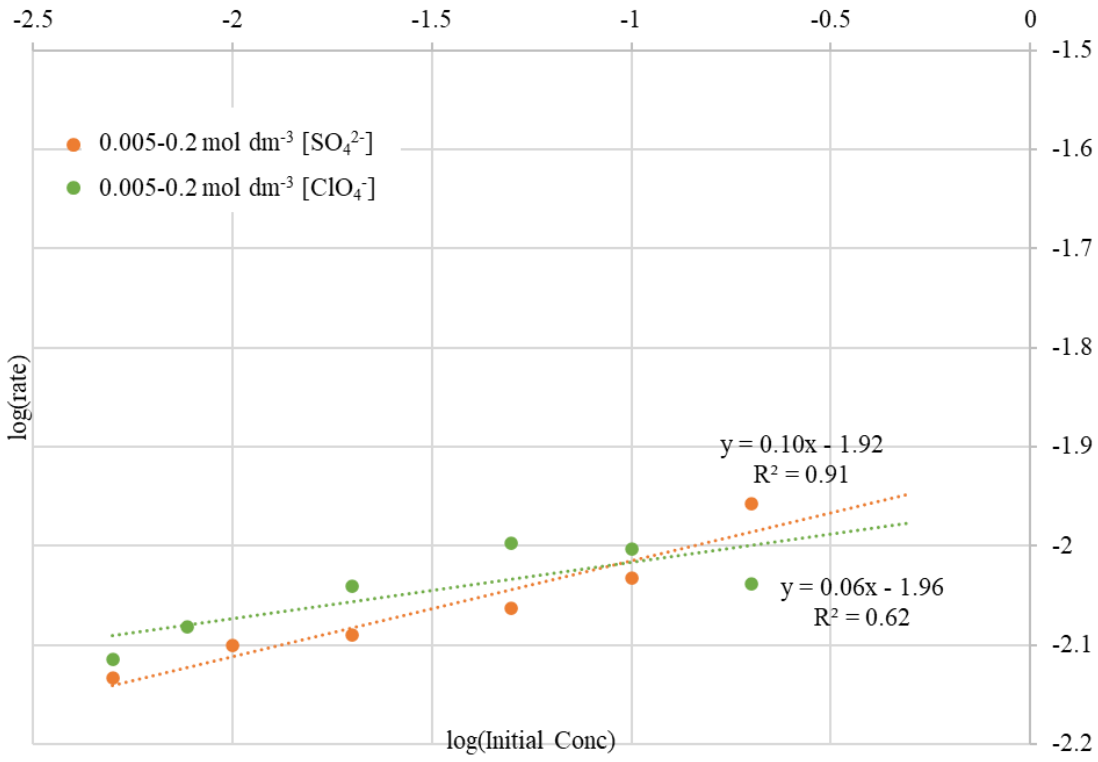

Figure 4-5 Determination of reaction orders with respect to SO_4^{2-} and ClO_4^-. (initial conditions: $[VO_2^+]$ = 12.5 mmol dm^{-3}, $[HNO_2]$ = 30 mmol dm^{-3}, $[H^+]$ = 1 mol dm^{-3}).

4.1.5 Discussion on the Mechanism of Reaction

4.1.5.1 Nitric Acid

As previously detailed in Section 1.2.3, Precek and Paulenova have reported the rate equation for the reduction of Np(VI) by HNO_2 in nitric acid to be given by equation 4.13 below.[88] From this and the similarities in reaction orders for the V(V)/HNO_2 and Np(VI)/HNO_2 systems noted above, we can deduce a similar form for the rate equation for the reduction of vanadium

in nitric acid, equation 4.14, where k_{Np} is the rate constant for the reduction of Np(VI) by HNO_2 and k_V is the rate constant for the reduction of V(V) by HNO_2.

$$-\frac{d[Np(VI)]}{dt} = [Np(VI)]\left(k_1\frac{[HNO_2]}{[H^+]} + k_2\frac{[HNO_2]^{1.5}}{[H^+]^{0.5}[NO_3^-]^{0.5}}\right) = k_{Np}\frac{[Np(VI)][HNO_2]^{1.2}}{[H^+]} \quad 4.13$$

$$-\frac{d[V(V)]}{dt} = k_V[V(V)][HNO_2]^{1.24} \quad 4.14$$

Using equation 4.14, a value of the overall rate parameter k_V can be calculated from the initial rate data of Figure 4-1. This is found to be $k_V = 5.4 \times 10^{-3}$ $dm^{3.72}$ $mol^{-1.24}$ s^{-1} at 20°C for the V(V)/HNO_2 system. Whilst the rate constants for that of the Np(VI) reduction by HNO_2 and that of the V(V) reduction by HNO_2 cannot be directly compared due to differing units arising from the difference in dependence on $[H^+]$, by taking $[H^+]$ to be 1 mol dm^{-3}, a value for $k_{Np}/[H^+]$ of 0.159 $dm^{3.6}$ $mol^{1.2}$ s^{-1} can be found from the k_{Np} value given by Precek and Paulenova for the analogous Np(VI) reduction.[88] By comparing this value to that calculated for k_V above, we can therefore see that k_V is approximately thirty times smaller than that of $k_{Np}/[H^+]$. This difference is consistent with the timescales for the vanadium experiment which reached a steady state at about a 50% conversion to the VO^{2+} after approximately 7 hours, compared to the neptunium reduction which is reported by Precek and Paulenova to occur over a few minutes.[88] A decrease in the rate of reduction is likely due to the breaking of the metal-oxygen bond associated with the loss of one of the vanadium bonded oxygens occurring during the vanadium reduction from the VO_2^+ ion to the VO^{2+} ion alluded to earlier in Section 1.4; no such loss of axial oxygen occurs in the analogous reduction of NpO_2^{2+} to NpO_2^+.

Based on the similarity between the rate equations for the Np(VI) and V(V) reduction deduced above, most especially the similarity in non-integer partial orders seen with respect to $[HNO_2]$, it is not unreasonable to propose that the reduction of vanadium by nitrous acid occurs *via* a similar two pathway mechanism to that of the reduction of Np(VI) by HNO_2 given in equations

1.45 and 1.46 of Section 1.2.3. Using the mechanism given for the neptunium reduction along with the standard reduction half equations given in Bard *et al*.,[81] the mechanism for the reduction of V(V) by nitrous acid is given as follows in equations 4.15 to 4.17,

Pathway 1:

$$VO_2^+ + NO_2^- + 2H^+ \rightleftharpoons VO^{2+} + NO_2 + H_2O \qquad 4.15$$

Pathway 2:

$$3HNO_2 \rightleftharpoons H^+ + NO_3^- + 2NO + H_2O \qquad 4.16$$

$$VO_2^+ + NO + H^+ \rightleftharpoons VO^{2+} + HNO_2 \qquad 4.17$$

Taken as a single step process, the direct reduction of V(V) by nitrous acid, given by equation 4.15 for pathway 1, gives an expected order of reaction with respect to [H^+] of 1, a result inconsistent with the experimentally determined order of zero indicated by equation 4.14. This suggests that equation 4.15 is the net result of a multi-step process, rather than it being a single step as written. By comparison with the derivation of the rate equation for pathway 1 in the Np(VI)/nitrous system given by equations 1.47 to 1.50 in Chapter 1, the lack of a dependence on [H^+] in equation 4.14 suggests the presence of a fast protonation step/pre-equilibrium preceding the reaction of the deprotonated nitrous with the V(V) centre. This protonation most likely involves initial protonation of one of the oxygens in the VO_2^+ ion, as outlined in equation 4.18, followed by the reduction of the protonated V(V) by the half reaction given by equations 4.19a and 4.20.

$$VO_2^+ + H^+ \rightleftharpoons [V(O)(OH)]^{2+} \quad 4.18$$

$$[V(O)(OH)]^{2+} + e^- \rightleftharpoons [V(O)(OH)]^+ \quad 4.19a$$

$$[V(O)(OH)]^+ + H^+ \rightleftharpoons VO^{2+} + H_2O \quad 4.20$$

This 3 step reaction mechanism for the half reaction describing the reduction of V(V) to V(IV) is supported by previous electrochemical studies on the electroreduction of VO_2^+ which has been shown to proceed *via* a chemical-electrochemical-chemical (CEC) process, in accordance with Gattrell *et al*.[159]

By analogy and replacing the reductant electron in equation 4.19a with NO_2^-, as in equation 4.19b, equation 4.15 and hence pathway 1, can then be seen to proceed as follows.[159, 160]

$$VO_2^+ + H^+ \rightleftharpoons [V(O)(OH)]^{2+} \quad 4.18$$

$$[V(O)(OH)]^{2+} + NO_2^- \rightleftharpoons [[V(O)(OH)]^+ + NO_2 \quad 4.19b$$

$$[V(O)(OH)]^+ + H^+ \rightleftharpoons VO^{2+} + H_2O \quad 4.20$$

If it is then assumed that the rate determining step is equation 4.19b, i.e. the reduction of the protonated vanadium centre by the deprotonated nitrous acid (the latter as per the analogous Np(VI) mechanism) then equation 4.21 may be written and the overall rate equation, written in terms of the initial reactants, derived in accordance with equations 4.21 to 4.25. As can be seen from equation 4.25, this results in a rate equation that is zero order with respect to $[H^+]$ and is consistent with the experimentally derived rate equation given by equation 4.14. The relationship between rate constants k_1 and k_1' can then also be given as in equation 4.26.

$$Rate = k_1[V(O)(OH)^{2+}][NO_2{}^-] \quad 4.21$$

Since; $$K_{HNO2} = \frac{[H^+][NO_2{}^-]}{[HNO_2]} \quad 4.22$$

And; $$K_{protonation} = \frac{[V(O)(OH)^{2+}]}{[VO_2^+][H^+]} \quad 4.23$$

$$Rate = k_1 K_{HNO2} K_{protonation}[VO_2^+][H^+]\frac{[HNO_2]}{[H^+]} \quad 4.24$$

$$Rate = k_1'[VO_2^+][HNO_2] \quad 4.25$$

$$k_1' = k_1 K_{HNO2} K_{protonation} \quad 4.26$$

If an initial protonation is also assumed for pathway 2, the observed zeroth order of reaction with respect to $[H^+]$ can be maintained through writing equation 4.17 as a multi-step process in a similar manner as previously implemented for equation 4.15. This results in the mechanism outlined in equations 4.27 and 4.28. By assuming equation 4.28 to be the rate determining step, we can obtain the rate equation for the pathway 2 as equation 4.29. By using equation 4.23 along with the equilibrium expression for the reaction shown in equation 4.16, given by equation 4.30, we can display the rate equation in the form given in equation 4.31. Given the assumption in nitric acid that $[NO_3^-] = [H^+]$, this can be further simplified to equation 4.32, and thus equation 4.33. The relationship between rate constants k_2 and k_2' can then also be given as in equation 4.34.

$$VO_2{}^+ + H^+ \rightleftharpoons [V(O)(OH)]^{2+} \quad 4.27$$

$$[V(O)(OH)]^{2+} + NO \rightleftharpoons VO^{2+} + HNO_2 \quad 4.28$$

$$Rate = k_2[V(O)(OH)^{2+}][NO] \quad 4.29$$

$$K_{NO} = \frac{[NO]^2[NO_3^-][H^+]}{[HNO_2]^3} \quad 4.30$$

$$Rate = k_2 K_{protonation}[VO_2^+][H^+]\frac{K_{NO}^{0.5}[HNO_2]^{1.5}}{[NO_3^-]^{0.5}[H^+]^{0.5}} \quad 4.31$$

$$Rate = k_2 K_{NO}^{0.5} K_{protonation}[VO_2^+][H^+]\frac{[HNO_2]^{1.5}}{[H^+]} \quad 4.32$$

$$Rate = k_2'[VO_2^+][HNO_2]^{1.5} \quad 4.33$$

$$k_2' = \frac{k_2 K_{protonation} K_{NO}^{0.5}[H^+]}{[NO_3^-]^{0.5}[H^+]^{0.5}} \quad 4.34$$

Therefore, by combining the kinetic expressions given for both pathways 1 and 2, equations 4.25 and 4.33 respectively, we obtain the full kinetic expression for the reduction of V(V) by nitrous acid as equation 4.35. This expression can be seen to be analogous to that given for the Np(VI) reduction by nitrous acid, equation 4.13, and can be seen to account for the orders of reaction for the different species in the observed rate equation, equation 4.14.

$$Rate = [VO_2^+](k_1'[HNO_2] + k_2'[HNO_2]^{1.5}) \quad 4.35$$

4.1.5.2 Non-Nitrogen-Oxygen Based Acids

In the derivation of the kinetic rate law of equation 4.33 for pathway 2 from equation 4.31, it is assumed that $[NO_3^-] = [H^+]$. However, this assumption and subsequent derivation will not hold in the presence of other acidic media such as sulphuric and perchloric acid due to no nitrate being present. Therefore, in experiments performed in sulphuric or perchloric acid such as shown in Figure 4-3, equation 4.31 is instead simplified to give the kinetic expression shown in equation 4.36.

$$Rate = k_2'[VO_2^+][HNO_2]^{1.5}\frac{[H^+]^{0.5}}{[NO_3^-]^{0.5}} \quad 4.36$$

This change in the form of the rate equation for pathway 2 can be used to account for the order with respect to $[H^+]$ deviating from zeroth order (as might be expected if equation 4.33 still held), which was previously seen in Figure 4-3. The observed order of reaction with respect to $[H^+]$ of 0.11 is therefore due to the combination of the theoretical orders of reaction from both pathways 1 and 2, of 0 and 0.5 respectively. Similarly, the observed order of reaction with respect to $[NO_3^-]$ of -0.21 lies between that of the pathways 1 and 2, of 0 and -0.5 respectively. These non-zeroth orders for both $[H^+]$ and $[NO_3^-]$ are further supported by the subsequent modelling work presented in Section 4.1.6 below. Referring forward, this uses an equation of the form of equation 4.36, specifically equation 4.39, as part of a suite of kinetic equations used to calculate theoretical fits to experimental data recorded in both nitric and sulphuric acid. This fitting process shows that the orders of reaction with respect to $[H^+]$ and $[NO_3^-]$ within equation 4.39 that provide the best modelled fit to the experimental data are 0.5 and -0.5 respectively i.e. the orders as given in equation 4.36. We shall return to this point when discussing equation 4.39 upon its introduction in Section 4.1.6 below.

It can also be seen that, for the reduction of V(V) by nitrous acid in non-nitrogen containing acids such as sulphuric or perchloric acid, the order of reaction with respect to nitrous acid is observed to be higher than observed if the reduction is conducted in nitric acid. This can be attributed to the reaction in non-nitrogen containing acids going predominantly *via* pathway 2, outlined in equations 4.16 to 4.17. This pathway would be seen to dominate in non-nitrogen containing acids due to the absence of nitrate ions. For the reductions conducted within nitric acid, the presence of nitrate ions would push the nitrous decomposition equation given by equation 4.16 to the left-hand side, so suppressing the solution concentration of NO. In the absence of nitric acid, this suppression is nearly absent, allowing for the nitrous decomposition reaction of equation 4.16 to proceed freely to the right-hand side resulting in the generation of NO and so increasing the rate of reduction *via* pathway 2.

4.1.6 Modelling work for the Nitrous Acid-Driven Reduction of V(V)

In Section 4.1.3.1, Figure 4-3 it was seen that, based on an initial rate analysis, the experimentally determined orders with respect to $[H^+]$ and $[NO_3^-]$ for the nitrous-driven reduction of V(V) were both near zero, being 0.11 and -0.21 respectively. This result is in contrast to the analogous reaction for Np(VI) for which Paulenova and Precek report an order with respect to $[H^+]$ of -1.[88] The mechanistic analysis of Section 4.1.5, again informed by the initial rate analyses of Figure 4-1 to Figure 4-5, provides a rationale for this difference. In order to test this analysis, modelling of experimental data for the reduction of V(V) by nitrous over the entire timescale of each experiment conducted was performed. This includes data recorded at times beyond the first 15 minutes interrogated by the initial rate method and thus provides additional information with which to test the proposed mechanism of Section 4.1.5.

Modelling of the vanadium/nitrous system was performed by A. Jackson at Lancaster University using MATLAB. The approach used was as follows and is based on the two-pathway mechanism proposed in Section 4.1.5 above, with the full code used shown in Appendix D-1.

Implementing this two-pathway mechanism in our analysis requires that equations 4.15 and 4.17 for pathways 1 and 2 respectively are written as equilibria and thus are each comprised of both the forward and back reactions. Rate equations for these forward and back reactions may then be written for each equilibrium/pathway. For pathway 1, the rate equations 4.37 and 4.38 can be written for the forward and back reactions comprising the equilibrium shown in equation 4.15, where the forward rate equation has been shown to be as in equation 4.25 in Section 4.1.5, with k_{1f} being the rate constant for the forward reaction of pathway 1, k_{1b} being the rate constant for the back reaction of pathway 1.

$$Rate_{1f} = k_{1f}[HNO_2][VO_2^+] \qquad 4.37$$

$$Rate_{1b} = k_{1b}[NO_2][VO^{2+}] \qquad 4.38$$

Similarly, forward and reverse rate equations for pathway 2 can be deduced from the equilibria shown in equations 4.16 and 4.17, with the forward rate equation being that given in equation 4.36 in terms of initial reactants that may be controlled by the experimenter when setting up the experiment. The forward and reverse rate equations can therefore be written as equations 4.39 and 4.40, with k_{2f} being the rate constant for the forward reaction of pathway 2, and k_{2b} being the rate constant for the back reaction of pathway 2.

$$Rate_{2f} = \frac{k_{2f}[HNO_2]^{1.5}[VO_2^+][H^+]^{0.5}}{[NO_3^-]^{0.5}} \quad 4.39$$

$$Rate_{2b} = k_{2b}[VO^{2+}][HNO_2] \quad 4.40$$

Rate equations 4.37 to 4.40 may then be used, along with a rate equation for the loss/decomposition of nitrous acid, equation 4.41, and the discretised time differential equations outlined in equations 4.42 to 4.48, to derive, in MATLAB, calculated fits to the experimental data. By fitting the model to experimental data taken for the reduction of vanadium by nitrous acid in both nitric acid and the non-nitrogen containing acid sulphuric acid, rate constants for both the forward and backward reactions may be found.

$$Rate_{HNO2} = k_{HNO2}[HNO_2] \quad 4.41$$

$$[VO_2^+]_{t+1} = [VO_2^+]_t + t_{step}\left(-Rate_{1f} - Rate_{2f} + Rate_{1b} + Rate_{2b}\right) \quad 4.42$$

$$[VO^{2+}]_{t+1} = [VO^{2+}]_t + t_{step}\left(Rate_{1f} + Rate_{2f} - Rate_{1b} - Rate_{2b}\right) \quad 4.43$$

$$[NO_2]_{t+1} = [NO_2]_t + t_{step}\left(Rate_{1f} - Rate_{1b}\right) \quad 4.44$$

$$[NO]_{t+1} = [NO]_t + t_{step}\left(\frac{2}{3} \times Rate_{HNO2}\right) \quad 4.45$$

$$[HNO_2]_{t+1} = [HNO_2]_t + t_{step}\left(-Rate_{1f} - \frac{1}{2}\times Rate_{2f} + Rate_{1b} + \frac{1}{2}\times Rate_{2b} - Rate_{HNO2}\right) \quad 4.46$$

$$[NO_3^-]_{t+1} = [NO_3^-]_t + t_{step}\left(\frac{1}{3}\times Rate_{HNO2} + \frac{1}{2}\times Rate_{2f} - \frac{1}{2}\times Rate_{2b}\right) \quad 4.47$$

$$[H^+]_{t+1} = [H^+]_t + t_{step}\left(\frac{1}{3}\times Rate_{HNO2} - \frac{1}{2}\times Rate_{2f} + \frac{1}{2}\times Rate_{2b} - Rate_{1f} + Rate_{1b}\right) \quad 4.48$$

All runs were fitted simultaneously, so generating a common set of values for k_{1f}, k_{1b}, k_{2f} and k_{2b}, all of which were allowed to float during all fitting procedure runs. Example best fits for the model to the experimental data for both the nitric acid and sulphuric acid data sets are shown in Figure 4-6 to Figure 4-9, with the full set of fitted data being shown in Appendix D-2. As discussed in Section 2.4, vertical error bars of ±10% associated with each experimental data point are included within these plots to provide an indication of how closely the modelled values fit the experimental data. These best fits were found when the orders of reaction with respect to $[H^+]$ and $[NO_3^-]$ within the kinetic expression for the forward reaction of pathway 2 were the values of 0.5 and -0.5 respectively produced during the derivation of equation 4.39. When combined with kinetic expression for pathway 1 given by equation 4.37, which shows a zero order dependence on both $[H^+]$ and $[NO_3^-]$, the observed orders of 0.11 and -0.21 for $[H^+]$ and $[NO_3^-]$ respectively in Section 4.1.3.1, can be accounted for. The slight difference in the observed order values from zero can therefore be seen to be due to a change in the validity of the assumption that the $[H^+] = [NO_3^-]$ from the nitric acid to the sulphuric acid data sets explored in Section 4.1.5.2.

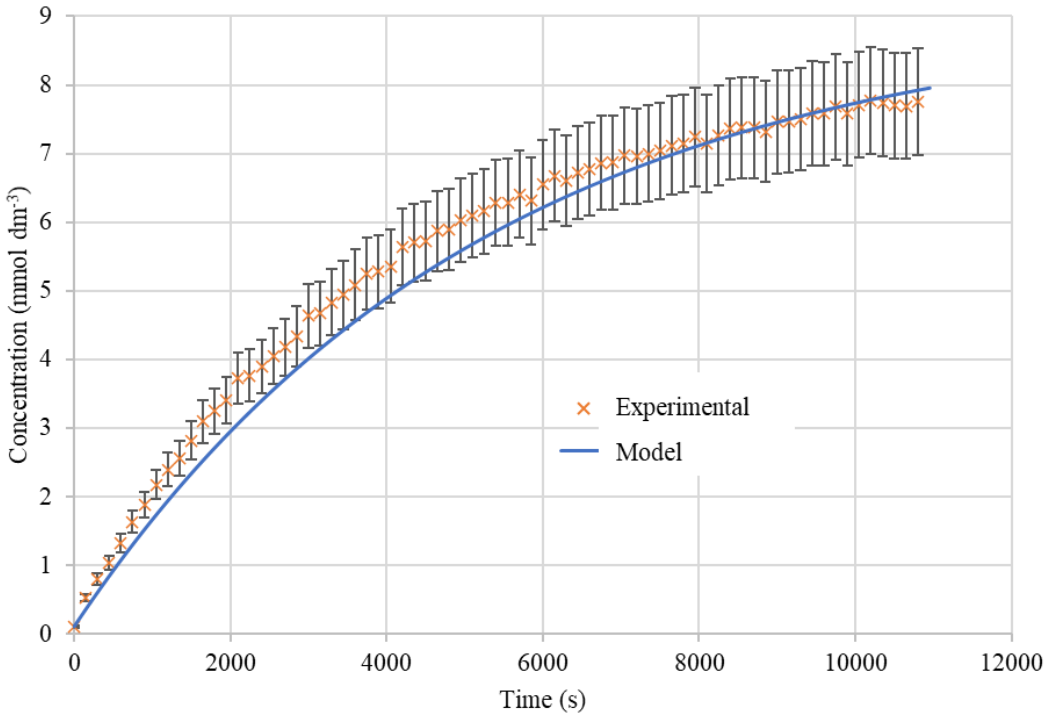

Figure 4-6 Model and experimental V(IV) concentration vs time data in HNO_3. (initial conditions: $[HNO_2]$ = 30 mmol dm^{-3}, $[VO_2^+]$ = 12.5 mmol dm^{-3}; $[HNO_3]$ = 0.1 mol dm^{-3}).

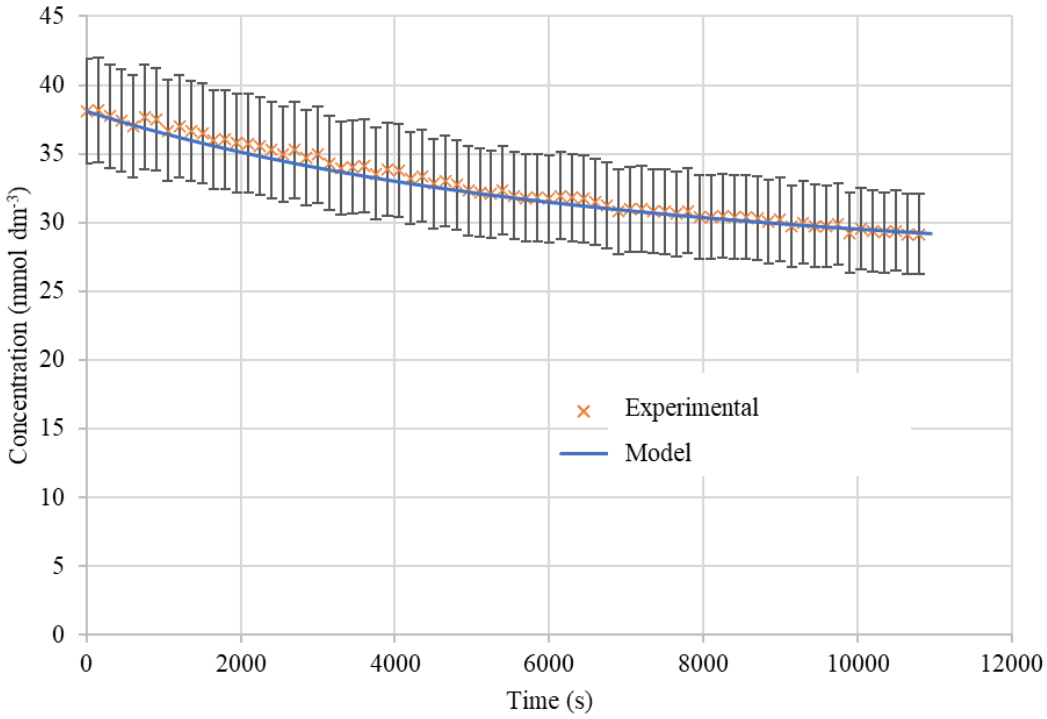

Figure 4-7 Model and experimental HNO_2 concentration vs time data in HNO_3. (initial conditions: $[HNO_2]$ = 30 mmol dm^{-3}, $[VO_2^+]$ = 12.5 mmol dm^{-3}; $[HNO_3]$ = 0.1 mol dm^{-3}).

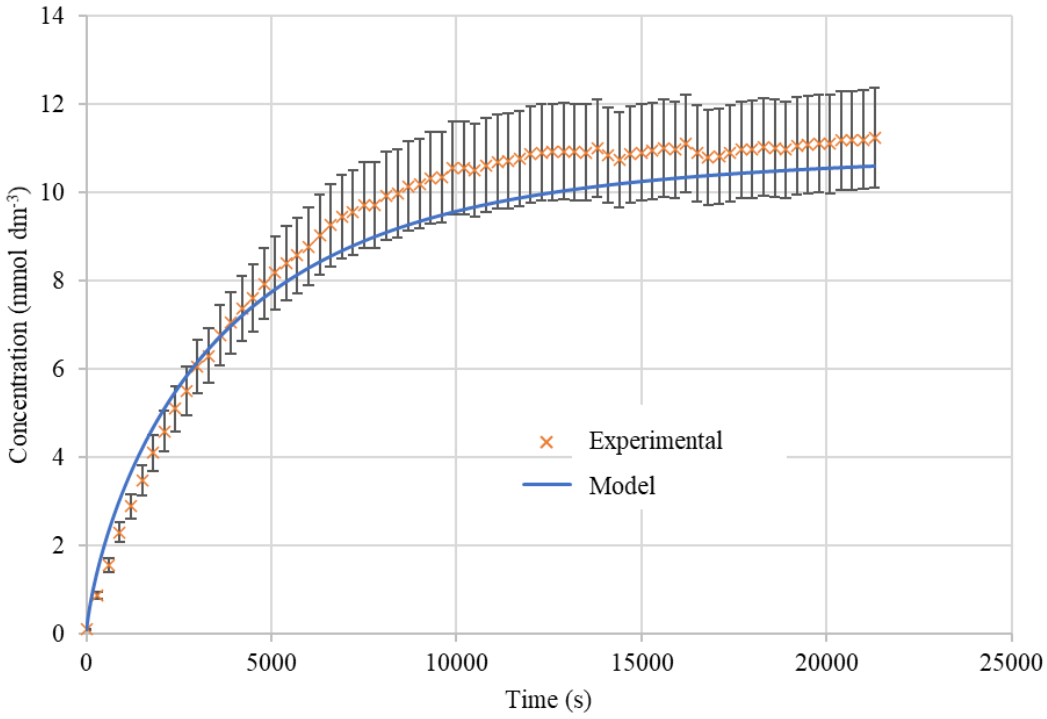

Figure 4-8 Model and experimental V(IV) concentration vs time data in H_2SO_4. (initial conditions: $[HNO_2]$ = 30 mmol dm^{-3}, $[VO_2^+]$ = 12.5 mmol dm^{-3}; $[H_2SO_4]$ = 0.1 mol dm^{-3}).

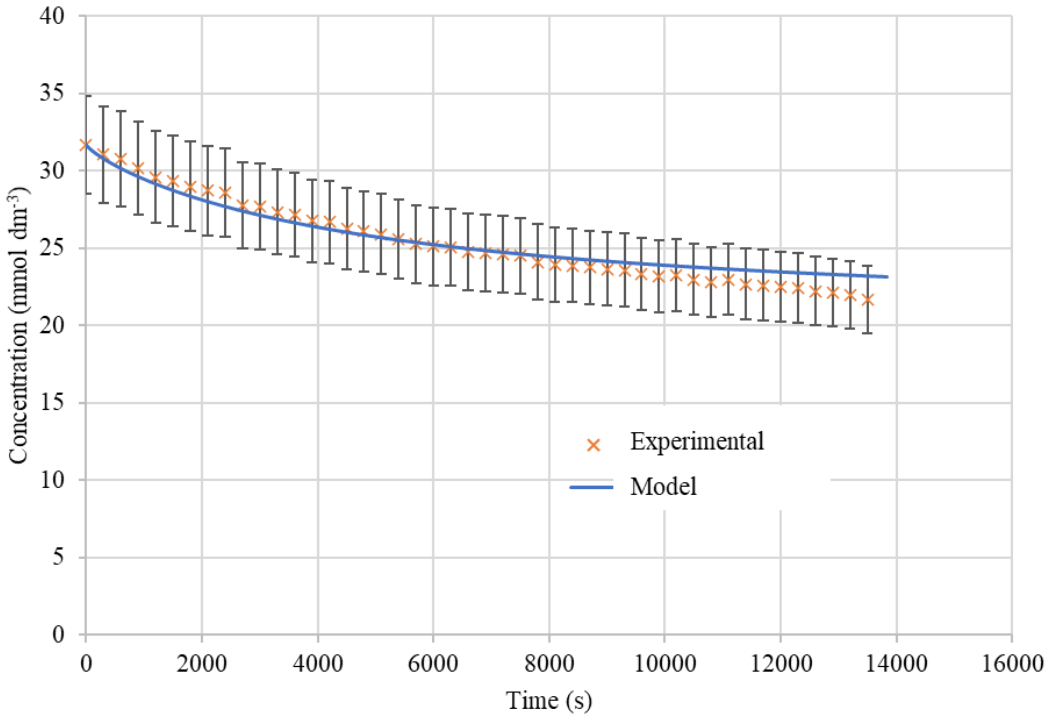

Figure 4-9 Model and experimental HNO_2 concentration vs time data in H_2SO_4. (initial conditions: $[HNO_2]$ = 30 mmol dm^{-3}, $[VO_2^+]$ = 12.5 mmol dm^{-3}; $[H_2SO_4]$ = 0.1 mol dm^{-3}).

The goodness of fit for the modelled V(IV) and HNO_2 concentrations were evaluated across 6 experimental data sets each in both nitric and sulphuric acids – resulting in 24 plots total – using a chi-squared statistical test which compares a calculated chi-squared value to a critical value for a given number of degrees of freedom. If the calculated chi-squared value is below that of the critical value, then there is a high correlation between the two sets of data. These modelled V(IV) and HNO_2 concentrations over time were calculated to have chi-squared values of 38.33 and 90.73 respectively, which are both seen to be below the chi-squared critical value for each concentration dataset of 700.73 taken from standard tabulated values at 800 degrees of freedom when evaluated at a 99.5% confidence level.[161]

From the modelling of the experimental data, rate constants were also found for both the forward and backward aspects of each of the mechanistic pathways. These were found to be as follows; $k_{1f} = 3 \times 10^{-6}$ dm^3 mol^{-1} s^{-1}, $k_{1b} = 5 \times 10^{-6}$ dm^3 mol^{-1} s^{-1}, $k_{2f} = 1 \times 10^{-7}$ dm$^{4.5}$ mol$^{-1.5}$ s^{-1}, and $k_{2b} = 1 \times 10^{-8}$ dm^3 mol^{-1} s^{-1}.

In order to determine whether pathways 1 or 2 will therefore dominate in solutions wherein concentrations of HNO_2 and NO were comparable, rate constants k_1 and k_2, which pertain to the rate equations 4.21 and 4.29 for the actual reacting species and not the initial reactants present, needed to be calculated. At short time intervals the presence of any significant back reaction associated with the rate equations given in 4.38 and 4.40 can be discounted due to the presence of minimal amounts of the VO^{2+} and NO_2 species and the rate constants k_{1f} and k_{2f} can therefore be equated to the rate constants k_1' and k_2' respectively for the rate equations given in equations 4.25 and 4.33. Using the relationships between k_1' and k_2', and k_1 and k_2 given in equations 4.26 and 4.34 respectively, along with values of $K_{HNO2} = 5.62 \times 10^{-4}$ mol dm^{-3} and $K_{NO} = 37.45$ mol dm^{-3} taken from the literature,[162, 163] values were calculated of $k_1K_{protonation} = 5.3 \times 10^{-3}$ dm^6 mol^{-2} s^{-1} and $k_2K_{protonation} = 1.63 \times 10^{-8}$ dm^6 mol^{-2} s^{-1}. From these values it can therefore be seen that the major pathway will be that of the reduction by the dissociated NO_2^- ion, even at comparable NO concentrations. However, it should be noted that, due to the assumptions made in the modelling work performed within this work such as both

reaction pathways going *via* the initial protonation of VO_2^+ and that the back reactions can be discounted at shorter timescales, these values should be taken with caution.

The use of the V(V) reduction as an analogue for the reduction of Np(VI) by nitrous acid in a nitrate medium has been shown to give reaction orders with respect to the concentrations of both V(V) and HNO_2 that are in reasonable agreement with the analogous reaction orders for the reduction of Np(VI) by nitrous acid previously reported by Precek and Paulenova[88] – suggesting that, for this particular reduction, V(V) can serve as a good mechanistic analogue for Np(VI). The rate parameter for the reduction of V(V) by nitrous acid is found to be two orders of magnitude smaller than that for the reduction of Np(VI) by HNO_2, a difference that is attributable to the breaking of the metal-oxygen bond associated with the loss of one of the axial oxygens during the VO_2^+ to VO^{2+} reduction reaction. Thus, the V(V)/HNO_2 system can be considered a good mechanistic, albeit kinetically slower analogue for the Np(VI)/HNO_2 and its use as such should always take account of this limitation. The role of NO in the reduction of Np(VI) to Np(V) can therefore be studied further through the use of the analogous V(V) to V(IV) reduction.

4.2 Nitric Oxide-Driven Reduction of Vanadium(V)

4.2.1 Preliminary Studies of Reduction of Vanadium(V) by Gaseous NO

A series of preliminary experiments were conducted in order to investigate the feasibility of V(V) reduction by NO. These were carried out by simply bubbling NO gas at a rate of 150 mL min^{-1} through a solution of V(V) and monitoring the concentrations of different species by UV-vis, Figure 4-10. Whilst this showed the expected increase in V(IV) and decrease in V(V) absorption peaks, the ingrowth of characteristic HNO_2 peaks were also seen, indicating formation of nitrous acid due to either reaction with the HNO_3 media or as a product of the vanadium reduction as per the pathway 2 reaction given by equation 4.17. It should be noted however that whilst this qualitative analysis of spectra taken gives an approximate indication of the species present, quantitative analysis of the preliminary data taken within this section should be treated with caution where calculation of concentrations has used absorbances above approximately 1.5 due to possible deviation from linearity being seen.

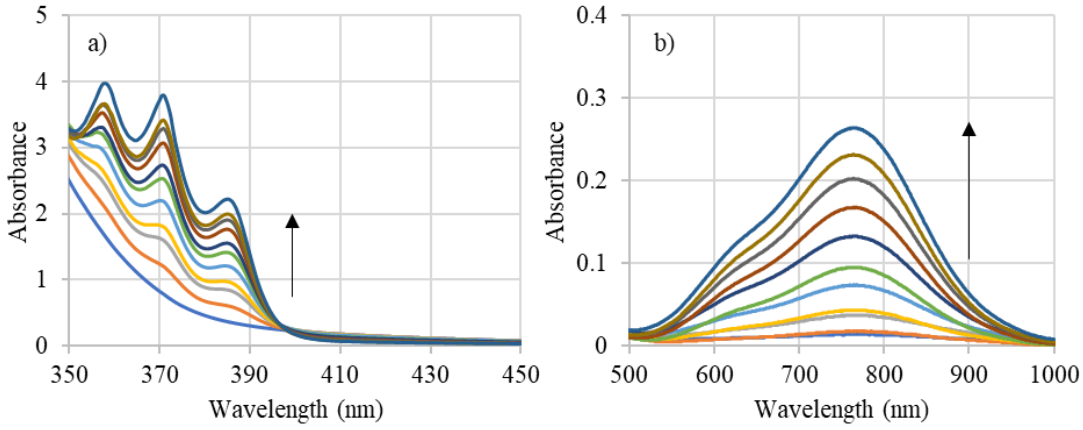

Figure 4-10 UV spectra showing the change in a) V(V) and HNO_2, and b) V(IV) over time.

By plotting the concentration of the V(V), V(IV), and HNO_2 species *vs.* time, Figure 4-11, we can see that the initial rate of V(V) reduction is slow, with the rate increasing with time. At the

same time the concentration of HNO_2 in solution is seen to increase nearly linearly with time. This increase in rate in V(V) reduction over time is likely seen due to the initial reduction at the shorter timescales occurring *via* a single pathway, with the in-growth of a second, nitrous-related reduction pathway contributing over the longer timescales and thus causing an increase in the observed overall rate of V(V) loss.

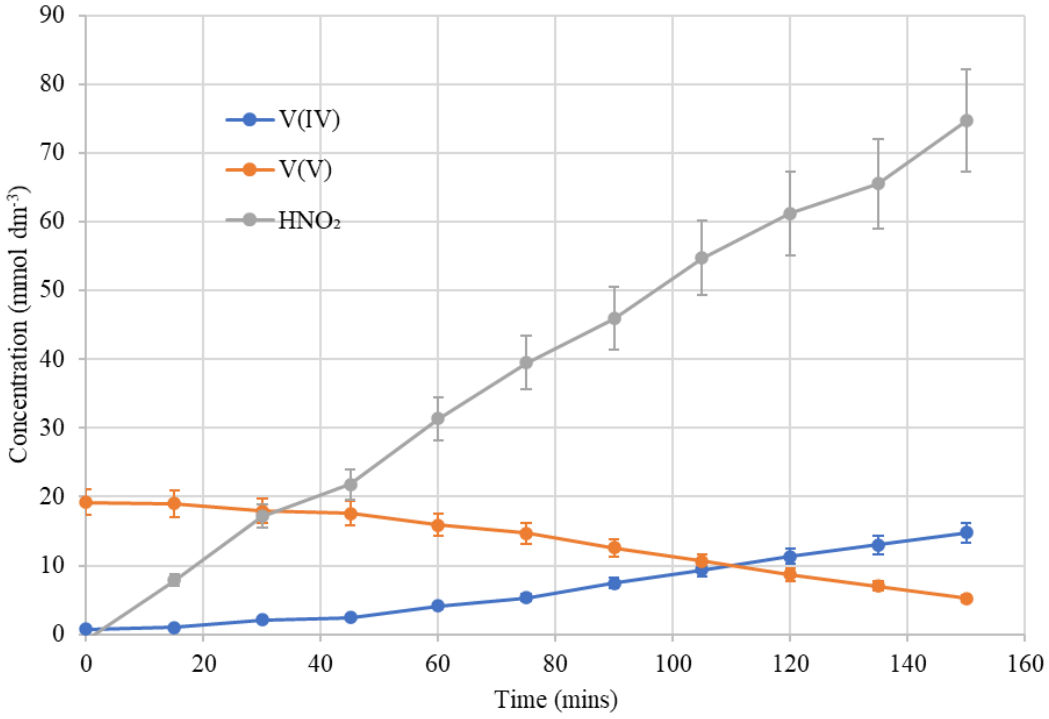

Figure 4-11 Plot of concentration of different species vs time for an initial solution of 20 mmol dm^{-3} V(V) in 1 mol dm^{-3} HNO_3 with NO gas bubbled through at a rate of approximately 150 mL min^{-1}.

The initial, slow reduction could potentially be due to one of two processes; the direct reduction of the V(V) to V(IV) by NO in accordance with equation 4.17, or indirect reduction of V(V) by HNO_2, in accordance with equations 4.18 to 4.20, with said HNO_2 having been generated by the reaction of NO with HNO_3 in accordance with equation 4.49.[164]

$$HNO_3 + 2NO + H_2O \rightleftharpoons 3HNO_2 \qquad 4.49$$

Given that equation 4.49 is a multi-step equilibrium process that involves the breaking and forming of numerous N-O bonds, it might be expected to be kinetically slow. Direct reduction of the V(V) to V(IV) by NO, however, would be expected to be kinetically fast due to the oxidation of NO to NO^+ being a facile reversible one-electron transfer reaction and that the process only involves the breaking of a single V-O bond (rather than numerous N-O bonds).[83] This suggests that the very short time reduction of V(V) is dominated by the direct V(V)/NO process of equation 4.17.

The subsequent acceleration in rate seen over longer timescales in Figure 4-11 is then likely due to the accumulation of the reductant HNO_2, with this accumulation being derived from two possible sources. The first is as a result of constant NO bubbling and thence equation 4.49. This mechanism was also postulated by Bennett and Kelmers for the analogous reduction of Pu(VI) to Pu(IV) by NO[86]. The second is the generation in solution of HNO_2 as a result of it being a product of the reaction given by equation 4.17. In order to determine which of these possible sources was the cause of the HNO_2 present in the reduction of V(V) by NO performed above, bubbling of NO through nitric acid was to be performed in the absence of vanadium and compared to those in the presence of vanadium. The results of this are shown in Section 4.2.2.

4.2.2 *Effect of the Absence and Presence of Vanadium on the Formation of Nitrous Acid During NO Bubbling*

Comparison of the formation rates of HNO_2 in solutions of 1 mol dm^{-3} HNO_3 both with and without vanadium present, shown by the blue circles and orange circles of Figure 4-12 respectively, was done to determine the source of HNO_2 in reduction reactions of V(V) by NO.

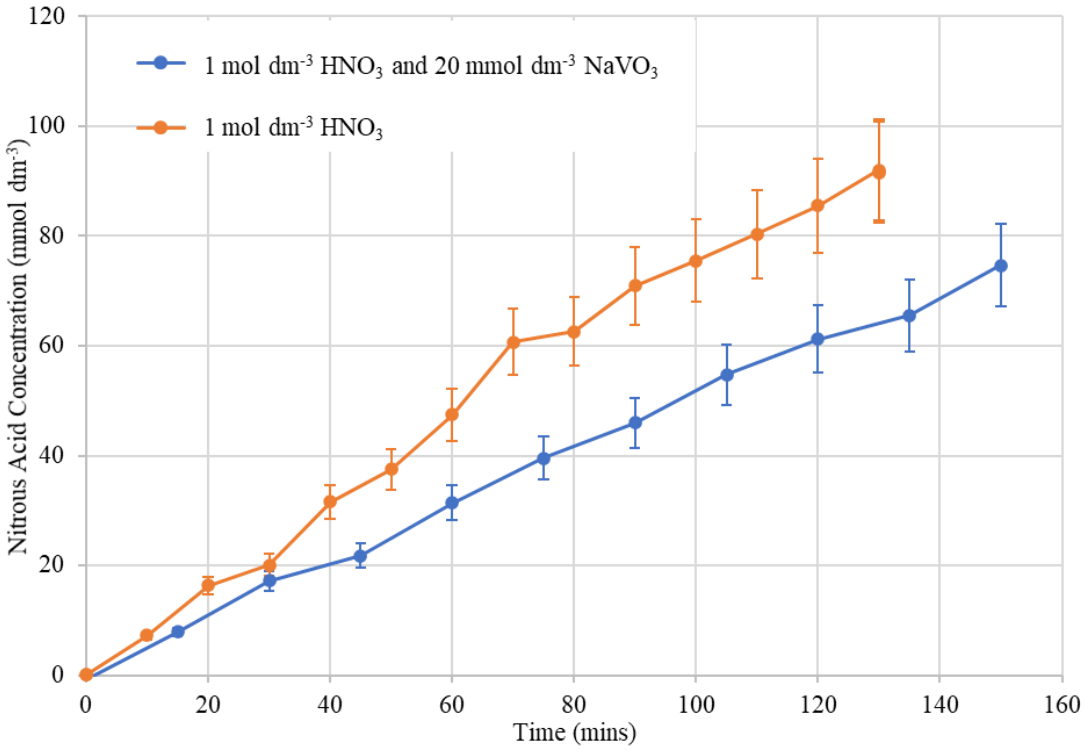

Figure 4-12 Rate of production of HNO_2 from NO when bubbled through 1 mol dm^{-3} HNO_3 both with and without vanadium.

From comparing the results of these experimental runs, it could be seen that, whilst differing amounts of HNO_2 were generated in the two systems studied, HNO_2 was seen to form readily in both. This suggests that the reaction of HNO_3 with NO by equation 4.49 is the main contributor to the formation of HNO_2, with some further contribution to the measured HNO_2 concentration from equation 4.17. Surprisingly, the amount of nitrous acid generated in solutions containing vanadium is seen to be approximately 25-30% lower at t = 120 mins. This reduction in the amount of nitrous seen is potentially due to either;

i. the consumption of some of the nitrous acid by the V(V)/HNO_2 reduction, as per equation 4.15;

or

ii. V(V) interrupting HNO_2 production by consumption of NO *via* equation 4.28 prior to its participation in the reaction in equation 4.49

Or from a combination of both of the above. It should be noted that whilst the reduction of V(V) by NO in point (ii) would also result in the formation of some nitrous acid, this pathway will produce 1 nitrous acid per 1 NO consumed, whereas reaction of the NO with the nitric acid media as per equation 4.49 would result in the formation of 1.5 nitrous acid per 1 NO consumed. Therefore, reduction of V(V) by NO would interrupt the more efficient nitrous acid production route and thus result in the observed suppression of the overall nitrous acid yield. Though the cause of the suppression of nitrous acid formation in the presence is therefore not clear, either of the above explanations are consistent with the majority formation route of nitrous acid being from reaction of NO with the nitric acid media seen in equation 4.49.

With the main cause of nitrous acid formation being seen to be due to reaction of the NO with the nitric acid media, minimisation of this reaction and hence minimisation of nitrous acid formation was needed in order to study the reduction of V(V) by NO.

4.2.3 NO Bubbling through varying pH Nitrate Solutions

With the formation of HNO_2 suggested to be mainly due to the reaction of HNO_3 with NO, the need to supress the formation of HNO_2 became apparent within the studies into the reduction of V(V) by NO due to its own potential to act as a reductant for V(V). Therefore, a series of experiments were conducted to measure the formation of HNO_2 in solutions of HNO_3 bubbled with NO, where the pH was varied whilst keeping the nitrate concentration constant using sodium nitrate with the objective of identifying a pH where no nitrous acid is seen to be generated. Results are shown in Figure 4-13.

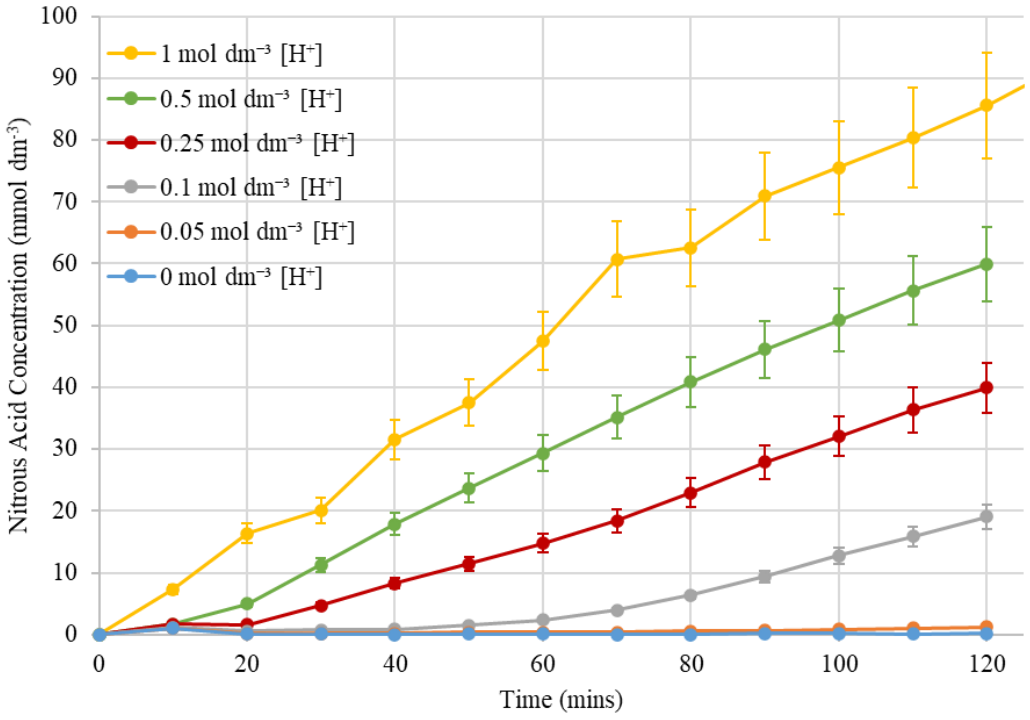

Figure 4-13 Rate of production of HNO_2 in nitrate solutions of varying pH. Nitrate concentration was kept constant at 1 mol dm^{-3} using $NaNO_3$.

From this we can see that the amount of HNO_2 formed within solution is seen to increase with increasing proton concentration. Bubbling of NO through solutions of 1 mol dm^{-3} $NaNO_3$ with no H^+ present was observed to result in the formation of no HNO_2 at all suggesting that the formation of HNO_2 by NO is possible *via* a mechanism involving the protonation of nitrate and

is not possible *via* unprotonated nitrate. Therefore, by utilising solution media at suitably low pH, we can ensure any HNO_2 present is as a result equation 4.17 and thereby examine the reduction of V(V) by NO independently of its reduction by HNO_2.

4.2.4 Identification of the V(V) Reducing Species in NO Bubbled Solutions

In order to elucidate whether the reduction of V(V) in NO bubbled solutions is occurring with the NO or the formed HNO_2 acting as the reductant, as seen in Figure 4-11, reduction experiments were done in solutions of 50 mmol dm^{-3} H^+ and compared to those done in 1 mol dm^{-3} H^+, with $[NO_3^-]$ being kept constant at 1 mol dm^{-3} in both. The lower acidity concentration was chosen due to the bubbling of NO through this solution having previously shown in Section 4.2.3 to form negligible amounts of HNO_2 compared to higher acidities. This acidity also had the advantage of being at an acidity where the reduction *via* nitrous acid had previously been seen to not occur (Section 4.1.3.2). Comparison of the results of bubbling NO through 1 mol dm^{-3} H^+ and 50 mmol dm^{-3} H^+ solutions are shown in Figure 4-14.

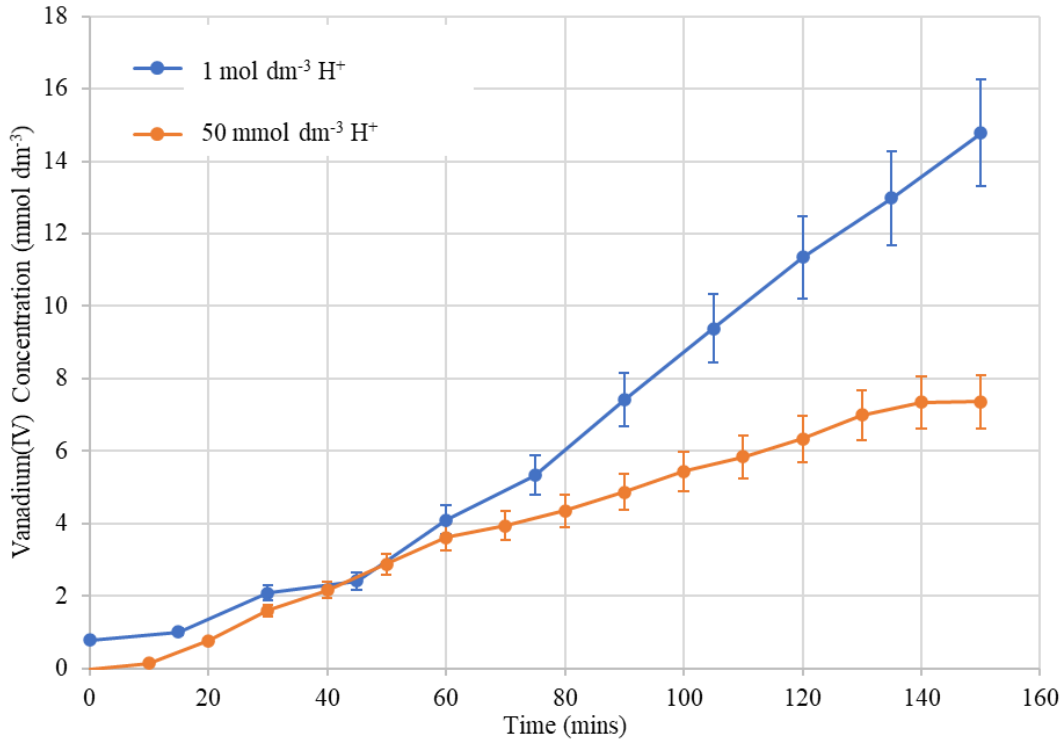

Figure 4-14 Concentration of V(IV) vs time for NO bubbled solutions of 1 mol dm^{-3} H$^+$ and 50 mmol dm^{-3} H$^+$, with 1 mol dm^{-3} NO_3^-. Total vanadium concentration was 20 mmol dm^{-3}, with NO gas bubbled through at a rate of approximately 150 mL min^{-1}.

It can be seen from this comparison of the rate of formation of V(IV) that, though the initial rate is similar in both 1 mol dm^{-3} H$^+$ and 50 mmol dm^{-3} H$^+$ solutions, an increase in the rate can be seen after approximately 60 minutes in the 1 mol dm^{-3} H$^+$ solution. This increase is likely due to the ingrowth of the nitrous acid giving a second reaction pathway, i.e. the reduction of the V(V) by nitrous acid as per equation 4.15, in the 1 mol dm^{-3} H$^+$ solution.

Whilst the ingrowth of the HNO_2 will also be present in the 50 mmol dm^{-3} H$^+$ solution due to nitrous acid being a product of the reduction of V(V) by NO, equation 4.17, the ingrowth of nitrous acid by this route will be slower. Additionally, the pathway in which the V(V) is reduced by nitrous acid has been previously been shown not to occur at these lower acidities (Section 4.1.3.2), meaning that any HNO_2 present in the 50 mmol dm^{-3} H$^+$ solutions will not be able to reduce the V(V) present and any reduction of V(V) will be due to reduction by NO.

It can also be seen that, over the monitored time period, the increase in V(IV) can be seen to be approximately linear for the 50 mmol dm^{-3} H^+ solution. This linear increase in V(IV) concentration likely due to two factors.

i. the concentration of NO in solution available for the reduction being at a pseudo-steady state, where it is being replenished by the gas bubbled through as fast as it is being consumed by the reaction and;
ii. the concentration of NO in solution being relatively low compared to that of vanadium, causing the order of reaction with respect to V(V) to be pseudo-zeroth order – this is consistent with studies on the order of reaction with respect V(V) seen later in Section 4.2.5

In order to minimise any re-oxidation of the V(IV) back to V(V), such as the nitrous acid catalysed re-oxidation of V(IV) to V(V) in nitric acid previously seen in the presence of nitrate (Section 4.1.3.3), a number of bubbling experimental runs were also done in sulphuric acid, for which no back reaction had been previously seen to occur for the reduction of V(V) by nitrous acid due to the absence of nitric acid. The absence of any nitric acid will also mean that no nitrous acid will be formed as a result of reactions with the solution media and any nitrous formed will be as a result of the vanadium reduction. The results of this experimental run can be seen in Figure 4-15.

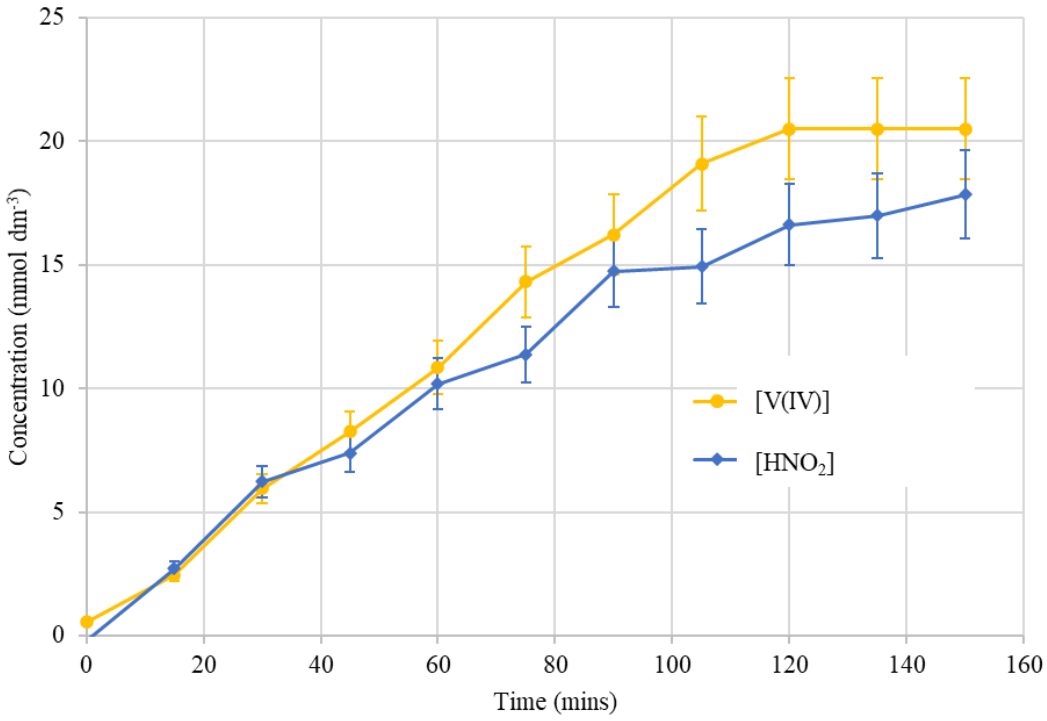

Figure 4-15 Plot of concentration of V(IV) and HNO_2 vs time for an initial solution of 20 mmol dm^{-3} V(V) in 1 mol dm^{-3} H_2SO_4 with NO gas bubbled through at a rate of approximately 150 mL min^{-1}.

From this we can see that the vanadium underwent complete conversion from V(V) to V(IV), and we can also see that we observe slightly less than stoichiometric formation of HNO_2. This is consistent with equation 4.17 for the second pathway as the nitric oxide reduction pathway previously discussed (Section 4.1.5), where one mole of nitrous acid is formed for every mole of V(V) reduced. The slightly less that stoichiometric formation of HNO_2 can be explained through it acting as a further reductant for the V(V) as outlined in Section 4.1.5.2.

Similarly to the reduction done in 50 mmol dm^{-3} H^+ solution, Figure 4-14, the rate of increase in V(IV) concentration can be seen to be approximately linear. This can again be attributed to both the replenishment of NO in solution by the continual bubbling of NO through the solution and to the NO concentration in solution being low compared to that of vanadium, causing a pseudo zeroth order with respect to V(V), as detailed above and further examined in Section 4.2.5.

With NO having been shown to play a direct role in the reduction of V(V), and with experimental conditions being found where interfering nitrous acid reduction pathways will play a minimal or no role, the kinetics of the NO reduction pathway were to be probed further. For this purpose, the orders of reaction were to be determined for both V(V) and H^+ species, in order to elucidate both the kinetic rate expression and the mechanism of reaction for the reduction of V(V) to V(IV) by NO.

4.2.5 Determination of Reaction Orders with respect to V(V)

Reduction reactions were run with varying V(V) concentration in solutions of both 0.1 mol dm^{-3} and 1 mol dm^{-3} H_2SO_4 in order to determine the order of reaction with respect to V(V). The reaction order was found from the slope of the plot of log(rate) vs. log(initial reactant concentration), Figure 4-16. Measured plots of [V(IV)] *vs.* time as a function of the initial [V(V)] are given in Appendix C-5, from which initial rates could be determined by taking the slope of each plot over the first 10 to 30 minutes. From this analysis, reaction orders with respect to V(V) were found to be 0.87 in 0.1 mol dm^{-3} H_2SO_4, whilst in the higher acidity 1 mol dm^{-3} H_2SO_4 a zeroth order and no dependence was seen on [V(V)] – as is consistent with results showing linear rates for the increase of V(IV) previously seen in Section 4.2.4. The implications of this on the mechanism of reaction are discussed further in Section 4.2.7.

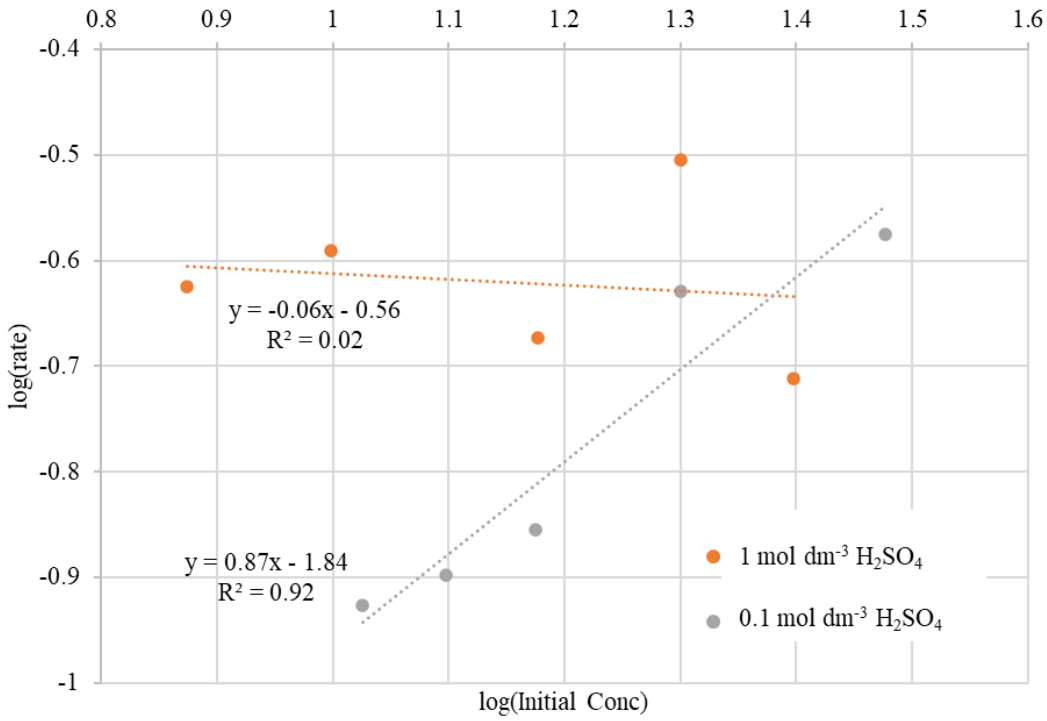

Figure 4-16 Determination of reaction orders with respect to V(V) in 0.1 mol dm^{-3} H_2SO_4, and 1 mol dm^{-3} H_2SO_4 (initial conditions: [VO_2^+] = 7.5-30 mmol dm^{-3})

4.2.6 Determination of Reaction Orders with respect to H^+

Reduction reactions were also done at varying H_2SO_4 concentration in order to determine the order of reaction with respect to [H^+]. Proton concentrations were calculated based on the sulphate acid speciation calculations conducted by Casas *et al.*[165] wherein, at the pHs under which the experiments herein were performed, 80% of the [H_2SO_4] would undergo monoprotic dissociation and the remaining 20% would undergo diprotic dissociation. Initial rates were determined by taking the slope of each of the measured plots of [V(IV)] *vs.* time as a function of the initial [H^+] (Appendix C-6) over the first 10 to 30 minutes and were then used to create the log-log plot shown in Figure 4-17. The linear trendline shown was calculated using data for H_2SO_4 concentrations of ≥ 1 mol dm^{-3} with R^2 values obtained of 0.97.

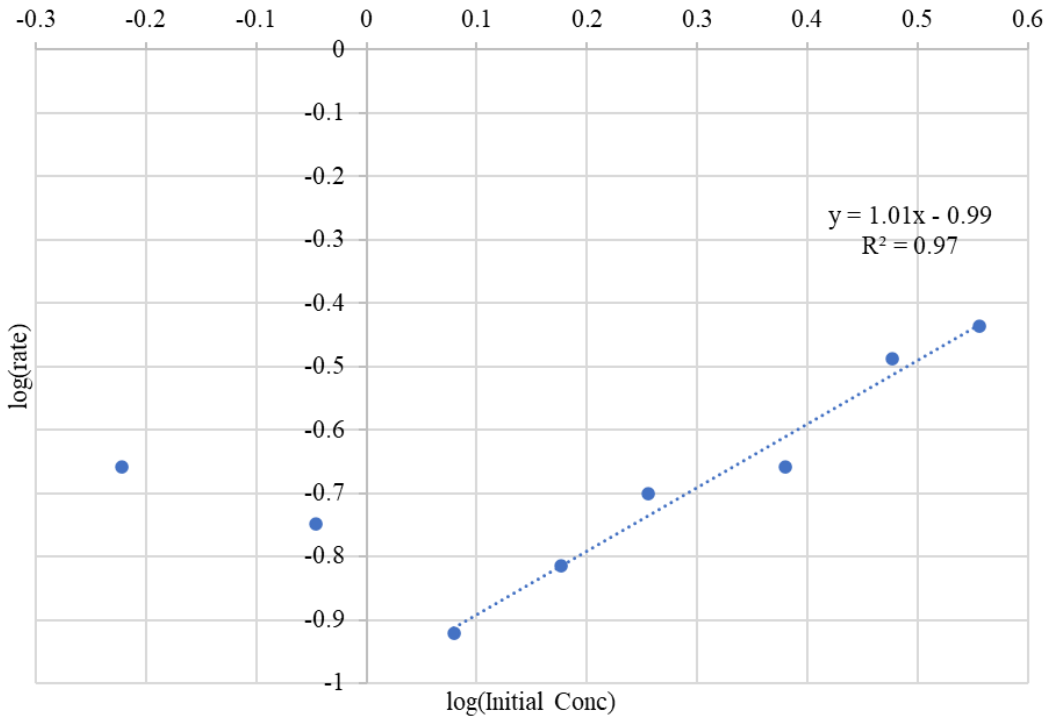

Figure 4-17 Determination of reaction orders with respect to H_2SO_4. (initial conditions: $[VO_2^+]$ = 25 mmol dm^{-3}; $[H_2SO_4]$ = 0.5-3 mol dm^{-3}).

The reaction order with respect to $[H^+]$ was seen to be 1.01 at sulphuric acid concentrations > 1 mol dm^{-3}. However, at sulphuric acid concentrations < 1 mol dm^{-3}, the rate of reaction was seen to be independent of H_2SO_4. This change in the order of reaction, as well as the difference in the order of reaction with respect to V(V) seen in Section 4.2.5 between high and low acidities indicates a change in the mechanism of reaction was occurring. This will be discussed further in Section 4.2.7.

4.2.7 Discussion on the Mechanism of Reaction

By using the experimental data collected on the rate of V(V) reduction by bubbled NO, the mechanism for the direct reduction of V(V) by NO could now be determined. From the data shown in Sections 4.2.5 and 4.2.6, it could be seen that for the reduction of V(V) by NO at higher acidities, the reaction appeared to be approximately first order with respect to proton

concentration and independent of [V(V)], whilst at lower acidities the reaction was seen to be first order with respect to [V(V)] but independent of proton concentration. This change in dependence from [V(V)] to [H^+] indicates that a change in mechanism for pathway 2 outlined in equation 4.17, is occurring between the two acidities. We therefore propose the following mechanism outlined in equations 4.50 to 4.53, which is consistent with the observed orders of reaction for the direct reduction of V(V) by NO.

$$NO + H^+ \underset{k_{-1}}{\overset{k_1}{\rightleftharpoons}} HNO^+ \quad 4.50$$

$$HNO^+ + VO_2^+ \overset{k_2}{\rightarrow} VO^{2+} + HNO_2 \quad 4.51$$

$$VO_2^+ + NO \underset{k_{-3}}{\overset{k_3}{\rightleftharpoons}} VO_2^+ \cdot NO \quad 4.52$$

$$VO_2^+ \cdot NO + H^+ \overset{k_4}{\rightarrow} VO^{2+} + HNO_2 \quad 4.53$$

Within this mechanism, the reduction of V(V) by NO goes *via* two potential pathways. The first of which involves the protonation of NO to form a HNO^+ species, equation 4.50, which then reduces the V(V) to give V(IV) and HNO_2, equation 4.51. The second involves an initial coordination of the NO to the V(V), equation 4.52, which then undergoes reaction with a proton to again give V(IV) and HNO_2, equation 4.53. This coordination of the NO to the vanadium to form the oxycation-NO adduct having previously been seen in the literature under certain conditions.[166] By assuming equations 4.51 and 4.53 are the rate determining steps due to being cation-cation interactions – as opposed to the cation-neutral species interactions for the steps shown in equations 4.50 and 4.52 – we can give the overall rate equation 4.54 which can be simplified further as shown in equations 4.55 to 4.63. These simplification calculations utilise the assumptions that both HNO^+ and $VO_2^+ \cdot NO$ are at steady state in order to get equations 4.56 and 4.59 respectively, and that the rate constants k_{-1} and k_{-3} associated with the back

reactions of equations 4.50 and 4.52 are small compared to the forward reactions given in equations 4.51 and 4.53, in order to simplify equation 4.62 to that given in equation 4.63.

$$\frac{d[VO^{2+}]}{dt} = k_2[HNO^+][VO_2^+] + k_4[VO_2^+ \cdot NO][H^+] \quad 4.54$$

Since; $$\frac{d[HNO^+]}{dt} = k_1[NO][H^+] - k_{-1}[HNO^+] - k_2[HNO^+][VO_2^+] \quad 4.55$$

At steady state; $$k_1[NO][H^+] = k_{-1}[HNO^+] + k_2[HNO^+][VO_2^+] \quad 4.56$$

$$[HNO^+] = \frac{k_1[NO][H^+]}{k_{-1} + k_2[VO_2^+]} \quad 4.57$$

And; $$\frac{d[VO_2^+ \cdot NO]}{dt} = k_3[VO_2^+][NO] - k_{-3}[VO_2^+ \cdot NO] - k_4[VO_2^+ \cdot NO][H^+] \quad 4.58$$

At steady state; $$k_3[VO_2^+][NO] = k_{-3}[VO_2^+ \cdot NO] + k_4[VO_2^+ \cdot NO][H^+] \quad 4.59$$

$$[VO_2^+ \cdot NO] = \frac{k_3[VO_2^+][NO]}{k_{-3} + k_4[H^+]} \quad 4.60$$

$$\frac{d[VO^{2+}]}{dt} = \frac{k_1k_2[VO_2^+][NO][H^+]}{k_{-1} + k_2[VO_2^+]} + \frac{k_3k_4[VO_2^+][NO][H^+]}{k_{-3} + k_4[H^+]} \quad 4.61$$

$$\frac{d[VO^{2+}]}{dt} = [VO_2^+][NO][H^+]\left(\frac{k_1k_2}{k_{-1} + k_2[VO_2^+]} + \frac{k_3k_4}{k_{-3} + k_4[H^+]}\right) \quad 4.62$$

$$\frac{d[VO^{2+}]}{dt} = [VO_2^+][NO][H^+]\left(\frac{k_1}{[VO_2^+]} + \frac{k_3}{[H^+]}\right) \quad 4.63$$

At high $[H^+]$, the observed first order dependence with respect to proton concentration and independence on [V(V)] can therefore be explained with the k_3 term of equation 4.63 becoming small and the equation being able to be reduced to the form given in equation 4.64. Similarly, at low $[H^+]$, the k_1 term of equation 4.63 becomes negligible and thus the equation can be reduced to the form given in equation 4.65.

At high [H^+]; $$\frac{d[VO^{2+}]}{dt} = k_1\,[NO][H^+] \quad (4.64)$$

At low [H^+]; $$\frac{d[VO^{2+}]}{dt} = k_3[VO_2^+][NO] \quad (4.65)$$

Using these rate equations given above along with the data gathered in Section 4.2.5, and assuming a saturated NO concentration of 3.02 mmol dm^{-3}, rate constants for the two pathways could therefore be calculated of $k_1 = 1.12 \times 10^{-3}$ dm^3 mol^{-1} s^{-1} and $k_3 = 5.66 \times 10^{-2}$ dm^3 mol^{-1} s^{-1} respectively. This suggests that the V(V) reduction route that involves the formation of the VO_2^+·NO adduct in accordance with equation 4.52 is > 50 times faster than the route that involves formation of the HNO^+ prior to action upon VO_2^+ in accordance with equations 4.50 and 4.51. However, caution should be exercised in the interpretation of these values given the preliminary nature of this analysis and the associated assumptions underlying the use of equations 4.64 and 4.65 (e.g. the assumed value for the solution phase concentration of NO).

In comparing the above two pathway mechanism, determined in experiments wherein NO was bubbled through a V(V) solution, with the NO pathway proposed in Section 4.1.5 for the reduction of V(V) by HNO_2, we can explain the condition dependence for the reduction of V(V) by NO as being down to the interaction of four different species; these being VO_2^+, $V(O)(OH)^{2+}$, NO, and HNO^+. For NO-bubbled V(V) reductions, the concentration of NO will be high, and the reaction will therefore go *via* either the initial protonation of NO or the complexation of the V and NO, as detailed above. Whereas in experiments performed in Section 4.1 for the reduction of V(V) by HNO_2, the NO concentration is comparatively low, and the NO pathway is seen to proceed *via* the protonation of the V followed by reaction with NO. The final possible interaction of $V(O)(OH)^{2+}$ with HNO^+ not being observed in either set of experiments is likely due to it being a minor pathway due to the charges of the individual ions. For each of these pathways, the determined rate constants can be summarised as given in Table 4-1.

Reaction	Rate Constant
V(V) reduction by NO_2^-	5.30×10^{-3} dm^6 mol^{-2} s^{-1}
Protonated V(V) reduction by NO	1.63×10^{-8} dm^6 mol^{-2} s^{-1}
Initial V-NO complexation	5.66×10^{-2} dm^3 mol^{-1} s^{-1}
V(V) reduction by HNO^+	1.12×10^{-3} dm^3 mol^{-1} s^{-1}

Table 4-1 Summary of rate constants for the reduction of V(V) by HNO_2 and NO

4.3 Chapter Summary

V(V) has been shown to be a suitable non-active surrogate for Np(VI) in the context of the reduction reaction by NO to be studied within this work. This was verified by studying the reduction of V(V) by HNO_2 and comparing the results to those given by Precek and Paulenova on the reduction of Np(VI) by HNO_2. Parallels taken from the referenced work, along with modelling of the data for the V(V) reduction by HNO_2, have also allowed for elucidation of the mechanism of reaction.

Reductions of V(V) performed using bubbled NO have demonstrated its potential role in the reduction of Np(VI) within the context of nuclear fuel reprocessing and have given further insight into the mechanism of reaction for both the direct reduction by NO and the pathway *via* NO for the reduction by HNO_2.

In order to verify the observed results on the V(V) reduction by NO are applicable to the Np(VI) system, studies were therefore to be done to expand the work to look at the reduction of Np(VI) by NO.

5 Nitric Oxide-Driven Reduction of Neptunium

5.1 Np(V) Electro-oxidation and Np(VI) Stability Tests

With the rate equation having been determined for the reduction of V(V), as a Np(VI) analogue, by NO and a two-pathway mechanism consistent with the orders of reaction observed (Sections 4.2.5 to 4.2.7) having been proposed, attention was then turned to studying the reduction of Np(VI) itself by NO. As was done for the reductions of V(V) by NO, experiments presented here were performed in H_2SO_4 in order to minimise the formation of HNO_2 from reaction of the NO with the nitric-bearing solution media, see equation 4.47.

Given that, for radiological safety purposes, a limited concentration stock of Np was used, there was therefore a need to reclaim and recondition the Np at the end of each batch of experiments. This process is described in detail in Section 2.1.2. However, it is worth mentioning here that, as it is not possible to drive off sulphate in a manner akin to the denitration that occurs during the driving off of nitrate during a nitrate-based reclamation / reconditioning run. Thus, the concentration of background sulphate increased from experiment to experiment throughout the campaign described below. This had unforeseen consequences for studies of the NO-driven reduction of Np(VI) conducted later in the campaign. We shall return to this point below.

Before experiments could be conducted to determine the rate equation and hence mechanism of the Np(VI) reduction by NO, tests first had to be done to ensure the Np could be efficiently preconditioned to the Np(VI) oxidation state and that the Np(VI) oxidation state would be stable over a long enough time period to conduct the reduction by NO.

5.1.1 Electrooxidation of Np(V) to Np(VI)

Electrooxidation of Np(V) for the purpose of preconditioning Np solutions to Np(VI) prior to reduction experiments was done using a solution of 1.65 mmol dm^{-3} Np in 0.1 mol dm^{-3} H_2SO_4. The extent of oxidation was then monitored by recording UV-vis spectra over the range of 350 nm to 1000 nm, Figure 5-1, at a range of intervals over the course of 72 hours. By using the molar absorption coefficient for Np(V) at 981 nm of 414.1 dm^3 mol^{-1} cm^{-1} as determined in Section 3.2.4 and given in Section 2.3, the concentration of Np(V) over time could be plotted, Figure 5-2. From this plot and the full UV-vis spectra, the extent of the electrooxidation could be observed by looking both at the decrease in the Np(V) peak at 981 nm and by checking any peaks arising from other oxidation states[91] (e.g. Np(IV) from disproportionation of the Np(V)) were absent.

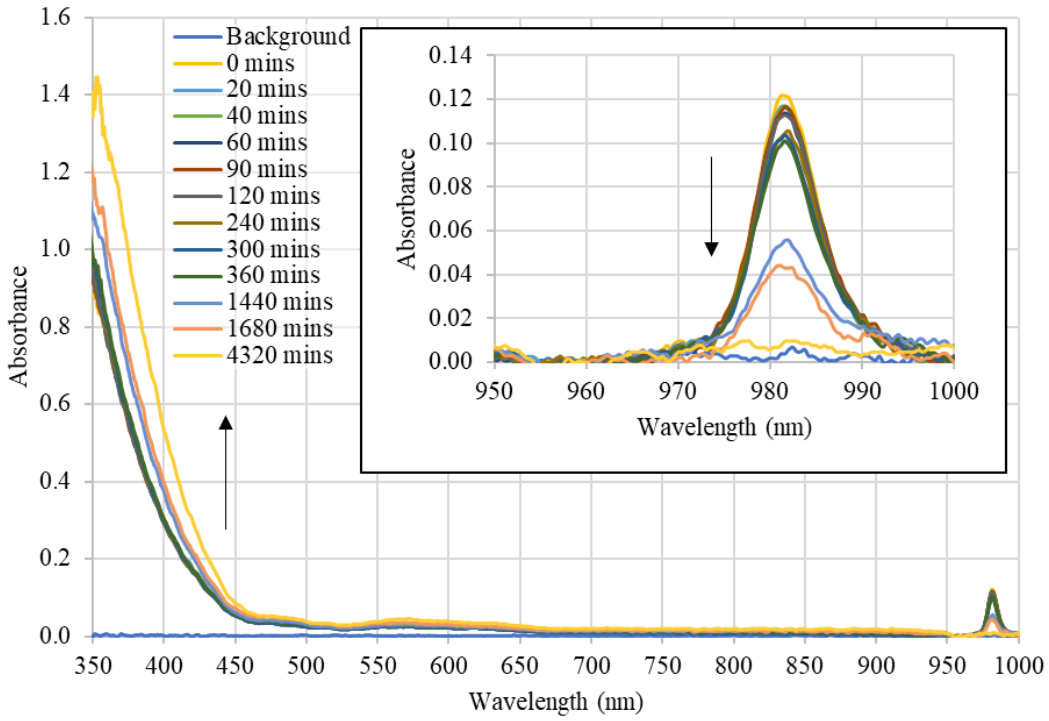

Figure 5-1 Spectral change for the electrooxidation of Np(V) to Np(VI) over the course of 72 hours. Insert shows decrease in the absorbance of the Np(V)at approx. 981 nm.

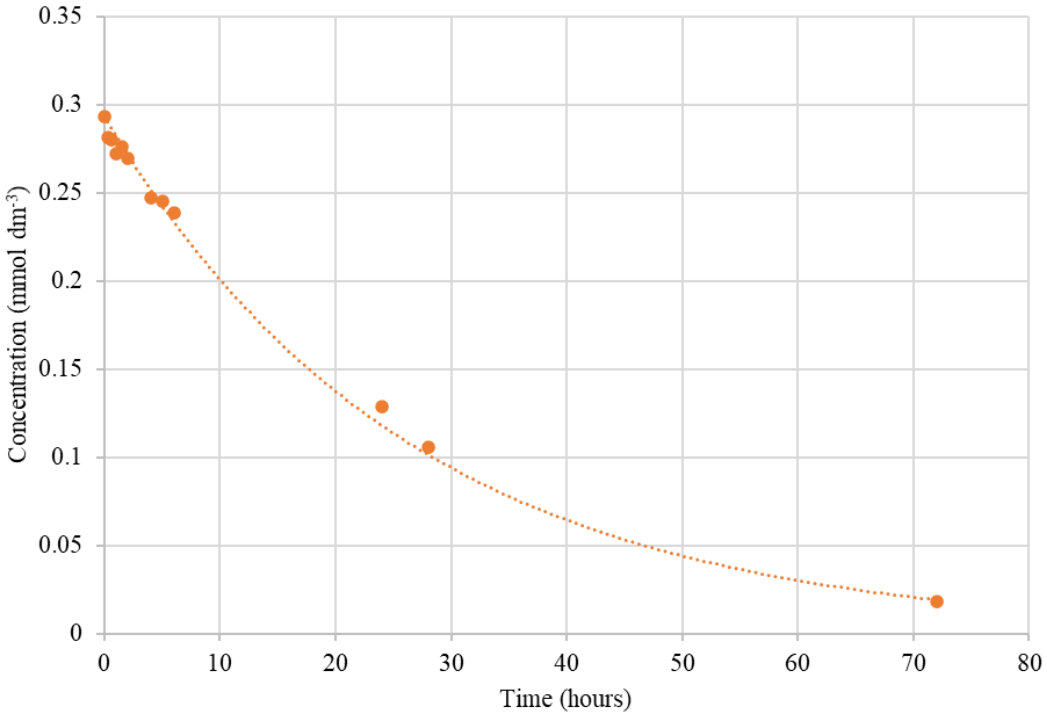

Figure 5-2 Plot of concentration of Np(V) vs time for the electrooxidation of Np(V) to Np(VI) in 0.1 mol dm^{-3} H_2SO_4 (no additional sulphate) taken over the course of 72 hours.

Whilst the initial observed concentration of Np(V) of approximately 0.3 mmol dm^{-3} is lower than the total amount of Np present, 1.65 mmol dm^{-3}, this is likely due to the starting solution already containing a significant fraction of Np in the Np(VI) oxidation state, evidenced by both the absorbance seen between 350 nm and 450 nm and by the small features at approximately 470 nm and 570 nm. The presence of any Np(IV) can also be seen to be negligible due to the absence of peaks at approximately 700 nm and 800 nm Use of the attenuation coefficient of 6.8 dm^3 mol^{-1} cm^{-1} at 557 nm given by Sjoblom and Hindman[53] allows for calculation of a solution phase concentration of Np(VI) of 1.62 mmol dm^{-3} – although this value is close to the total [Np] concentration, suggesting the Np is present mostly in the +VI oxidation state, this value should be treated with caution given the relatively weak intensity of the peaks at 470 nm and 570 nm.

It can be seen from Figure 5-2 that the concentration of Np(VI) decreases to < 2% of the total Np present; thus the electrooxidation was taken to be successful in preconditioning the Np to the Np(VI) oxidation state for the reduction reactions to be performed. However, depending on the initial amount of Np(V) present at the start of the electrooxidation process in subsequent experimental campaigns, future electrooxidation preconditioning steps may need to be run for longer with the amounts of Np(V) and Np(VI) being monitored by UV-vis.

5.1.2 Np(VI) Stability Test

After electrooxidation had been performed to ensure the Np was in the Np(VI) oxidation state, the stability of this was monitored by recording UV-vis spectra of a 1 mL aliquot of the solution every hour over the course of 92 hours. As was done with the electrooxidation test performed above, the molar attenuation coefficient of Np(V) at 981 nm of 414.1 $dm^3\ mol^{-1}\ cm^{-1}$ (as determined in Section 2.3), was used in order to create a plot of Np(V) concentration *vs.* time over the course of 92 hours, Figure 5-3.

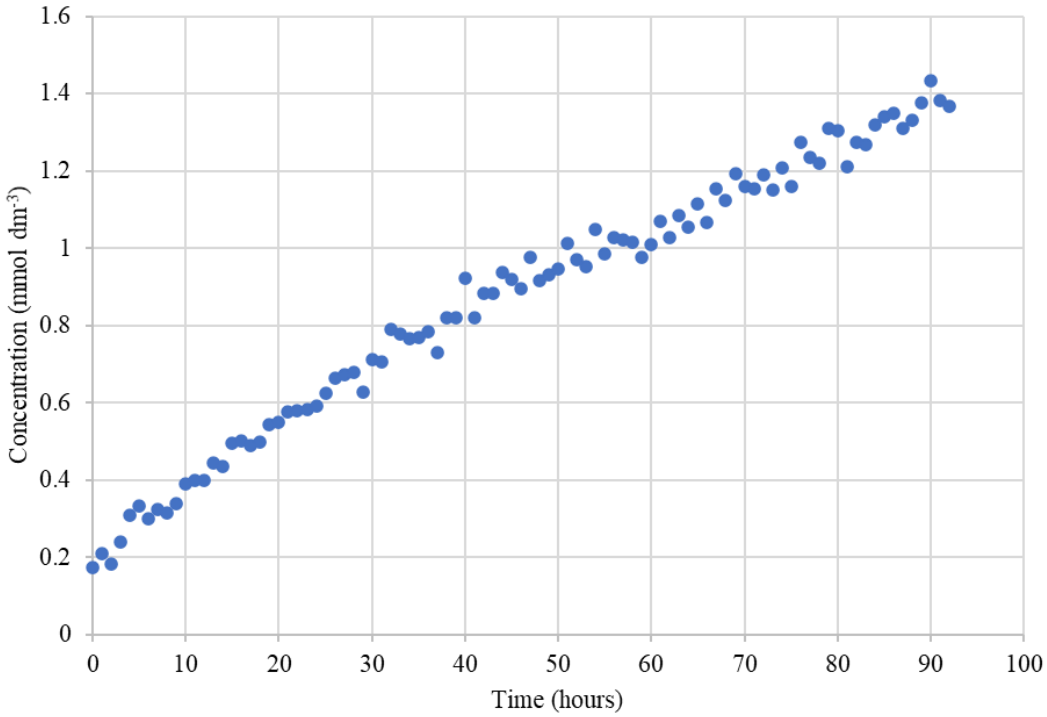

Figure 5-3 Plot of concentration of Np(V) vs time for an initial solution of approximately 1.65 mmol dm^{-3} Np(VI) in 0.1 mol dm^{-3} H_2SO_4 with spectra recorded every hour over the course of 92 hours.

Whilst the Np(VI) was seen to slowly be reduced to Np(V) over the 92 hour time period monitored, given that the experiments studying the reduction of Np(VI) to Np(V) by NO took place immediately after the electrooxidation pre-treatment had been completed and took no longer than 30 minutes, the slow rate at which the background reduction of Figure 5-3 occurred meant that the Np(VI) was stable enough for us to be able to run experiments looking specifically at its reduction by NO, with negligible Np(V) being formed in accordance with the process of Figure 5-3.

5.2 Determination of Reaction Orders with respect to H^+

With Np(VI) having been shown to be stable over the time periods for which its reduction by NO was to be studied, NO-driven reduction reactions were first conducted at varying H_2SO_4 concentrations in order to determine the order of reaction with respect to $[H^+]$. These were performed at a constant neptunium concentration of 0.61875 mmol dm^{-3} with a constant NO gas flow rate of 20 mL min^{-1}. As discussed in Section 2.5, this rate would be sufficient to generate a saturated solution of NO, with a concentration of 3.02 mol dm^{-3}.[138] In this, it is assumed that its reaction with Np(VI) is not sufficient to substantially deplete NO in solution – a not unreasonable assumption given the constant replenishing of the NO concentration by the bubbling process.

Preconditioning of neptunium to ensure its presence as the +VI oxidation state was done using bulk electrolysis, with electrochemical current-time curves for these being given in Appendix E-1. Based on the sulphate acid speciation calculations conducted by Casas *et al.*[165], proton concentration was again calculated, as for experiments outlined in Section 4.2.6, by assuming 80% of the H_2SO_4 underwent monoprotic dissociation and the remaining 20% underwent diprotic dissociation, as would be expected at the pHs present.

Plots of Np(V) concentration *vs.* time could then be made in order to see the rate of Np(V) ingrowth into NO bubbled solutions of Np(VI), Figure 5-4. In comparing the concentration *vs.* time profiles for the reductions performed of V(V) by NO in Section 4.2, similar shapes could be seen to that of the reductions performed of Np(VI) by NO, wherein the reduction of the metal ion was preceded by a small induction period. An example of such similarity can be seen when comparing the concentration-time plot given in Figure 5-5 for the V(V) reduction by NO in 0.5 mol dm^{-3} H_2SO_4 to the Np(VI) reduction by NO in 0.5 mol dm^{-3} H_2SO_4 shown in Figure 5-4.This induction period is likely due to time taken for bubbled NO to saturate the reaction solution and not due to ingrowth of HNO_2 which then causes the metal ion reduction for reasons outlined in Section 4.2.4.

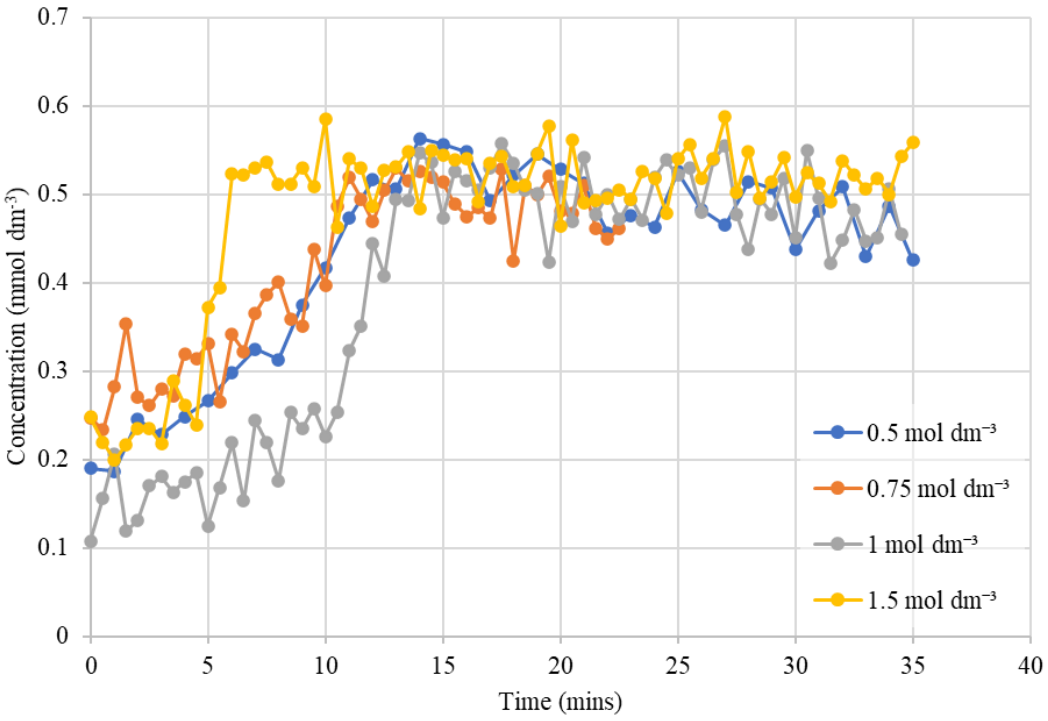

Figure 5-4 Plot of the concentration of Np(V) vs time for solutions of 0.61875 mmol dm^{-3} [Np(VI)] with 0.5-1.5 mol dm^{-3} [H_2SO_4] with NO gas bubbled through at a rate of 20 mL min^{-1}.

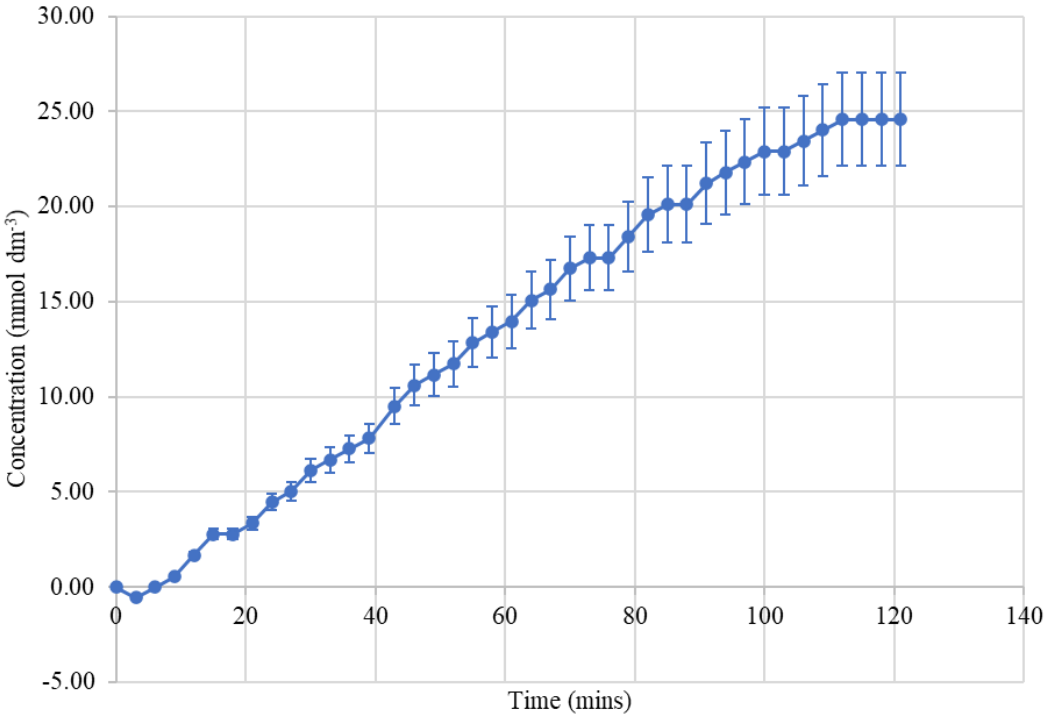

Figure 5-5 Plot of the concentration of V(IV) vs time for solutions of 25 mmol dm^{-3} [V(V)] with 0.5 mol dm^{-3} [H_2SO_4] with NO gas bubbled through at a rate of 150 mL min^{-1}.

Initial rates could be determined by taking the slope of each plot over the 2 to 10 minute interval, discarding the induction period as in Sections 4.2.5 and 4.2.6, and information on the order of reaction with respect to H^+ could be taken from the observed slopes of the plot of log(initial rate) *vs.* log([H^+]), Figure 5-6.

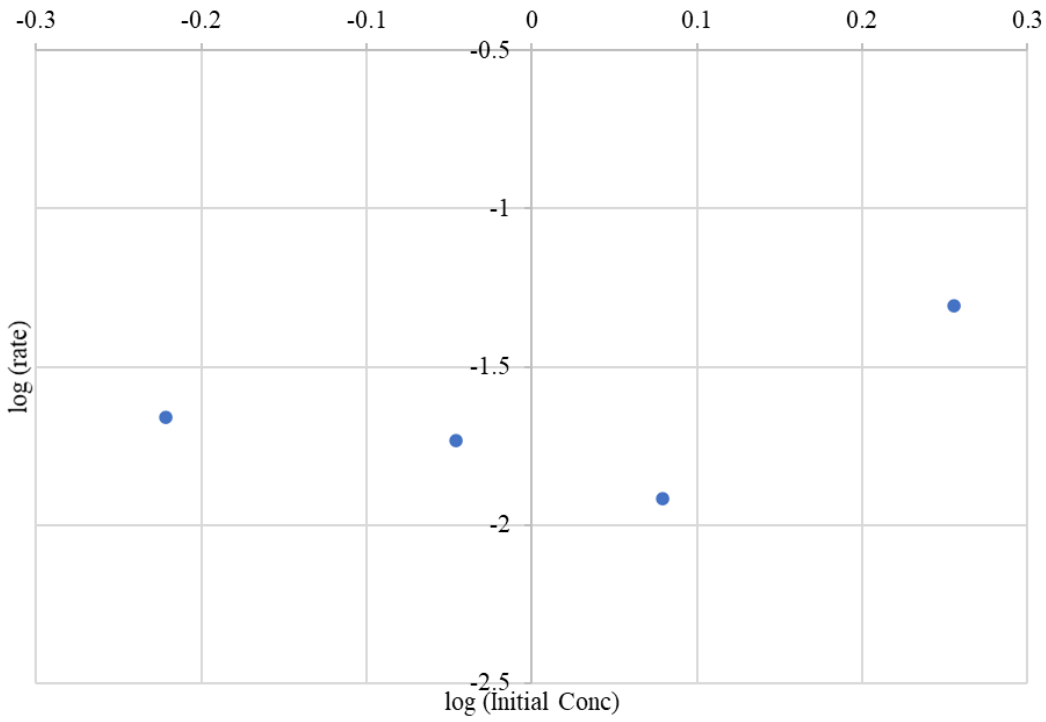

Figure 5-6 Determination of reaction orders with respect to H_2SO_4. (initial conditions: [NpO_2^{2+}] = 0.61875 mmol dm^{-3}; [H_2SO_4] = 0.5-1.5 mol dm^{-3}, no additional sulphate).

Comparison of the data of Figure 5-6 with that recorded for the reduction of V(V) under similar conditions, Figure 4-17 in Section 4.2.6, indicates that they have similar forms. Specifically, as was seen previously for the reduction of V(V) by NO, the rate of reaction was observed to be approximately independent of the [H^+] at H_2SO_4 concentrations < 1 mol dm^{-3}, whilst a dependency was seen to start to emerge at concentrations ≥ 1 mol dm^{-3}. The implications of this for the utilising of the mechanism for the V(V) reduction by NO determined in Section 4.2.7 to determine the analogous mechanism for the Np(VI) reduction by NO are discussed further in Section 5.5.

5.3 Determination of Reaction Orders with respect to Np(VI)

In order to determine if the order of reaction with respect to Np(VI) changed from 0 to 1 when moving from high to low acidity, as was seen for the dependence on V(V) in Section 4.2.5, reduction reactions were planned to be run with varying Np(VI) concentrations in both 0.1 mol dm^{-3} and 1 mol dm^{-3} H_2SO_4. Preconditioning of neptunium to ensure its presence as the VI oxidation state was done using bulk electrolysis, with electrochemical current-time curves for these being given in Appendix E-2. Reduction reactions were first run with varying Np(VI) concentrations in a 1 mol dm^{-3} H_2SO_4 solution. By plotting the absorbance at 981 nm from Np(V), Figure 5-7, it could be seen that the reduction of Np(VI) by NO was being seen to not occur.

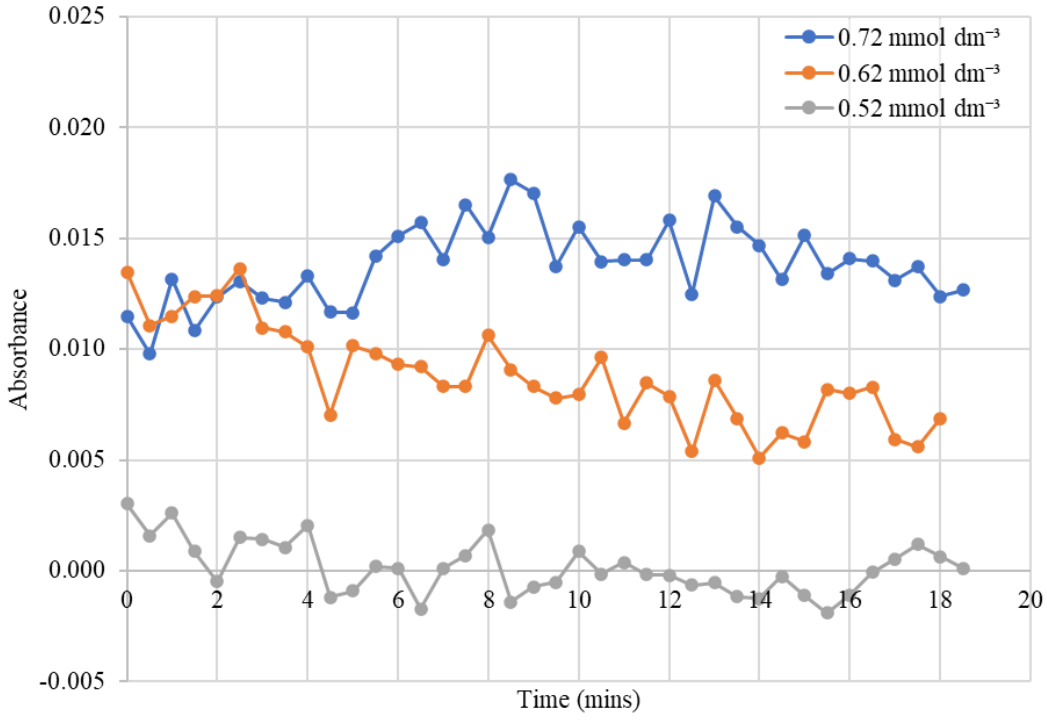

Figure 5-7 Plot of absorbance taken at 981 nm vs time for solutions of varying initial [Np(VI)] in 1 mol dm^{-3} H_2SO_4 with saturated sulphate (estimated approximately 3.4 mol dm^{-3}) and NO gas bubbled through at a rate of approximately 20 mL min^{-1}.

This lack of reduction reaction occurring was postulated to be due to high sulphate loadings in the stock Np solution caused by the recycle procedure outlined in Section 2.1.2 not removing

sulphate as planned. This occurred due to the water present in solution being preferentially evaporated over the H_2SO_4 in solution, resulting in a more concentrated acid solution, which then had to be partially neutralised using NaOH in order to allow for dilution of the stock to the concentrations needed in the reduction reactions. The presence of high amounts of sulphate in solution was also indicated by the presence of a white precipitate which had seen to be formed in the Np stock solution and was expected to be Na_2SO_4.

5.4 Cyclic Voltammetry of Saturated Sulphate Neptunium Solutions

The effect of high sulphate loadings on the reduction of Np(VI) by NO was therefore investigated further due to its presence potentially effecting the reduction, whilst previous experiments had indicated no effect of the rate for the reduction of V(V) by HNO_2 on the presence of sulphate, Section 4.1.4. This was done using cyclic voltammetry and comparing those taken in the high sulphate loaded solution, shown in Figure 5-8a, to those done previously in 0.5 mol dm^{-3} HNO_3 in Figure 3-6, Section 3.2.1.3 and shown again here in Figure 5-8b.

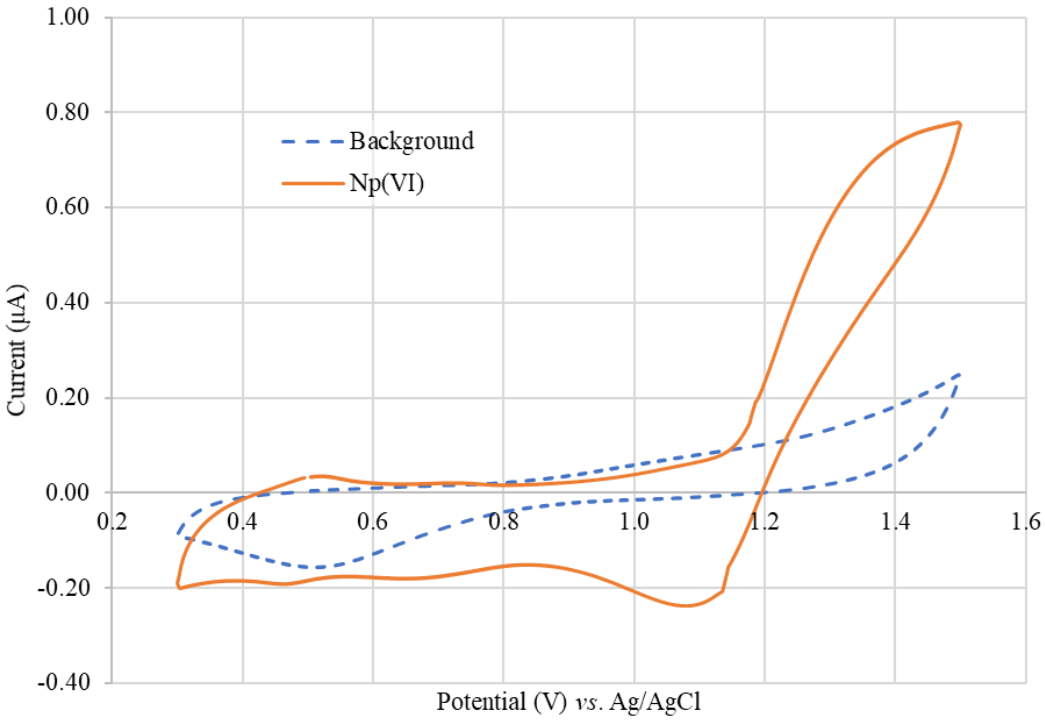

Figure 5-8a CVs of 1.65 mmol dm^{-3} Np in a saturated sulphate, 2 mol dm^{-3} H_2SO_4 solution on Pt (250 µm diameter) showing the final scan only for clarity. Scan rate = 100 mV s^{-1}.

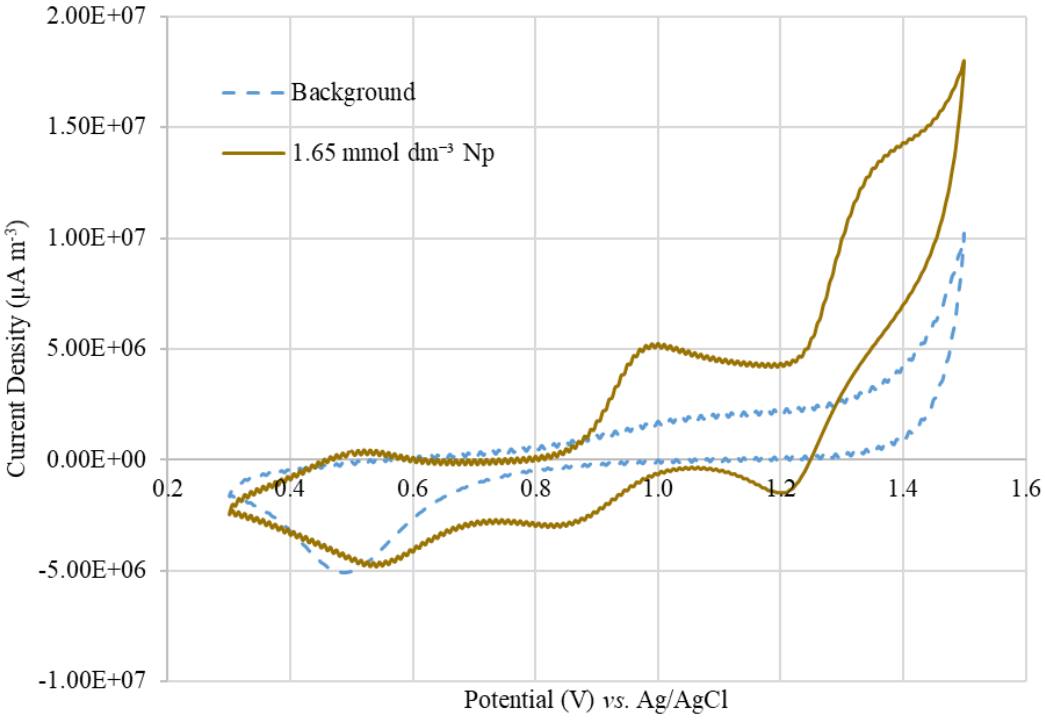

Figure 5-8b CVs of 1.65 mmol dm^{-3} Np(V) in 0.5 mol dm^{-3} HNO_3 on Pt (250 µm diameter) showing the final scan only for clarity. Scan rate = 100 mV s^{-1}.

The oxidation peak present at approximately 1.35 V *vs.* Ag/AgCl within the Np CV shown above was also previously seen in the CVs performed in HNO_3 and was attributed to the NpO_2^{2+}-assisted solvent oxidation, consistent with Chatterjee *et al.*[150] Whilst the mechanism for this NpO_2^{2+}-assisted solvent oxidation, having been described in Section 3.2.1.3 as an EC' process, involves the reduction of the electrogenerated Np(VI) (the E step) by either simultaneously electrogenerated H_2O_2 or $HO_2\cdot$(the C' step from the perspective of the Np(V)/(VI) couple), a negative shift in the electrochemical potential for the Np(V)/Np(VI) couple explained further below may make the reduction of Np(VI) by H_2O_2 no longer thermodynamically possible, and thus the putative EC' mechanism would proceed only by involvement of the electrogenerated $HO_2\cdot$ (in the C' step).

In contrast to the CVs taken in HNO_3 and shown in Figure 5-8b, CVs of Np in high sulphate loadings appeared to show an absence of the oxidation peak previously observed at approximately 1 V *vs.* Ag/AgCl and attributed to the Np(V)/Np(VI) couple. The absence of this couple is likely due to complexation of the Np with sulphate making the couple irreversible, with previous work done by Hennig *et al.*[167] into the sulphate coordination of neptunium supporting a complexation-driven change in the reversibility of the Np(V)/Np(VI) electrochemical couple, with the couple becoming more irreversible when moving to higher sulphate concentrations.

Work done by Hennig *et al.* also suggests that additional thermodynamic stability will be afforded to the Np(VI) ion through complexation with the sulphate anion, with this conceivably shifting the potential for the Np(V)/Np(VI) electrochemical couple to more negative potentials – and potentially to values more negative than the NO/NO^+ couple. As was done previously in Section 4.1.3.2 to adjust for changes in pH, the potential for the Np(V)/Np(VI) electrochemical couple was adjusted using the Nernst equation as given in equation 5.1. These calculations are given in equations 5.2 to 5.12 and use both the value for the reduction potential given by Bard *et al.* of 1.24 V *vs.* NHE[81] and the value for the log of the equilibrium constant for the formation of the Np(VI) disulphate complex given by Guillaumont *et al.* of 4.70.[168]

$$E = E^0 + \frac{RT}{nF} ln\left(\frac{C_{Ox}}{C_{Red}}\right) \quad 5.1$$

$$E = E^0 + \frac{RT}{nF} \ln\left(\frac{[NpO_2^{2+}]}{[NpO_2^{+}]}\right) \quad 5.2$$

Since; $$K = \frac{[NpO_2(SO_4)_2]}{[NpO_2^{2+}][SO_4^{2-}]^2} \quad 5.3$$

$$E = E^0 + \frac{RT}{nF} \ln\left(\frac{[NpO_2(SO_4)_2]/K[SO_4^{2-}]^2}{[NpO_2^{+}]}\right) \quad 5.4$$

$$E = E^0 + \frac{RT}{nF} \ln\left(\frac{[NpO_2(SO_4)_2]}{[NpO_2^{+}][SO_4^{2-}]^2}\right) - \frac{\mathrm{RT}}{\mathrm{nF}} \ln(\mathrm{K}) \quad 5.5$$

$$E = E^0 + \frac{RT}{nF} \ln\left(\frac{[NpO_2(SO_4)_2]}{[NpO_2^{+}][SO_4^{2-}]^2}\right) - \frac{\mathrm{RT}}{\mathrm{nF}} \times 2.303 \times \log(\mathrm{K}) \quad 5.6$$

$$E = E^0 + \frac{RT}{nF} \ln\left(\frac{[NpO_2(SO_4)_2]}{[NpO_2^{+}][SO_4^{2-}]^2}\right) - 0.059 \times \log(\mathrm{K}) \quad 5.7$$

By taking the reduction potential of Np(VI) as 1.24 V *vs.* NHE;

$$E^0 + \frac{RT}{nF} ln\left(\frac{[NpO_2(SO_4)_2]}{[NpO_2^{+}][SO_4]}\right) = 1.24 \quad 5.8$$

And taking log(K) = 4.70 from Guillaumont *et al.[168]*, therefore;

$$E = 1.24 - 0.059 \times 4.7 \quad 5.9$$

$$E = 0.9627V\ vs\ NHE \\ = 0.7657V\ vs\ Ag/AgCl \quad 5.10$$

This shifted value for the potential for the electrochemical reduction of Np(VI) to Np(V) is now seen to be sufficiently close to that of NO found in Figure 3-1, Section 3.1.1 as 0.7 V *vs.* Ag/AgCl causing the reduction of Np(VI) by NO to not be thermodynamically viable due to the thermodynamic stability afforded to the Np(VI) ion by its complexation with sulphate.

5.5 Discussion on the Mechanism of Reaction

Using the half equation for the Np(V)/Np(VI) electrochemical couple and mechanism outlined for the reduction of V(V) by NO in equations 4.50 to 4.53, Section 4.2.7, and based on the two ranges of Np(V) reduction rate dependence on [H^+] seen in the preliminary data of Figure 5-6, an analogous mechanism for the Np(VI) reduction by NO can be postulated. As with the V(V) system, this involves two mechanistic pathways. The first of these pathways involves the initial protonation of NO followed by reduction of the Np(VI) by the formed HNO^+ species, equations 5.11 and 5.12. The second involves the coordination of the NO with the Np(VI) ion, followed by the reduction of the formed Np(VI) complex, equations 5.13 and 5.14.

$$NO + H^+ \underset{k_{-1}}{\overset{k_1}{\rightleftharpoons}} HNO^+ \qquad 5.11$$

$$HNO^+ + NpO_2^{2+} + H_2O \overset{k_2}{\rightarrow} NpO_2^+ + HNO_2 + 2H^+ \qquad 5.12$$

$$NpO_2^{2+} + NO \underset{k_{-3}}{\overset{k_3}{\rightleftharpoons}} NpO_2^{2+} \cdot NO \qquad 5.13$$

$$NpO_2^{2+} \cdot NO + H_2O \overset{k_4}{\rightarrow} NpO_2^+ + HNO_2 + H^+ \qquad 5.14$$

As with the V(V) system, by taking equations 5.12 and 5.14 as the rate determining steps we can give the overall rate equation 5.15 which can be simplified further, equations 5.16 to 5.24. These simplification calculations utilise the assumptions that both HNO^+ and NpO_2^{2+}·NO are at steady state in order to get equations 5.17 and 5.20 respectively, and that the rate constants k_{-1} and k_{-3} associated with the back reactions of equations 5.11 and 5.13 are small compared to the forward reactions given in equations 5.12 and 5.14, in order to simplify equation 5.23 to that given in equation 5.24. From this, we can again split this into two forms of the rate equation when operating at either high acidity, equation 5.25, or low acidity, equation 5.26.

$$\frac{d[NpO_2^+]}{dt} = k_2[HNO^+][NpO_2^{2+}][H_2O] + k_4[NpO_2^{2+} \cdot NO][H_2O] \quad 5.15$$

Since; $$\frac{d[HNO^+]}{dt} = k_1[NO][H^+] - k_{-1}[HNO^+] - k_2[HNO^+][NpO_2^{2+}][H_2O] \quad 5.16$$

At steady state; $$k_1[NO][H^+] = k_{-1}[HNO^+] + k_2[HNO^+][NpO_2^{2+}][H_2O] \quad 5.17$$

$$[HNO^+] = \frac{k_1[NO][H^+]}{k_{-1} + k_2[NpO_2^{2+}][H_2O]} \quad 5.18$$

And; $$\frac{d[NpO_2^{2+} \cdot NO]}{dt} = k_3[NpO_2^{2+}][NO] - k_{-3}[NpO_2^{2+} \cdot NO] - k_4[NpO_2^{2+} \cdot NO][H_2O] \quad 5.19$$

At steady state; $$k_3[NpO_2^{2+}][NO] = k_{-3}[NpO_2^{2+} \cdot NO] + k_4[NpO_2^{2+} \cdot NO][H_2O] \quad 5.20$$

$$[NpO_2^{2+} \cdot NO] = \frac{k_3[NpO_2^{2+}][NO]}{k_{-3} + k_4[H_2O]} \quad 5.21$$

$$\frac{d[NpO_2^+]}{dt} = \frac{k_1k_2[NpO_2^{2+}][NO][H^+][H_2O]}{k_{-1} + k_2[NpO_2^{2+}][H_2O]} + \frac{k_3k_4[NpO_2^{2+}][NO][H_2O]}{k_{-3} + k_4[H_2O]} \quad 5.22$$

$$\frac{d[NpO_2^+]}{dt} = [NpO_2^{2+}][NO][H_2O]\left(\frac{k_1k_2[H^+]}{k_{-1} + k_2[NpO_2^{2+}][H_2O]} + \frac{k_3k_4}{k_{-3} + k_4[H_2O]}\right) \quad 5.23$$

$$\frac{d[NpO_2^+]}{dt} = [NpO_2^{2+}][NO]\left(\frac{k_1[H^+]}{[NpO_2^{2+}]} + k_3\right) \quad 5.24$$

At high [H⁺]; $$\frac{d[NpO_2^+]}{dt} = k_1[H^+][NO] \quad 5.25$$

At low [H⁺]; $$\frac{d[NpO_2^+]}{dt} = k_3[NpO_2^{2+}][NO] \quad 5.26$$

Whilst the order of reaction with respect to [Np(VI)] unfortunately could not be verified experimentally due to issues outlined in Section 5.3, the change in the kinetic rate equation is consistent with the change in order with respect to [H^+] seen in Section 5.2 above.

Using these rate equations given above along with the data gathered in Section 5.2, and assuming a saturated NO concentration of 3.02 mmol dm^{-3}, rate constants for the two pathways could therefore be calculated of $k_1 = 5.58 \times 10^{-5}$ dm^3 mol^{-1} s^{-1} and $k_3 = 1.96 \times 10^{-1}$ dm^3 mol^{-1} s^{-1} respectively. In comparing these to the values obtained for the vanadium system in Section 4.2.7 of $k_1 = 1.12 \times 10^{-3}$ dm^3 mol^{-1} s^{-1} and $k_3 = 5.66 \times 10^{-2}$ dm^3 mol^{-1} s^{-1} it can be seen that for both the Np and V systems pathway 2, involving the formation of a oxycation-NO adduct in both instances, is faster than the HNO^+ mediated pathway 1. It can also be seen that pathway 1 is faster for the vanadium system than the neptunium, whereas pathway 2 is faster for the Np system than the V system. Whilst pathway 1 being faster for the vanadium system might be unexpected due to the loss of the axial oxygen when reducing V(V) to V(IV) and the Np(VI) to Np(V) reduction being a simple one electron process, we propose here that this slower rate is due to the higher charge on the NpO_2^{2+} ion compared to the VO_2^+ ion making its interaction with the HNO^+ ion more unfavourable.

5.6 Chapter Summary

An experimental plan was drawn up to determine the mechanism by which Np(VI) is reduced by NO. Both the electrochemical pre-conditioning formation of Np(VI) and the stability of Np(VI) was tested and monitored using UV-visible spectroscopy.

Similar forms of the concentration *vs* time plots for the NO-bubbled systems of Np(VI) to those for the NO-bubbled V(V) systems suggest that, in the presence of excess NO generated in such experiments, NO is the dominant reductant at short timescales (i.e. over approximately the initial 10 minutes the reduction by NO is not competing with a secondary reduction by the HNO_2 formed by the oxidation of the NO itself). Dependency of the rate of reaction to $[H^+]$ concentration was then found by performing reductions of Np(VI) with NO at varying sulphuric acid concentrations. Rates of reactions were found to be independent of $[H^+]$ at concentrations < 1 mol dm^{-3} whilst some dependency was seen at concentrations > 1 mol dm^{-3}. This is consistent with experiments perform on the analogous vanadium system in Section 4.2.6.

These results, along with those previously show in Section 4.2 of the vanadium system, were then used to propose both a mechanism and rate expressions for the reduction of Np(VI) by NO, wherein the rate expression is seen to change due to a shift in the mechanistic pathway when moving from low to high acidity.

Due to issues caused by high sulphate loadings of neptunium stock solutions after recycle, orders of reaction with respect to [Np(VI)] at both high and low acidity could not be verified experimentally. Further work to verify the mechanism proposed herein should be done by performing reduction of Np(VI) by NO at varying Np(VI) concentrations at both high and low H_2SO_4 concentrations. These being done after removal of the high sulphate loadings now present in solution by performing purification of the Np solution *via* column chromatography.

However, based on the relative sizes of the values determined for the $k_1K_{protonation}$ and $k_2K_{protonation}$ rate constants for the NO_2^- and NO pathways respectively determined for the

vanadium system, Section 4.1.6, and assuming the relative sizes remain the same for the neptunium system, then in wholly *solution phase* experiments where the NO is generated by the nitrous acid catalysed oxidation of Np(V) by nitrate, see equations 1.23 to 1.27, the NO_2^- also formed during the oxidation of Np(V) by nitrate as a result of the reaction of the so-formed NO with nitrate, see equation 1.13, will dominate kinetically over the effect of NO and drive the back reduction of Np(VI) to Np(V).

6 Conclusions & Further Work

6.1 Project Objectives

Whilst the effect of the concentrations of nitrous and nitric acid on the extent of oxidation of neptunium has been previously seen within the literature to be dependent on the HNO_3:HNO_2 ratio, previous work attempting to fit Np(V) oxidation data to the current accepted kinetic expressions has shown inconsistencies. The key scientific objective of this thesis was therefore to assess the thus far unstudied, possible reductive effect of nitric oxide on the oxidation state of neptunium within the context of spent nuclear fuel reprocessing.

In order to achieve this, studies were carried out to address the following;

- Investigate the electrochemistry of NO and elucidated the oxidation potential of the NO/NO^+ couple
- Determine suitability/feasibility of the use of electrochemical quantification of HNO_2 during V(V)/Np(VI) reduction experiments
- Establish the suitability of V(V) as an analogue in wider studies of the reduction of Np(VI) by nitrogen-oxygen containing species
- Determine the role of NO in the reduction of V(V) to V(IV)
- Verify the observed results on the V(V) reduction by NO are applicable to the Np(VI) system

6.2 Conclusions

6.2.1 Electrochemistry of Nitrogen-Oxygen Species

The development of an electrochemical sensor for HNO_2 in the context of reduction reactions of V(V) or Np(VI) was seen to be feasible using either gold or glassy carbon as an electrode material due to the different position of the V/Np and HNO_2 current peaks on gold and due to the absence of a current response for Np on glassy carbon. The limit of detection obtainable by using an electrochemical method could also be improved by increasing the electrode area, however, this was impractical for the neptunium reduction experiments which were to be done within small volume reaction vessels for radiological safety reasons. Therefore, when comparing the achievable limits of detection for electrochemical methods to quantification by spectrophotometric methods also explored, the use of UV-vis was found to be a much more practical and reliable method to sense nitrous acid at the concentrations within this study. For this reason, and since UV-vis spectroscopy was to be utilised for quantification of the different metal oxidation states present anyway, for future reduction experiments concentrations of nitrous acid were determined by UV-vis, with any overlapping species being considered by the subtraction of their calculated absorbance – as detailed in Section 2.3.

Investigation into the electrochemical potential of the NO/NO^+ couple has found the onset of NO oxidation to occur at a potential at which the reduction of either Np(VI) or V(V) would be thermodynamically viable, highlighting the feasibility of direct reduction of Np(VI) and V(V) by NO.

More generally, consideration of the electrochemistry of the Np(V)/Np(VI) couple during investigation into electrochemical detection methods for HNO_2 has led us to advance a mechanism for the Np-assisted solvent wave oxidation. This was found to be due to an EC' mechanism in which, from the perspective of the neptunium couple, the electrochemical step of oxidation of Np(V) to Np(VI) is followed by a chemical step which regenerates the reactant

species for the electrochemical step, said chemical step caused by the reductive effect of electrogenerated H_2O_2 and $HO_2\cdot$ species.

6.2.2 Vanadium as a Neptunium Analogue

Studies into the reduction of V(V) by HNO_2 and comparing the results to those given by Precek and Paulenova on the reduction of Np(VI) by HNO_2 have shown the reduction of V(V) to V(IV) to be a suitable non-active surrogate for Np(VI) in the context of the reduction reaction by NO to be studied within this work. Parallels taken from the referenced works, along with modelling of the data for the V(V) reduction by HNO_2, have also allowed for elucidation of the mechanism of the reduction of V(V) by HNO_2, with the reduction being seen to go *via* the two pathways show again here for the convenience of the reader in equations 6.1 and 6.2, and for the calculation of rate parameters for the different mechanistic pathways involved.

$$VO_2^+ + NO_2^- + 2H^+ \rightleftharpoons VO^{2+} + NO_2 + H_2O \qquad 6.1$$

$$VO_2^+ + NO + H^+ \rightleftharpoons VO^{2+} + HNO_2 \qquad 6.2$$

Reductions of V(V) performed using bubbled NO have demonstrated its potential role in the reduction of Np(VI) within the context of nuclear fuel reprocessing and have given further insight into the mechanism of reaction for the direct reduction by NO wherein the reaction is seen to go via two mechanistic pathways; these pathways being either the initial protonation of NO, equations 6.3 and 6.4, or the initial formation of the oxycation-NO adduct, equations 6.5 and 6.6, the major pathway involved being seen to be dependent on the solution pH.

$$NO + H^+ \underset{k_{-1}}{\overset{k_1}{\rightleftharpoons}} HNO^+ \qquad 6.3$$

$$HNO^+ + VO_2^+ \overset{k_2}{\rightarrow} VO^{2+} + HNO_2 \qquad 6.4$$

$$VO_2^+ + NO \underset{k_{-3}}{\overset{k_3}{\rightleftharpoons}} VO_2^+ \cdot NO \quad 6.5$$

$$VO_2^+ \cdot NO + H^+ \overset{k_4}{\rightarrow} VO^{2+} + HNO_2 \quad 6.6$$

6.2.3 Nitric Oxide-Driven Reduction of Neptunium

Firstly, both the electrochemical pre-conditioning formation of Np(VI) and the stability of Np(VI) was tested and were found to be successful over the time periods for which experiments looking at the reduction of Np(VI) by NO were to be studied.

Reductions of Np(VI) by bubbled NO were performed and showed similar forms of the concentration *vs* time plots for the NO-bubbled systems of Np(VI) to those for the NO-bubbled V(V) systems. This suggested that, in the presence of excess NO generated in such experiments, NO is the dominant reductant at short timescales. Dependency of the rate of reaction to $[H^+]$ concentration was then found by performing reductions of Np(VI) with NO at varying sulphuric acid concentrations. Rates of reactions were found to be independent of $[H^+]$ at concentrations < 1 mol dm^{-3} whilst some dependency was seen at concentrations > 1 mol dm^{-3}. This is consistent with experiments perform on the analogous vanadium system in Section 4.2.6.

Due to issues caused by high sulphate loadings of neptunium stock solutions after recycle, orders of reaction with respect to [Np(VI)] at both high and low acidity could not be verified experimentally. However, results found for the dependence of the reaction on $[H^+]$, along with those previously show in Section 4.2 of the vanadium system, could be used to propose both a mechanism and rate expressions for the reduction of Np(VI) by NO. For this mechanism, the rate expression was seen to change when moving from high to low acidity due to a shift in the mechanistic pathway wherein the dominant pathway shifted from the initial protonation of NO, equation 6.7, to initial complexation of the metal ion with NO, equation 6.9, both then followed by the reduction step, equations 6.8 and 6.10 respectively.

$$NO + H^+ \underset{k_{-1}}{\overset{k_1}{\rightleftharpoons}} HNO^+ \quad 6.7$$

$$HNO^+ + NpO_2^{2+} + H_2O \overset{k_2}{\rightarrow} NpO_2^+ + HNO_2 + 2H^+ \quad 6.8$$

$$NpO_2^{2+} + NO \underset{k_{-3}}{\overset{k_3}{\rightleftharpoons}} NpO_2^{2+} \cdot NO \quad 6.9$$

$$NpO_2^{2+} \cdot NO + H_2O \overset{k_4}{\rightarrow} NpO_2^+ + HNO_2 + H^+ \quad 6.10$$

The derived rate parameter data for each of the above mechanistic pathways indicates that for both the Np and V systems pathway 2, involving the formation of an oxycation-NO adduct in both instances, is faster than the HNO^+ mediated pathway 1. It can also be seen that pathway 1 is faster for the vanadium system than the neptunium, whereas pathway 2 is faster for the Np system than the V system with this difference likely being due to cation-cation repulsions playing a role in pathway 1, whilst no such difficulties are encounter in the oxycation-NO adduct based mechanism of pathway 2.

Based on the relative sizes of the values determined for the $k_1K_{protonation}$ and $k_2K_{protonation}$ rate constants for the NO_2^- and NO pathways respectively determined for the vanadium system, Section 4.1.6, and assuming the relative sizes remain the same for the neptunium system, then in solution phase experiments where the NO is generated by the nitrous acid catalysed oxidation of Np(V) by nitrate, the NO_2^- concentration also formed during the oxidation of Np(V) by nitrate will dominate over the low concentration of NO and drive the back reduction of Np(VI) to Np(V).

6.3 Further Work

Whilst the work presented in this thesis has given insight into identifying the mechanism by which Np(VI) may be reduced by NO, further work to verify the mechanism proposed herein should be done by performing reduction of Np(VI) by NO at varying Np(VI) concentrations at both high and low H_2SO_4 concentrations (these having not been performed due to issues with high sulphate loadings wherein the thermodynamic stability afforded to the Np(VI) ion by its complexation with sulphate caused the reduction of the +VI ion by NO to be turned off). This would therefore allow for the order of reaction with respect to neptunium to be determined through the method of initial rates, as was done for the vanadium system studied in Section 4.2.5. These reductions should be done after removal of the high sulphate loadings now present in solution by performing purification of the Np solution *via* column chromatography.

Further information on the mechanism of reaction for the reduction of both V(V) and Np(VI) by NO could also be found by performing these reductions at varying NO gas flow rates. This experimental data could then be used along with equations for the gas-liquid mass transfer kinetics to determine the order of reaction with respect to NO, and hence validate the mechanisms proposed within this thesis.

Work presented within this thesis should also be restructured for publication into a series of journal papers, with the tentative outlines of these papers being as follows.

The first of these papers should cover the results presented in Chapter 3 as an analytical chemistry paper, potentially submitted to the Journal of Electroanalytical Chemistry, looking at the electrochemical detection of nitrous acid and other NOx species in the context of nuclear fuel reprocessing. This paper will include the cyclic voltammograms of nitrous acid measured on the different materials of platinum, gold, and glassy carbon, the mechanistic electrode surface behaviour determined on these different materials, and the potential benefits and limits in use of electrochemical methods for NOx detection.

The second paper should cover results presented in Chapter 4 and first show the work done for the validation of use of V(V) as a Np(VI) analogue by studying the reduction of V(V) by HNO_2 and comparing the results to those given by Precek and Paulenova on the reduction of Np(VI) by HNO_2. This will also include the additional mechanistic information determined through modelling of the experimental results. Results and discussion on the mechanism for the reduction of V(V) by nitric oxide will then also be included.

The final paper, covering the results presented in Chapter 5 and potentially submitted to the Journal of Inorganic and Nuclear Chemistry, will be structured to show the results found for the reduction of Np(VI) by nitric oxide, the discussion on the proposed mechanism consistent with the experimental observations, as well as the turning off of the reduction at high sulphate loadings due to the extra thermodynamic stability afforded to the neptunium with sulphate complexation.

Bibliography

1. IEA. *World electricity final consumption by sector, 1974-2019*. 2022 July 2022 [cited 2022 09/12/2022]; Available from: https://www.iea.org/data-and-statistics/charts/world-electricity-final-consumption-by-sector-1974-2019.
2. Agency, I.E., *World Energy Outlook 2022*. 2022.
3. *Outline History of Nuclear Energy*. 2022 12/12/22]; Available from: https://world-nuclear.org/information-library/current-and-future-generation/outline-history-of-nuclear-energy.aspx.
4. Wydler, J.W., U.S.C.H.C.o. Science, and Technology, *Oversight of Breeder Reactor Development in the United Kingdom: To the Committee on Science and Technology, U.S. House of Representatives, Ninety-sixth Congress, Second Session*. 1981: U.S. Government Printing Office.
5. *Nuclear Development in the United Kingdom*. 2022 12/12/22]; Available from: https://www.world-nuclear.org/information-library/country-profiles/countries-t-z/appendices/nuclear-development-in-the-united-kingdom.aspx.
6. *Nuclear power in a clean energy system*. 2019 01/07/2019]; Available from: https://www.iea.org/publications/nuclear/.
7. *Nuclear Power in the World Today*. 2019 01/07/19]; Available from: http://www.world-nuclear.org/information-library/current-and-future-generation/nuclear-power-in-the-world-today.aspx.
8. *Nuclear Energy Data*. 2018, OECD NEA. p. 104.
9. *Energy Trends: March 2019*, E.I.S. Department for Business, Editor. 2019: United Kingdom.
10. *Energy Trends: March 2020*, E.I.S. Department for Business, Editor. 2020: United Kingdom.

11. *Nuclear Power in the United Kingdom*. 2020 [cited 2020 10/03/2020]; Available from: https://www.world-nuclear.org/information-library/country-profiles/countries-t-z/united-kingdom.aspx.

12. *Nuclear Power in the United Kingdom*. 2022 [cited 2022 30/11/2022]; Available from: https://www.world-nuclear.org/information-library/country-profiles/countries-t-z/united-kingdom.aspx.

13. *Meeting the Energy Challenge: A White Paper on Nuclear Power*, E.R.R. Department for Business, Editor. 2008: United Kingdom.

14. *The UK's Nuclear Future*, I.S.a.D.o.E.C.C. Department for Business, Editor. 2013: United Kingdom.

15. *Processing of Used Nuclear Fuel*. 2018 [cited 2020 10/03/2020]; Available from: http://www.world-nuclear.org/information-library/nuclear-fuel-cycle/fuel-recycling/processing-of-used-nuclear-fuel.aspx.

16. *Uranium 2018: Resources, Production and Demand*. 2018, OECD NEA, IAEA. p. 462.

17. Corkhill, C. and N. Hyatt, *Nuclear Waste Management*. 2018, IOP Publishing.

18. Management, R.W. *Guidance - Geological Disposal*. 02/06/2021]; A permanent solution for the UK's higher-activity radioactive waste]. Available from: https://www.gov.uk/guidance/geological-disposal.

19. *Nuclear Energy Research and Development Roadmap: Future Pathways*, I.S. Department for Business and D.o.E.C. Change, Editors. 2013: United Kingdom.

20. *Fuelling Net Zero: Advanced Nuclear Fuel Cycle Roadmaps for a Clean Energy Future*. 2021.

21. Hiezl, Z., *Processing and microstructural characterisation of UO2-based simulated spent nuclear fuel ceramics for the UK`s advanced gas-cooled reactors*, in *Department of Materials*. 2015, Imperial College London. p. 260.

22. Herbst, R.S., P. Baron, and M. Nilsson, *Standard and advanced separation: PUREX processes for nuclear fuel reprocessing*, in *Advanced Separation Techniques for*

Nuclear Fuel Reprocessing and Radioactive Waste Treatment. 2011, Elsevier Science. p. 141-175.

23. Baron, P., et al., *A review of separation processes proposed for advanced fuel cycles based on technology readiness level assessments.* Progress in Nuclear Energy, 2019. **117**: p. 103091.
24. Sood, D.D. and S.K. Patil, *Chemistry of nuclear fuel reprocessing: Current status.* Journal of Radioanalytical and Nuclear Chemistry, 1996. **203**(2): p. 547-573.
25. Choppin, G., et al., *The Nuclear Fuel Cycle*, in *Radiochemistry and Nuclear Chemistry*. 2013, Elsevier. p. 685-751.
26. Joly, P. and E. Boo, *SACESS Roadmap: Actinide separation processes*. 2015.
27. *State-of-the-Art Report on the Progress of Nuclear Fuel Cycle Chemistry*. 2018, OECD NEA. p. 304.
28. Todd, T.A. and R.A. Wigeland, *Advanced Separation Technologies for Processing Spent Nuclear Fuel and the Potential Benefits to a Geologic Repository*, in *Separations for the Nuclear Fuel Cycle in the 21st Century*. 2006, American Chemical Society. p. 41-55.
29. Sakurai, T., et al., *The Composition of NOx Generated in the Dissolution of Uranium Dioxide.* Nuclear Technology, 1988. **83**(1): p. 24-30.
30. Carrott, M.J., et al., *The Chemistry of (U,Pu)O2 Dissolution in Nitric Acid.* Procedia Chemistry, 2012. **7**: p. 92-97.
31. Nikitina, G.P., et al., *Existing methods of plutonium dioxide dissolution 2 Reduction-oxidation plutonium dioxide dissolution using homogeneous catalysts.* Radiokhimiya, 1997. **39**(2): p. 109-122.
32. Zundelevich, Y., *The mediated electrochemical dissolution of plutonium oxide: kinetics and mechanism.* Journal of Alloys and Compounds, 1992. **182**(1): p. 115-130.
33. Bourges, J., et al., *Dissolution du bioxyde de plutonium en milieu nitrique par l'argent(II) electrogenere.* Journal of the Less Common Metals, 1986. **122**: p. 303-311.

34. Burrows, C., C. Phillips, and A. Milliken, *The Thermal Oxide Reprocessing Plant at Sellafield - Lessons Learned from 10 Years of Hot Operations and their Applicability to the DOE Environmental Management Program*, in *WM'06 Conference*. 2006: Tucson, Arizona.

35. Alcock, K., et al., *Tri-n-butyl phosphate as an extracting solvent for inorganic nitrates—V: Further results for the tetra- and hexavalent actinide nitrates.* Journal of Inorganic and Nuclear Chemistry, 1958. **6**(4): p. 328-333.

36. Best, G.F., H.A.C. McKay, and P.R. Woodgate, *Tri-n-butyl phosphate as an extracting solvent for inorganic nitrates—III The plutonium nitrates.* Journal of Inorganic and Nuclear Chemistry, 1957. **4**(5): p. 315-320.

37. Natrajan, L.S. and M.H. Langford Paden, *CHAPTER 6 F ‐ block Elements Recovery*, in *Element Recovery and Sustainability*. 2013, The Royal Society of Chemistry. p. 140-184.

38. Kim, S.Y., T. Asakura, and Y. Morita, *Electrochemical and spectroscopic studies of Pu(IV) and Pu(III) in nitric acid solutions.* Journal of Radioanalytical and Nuclear Chemistry, 2013. **295**(2): p. 937-942.

39. Collins, E.D., *12 - Advanced thermal denitration conversion processes for aqueous-based reprocessing and recycling of spent nuclear fuels*, in *Reprocessing and Recycling of Spent Nuclear Fuel*, R. Taylor, Editor. 2015, Woodhead Publishing: Oxford. p. 313-323.

40. *Mixed Oxide (MOX) Fuel*. 2022 [cited 2022 30/11/2022]; Available from: https://world-nuclear.org/information-library/nuclear-fuel-cycle/fuel-recycling/mixed-oxide-fuel-mox.aspx.

41. Phillips, C., *The Thermal Oxide Reprocessing Plant at Sellafield: Four Years of Successful Treatment of Irradiated Nuclear Fuel* in *WM'99 CONFERENCE*. 1999: Tucson, Arizona.

42. Greintz, R.M. and D.H. Neal, *Plutonium(IV) oxalate precipitation and calcination process for plutonium nitrate to oxide conversion*. 1978: United States.

43. Ondrejcin, R.S. and T.P. Garrett, Jr., *THE THERMAL DECOMPOSITION OF ANHYDROUS URANYL NITRATE AND URANYL NITRATE DIHYDRATE1*. The Journal of Physical Chemistry, 1961. **65**(3): p. 470-473.

44. Collins, E.D., S.L. Voit, and R.J. Vedder, *Evaluation of Co-precipitation Processes for the Synthesis of Mixed-Oxide Fuel Feedstock Materials*. 2011: United States.

45. Basunia, M.S., *Nuclear Data Sheets for A = 237.* Nuclear Data Sheets, 2006. **107**(8): p. 2323-2422.

46. Eckhardt, R.C., et al., *Yucca Mountain: Looking ten thousand years into the future*, in *Los Alamos Science*, N.G. Cooper, Editor. 2000, Los Alamos National Laboratory: Los Alamos.

47. Law, G.T.W., et al., *Geomicrobiological Redox Cycling of the Transuranic Element Neptunium.* Environmental Science & Technology, 2010. **44**(23): p. 8924-8929.

48. Choppin, G., et al., *22. Behavior of Radionuclides in the Environment*, in *Radiochemistry and Nuclear Chemistry*. Elsevier.

49. Tanaka, S., et al., *Geochemical Behavior of Neptunium.* Journal of Nuclear Science and Technology, 1992. **29**(7): p. 706-718.

50. Sarsfield Mark, J., J. Taylor Robin, and J. Maher Chris, *Neptunium(V) disproportionation and cation–cation interactions in TBP/kerosene solvent.* Radiochimica Acta, 2007. **95**(12): p. 677.

51. Escure, H., D. Gourisse, and J. Lucas, *Dismutation du neptunium pentavalent en solution nitrique—I: Etudes a l'equilibre.* Journal of Inorganic and Nuclear Chemistry, 1971. **33**(6): p. 1871-1876.

52. Hindman, J.C., J.C. Sullivan, and D. Cohen, *The Effect of Deuterium on the Kinetics of Reactions Involving Neptunium(IV), (V) and (VI) Ions1.* Journal of the American Chemical Society, 1959. **81**(10): p. 2316-2319.

53. Sjoblom, R. and J.C. Hindman, *Spectrophotometry of Neptunium in Perchloric Acid Solutions1*. Journal of the American Chemical Society, 1951. **73**(4): p. 1744-1751.

54. Sullivan, J.C., D. Cohen, and J.C. Hindman, *Kinetics of Reactions Involving Neptunium(IV), Neptunium(V) and Neptunium(VI) Ions in Sulfate Media1*. Journal of the American Chemical Society, 1957. **79**(15): p. 4029-4034.

55. Hindman, J.C., J.C. Sullivan, and D. Cohen, *Kinetics of Reactions between Neptunium Ions. The Neptunium(IV)-Neptunium(VI) Reaction in Perchlorate Solution.* Journal of the American Chemical Society, 1954. **76**(12): p. 3278-3280.

56. Takanashi, M., et al., *Numerical simulation of neptunium extraction behavior in Co-decontamination stage for late split purex system.* Journal of Nuclear Science and Technology, 1997. **34**(8): p. 817-822.

57. Takanashi, M., et al., *Neptunium concentration profiles in the Purex process.* Journal of Alloys and Compounds, 1998. **271–273**: p. 689-692.

58. Dey, P.K., et al., *Spent Fuel Reprocessing Options*. IAEA TECDOC Series. 2008, Vienna: International Atomic Energy Agency.

59. Birkett, J.E., et al., *Controlling Neptunium and Plutonium within Single Cycle Solvent Extraction Flowsheets for Advanced Fuel Cycles.* Journal of Nuclear Science and Technology, 2007. **44**(3): p. 337-343.

60. Roube, C.V., *A Review of Neptunium Behaviour in the Purex Process*. 2004, British Nuclear Fuels Limited.

61. Taylor, R.J., et al., *Progress towards the Full Recovery of Neptunium in an Advanced PUREX Process.* Solvent Extraction and Ion Exchange, 2013. **31**(4): p. 442-462.

62. Taylor, R.J., et al., *The applications of formo- and aceto-hydroxamic acids in nuclear fuel reprocessing*. Journal of Alloys and Compounds, 1998. **271–273**: p. 534-537.

63. Fox, O.D., et al., *Advanced PUREX Flowsheets for Future Np and Pu Fuel Cycle Demands*, in *Separations for the Nuclear Fuel Cycle in the 21st Century*. 2006, American Chemical Society. p. 89-102.

64. Andrieux, F., et al., *Modelling the Hydrolysis of Actinide Complexed Hydroxamic Acid Ligands*, in *Recent Advances in Actinide Science*, I. May, R. Alvares, and N. Bryan, Editors. 2006, Royal Society of Chemistry. p. 626-628.

65. Edwards, S., et al., *Neptunium(iv)-hydroxamate complexes: their speciation, and kinetics and mechanism of hydrolysis.* Dalton Transactions, 2019. **48**(2): p. 673-687.

66. Kim, K.-W., et al., *Oxidation State and Extraction of Neptunium with TBP*. Journal of Radioanalytical and Nuclear Chemistry, 2000. **246**(1): p. 215-219.

67. Uchiyama, G., S. Hotoku, and S. Fujine, *Distribution of Nitrous Acid Between Tri-N-Butyl Phosphate/ N-Dodecane and Nitric Acid.* Solvent Extraction and Ion Exchange, 1998. **16**(5): p. 1177-1190.

68. Ikeda-Ohno, A., et al., *Electrochemical and Complexation Behavior of Neptunium in Aqueous Perchlorate and Nitrate Solutions.* Inorganic Chemistry, 2008. **47**(18): p. 8294-8305.

69. Roube, C.V., et al., *Investigations into Np Routing in THORP HA/HS*. 2005, British Nuclear Fuels Limited.

70. Siddall, T.H. and E.K. Dukes, *Kinetics of HNO2 Catalyzed Oxidation of Neptunium(V) by Aqueous Solutions of Nitric Acid.* Journal of the American Chemical Society, 1959. **81**(4): p. 790-794.

71. Swanson, J.L., *Oxidation of Neptunium(V) in Nitric Acid Solution: Laboratory Study of Rate Accelerating Materials (RAM)*, in *Other Information: UNCL. Orig. Receipt Date: 31-DEC-69*. 1969. p. Medium: ED; Size: Pages: 29.

72. Koltunov, V.S., *Reaction kinetics of the actinides; Kinetika reaktsii aktinoidov*. Other Information: Orig. Receipt Date: 31-DEC-74. 1974. Medium: X; Size: Pages: 312.

73. Koltunov, V.S., et al., *Kinetics and Mechanism of the Oxidation of Neptunium(IV) by Nitric Acid in Tributyl Phosphate Solution.* Radiochimica Acta, 1997. **76**(1-2): p. 45.

74. Moulin, J.P., *Oxidation – reduction kinetics of neptunium in nitric acid solution*, in *Cinetiques Des Reactions D'Oxydo-reduction du Neptunium en Solution Nitrique*

Oxydation du Neptunium (IV) en Neptunium (V) Oxydation du Neptunium (V) en Neptunium (VI) Par L'acide Nitrique, Catalysees Par L'acide Nitreux. 1978.

75. Tochiyama, O., et al., *Kinetics of Nitrous Acid-Catalyzed Oxidation of Neptunium in Nitric Acid-TBP Extraction System.* Journal of Nuclear Science and Technology, 1995. **32**(2): p. 118-124.

76. Tochiyama, O., et al., *Equilibrium of Nitrous Acid-Catalyzed Oxidation of Neptunium in Nitric Acid-TBP Extraction System.* Journal of Nuclear Science and Technology, 1995. **32**(1): p. 50-59.

77. Homma, S., et al., *An Approach for Evaluating Equilibrium and Rate Constants for the Reaction of Np(V) with Nitric Acid in the Purex Process Using Process Data.* Nuclear Technology, 1996. **116**(1): p. 108-114.

78. Koltunov, V.S., et al., *Features of Kinetics and Mechanism of some Oxidation–Reduction Reactions of Np, Pu and U,* in *Proceedings of the Moscow Symposium on the Chemistry of Transuranium Elements*, J.J. Katz, Editor. 1976, Pergamon. p. 189-196.

79. Jianyu, H., et al., *Behavior of Neptunium in HNO3-HNO2 System (A Simulation Experiment for Dissolution of Spent Fuel Elements).* Radiochimica Acta, 1998. **83**(4): p. 183.

80. Topol, L.E., R.A. Osteryoung, and J.H. Christie, *Electrochemical Studies of NO + and NO 2 + in Concentrated H 2 S 04.* Journal of The Electrochemical Society, 1965. **112**(8): p. 861-864.

81. Bard, A.J., R. Parsons, and J. Jordan, *Standard Potentials in Aqueous Solution*. 1985: Taylor & Francis.

82. Lee, K.Y., D.J. Kuchynka, and J.K. Kochi, *Redox equilibria of the nitrosonium cation and of its nonbonded complexes.* Inorganic Chemistry, 1990. **29**(21): p. 4196-4204.

83. Tamayo García, C., A.J. Calandra, and A.J. Arvía, *The electrochemical reduction of nitrosonium ion in concentrated sulphuric acid: The NO+/NO redox couple.* Electrochimica Acta, 1972. **17**(12): p. 2181-2194.

84. Patel, B.A., et al., *Detection of Nitric Oxide Release from Single Neurons in the Pond Snail, Lymnaea stagnalis.* Analytical Chemistry, 2006. **78**(22): p. 7643-7648.

85. Boughriet, A. and M. Wartel, *Electrochemical and thermodynamic properties of oxygenated nitrogen compounds and aromatics in nitromethane. Application to the energetic aspects of the nitration process via inner-sphere and/or outer-sphere electron-transfer mechanisms.* Journal of the Chemical Society, Chemical Communications, 1989(13): p. 809-810.

86. Bennett, M.R. and A.D. Kelmers, *Reduction of plutonium(VI) to plutonium(IV) in nitric acid by nitric oxide or nitrogen dioxide gases*. 1978, Oak Ridge National Laboratory: United States.

87. Woods, M., T.A. Montag, and J.C. Sullivan, *A kinetic study of the oxidation of nitrous acid by Np(VI) and Am(VI) in perchlorate media.* Journal of Inorganic and Nuclear Chemistry, 1976. **38**(11): p. 2059-2061.

88. Precek, M. and A. Paulenova, *Kinetics of reduction of hexavalent neptunium by nitrous acid in solutions of nitric acid.* Journal of Radioanalytical and Nuclear Chemistry, 2010. **286**(3): p. 771-776.

89. Edwards, S., *Neptunium(V) oxidation by nitrous acid in nitric acid - A summary*.

90. Gregson, C., et al., *Neptunium (V) Oxidation by Nitrous Acid in Nitric Acid.* Procedia Chemistry, 2012. **7**: p. 398-403.

91. Mincher, B.J., et al., *The redox chemistry of neptunium in γ-irradiated aqueous nitric acid.* Radiochimica Acta, 2013. **101**(4): p. 259.

92. Mincher, B., M. Precek, and A. Paulenova, *The redox chemistry of neptunium in γ-irradiated aqueous nitric acid in the presence of an organic phase.* Journal of Radioanalytical and Nuclear Chemistry, 2015: p. 1-5.

93. Mincher, B.J., et al., *The role of oxidizing radicals in neptunium speciation in γ-irradiated nitric acid.* Journal of Radioanalytical and Nuclear Chemistry, 2013. **296**(1): p. 27-30.

94. Precek, M., et al., *Effect of Gamma Irradiation on the Oxidation State of Neptunium in Nitric Acid in the Presence of Selected Scavengers.* Separation Science and Technology, 2010. **45**(12-13): p. 1699-1705.

95. Gourisse, D., *Oxydation du neptunium(V) par les solutions aqueuses d'acide nitrique en presence d'acide nitreux.* Journal of Inorganic and Nuclear Chemistry, 1971. **33**(3): p. 831-837.

96. McLachlan, F., et al., *Neptunium Two Phase Trials 2007-2008*. 2008, Nexia Solutions.

97. Maher, C.J., *Current headend technologies and future developments in the reprocessing of spent nuclear fuels*, in *Reprocessing and Recycling of Spent Nuclear Fuel*, R. Taylor, Editor. 2015, Woodhead Publishing: Oxford. p. 93-124.

98. Lacher, J.R., J.D. Salzman, and J.D. Park, *Dissolving Uranium in Nitric Acid.* Industrial & Engineering Chemistry, 1961. **53**(4): p. 282-284.

99. Shabbir, M. and R.G. Robins, *Kinetics of the dissolution of uranium dioxide in nitric acid. I.* Journal of Applied Chemistry, 1968. **18**(5): p. 129-134.

100. Adachi, T., et al., *Dissolution study of spent PWR fuel: Dissolution behavior and chemical properties of insoluble residues.* Journal of Nuclear Materials, 1990. **174**(1): p. 60-71.

101. Marchenko, V.I., K.N. Dvoeglazov, and V.I. Volk, *Use of redox reagents for stabilization of Pu and Np valence forms in aqueous reprocessing of spent nuclear fuel: Chemical and technological aspects.* Radiochemistry, 2009. **51**(4): p. 329-344.

102. Ikeda, Y., et al., *Kinetic study on dissolution of UO2 powders in nitric acid.* Journal of Nuclear Materials, 1995. **224**(3): p. 266-272.

103. Taylor, R.F., et al., *Dissolution rates of uranium dioxide sintered pellets in nitric acid systems.* Journal of Applied Chemistry, 1963. **13**(1): p. 32-40.

104. Mineo, H., et al., *An Investigation into Dissolution Rate of Spent Nuclear Fuel in Aqueous Reprocessing.* Journal of Nuclear Science and Technology, 2004. **41**(2): p. 126-134.

105. Yakabuskie, P.A., et al., *Long-Term γ-Radiolysis Kinetics of NO3− and NO2− Solutions.* The Journal of Physical Chemistry A, 2011. **115**(17): p. 4270-4278.

106. Mark, G., et al., *The photochemistry of aqueous nitrate ion revisited.* Journal of Photochemistry and Photobiology A: Chemistry, 1996. **101**(2–3): p. 89-103.

107. Scharko, N.K., A.E. Berke, and J.D. Raff, *Release of Nitrous Acid and Nitrogen Dioxide from Nitrate Photolysis in Acidic Aqueous Solutions.* Environmental Science & Technology, 2014. **48**(20): p. 11991-12001.

108. Park, J.Y. and Y.N. Lee, *Solubility and decomposition kinetics of nitrous acid in aqueous solution.* The Journal of Physical Chemistry, 1988. **92**(22): p. 6294-6302.

109. Bhattacharyya, P.K. and R.D. Saini, *Radiolytic yields G(HNO2) and G(H2O2) in the aqueous nitric acid system.* International Journal for Radiation Physics and Chemistry, 1973. **5**(1): p. 91-99.

110. Jiang, P.-Y., et al., *γ-Radiolysis study of concentrated nitric acid solutions.* Journal of the Chemical Society, Faraday Transactions, 1994. **90**(1): p. 93-95.

111. Daniels, M. and E.E. Wigg, *Radiation chemistry of the aqueous nitrate system. I. γ-Radiolysis of dilute solutions.* The Journal of Physical Chemistry, 1967. **71**(4): p. 1024-1033.

112. Precek, M., A. Paulenova, and B.J. Mincher, *Reduction of Np(VI) in Irradiated Solutions of Nitric Acid.* Procedia Chemistry, 2012. **7**: p. 51-58.

113. Kazanjian, A.R., et al., *Radiolysis of nitric acid solution : L.E.T. effects.* Transactions of the Faraday Society, 1970. **66**(0): p. 2192-2198.

114. Abel, E. and H. Schmid, *The kinetics of nitrous acid.* Zeitschrift für Physikalische Chemie, 1928. **134**: p. 279-300.

115. Rayson, M.S., et al., *Accurate Rate Constants for Decomposition of Aqueous Nitrous Acid.* Inorganic Chemistry, 2012. **51**(4): p. 2178-2185.

116. Komiyama, H. and H. Inoue, *Reaction and Transport of Nitrogen Oxides in Nitrous Acid Solutions.* Journal of Chemical Engineering of Japan, 1978. **11**(1): p. 25-32.

117. Beake, B.D. and R.B. Moodie, *Role of the reaction of nitric oxide with oxygen in the decomposition of nitrous acid in aqueous acid solution.* Journal of the Chemical Society, Perkin Transactions 2, 1995(6): p. 1045-1048.

118. Nishimura, K., et al., *Effect of Nitrous Acid on Dissolution of UO2 Powders in Nitric Acid Optimal Conditions for Dissolving UO2.* Journal of Nuclear Science and Technology, 1995. **32**(2): p. 157-159.

119. Zhang, H., et al., *The reversible reaction kinetics of neptunium with nitrous and nitric acids.* Journal of Radioanalytical and Nuclear Chemistry, 2015: p. 1-6.

120. Garcia, E.E., *Determination of nitrite ion using the reaction with p-nitroaniline and azulene*. Analytical Chemistry, 1967. **39**(13): p. 1605-1607.

121. Hetrick, E.M. and M.H. Schoenfisch, *Analytical Chemistry of Nitric Oxide.* Annual Review of Analytical Chemistry, 2009. **2**(1): p. 409-433.

122. Yilong, Z., Z. Dean, and D. Li, *Electrochemical and Other Methods for Detection and Determination of Dissolved Nitrite: A Review*. Vol. 10. 2015. 1144-1168.

123. Brust, A.S., et al., *UV absorption cross sections of nitrous acid.* Atmospheric Environment, 2000. **34**(1): p. 13-19.

124. Hasegawa, S., et al., *Redox behavior of VO2+/VO2+as a simulant of NpO2+/NpO22+in boiling nitric acid solution.* Journal of Radioanalytical and Nuclear Chemistry, 2018. **317**(3): p. 1319-1328.

125. Fauvet, P., et al., *Corrosion mechanisms of austenitic stainless steels in nitric media used in reprocessing plants.* Journal of Nuclear Materials, 2008. **375**(1): p. 52-64.

126. Scheidt, W.R., *Crystallographic study of the structural trans effect. Molecular structure of oxoisopropoxobis(8-hydroxyquinolinato)vanadium(V).* Inorganic Chemistry, 1973. **12**(8): p. 1758-1761.

127. Dikshitulu, L.S.A., et al., *Kinetics and mechanism of oxidation of nitrous acid by vanadium(V).* Journal of Inorganic and Nuclear Chemistry, 1981. **43**(10): p. 2455-2457.

128. *11 - Nitrogen*, in *Chemistry of the Elements (Second Edition)*, N.N. Greenwood and A. Earnshaw, Editors. 1997, Butterworth-Heinemann: Oxford. p. 406-472.

129. Aga, R.G. and M.N. Hughes, *Chapter Three - The Preparation and Purification of NO Gas and the Use of NO Releasers: The Application of NO Donors and Other Agents of Nitrosative Stress in Biological Systems*, in *Methods in Enzymology*, K.P. Robert, Editor. 2008, Academic Press. p. 35-48.

130. Brauer, F.P., et al., *The specific activity and half-life of 237Np.* Journal of Inorganic and Nuclear Chemistry, 1960. **12**(3): p. 234-235.

131. *Specific Activities*. [cited 2020 06/04/2020]; Available from: http://www.iem-inc.com/information/tools/specific-activities.

132. Choi, N.H., S.-k. Kwon, and H. Kim, *Analysis of the Oxidation of the V(II) by Dissolved Oxygen Using UV-Visible Spectrophotometry in a Vanadium Redox Flow Battery.* Journal of The Electrochemical Society, 2013. **160**(6): p. A973-A979.

133. Brooker, R.P., et al., *Determining Vanadium Concentrations Using the UV-Vis Response Method.* Journal of The Electrochemical Society, 2015. **162**(4): p. A608-A613.

134. Burney, G.A. and R.M. Harbour, *Radiochemistry of Neptunium*. 1974: Technical Information Center, Office of Information Services, United States Atomic Energy Commission.

135. Blanc, P., C. Madic, and J.P. Launay, *Spectrophotometric identification of a mixed-valence cation-cation complex between aquadioxovanadium(V) and aquaoxovanadium(IV) ions in perchloric, sulfuric, and hydrochloric acid media.* Inorganic Chemistry, 1982. **21**(8): p. 2923-2928.

136. Chen, G. and H. Liu, *Understanding the Reduction Kinetics of Aqueous Vanadium(V) and Transformation Products Using Rotating Ring-Disk Electrodes.* Environmental Science & Technology, 2017. **51**(20): p. 11643-11651.

137. Wu, X., et al., *Study of vanadium(IV) species and corresponding electrochemical performance in concentrated sulfuric acid media.* Electrochimica Acta, 2011. **56**(27): p. 10197-10203.

138. Young, C.L., *Oxides of nitrogen*. 1981, Oxford [Oxfordshire]; New York: Pergamon Press.

139. Angerstein-Kozlowska, H., B.E. Conway, and W.B.A. Sharp, *The real condition of electrochemically oxidized platinum surfaces: Part I. Resolution of component processes.* Journal of Electroanalytical Chemistry and Interfacial Electrochemistry, 1973. **43**(1): p. 9-36.

140. Wang, Y., E. Laborda, and R.G. Compton, *Electrochemical oxidation of nitrite: Kinetic, mechanistic and analytical study by square wave voltammetry*. Journal of Electroanalytical Chemistry, 2012. **670**: p. 56-61.

141. Casella, I.G. and A.M. Salvi, *Voltammetric behavior and ion chromatographic detection of nitrite at a dispersed platinum glassy carbon electrode.* Electroanalysis, 1997. **9**(8): p. 596-601.

142. Bard, A.J., *Electrochemical methods : fundamentals and applications*. 2nd ed. ed, ed. L.R. Faulkner. 2000: New York : John Wiley.

143. Nicholson, R.S. and I. Shain, *Theory of Stationary Electrode Polarography. Single Scan and Cyclic Methods Applied to Reversible, Irreversible, and Kinetic Systems.* Analytical Chemistry, 1964. **36**(4): p. 706-723.

144. Kissinger, P.T. and W.R. Heineman, *Cyclic voltammetry.* Journal of Chemical Education, 1983. **60**(9): p. 702.

145. Vetter, K.J., *Entgegnung auf die vorstehende Arbeit von G. Schmid über „Die autokatalytische Natur der kathodischen Reduktion von Salpetersäure zu salpetriger Säure"*. Zeitschrift für Elektrochemie, Berichte der Bunsengesellschaft für physikalische Chemie, 1959. **63**(9-10): p. 1189-1191.

146. Schmid, G. and G. Krichel, *Die autokatalytische Natur der kathodischen Reduktion von Salpetersäure zu salpetriger Säure IV. Der potentiostatische Einschaltvorgang [1].* Berichte der Bunsengesellschaft für physikalische Chemie, 1964. **68**(7): p. 677-688.

147. Abel, E., H. Schmid, and S. Babad, *The kinetics of nitrous acid. V. Kinetics of nitrous acid-nitric acid-nitric oxide reaction.* Zeitschrift für Physikalische Chemie, 1928. **136U**(1): p. 419.

148. Abel, E., H. Schmid, and S. Babad, *Kinetik der salpetrigen Säure IV.* Zeitschrift für Physikalische Chemie, 1928. **136U**(1): p. 135.

149. Balbaud, F., et al., *Cathodic Reactions Involved in Corrosion Processes Occurring in Concentrated Nitric Acid at 100 °C.* European Journal of Inorganic Chemistry, 2000. **2000**(4): p. 665-674.

150. Chatterjee, S., et al., *Mechanisms of neptunium redox reactions in nitric acid solutions.* Inorganic Chemistry Frontiers, 2017. **4**(4): p. 581-594.

151. Chanon, M., et al., *Role of Single Electron Transfer in Dioxygen Activation. Swing Activation in Photochemistry, Electrochemistry, Thermal Chemistry.* New Journal of Chemistry, 1992. **16**: p. 171-201.

152. Shackleford, S.G.D., et al., *An in situ electrochemical quartz crystal microbalance study of polycrystalline gold electrodes in nitric acid solution.* Journal of Electroanalytical Chemistry, 2002. **538-539**: p. 109-119.

153. Hirabayashi, M., et al., *DNA immobilization on high aspect ratio glassy carbon (GC-MEMS) microelectrodes for bionanoelectronics applications.* Microsystem Technologies, 2015. **21**(11): p. 2359-2365.

154. Sharma, S., *Glassy Carbon: A Promising Material for Micro- and Nanomanufacturing.* Materials, 2018. **11**(10).

155. Vomero, M., et al., *Highly Stable Glassy Carbon Interfaces for Long-Term Neural Stimulation and Low-Noise Recording of Brain Activity.* Scientific Reports, 2017. **7**(1): p. 40332.

156. Friedman, H.A. and L.M. Toth, *Absorption spectra of Np(III), (IV), (V) and (VI) in nitric acid solution.* Journal of Inorganic and Nuclear Chemistry, 1980. **42**(9): p. 1347-1349.

157. Pope, M.T. and B.W. Dale, *Isopoly-vanadates, -niobates, and -tantalates.* Quarterly Reviews, Chemical Society, 1968. **22**(4): p. 527-548.

158. Krishtalik, L.I., *pH-dependent redox potential: how to use it correctly in the activation energy analysis.* Biochimica et Biophysica Acta (BBA) - Bioenergetics, 2003. **1604**(1): p. 13-21.

159. Gattrell, M., et al., *The electrochemical reduction of VO2+ in acidic solution at high overpotentials.* Electrochimica Acta, 2005. **51**(3): p. 395-407.

160. Littler, J.S. and W.A. Waters, *603. Oxidations of organic compounds with quinquevalent vanadium. Part II. The oxidation of ketones.* Journal of the Chemical Society (Resumed), 1959(0): p. 3014-3019.

161. Ltd, M.S. *Values of the Chi-squared distribution*. 2022 [cited 2022 30/01/2022]; Available from: https://www.medcalc.org/manual/chi-square-table.php.

162. Burrows, A., et al., *Chemistry³: Introducing Inorganic, Organic and Physical Chemistry*. 2013: OUP Oxford.

163. Lewis, G.N. and A. Edgar, *THE EQUILIBRIUM BETWEEN NITRIC ACID, NITROUS ACID AND NITRIC OXIDE.* Journal of the American Chemical Society, 1911. **33**(3): p. 292-299.

164. Zhaowu, Z., et al., *Generation of HNO2 by bubbling NO in HNO3 system and its application in the PUREX process.* Journal of Radioanalytical and Nuclear Chemistry, 2003. **258**(3): p. 557-561.

165. Casas, J.M., F. Alvarez, and L. Cifuentes, *Aqueous speciation of sulfuric acid–cupric sulfate solutions.* Chemical Engineering Science, 2000. **55**(24): p. 6223-6234.

166. Hayton, T.W., B.O. Patrick, and P. Legzdins, *New Details Concerning the Reactions of Nitric Oxide with Vanadium Tetrachloride.* Inorganic Chemistry, 2004. **43**(22): p. 7227-7233.

167. Hennig, C., et al., *The Sulfate Coordination of Np(IV), Np(V), and Np(VI) in Aqueous Solution.* Inorganic Chemistry, 2009. **48**(12): p. 5350-5360.

168. Guillaumont, R., et al., *Update on the Chemical Thermodynamics of Uranium, Neptunium, Plutonium, Americium and Technetium*. 2003: Elsevier Science.

Appendix A.

A-1. Thermogravimetric and couple mass spectrometric plot for the determination of the number of waters of crystallization present in $VOSO_4 \cdot xH_2O$

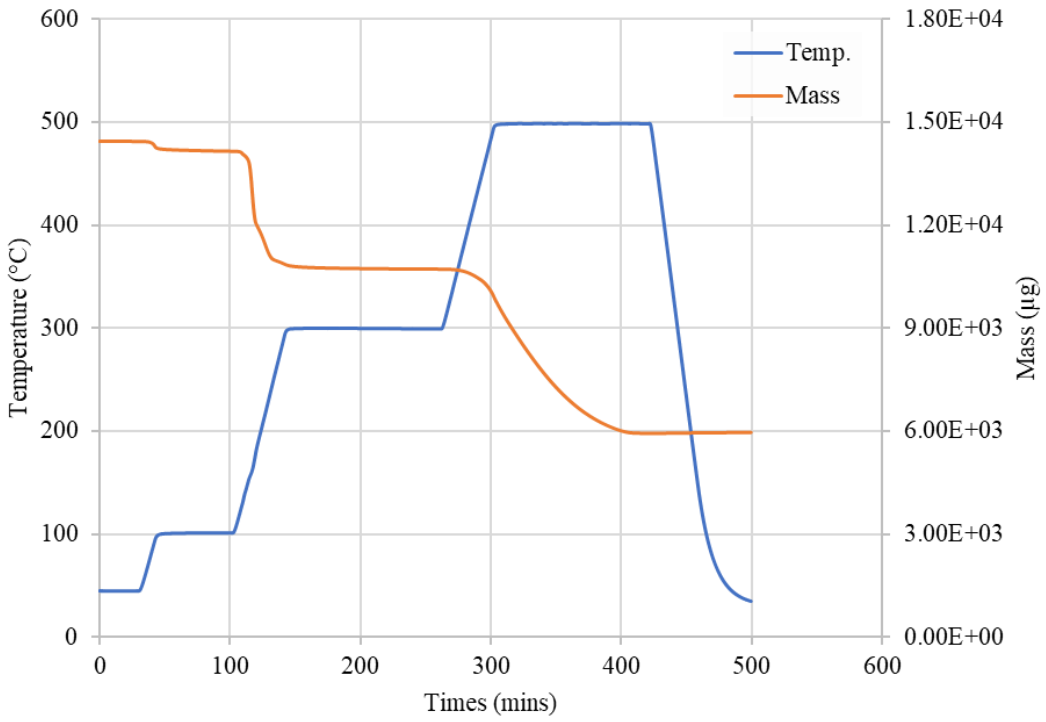

Figure A-1 Thermogravimetric analysis for a sample of $VOSO_4 \cdot xH_2O$

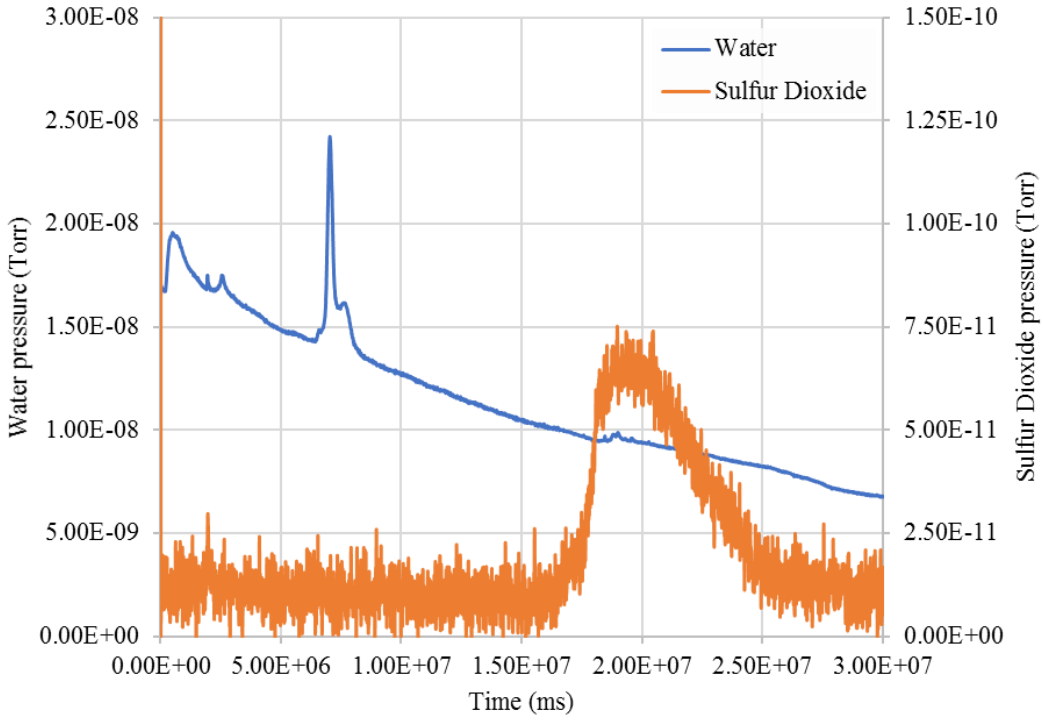

Figure A-2 Mass spectrometry analysis showing the evolution times of both water and sulfur dioxide during thermogravimetric analysis of .$VOSO_4 \cdot xH_2O$

A-2. Elemental analysis plot for the determination of the number of waters of crystallization present in $VOSO_4 \cdot xH_2O$

	Sample Weight / mg	Weight % N	Weight % C	Weight % H	Weight % S
Run 1	1.69	0.08	0.02	2.80	14.73
Run 2	1.17	0.11	0.02	2.79	14.63

Table A-1 Elemental analysis for a sample of $VOSO_4 \cdot xH_2O$

Appendix B.

t / days	Np-237 mass / g	Pa-233 mass present after Np-237 decay / g	Pa-233 mass remaining after Pa-233 decay / g	Pa-233 activity / Bq	%
1	m_{Np1}	$= m_{Np1} - \left(m_{Np1} \times \frac{1}{2}^{\left(\frac{1}{t_{1/2Np}}\right)} \right)$	$= m_{Pa1f} \times \frac{1}{2}^{\left(\frac{1}{t_{1/2Pa}}\right)}$	$= a_{Pa} \times m_{Pa1r}$	$= \frac{A_{Pa1}}{A_{Np0}} \times 100$
2	$= m_{Np1} - m_{Pa1f}$	$= m_{Pa1r} + m_{Np2} - \left(m_{Np2} \times \frac{1}{2}^{\left(\frac{1}{t_{1/2Np}}\right)} \right)$	$= m_{Pa2f} \times \frac{1}{2}^{\left(\frac{1}{t_{1/2Pa}}\right)}$	$= a_{Pa} \times m_{Pa2r}$	$= \frac{A_{Pa2}}{A_{Np0}} \times 100$
3	$= m_{Np2} - m_{Pa2f}$	$= m_{Pa2r} + m_{Np3} - \left(m_{Np3} \times \frac{1}{2}^{\left(\frac{1}{t_{1/2Np}}\right)} \right)$	$= m_{Pa3f} \times \frac{1}{2}^{\left(\frac{1}{t_{1/2Pa}}\right)}$	$= a_{Pa} \times m_{Pa3r}$	$= \frac{A_{Pa3}}{A_{Np0}} \times 100$

Table B-1 Calculation of Pa-233 ingrowth in samples of Np-237.

Appendix C.

C-1. Plots of Concentration vs. Time for the reduction of V(V) by HNO_2 at varying [V(V)]

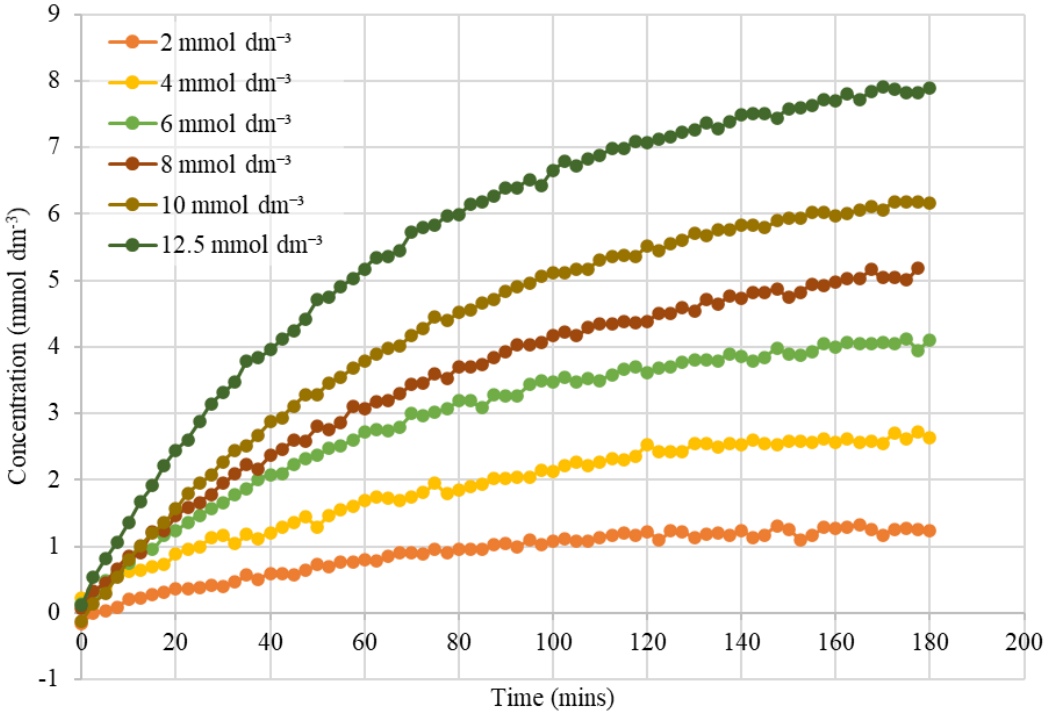

Figure C-1 Plot of the concentration of V(IV) vs time for solutions of varying [V(V)] in 0.1 mol dm^{-3} HNO_3. (initial conditions: [HNO_2] = 30 mmol dm^{-3}, [VO_2^+] = 2-12.5 mmol dm^{-3})

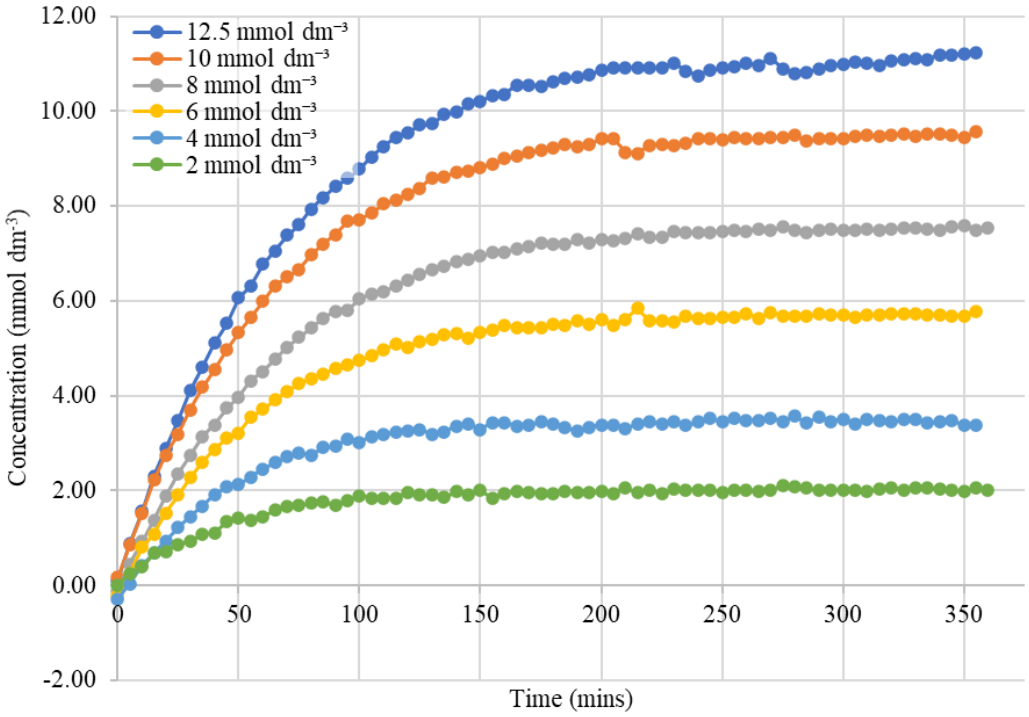

Figure C-2 Plot of the concentration of V(IV) vs time for solutions of varying [V(V)] in 0.1 mol dm^{-3} H_2SO_4. (initial conditions: [HNO_2] = 30 mmol dm^{-3}, [VO_2^+] = 2-12.5 mmol dm^{-3})

C-2. Plots of Concentration vs. Time for the reduction of V(V) by HNO_2 at varying $[HNO_2]$

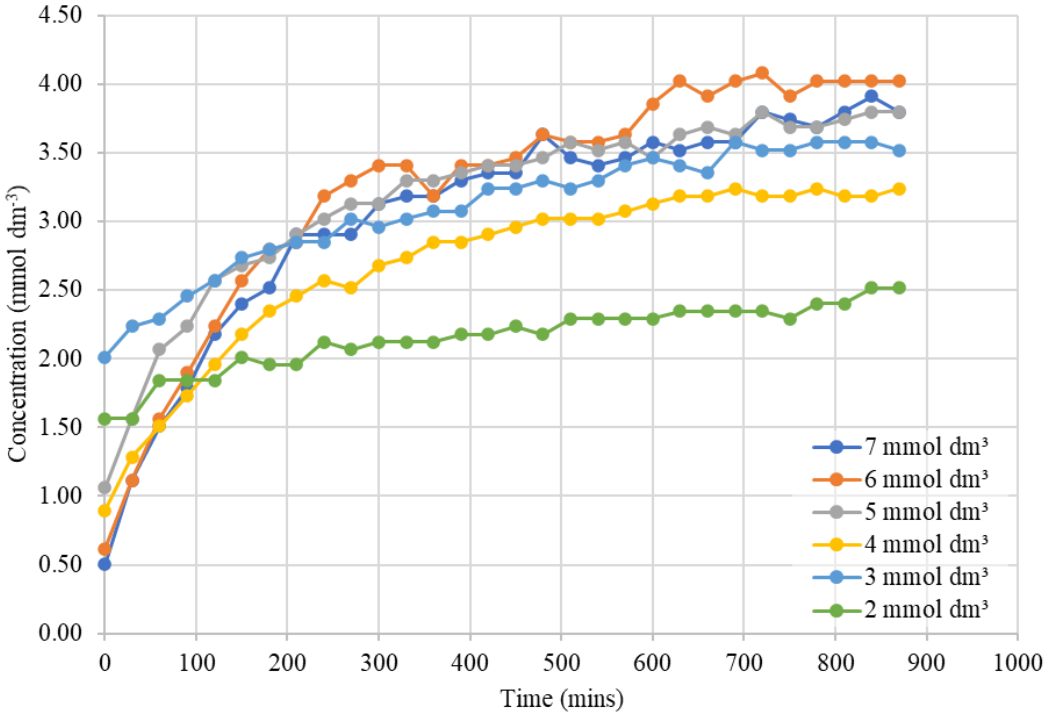

Figure C-3 Plot of the concentration of V(IV) vs time for solutions of [V(V)] in 0.1 mol dm^{-3} HNO_3. (initial conditions: $[HNO_2]$ = 2-7 mmol dm^{-3}, $[VO_2^+]$ = 15 mmol dm^{-3})

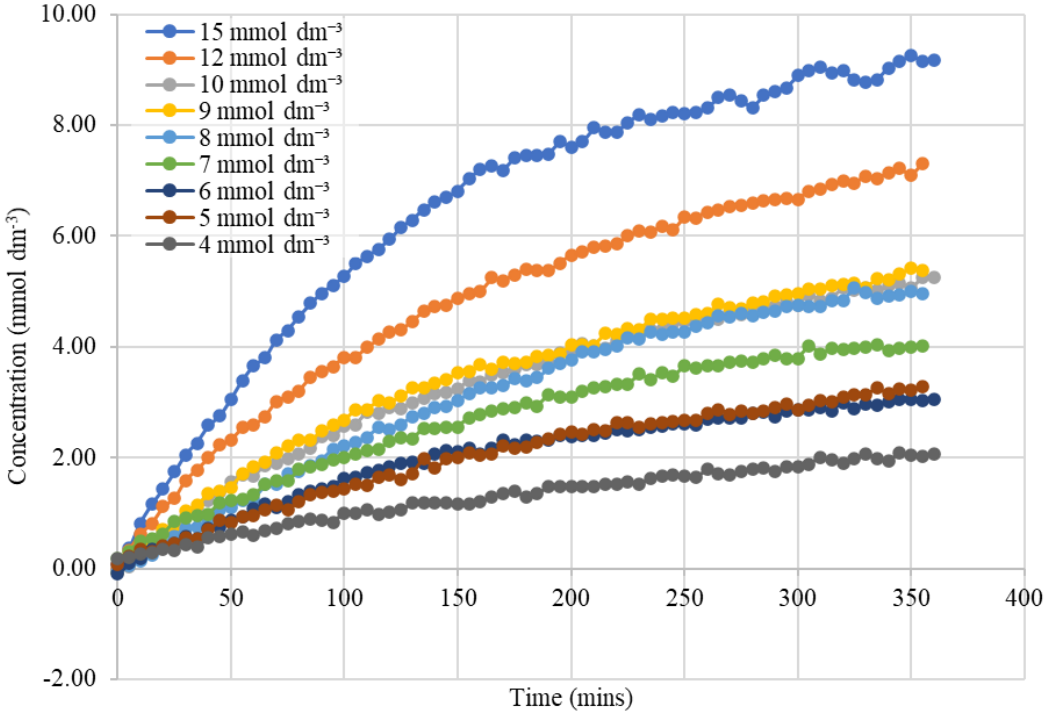

Figure C-4 Plot of the concentration of V(IV) vs time for solutions of [V(V)] in 0.1 mol dm^{-3} H_2SO_4. (initial conditions: $[HNO_2]$ = 4-15 mmol dm^{-3}, $[VO_2^+]$ = 15 mmol dm^{-3})

C-3. Plots of Concentration vs. Time for the reduction of V(V) by HNO_2 at varying $[H^+]$ and $[NO_3^-]$

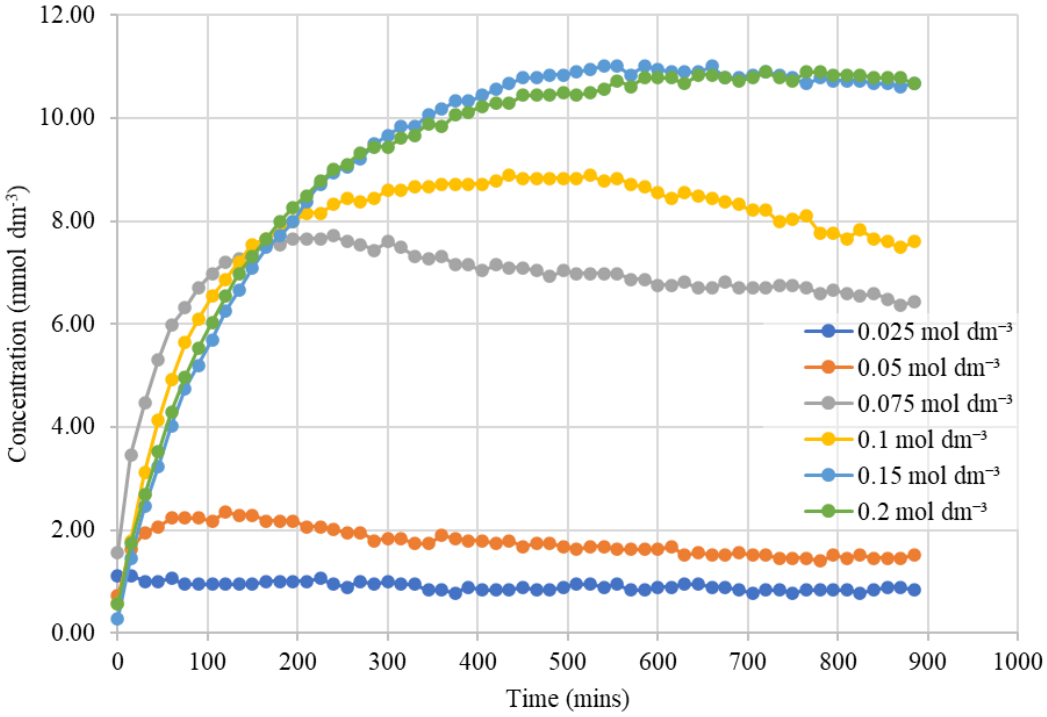

Figure C-5 Plot of the concentration of V(IV) vs time for solutions of [V(V)] in 0.025-0.2 mol dm^{-3} H^+ and 2 mol dm^{-3} NO_3^-. (initial conditions: $[HNO_2]$ = 30 mmol dm^{-3}, $[VO_2^+]$ = 12.5 mmol dm^{-3})

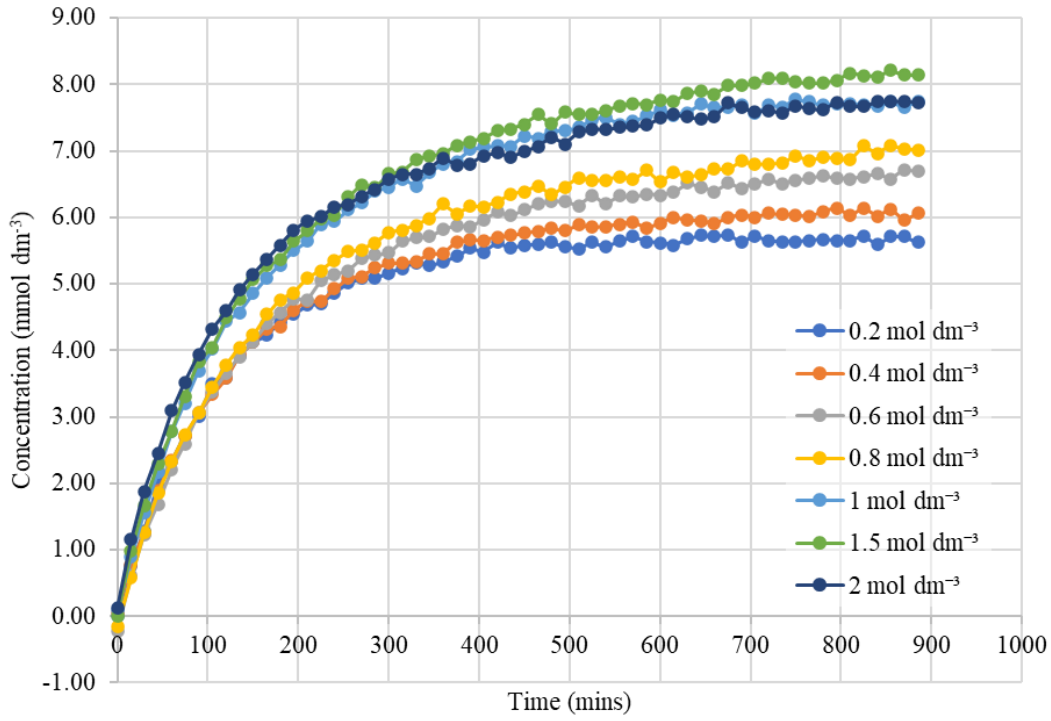

Figure C-6 Plot of the concentration of V(IV) vs time for solutions of [V(V)] in 0.2-2 mol dm^{-3} H^+ and 2 mol dm^{-3} NO_3^-. (initial conditions: [HNO_2] = 30 mmol dm^{-3}, [VO_2^+] = 12.5 mmol dm^{-3})

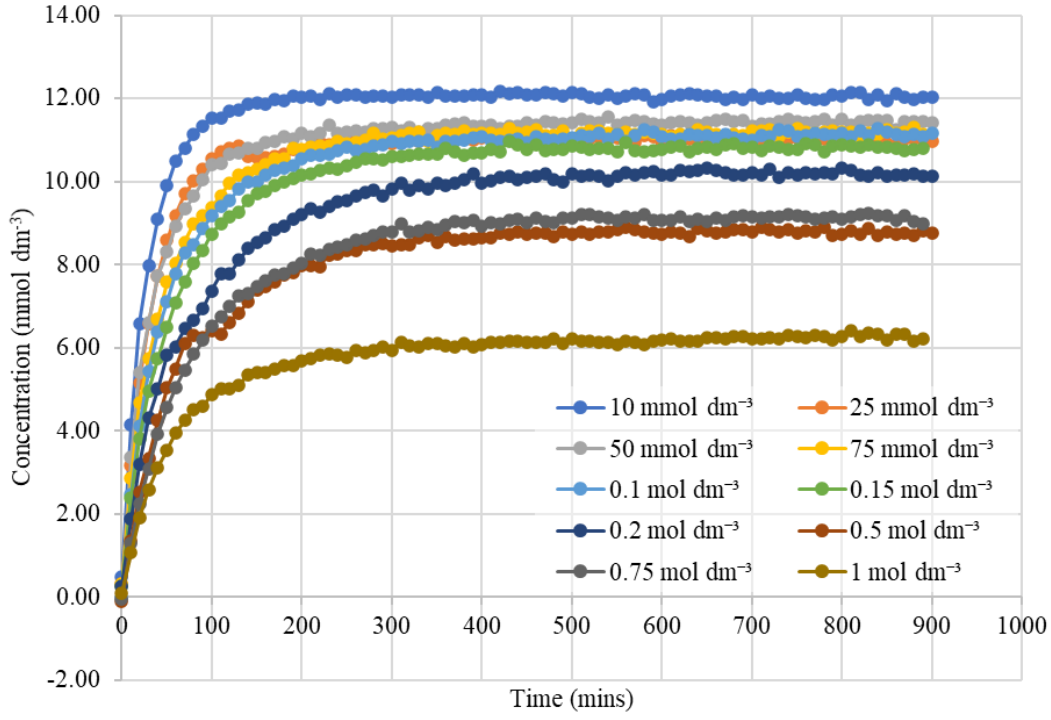

Figure C-7 Plot of the concentration of V(IV) vs time for solutions of [V(V)] in 1 mol dm^{-3} H^+ and 0.01-1 mol dm^{-3} NO_3^-. (initial conditions: [HNO_2] = 30 mmol dm^{-3}, [VO_2^+] = 12.5 mmol dm^{-3})

C-4. Plots of Concentration vs. Time for the reduction of V(V) by HNO_2 at varying $[SO_4^{2-}]$ and $[ClO_4^-]$

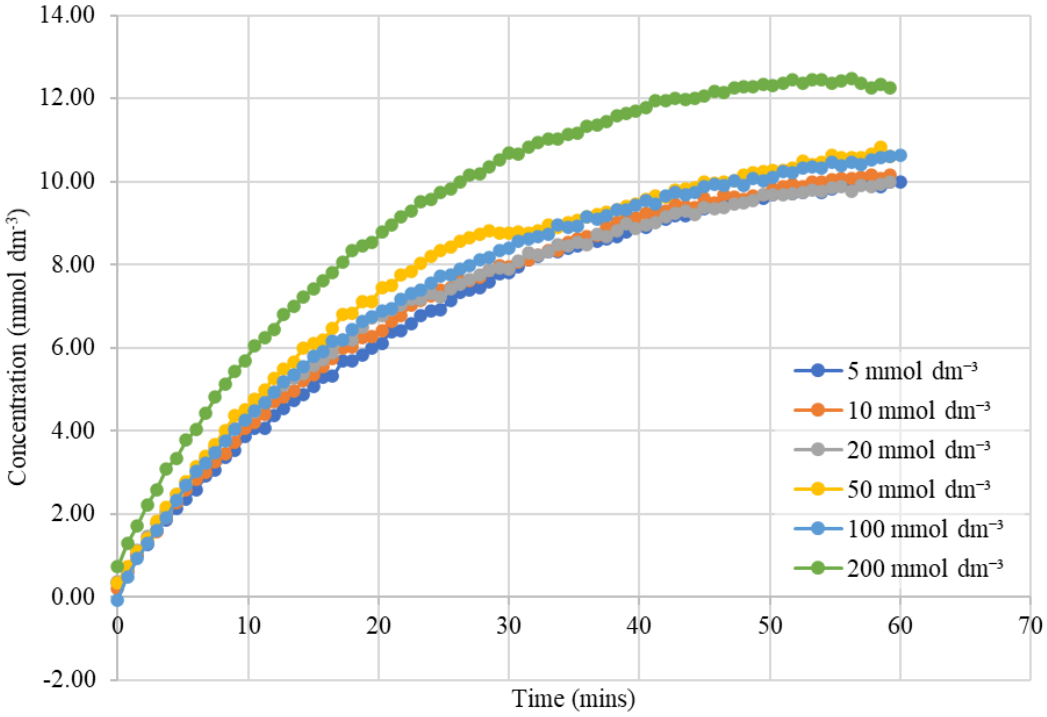

Figure C-8 Plot of the concentration of V(IV) vs time for solutions of [V(V)] in 1 mol dm^{-3} H^+ and 5-200 mmol dm^{-3} SO_4^{2-}. (initial conditions: $[HNO_2]$ = 30 mmol dm^{-3}, $[VO_2^+]$ = 12.5 mmol dm^{-3})

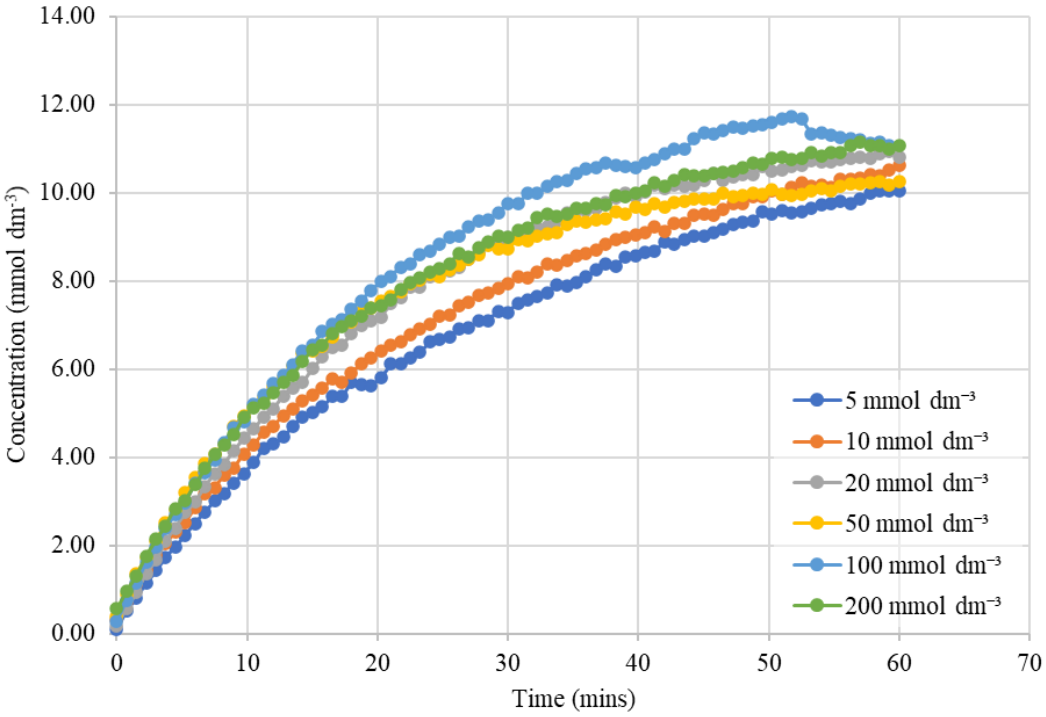

Figure C-9 Plot of the concentration of V(IV) vs time for solutions of [V(V)] in 1 mol dm^{-3} H^+ and 5-200 mmol dm^{-3} ClO_4^-. (initial conditions: [HNO_2] = 30 mmol dm^{-3}, [VO_2^+] = 12.5 mmol dm^{-3})

C-5. Plots of Concentration vs. Time for the reduction of V(V) by NO at varying [V(V)]

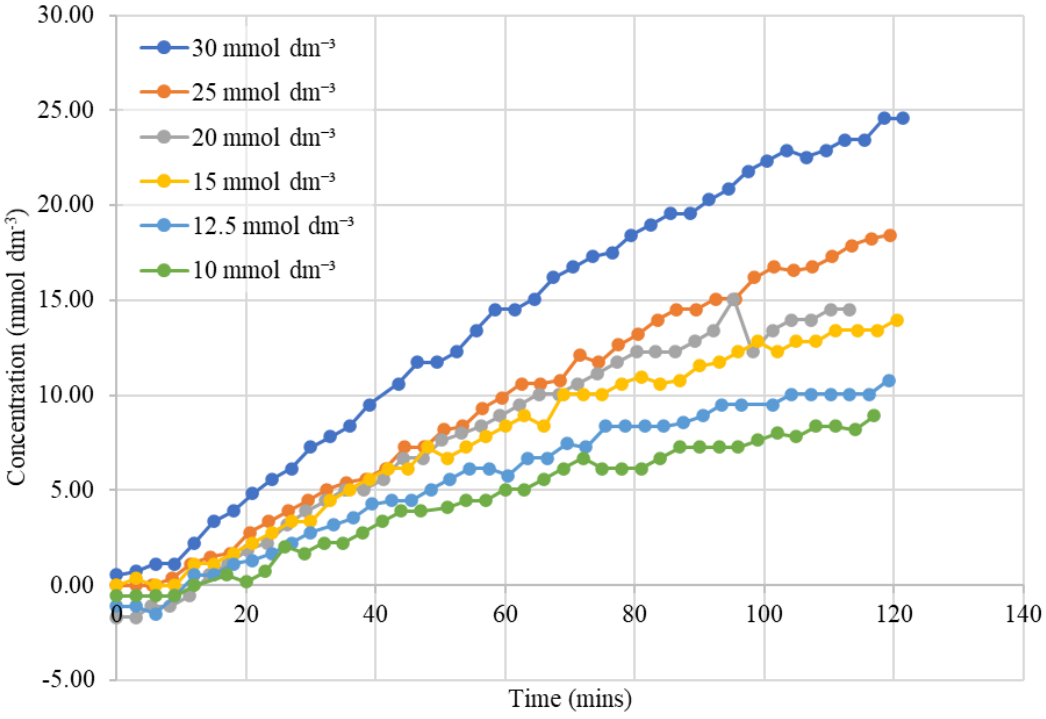

Figure C-10 Plot of the concentration of V(IV) vs time for solutions of 10-30 mmol dm^{-3} [V(V)] in 0.1 mol dm^{-3} H_2SO_4.

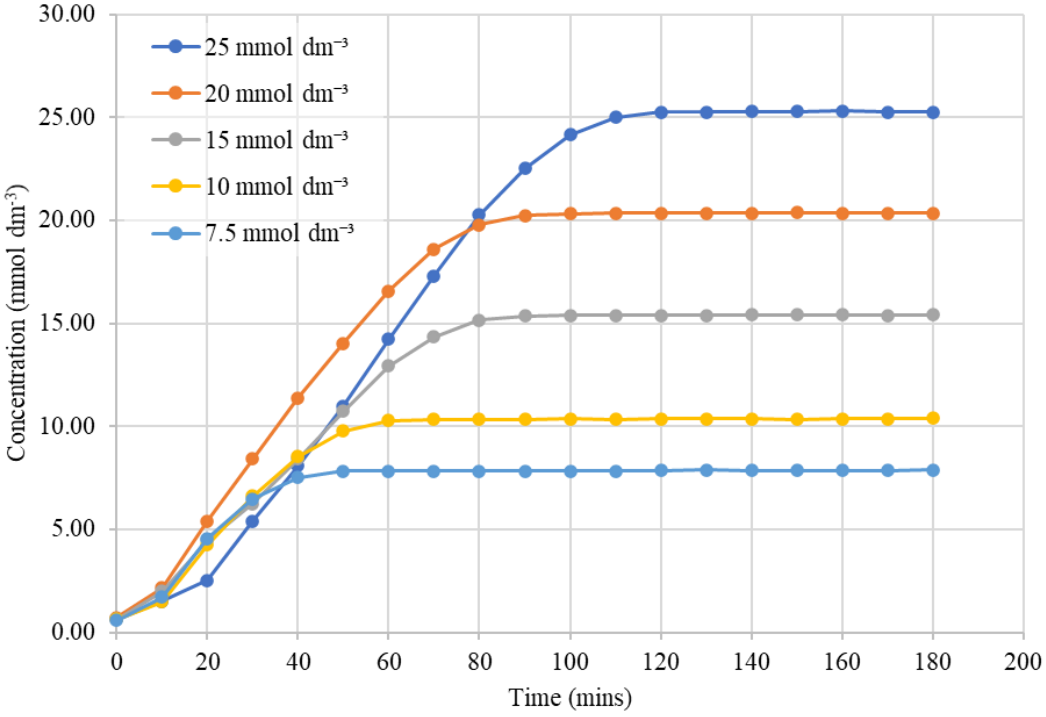

Figure C-11 Plot of the concentration of V(IV) vs time for solutions of 7.5-25 mmol dm^{-3} [V(V)] in 1 mol dm^{-3} H_2SO_4.

C-6. Plots of Concentration vs. Time for the reduction of V(V) by NO at varying [H^+]

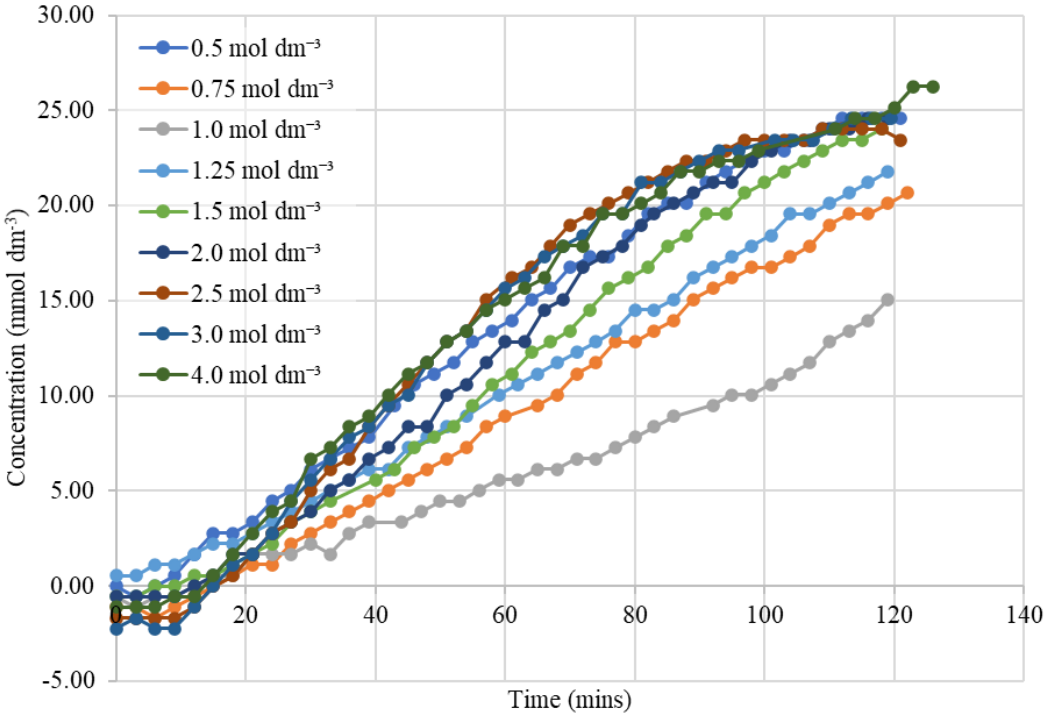

Figure C-12 Plot of the concentration of V(IV) vs time for solutions of 25 mmol dm^{-3} [V(V)] in 0.5-3 mol dm^{-3} H_2SO_4.

Appendix D.

D-1. MATLAB CODE

```
% Mike's model

% This model utilises the HNO3 concentration in solution - which the
% sulphuric experiments in Mike_Dataset2 doesn't have. Now the reaction
% rate constants can be set independently to fit data from both nitric and
% non-nitric experimental datasets. HNO3 concentration is in the
% denominator of pathway 2.

% Import all the data stored on Mike_Dataset2
% Matrix made with each row as new timestep, each column new dataset
Mike_Dataset3

% find out how many datasets are included
size_datasets = size(t) ;

% Model parameters
t_period = 21300 ; % s
t_step = 0.2 ; % s

% Kinetic rate constants
k1f = 3.2e-6 ;
k1b = 4.5e-6 ;
k2f = 5e-8 ;
k2b = 1e-8 ;
k_deg = 5e-6 ;

% Initialise time vector
t_m = [0:t_step:t_period] ;

% Find out how big time vector is
size_t_m = size(t_m) ;

% Initialise concentration vectors
C_V5_m = zeros(size_t_m(2),size_datasets(2)) ;
C_V4_m = zeros(size_t_m(2),size_datasets(2)) ;
C_NO2_m = zeros(size_t_m(2),size_datasets(2)) ;
C_NO_m = zeros(size_t_m(2),size_datasets(2)) ;
C_HNO2_m = zeros(size_t_m(2),size_datasets(2)) ;
C_NO3minus_m = zeros(size_t_m(2),size_datasets(2)) ;
C_proton_m = zeros(size_t_m(2),size_datasets(2)) ;

% Error vectors
err_V5 = 0.1*C_V5 ;
err_V4 = 0.1*C_V4 ;
err_HNO2 = 0.1*C_HNO2 ;

for data_index = 1:size_datasets(2)

% Initialise first row of matrix - i.e. across datasets
C_V5_m(1,data_index) = C_V5(1,data_index) ;
C_V4_m(1,data_index) = C_V4(1,data_index) ;
C_NO2_m(1,data_index) = 0 ;
```

```
53          C_NO_m(1,data_index) = 0 ;
54          C_HNO2_m(1,data_index) = C_HNO2(1,data_index) ;
55          C_NO3minus_m(1,data_index) = C_NO3minus(data_index) ;
56          C_proton_m(1,data_index) = C_proton(data_index) ;
57
58          for time_index = 1:size_t_m(2)-1
59
60          % rate equations
61          rate_1f = k1f*C_HNO2_m(time_index,data_index)*C_V5_m(time_index,
              data_index) ;
62          rate_1b = k1b*C_NO2_m(time_index,data_index)*C_V4_m(time_index,data_index)
              ;
63          rate_2f = k2f*C_HNO2_m(time_index,data_index)^1.5*C_V5_m(time_index,
              data_index)*C_proton_m(time_index,data_index)^0.5/C_NO3minus_m(time_index,data_index)
              ^0.5 ;
64          rate_2b = k2b*C_V4_m(time_index,data_index)*C_HNO2_m(time_index,
              data_index) ;
65          rate_deg = k_deg*C_HNO2_m(time_index,data_index) ;
66
67          % discretised time differentials
68          C_V5_m(time_index+1,data_index) = C_V5_m(time_index,data_index) + t_step*
              (-rate_1f - rate_2f + rate_1b + rate_2b) ;
69          C_V4_m(time_index+1,data_index) = C_V4_m(time_index,data_index) + t_step*
              (rate_1f + rate_2f - rate_1b - rate_2b) ;
70          C_NO2_m(time_index+1,data_index) = C_NO2_m(time_index,data_index) +
              t_step*(rate_1f - rate_1b) ;
71          C_NO_m(time_index+1,data_index) = C_NO_m(time_index,data_index) + t_step*
              ((2/3)*rate_deg) ;
72          C_HNO2_m(time_index+1,data_index) = C_HNO2_m(time_index,data_index) +
              t_step*(-rate_1f - 0.5*rate_2f + rate_1b + 0.5*rate_2b - rate_deg) ;
73          C_NO3minus_m(time_index+1,data_index) = C_NO3minus_m(time_index,
              data_index) + t_step*((1/3)*rate_deg + 0.5*rate_2f - 0.5*rate_2b) ;
74          C_proton_m(time_index+1,data_index) = C_proton_m(time_index,data_index) +
              t_step*((1/3)*rate_deg - 0.5*rate_2f + 0.5*rate_2b - rate_1f + rate_1b) ;
75
76          end
77
78          % plot conc data
79
80          figure(data_index);
81          subplot(3,3,1)
82          plot(t_m,C_V5_m(:,data_index),'b');
83          hold on
84          errorbar(t(:,data_index),C_V5(:,data_index),err_V5(:,data_index),'rx');
85          xlabel('t(s)'),ylabel('[V(V)] (mmol.dm^-^3)')
86          subplot(3,3,2)
87          plot(t_m,C_V4_m(:,data_index),'b');
88          hold on
89          errorbar(t(:,data_index),C_V4(:,data_index),err_V4(:,data_index),'rx');
90          xlabel('t(s)'),ylabel('[V(IV)] (mmol.dm^-^3)')
91          subplot(3,3,3)
92          plot(t_m,C_HNO2_m(:,data_index),'b');
93          hold on
94          errorbar(t(:,data_index),C_HNO2(:,data_index),err_HNO2(:,data_index),'rx');
95          xlabel('t(s)'),ylabel('[HNO_2] (mmol.dm^-^3)')
96          subplot(3,3,4)
97          plot(t_m,C_NO2_m(:,data_index),'b');
98          xlabel('t(s)'),ylabel('[NO_2] (mmol.dm^-^3)')
99          subplot(3,3,5)
100         plot(t_m,C_NO_m(:,data_index),'b');
```

```
101         xlabel('t(s)'),ylabel('[NO] (mmol.dm^-^3)')
102         subplot(3,3,6)
103         plot(t_m,C_NO3minus_m(:,data_index),'b');
104         xlabel('t(s)'),ylabel('[NO_3^-] (mmol.dm^-^3)')
105         subplot(3,3,7)
106         plot(t_m,C_proton_m(:,data_index),'b');
107         xlabel('t(s)'),ylabel('[H^+] (mdmol.m^-^3)')
108
109       end
```

D-2. All modelled concentrations

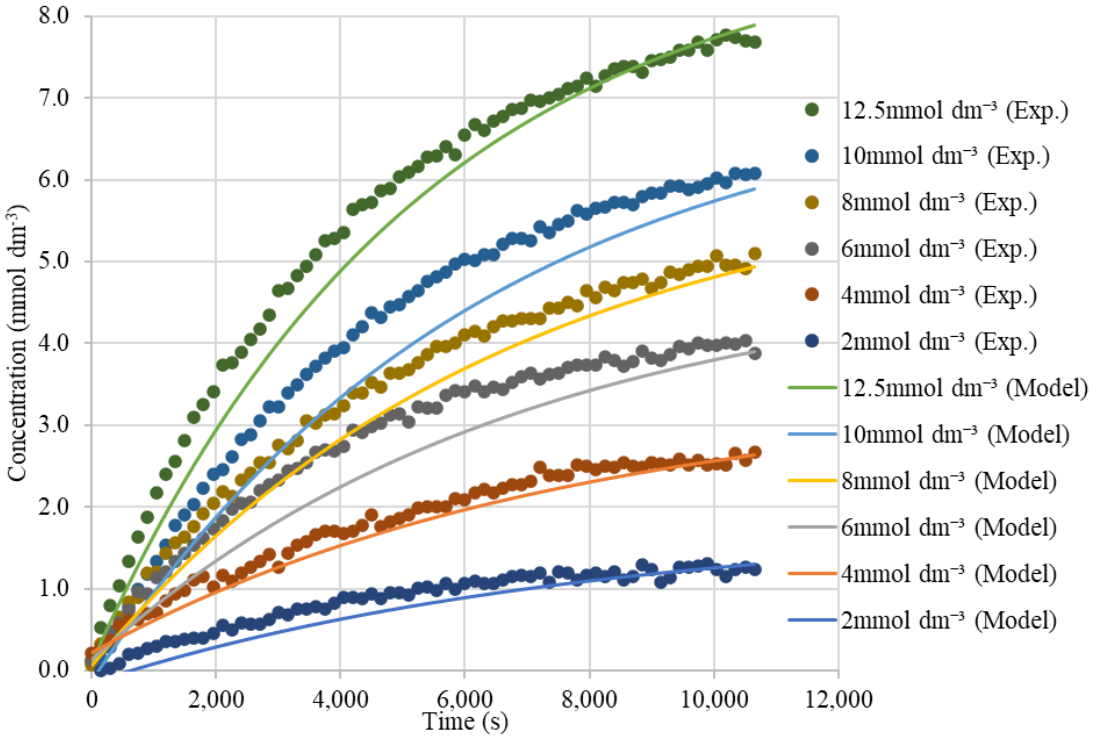

Figure D-1 Model and experimental V(IV) concentration vs time data in HNO_3. (initial conditions: $[HNO_2]$ = 30 mmol dm^{-3}, $[VO_2^+]$ = 2-12.5 mmol dm^{-3}; $[HNO_3]$ = 0.1 mol dm^{-3}).

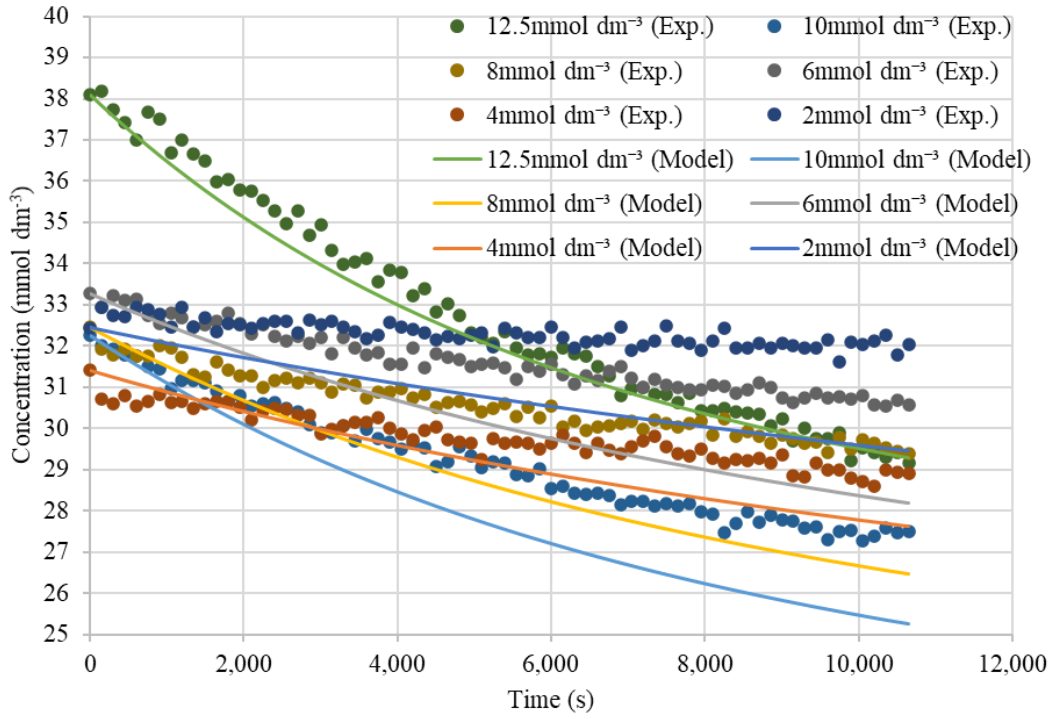

Figure D-2 Model and experimental HNO_2 concentration vs time data in HNO_3. (initial conditions: $[HNO_2]$ = 30 mmol dm^{-3}, $[VO_2^+]$ = 2-12.5 mmol dm^{-3}; $[HNO_3]$ = 0.1 mol dm^{-3}).

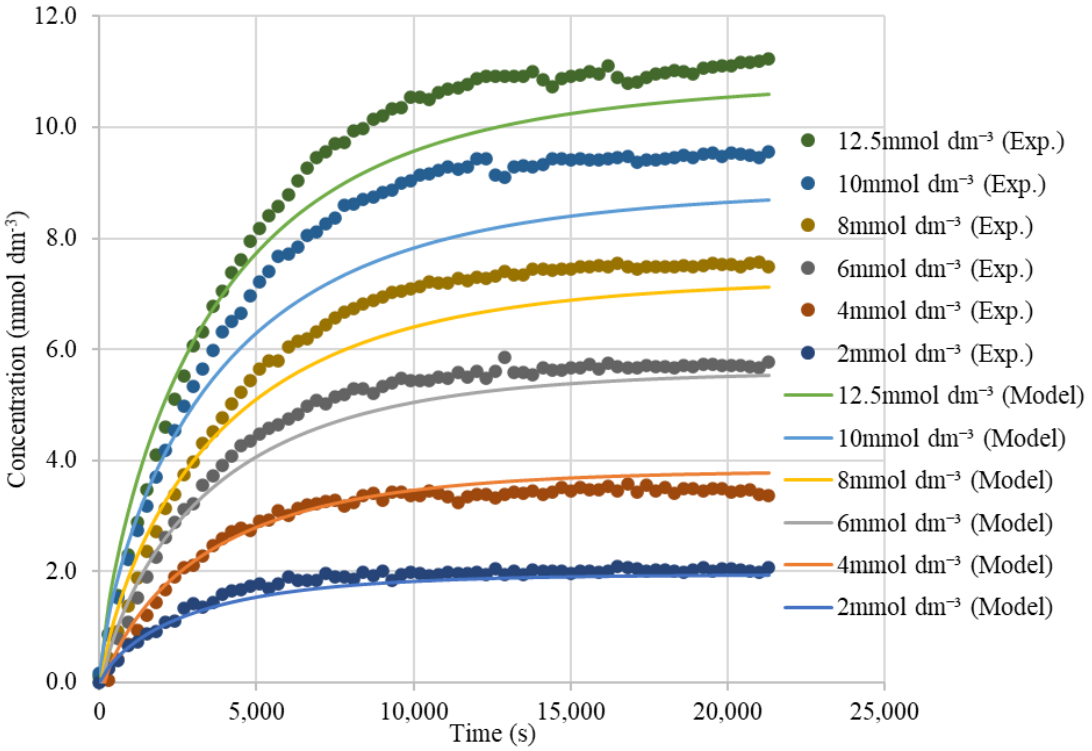

Figure D-3 Model and experimental V(IV) concentration vs time data in H_2SO_4. (initial conditions: [HNO_2] = 30 mmol dm^{-3}, [VO_2^+] = 2-12.5 mmol dm^{-3}; [H_2SO_4] = 0.1 mol dm^{-3}).

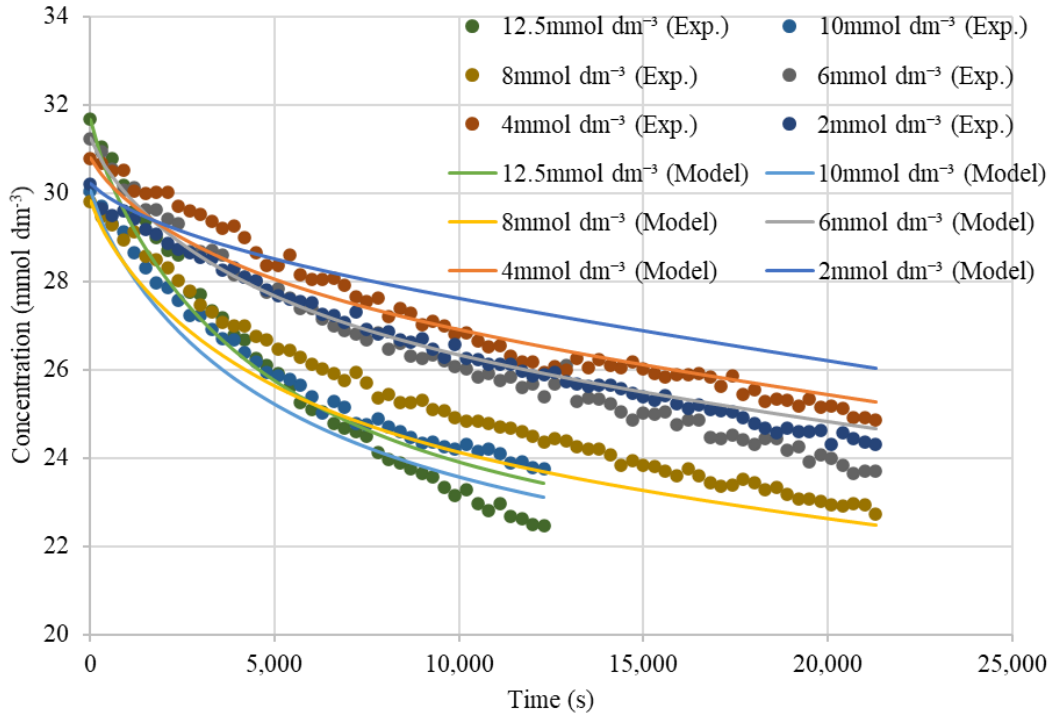

Figure D-4 Model and experimental HNO_2 concentration vs time data in H_2SO_4. (initial conditions: [HNO_2] = 30 mmol dm^{-3}, [VO_2^+] = 2-12.5 mmol dm^{-3}; [H_2SO_4] = 0.1 mol dm^{-3}).

Appendix E.

E-1. Preconditioning Plots of Current vs. Time for experiments into the reduction of Np(VI) by NO at varying [H^+]

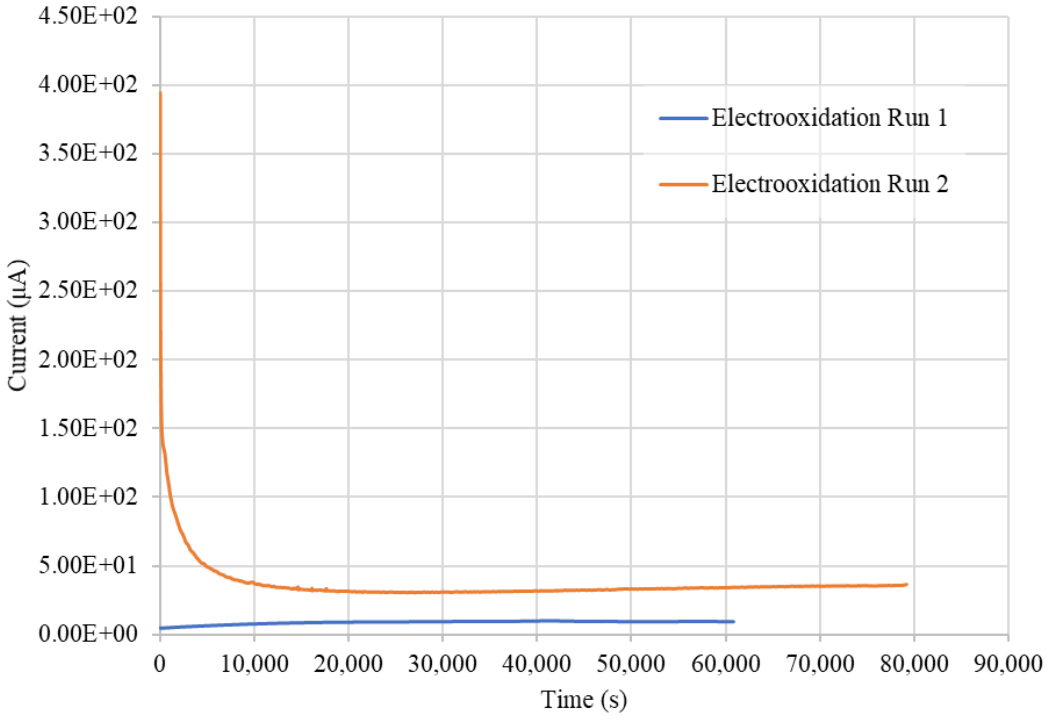

Figure E-1 Plots of Current vs time for the electrooxidation of Np(V) to Np(VI) before reduction experiment performed in 0.5 mol dm^{-3} H_2SO_4.

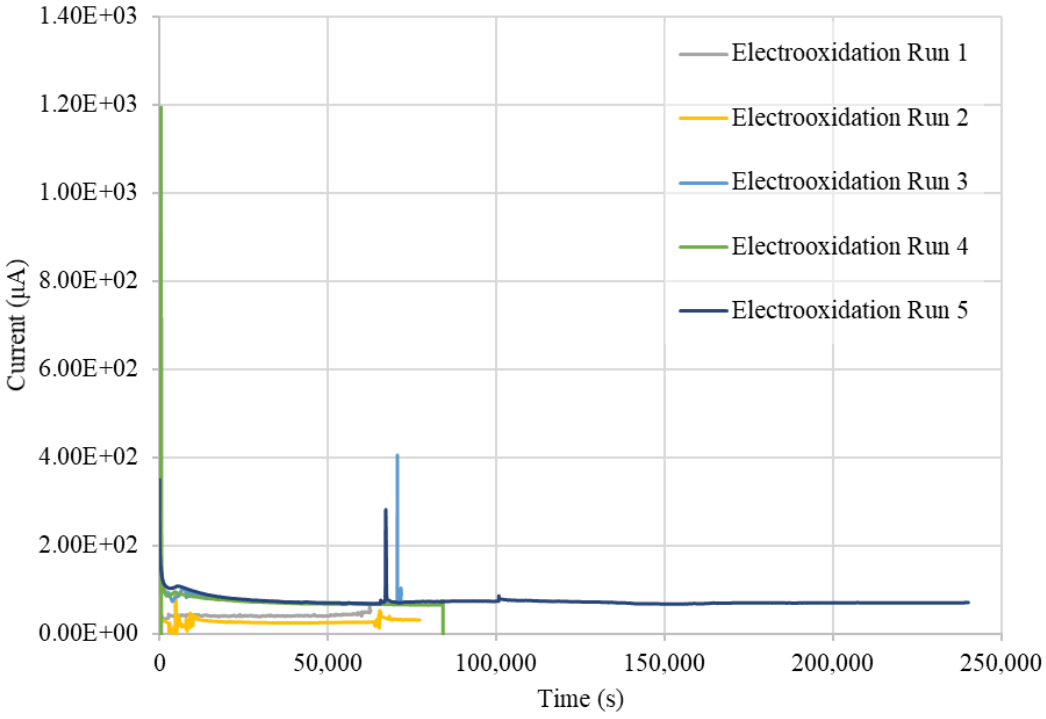

Figure E-2 Plots of Current vs time for the electrooxidation of Np(V) to Np(VI) before reduction experiment performed in 0.75 mol dm^{-3} H_2SO_4.

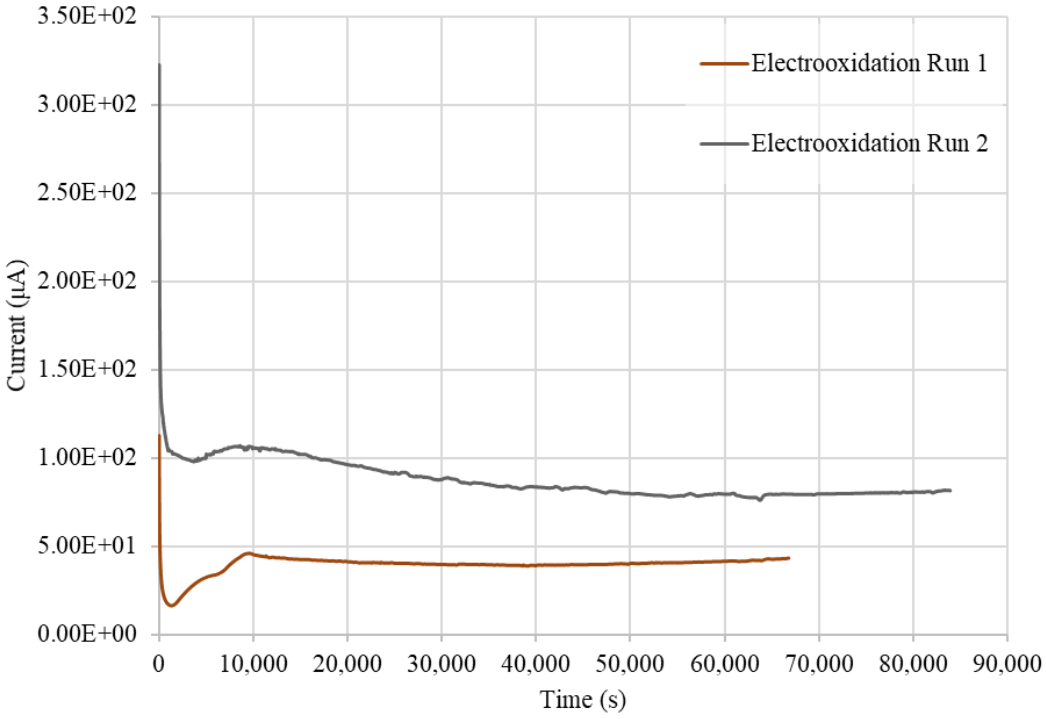

Figure E-3 Plots of Current vs time for the electrooxidation of Np(V) to Np(VI) before reduction experiment performed in 1 mol dm^{-3} H_2SO_4.

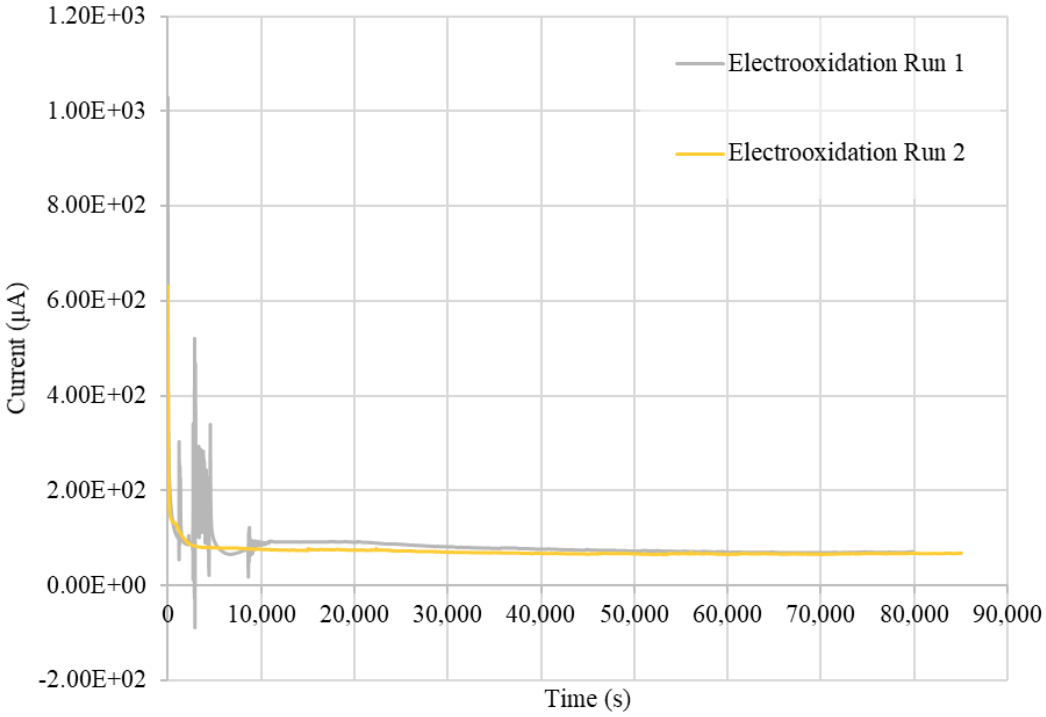

Figure E-4 Plots of Current vs time for the electrooxidation of Np(V) to Np(VI) before reduction experiment performed in 1.5 mol dm^{-3} H_2SO_4.

E-2. Preconditioning Plots of Current vs. Time for experiments into the reduction of Np(VI) by NO at varying [Np(VI)]

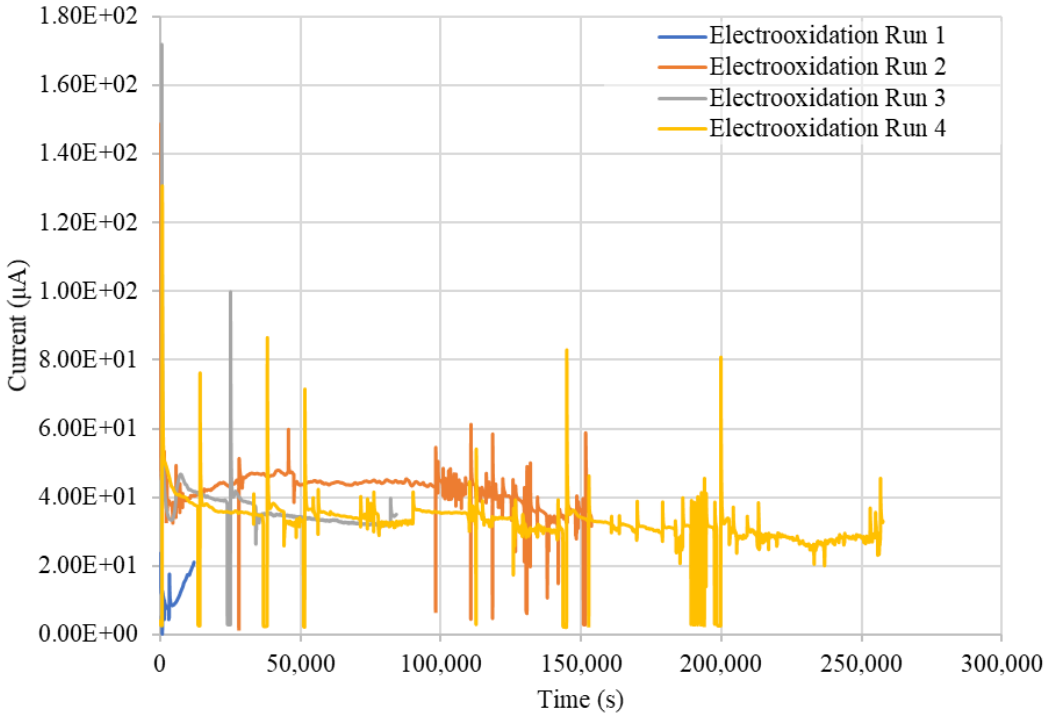

Figure E-5 Plots of Current vs time for the electrooxidation of 0.72 mmol dm–3 Np(V) to Np(VI) before reduction experiment performed in 1 mol dm^{-3} H_2SO_4.

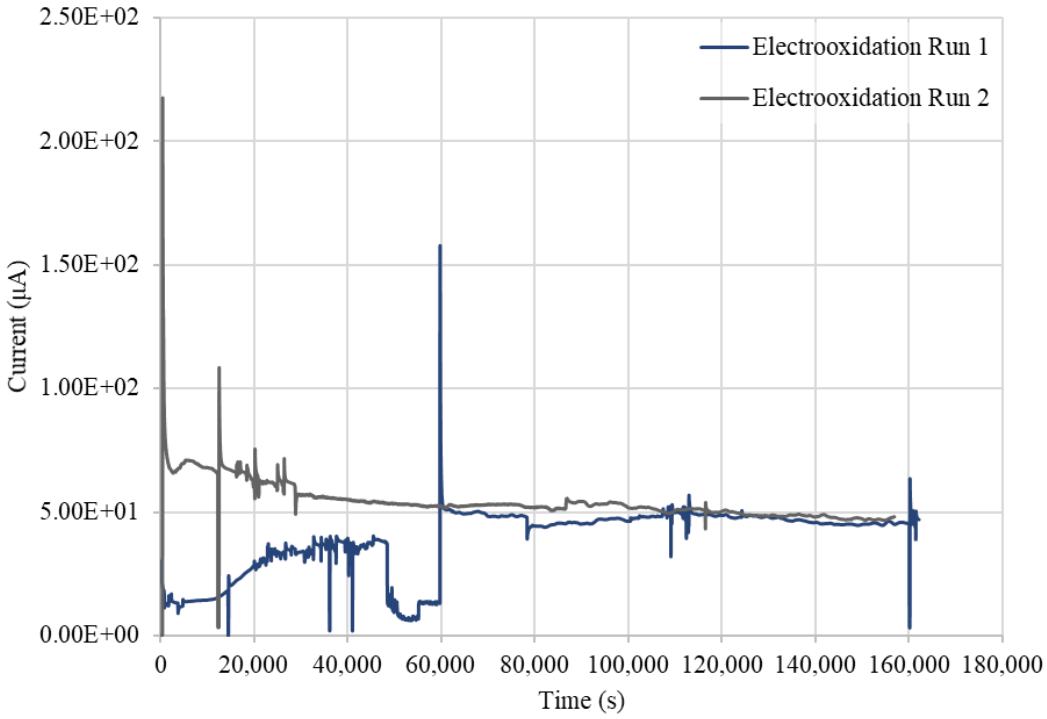

Figure E-6 Plots of Current vs time for the electrooxidation of 0.62 mmol dm–3 Np(V) to Np(VI) before reduction experiment performed in 1 mol dm^{-3} H_2SO_4.

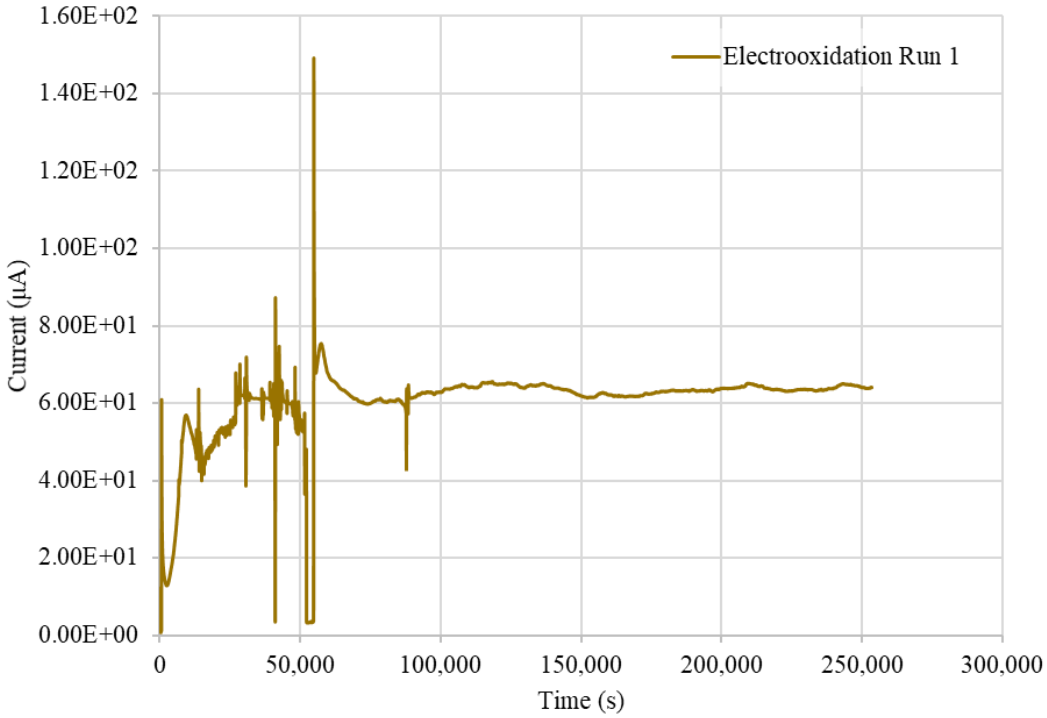

Figure E-7 Plots of Current vs time for the electrooxidation of 0.52 mmol dm^{-3} Np(V) to Np(VI) before reduction experiment performed in 1 mol dm^{-3} H_2SO_4.